

STRUCTURAL DYNAMICS OF RHODOPSIN:
RELATIONSHIPS BETWEEN RETINAL SCHIFF BASE
INTEGRITY AND RECEPTOR SIGNALING STATES

by

Jay M. Janz

A DISSERTATION

Presented to the Department of Biochemistry and Molecular Biology
and the Oregon Health and Science University School of Medicine
in partial fulfillment of the requirements for the degree of

Doctor of Philosophy

April 2004

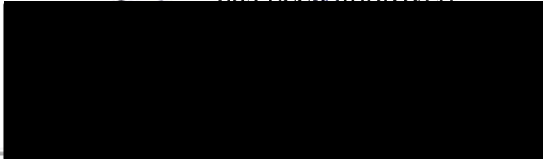
School of Medicine
Oregon Health & Science University

CERTIFICATE OF APPROVAL

This is to certify that the Ph.D. thesis of

Jay M. Janz

has been approved



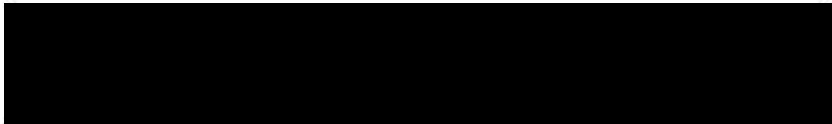
Professor in charge of thesis – Dr. David L. Farrens



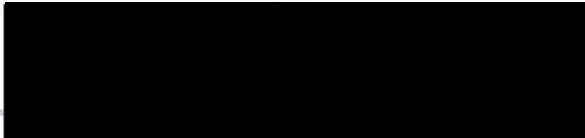
Thesis Committee Chair – Dr. Richard G. Brennan



Thesis Committee Member – Dr. Hans Peter Bächinger



Thesis Committee Member – Dr. Susan G. Amara



Thesis Committee Member – Dr. Jack H. Kaplan

TABLE OF CONTENTS

List of Tables	v
List of Figures	vi
List of Abbreviations	xii
Acknowledgments	xix
Abstract	xxi
Chapter 1: Introduction	
1. 1 G-protein coupled receptor signaling.	2
1. 2 Visual signal transduction.	3
1. 3 Rhodopsin structure.	7
1. 4 Rhodopsin structure/function relationship.	10
1. 5 Dissertation overview.	18
Chapter 2: Engineering a functional blue-wavelength shifted rhodopsin mutant.	
2. 1 Summary	41
2. 2 Introduction	42
2. 3 Materials and Methods	44
2. 4 Results	48
2. 5 Discussion	52
2. 6 Acknowledgments	59
2. 7 Supplementary Material	75

Chapter 3: Stability of dark-state rhodopsin is mediated by a conserved ion-pair in intradiscal loop E-2.

3. 1	Summary	84
3. 2	Introduction	85
3. 3	Materials and Methods	87
3. 4	Results	93
3. 5	Discussion	97
3. 6	Acknowledgments	106
3. 7	Supplementary Material	125

Chapter 4: Assessing structural elements that influence Schiff base stability: Mutants E113Q and D190N destabilize rhodopsin through different mechanisms.

4. 1	Summary	131
4. 2	Introduction	131
4. 3	Materials and Methods	134
4. 4	Results	138
4. 5	Discussion	142
4. 6	Acknowledgments	149
4. 7	Supplementary Material	163

Chapter 5: Role of retinal hydrogen bond network in Schiff base stability and hydrolysis.

5. 1	Summary	169
5. 2	Introduction	169

5.3	Materials and Methods	172
5.4	Results	174
5.5	Discussion	179
5.6	Acknowledgments	187
Chapter 6: Rhodopsin activation exposes a key hydrophobic binding site for the transducin α -subunit C-terminus.		
6.1	Summary	205
6.2	Introduction	205
6.3	Materials and Methods	207
6.4	Results	214
6.5	Discussion	218
6.6	Acknowledgments	221
6.7	Supplementary Material	239
Chapter 7: Summary and Conclusions		
7.1	Stabilization of the retinal Schiff base linkage in the dark state of rhodopsin.	243
7.2	Mechanism of rhodopsin activation.	244
7.3	Mechanism of rhodopsin interaction with transducin.	244
7.4	Retinal release and signaling attenuation.	245
7.5	Possible structural changes in rhodopsin during MII decay.	246

7.6	Future studies.	246
7.7	Concluding statements.	247
References		248
Appendix 1: Retinal Schiff base hydrolysis regulates resetting of TM Helix 6 during rhodopsin signal attenuation.		
A.1	Summary	282
A.2	Introduction	282
A.3	Materials and Methods	284
A.4	Results	286
A.5	Discussion	291

LIST OF TABELS

<i>Number</i>		<i>Page</i>
2. 1:	Functional characterization of wavelength-shifted single point mutants.	60
2. 2:	Relative transducin activation rates and rates of retinal release for wavelength-shifted mutants.	61
2. 3:	Functional properties of mutant T118A/E122D/A292S in comparison with WT rhodopsin.	62
3. 1:	Functional characterization of ion-pair mutants.	107
3. 2:	Thermodynamic parameters for the dark state thermal decay of WT and ion-pair mutant rhodopsins.	108
4. 1:	Schiff base hydrolysis characteristics for WT rhodopsin and mutants E113Q and D190N.	150
5. 1:	Spectral and functional properties of hydrogen bond network mutants.	188
5. 2:	Kinetic and thermodynamic parameters of Schiff base stability studies on hydrogen bond network rhodopsin mutants.	189
6. 1:	PDT-bimane labeling characteristics of single rhodopsin mutants.	222
6. 2:	PDT-bimane labeling characteristics of rhodopsin hydrophobic patch mutants.	223
6. 3:	Activation and peptide quenching characteristics of rhodopsin hydrophobic patch mutants.	224
A. 1:	Characterization of PDT-bimane labeled rhodopsin mutants.	296

LIST OF FIGURES

<i>Number</i>		<i>Page</i>
1. 1:	G-protein coupled receptor mediated signal transduction.	23
1. 2:	Rod cell morphology and rhodopsin adsorption.	25
1. 3:	Phototransduction cascade of the rod cell.	27
1. 4:	11- <i>cis</i> -retinal is recycled through the enzymatic processing of the retinoid cycle.	29
1. 5:	Three-dimensional structural model of rhodopsin in the dark state and a schematic showing the residues within 4.5 Å distance from the retinal chromophore.	31
1. 6:	Monitoring rhodopsin signaling states by absorption spectroscopy.	33
1. 7:	Rhodopsin photocycle indicating spectroscopically detected photointermediates.	34
1. 8:	Decay of Metarhodopsin intermediates.	37
1. 9:	Proposed mechanism of retinal Schiff base hydrolysis in rhodopsin.	39
2. 1:	Models of the bovine rhodopsin indicating sites introducing blue-wavelength shifting mutations.	64
2. 2:	UV/vis absorption spectra of WT and mutant rhodopsin pigments in the dark state.	66
2. 3:	UV/vis spectral properties of select blue wavelength shifted rhodopsin mutants.	68

2. 4:	Transducin activation by blue-wavelength shifted rhodopsin mutants.	70
2. 5:	Arrhenius plot of the retinal release rates from photobleached WT and mutant rhodopsins.	72
2. 6:	UV/vis spectral properties of rhodopsin mutant T118A/E122D/A292S relative to WT.	74
2. S1:	Three-dimensional model of rhodopsin residues making steric contact with the C ₉ -methyl of 11- <i>cis</i> -retinal.	78
2. S2:	Photobleaching characteristics of rhodopsin mutant I189A.	80
2. S3:	Characterization of the MII signaling state for mutant I189A.	82
3. 1:	Model of rhodopsin indicating R177/D190 ion-pair.	110
3. 2:	Sequence alignment of loop E-2 for rhodopsin, β -2 adrenergic and CB1 cannabinoid receptors.	112
3. 3:	Immunoblot analysis of mutant rhodopsins.	114
3. 4:	Disrupting the R177/D190 ion-pair does not impair MII stability or function in mutants that regenerate with 11- <i>cis</i> -retinal.	116
3. 5:	Rapid thermal decay of R177Q mutant correlates with loss of functional ability, loss of Schiff base linkage, and release of chromophore.	118

3. 6:	Ion-pair mutants show much faster rates of thermal decay than wild-type rhodopsin.	120
3. 7:	Arrhenius plots of dark state thermal decay rates show ion-pair mutants have similar activation energies for retinal hydrolysis yet faster rates than WT rhodopsin.	122
3. 8:	Ion-pair mutants do not show increased susceptibility to hydroxylamine.	124
3. S1:	Photobleaching properties of rhodopsin mutant R177Q/D190N.	127
3. S2:	Effects of 140 mM NaCl on the thermal decay process of rhodopsin mutant D190N.	129
4. 1:	How the rhodopsin structure influences the retinal Schiff base linkage.	152
4. 2:	Three-dimensional model of the rhodopsin intradiscal domain.	154
4. 3:	Monitoring retinal Schiff base stability in dark state and MII rhodopsin.	156
4. 4:	Spectral properties of two different rhodopsin mutants with perturbed Schiff base stabilities.	158
4. 5:	Mutations can alter the retinal Schiff base stability in rhodopsin in fundamentally different ways.	160
4. 6:	Hydroxylamine sensitivity indicates fundamental differences between mutants that exhibit altered Schiff base stability.	162

4. S1: Effects of pH on the thermal decay process of rhodopsin mutant D190N.	165
4. S2: Effects of pH on the process of MII decay and retinal release on rhodopsin mutant D190N.	167
5. 1: Residues involved in a hydrogen bond network around the retinal Schiff base linkage in rhodopsin.	191
5. 2: UV/vis absorption profiles of purified rhodopsin hydrogen bond network mutants.	193
5. 3: Spectral properties of mutant Y268F in comparison with WT following illumination.	195
5. 4: Arrhenius plots of dark state thermal decay rates.	197
5. 5: Hydrogen bond network rhodopsin mutations show location dependent effects on Schiff base stability in the MII state.	199
5. 6: Kinetic isotope effects of retinal Schiff base hydrolysis and retinal release.	201
5. 7: Proposed mechanism for retinal Schiff base hydrolysis from rhodopsin.	203
6. 1: Light activation of rhodopsin opens a cleft to enable binding of the G _{Tα} C-terminus.	228
6. 2: Peptide W23SV binding occludes site V250C.	230
6. 3: Peptide W23SV binding and quenching properties of PDT-bimane labeled rhodopsin mutants.	232

6. 4:	Peptide W23SV binds to rhodopsin near residues C140, K141 and F228.	234
6. 5:	Peptide W23SV binding to K141B is specific, requires the MII state, and requires an intact protonated Schiff base linkage.	236
6. 6:	Mutations in a “hydrophobic patch” on rhodopsin reduce but do not abolish peptide W23SV binding affinity.	238
6. S1:	Stabilization of MII state by G _{Tα} C-terminal tail peptide analogues.	241
A. 1:	Three-dimensional model of rhodopsin viewed toward the cytoplasmic face indicating sites of bimane label and tryptophan-quenching group incorporation.	298
A. 2:	Fluorescence resonance energy transfer between bimane fluorescence emission and rhodopsin absorbance.	300
A. 3:	UV/vis bleaching profiles of PDT-bimane labeled rhodopsin mutants during MII decay.	302
A. 4:	Movements in TM helix 6 during MII decay detected at site 250 from bimane fluorescence.	304
A. 5:	Movements in TM helix 6 during MII decay detected at site 248 from bimane fluorescence.	306
A. 6:	UV/vis bleaching profile and Steady state emission spectra of mutant E113Q-V139W-V250B.	308

A. 7:	Helix 6 resetting appears to be coupled to retinal Schiff base hydrolysis.	310
A. 8:	Cartoon model illustrating TM helix 6 resetting during decay of the rhodopsin MII state.	312

LIST OF ABBREVIATIONS

1D4	monoclonal antibody to rhodopsin-
23S	peptide: $\text{NH}_2\text{VLEDLKSCGLF}_{\text{COOH}}$
A	alanine
α	alpha
<i>A</i>	Arrhenius pre-exponential factor
Å	angstrom
ABCR	ATP-driven photoreceptor specific ABC binding Cassette transported
ADRP	Autosomal Dominant Retinitis Pigmentosa
Arr	arrestin
Asp	aspartate
ATP	adenosine triphosphate
ATR-al	all- <i>trans</i> -retinal
ATR-ol	All- <i>trans</i> -retinol
β	beta
B	bimane label
β AR	β -2 adrenergic receptor
BSI	blue-shifted intermediate
C	cysteine
C-	carboxyl-

Ca	calcium
CB1	cannabinoid 1 receptor
cGMP	cyclic
Cl	chloride
CNB	Congenital Night Blindness
Cys	cysteine
D (chemical compounds)	deuterium
D (protein context)	aspartic acid
D ₂ O	deuterium oxide
DEAE dextran	Diethylaminoethyl-Dextran
ΔG^\ddagger	change in Gibbs free energy
ΔH^\ddagger	change in enthalpy
DM	<i>n</i> -dodecyl- β -maltoside
DNA	deoxyribonucleic acid
DS	dark state rhodopsin
ΔS^\ddagger	change in entropy
DTT	dithiothreitol
ϵ	extinction coefficient
E (protein context)	glutamic acid
E (protein domain)	extracellular
E-2	second extracellular loop of rhodopsin
E _a	energy of activation

EC ₅₀	effective concentration
EDTA	ethylenediamine-tetraacetic acid
EPR	electron paramagnetic resonance
ExPASy	Expert Protein Analysis System
F	phenylalanine
FRET	fluorescence resonance energy transfer
FTIR	Fourier Transform Infrared Spectroscopy
γ	gamma
G	glycine
GC	guanylate cyclase
GCAP	guanylate cyclase activating protein
GDT	guanosine diphosphate
Glu	glutamic acid
GMP	guanosine monophosphate
GPCR	G-protein coupled receptor
G-protein	heterotrimeric guanine nucleotide-binding regulatory protein
G _T	transducin G-protein
G _{Tα}	alpha subunit of transducin G-protein
GTP	gaunosine triphosphate
GTPγS	gaunosine 5'-3-O-(thio)triphosphate
h	hour

h	Planck's constant
$h\nu$	light
HPLC	high pressure liquid chromatography
Hyd	hydroxylamine
Hz	hertz
I (chemical compound)	iodine
I (protein context)	isoleucine
I (protein domain)	intracellular
IMP	interphotoreceptor matrix space
IPBP	interphotoreceptor retinal binding protein
k	rate constant
k_n	rate constant in n amount D_2O
k_H	rate constant 100% H_2O
K (chemical compound)	potassium
K (protein context)	lysine
k_B	Boltzmann constant
kcal	kilocalories
K_d	equilibrium dissociation constant
kDa	kilodalton
K_{sv}	Stern-Volmer quenching constant
L	leucine
LRAT	Lecithin:retinol acyl-transferase

λ_{\max}	absorption maximum
M	Molar
MES	2-(N-Morpholino)-ethanesulfonic acid Monohydrate
MI	metarhodopsin I photointermediate
MII	metarhodopsin II photointermediate
MIII	metarhodopsin III photointermediate
min	minute
μL	microliter
ml	milliliter
μM	micromolar
mM	millimolar
n (chemical context)	mole fraction
MW	molecular weight
N-	amino-
N (chemical compounds)	nitrogen
N (protein context)	asparagine
Na	sodium
NADPH	nicotinamide adenine dinucleotide, reduced form
ng	nanogram
NH_2OH	hydroxylamine
nM	nanomolar
O	oxygen

°C	degrees Celsius
PBSSC	phosphate buffered saline
PCR	polymerase chain reaction
PDE	phosphodiesterase
PDT-bimane	2-Pyridyl-dithiobimane
pK _a	pH of the acid dissociation constant
PMSF	phenylmethanesulfonyl fluoride
preps	preparations
PSB	protonated Schiff base
PyMPO maleimide	1-(2-maleimidylethyl)-4-(5-(4-methoxyphenyl)oxazol-2-yl)-pyridinium methanesulfonate
Q	glutamine
θ	rhodopsin background mutant-C140S, C316S, C322S and C323S
Q	quenching agent
R	off state GPCR
R (equation context)	universal gas constant
R (protein context)	arginine
R*	active GPCR
RDH	retinol dehydrogenase
Rel	relative
rho	rhodopsin

RK	rhodopsin kinase
ROS	rod outer segment
RPE	retinal pigment epithelium
s	second
S	serine
SDS-PAGE	sodium dodecyl sulfate-poly-acrylamide gel electrophoresis
SDFL	Site-directed fluorescence labeling
SDSL	Site-directed spin labeling
T	threonine
TCA	trichloroacetic acid
TCEP	Tris(2-carboxyethyl)phosphine
TM	transmembrane
tris	2-Amino-2-hydroxymethyl-1-3-propanediol
Trp	tryptophan
UV/vis	ultraviolet-visible
V	valine
W	tryptophan
W23SV	peptide: $\text{NH}_2\text{WVLEDLKS VGLF}_{\text{COOH}}$
WT	wild type rhodopsin
Y	tyrosine

ACKNOWLEDGMENTS

First and foremost I would like to sincerely thank my advisor and mentor Dr. David L. Farrens, his guidance and friendship have truly been a gift. The past years of graduate school have been an excellent learning experience and he has instilled in me the importance of understanding the physical principles that govern biological processes. I further wish to thank him for all of his help with the work presented in this dissertation and his patience in teaching me and fostering my development as an investigator.

I would also like to thank the members of the Farrens' lab past and present who have made daily bench work thoroughly enjoyable. My gratitude is extended to Jonathon Fay, Martha Sommer, Steven Mansoor, Tom Dunham and Dr. Brian Nauert – it is wonderful to be able to call all of my co-workers friends. I thank them all for their support throughout my graduate studies and for being able to deal with “Surly-Jay” on more than one occasion. I have also been the beneficiary of many great friendships at OHSU and wish to thank fellow classmate Joel Walker for bringing me into his circle of friends several years ago.

I also would like to thank the members of my research advisory committee – Dr. Richard Brennan, Dr. Jack Kaplan, Dr. Hans Peter Bächinger and Dr. Susan Amara for their guidance and helpful comments.

Finally, I wish to thank my parents James and Joan for their untiring love and encouragement. An excellent education is one of the greatest gifts parents can bestow upon their children. My parents have always provided me with much-needed moral, spiritual and “occasional” financial support in all of my endeavors.

I also wish to thank all of my brothers for their years of support, encouragement, and occasional harassment.

This thesis is dedicated to *H. Power* through whose wisdom and strength I am granted my daily reprieve and lasting serenity.

ABSTRACT

The dim-light photoreceptor rhodopsin serves as the paradigm for G-protein coupled receptor (GPCR) structure/function investigations. This transmembrane protein contains an 11-*cis*-retinal chromophore covalently attached via a Schiff base linkage. Interactions between this ligand and the surrounding protein are thought to maintain rhodopsin stability and regulate the signaling states of the receptor. This dissertation presents studies investigating how the protein affects the retinal Schiff base stability and binding of the retinal ligand in the dark and active states of the receptor, as well as the molecular mechanisms involved in receptor activation and the structural dynamics underlying signal attenuation.

Data is presented which suggest the retinal Schiff base counter-ion (E113), a conserved ion-pair in the extracellular domain (R177/D190) and a network of hydrogen bonds that surround the retinal Schiff base site are integral to maintaining the stability of this linkage in the dark state of the receptor. These studies suggest the rhodopsin protein can mediate retinal Schiff base stability through three fundamentally different mechanisms – i) by affecting the hydrolysis chemistry, ii) by shielding the retinal linkage from solvent, or iii) by acting as a kinetic trap to slow retinal release.

The molecular mechanism of receptor activation and interactions that facilitate and stabilize signaling are also explored. Through site-directed mutagenesis in conjunction with biochemical and biophysical approaches the validity of the currently accepted “steric trigger” model of receptor activation is brought into question. In addition, site-directed fluorescence labeling studies are presented which indicate that movement of helix 6 during formation of the active MII state opens up a cleft on the

cytoplasmic face of rhodopsin, which binds the C-terminal tail of the transducin α -subunit. This interaction is further shown to be mediated by key hydrophobic interactions.

Finally, the dynamics of rhodopsin signal attenuation are explored as they relate to the decay of the active, MII signaling species. Highlights from these studies include the observation that residues T94, E113 and S186 are crucial to facilitate the chemical process of retinal Schiff base hydrolysis during the decay of the MII state. In addition, results are presented that are consistent with the hypothesis that the chemical event of Schiff base hydrolysis is the rate-limiting step in MII decay. Lastly, site-directed labeling studies are presented which suggest helix 6 moves back toward the helical bundle in tandem with hydrolysis of the retinal Schiff base linkage.

In summary, the results from this dissertation study provide further mechanistic detail into the process of retinal Schiff base stabilization by rhodopsin and demonstrate how the integrity of this linkage regulates to the signaling state of the receptor.

Chapter 1

Introduction

1. 1: G-protein Coupled Receptor Signaling.

G-protein coupled receptors (GPCRs) provide a molecular link uniting extracellular signals to intracellular response pathways (1-4). These receptors form one of the largest superfamilies of cell-surface receptors, mediating responses to a diverse array of signals including odorants, small molecules such as hormones, peptides, nucleotides and even proteins (1, 3). The entire superfamily of GPCRs share limited sequence homology (5), although all are thought to be integral membrane proteins that share a similar topology. In general, their structure consists of seven transmembrane (TM) spanning α -helical segments connected by alternating intracellular and extracellular loops, with the amino (N-) terminus located on the extracellular side and the carboxy (C-) terminus on the intracellular side of the cell. In addition, more significant sequence homology may be found within the three receptor subfamilies. The "A" subfamily (rhodopsin / B2 adrenergic receptor like-receptors) is by far the largest of these three subfamilies (2, 3, 5). The structure and function of rhodopsin mediated signal transduction is the focus of this dissertation.

As their name implies, GPCRs function primarily to recruit and regulate the activity of intracellular heterotrimeric G-proteins (guanine nucleotide-binding regulatory proteins). G-proteins consist of three subunits; α , β , and γ . Each of these subunit groupings may be further divided into different subtypes – to date 16 α , 5 β and 12 γ proteins have been cloned (1). This diverse array of subtypes greatly increases the number of signal transduction pathways in which G-proteins participate, as each subtype regulates the activity of different effector proteins (1, 6).

A general overview of GPCR activation is shown in Figure 1. 1. As shown, GPCRs act to catalyze guanine-nucleotide exchange in heterotrimeric G-proteins. That is, the binding of ligand to its respective GPCR induces conformational changes which activate the receptor (7, 8). The activated receptor binds and induces conformational changes in its respective G-protein α -subunit, thus inducing release of GDP followed by rapid binding of GTP (9, 10). Subsequently, the GTP-bound heterotrimeric G-protein dissociates from the receptor and the α -subunit separates from the $\beta\gamma$ subunits. The released α_{GTP} and $\beta\gamma$ subunits then modulate several cellular signaling pathways through interaction with their effector proteins such as adenylate cyclases, phospholipases, various channel proteins and second messenger systems (1, 11), (Figure 1. 1).

Importantly, GPCRs act catalytically – one receptor protein can elicit GDP/GTP exchange in many G-proteins. In turn, the G-protein subunits can subsequently modulate the activity of even more effector proteins. This resulting signal transduction cascade serves the important role of both amplifying the original signal as well as expediting the response time occurring within the cell.

Vision is an excellent example of a cellular process mediated by GPCR signal transduction cascades. Visual signal transduction is initiated by specialized GPCRs which have evolved to respond to light stimulus. Through years of extensive study, the visual system has become the best model system for studying the process of GPCR mediated signal transduction, and it is described below.

1. 2: Visual Signal Transduction.

Visual phototransduction occurs when photons of light are captured by a molecule of visual pigment, which results in generating an electrical signal in the brain (12-14).

Light enters the eye and is focused upon the retina, a specialized tissue of the central nervous system that is comprised of three layers (15). The innermost two layers of the retina are composed primarily of neuronal cells that relay light information to the optic nerve and ultimately the brain. The outer layer contains the photoreceptor cells, the rods and cones, which mediate dim light (scotopic) and bright light (photopic) vision, respectively (15). In higher primates cone cells respond to photons of different wavelengths (red, green and blue in humans), thus providing the basis for tri-chromatic vision (16, 17). Although most photoreceptors in humans are found predominately in rod cells (95%), this amount can vary in other species (18).

In both rods and cones, the proteins which mediate phototransduction are located within a modified and greatly enlarged cilium, referred to as the outer segment, as shown in Figure 1. 2 (15, 19, 20). The outer segment is filled with 1000 to 2000 specialized flattened membrane sacs called discs. These discs contain the opsin visual proteins, and are constantly renewed by new synthesis and assembly at the base of the photoreceptor and shedding of older material from its tip (19, 21, 22). Both rod and cone cells contain opsin photoreceptors, which are made up of a transmembrane opsin protein and a covalently attached light-sensitive chromophore called 11-*cis*-retinal (19, 21, 22). The signal transduction process is similar in both types of visual photoreceptor cells (18) and the phototransduction cascade for the rod cell system is detailed below.

The first stage in light capture and signal amplification. As mentioned above, the capture of photons by chromophores in the visual pigments initiates a series of biochemical cascades which ultimately result in neuronal firing and visual processing by the brain (Figure 1. 3), (12, 14, 19, 23-27). This light-to-voltage transition process is

highly amplified and thus must have a low amount of background noise to induce a high signal-to-noise ratio. This allows a high degree of sensitivity within the rod cells (28-31). Eye diseases such as *congenital night blindness*, (CNB) exemplify the importance of maintaining low background noise. This disease is thought to arise from inappropriate stimulation (constitutive activation) of rhodopsin in the dark state, which increases the background “noise” levels and eventually leads to photoreceptor death (32).

In rod cells, photon capture causes the 11-*cis*-retinal chromophore of rhodopsin to isomerize along the C₁₁=C₁₂ double bond to the all-*trans* configuration (14). This change in chromophore conformation is transduced through the rhodopsin receptor protein (R), which proceeds through a series of spectrally defined intermediates culminating in a conformational switch to the active R* or Metarhodopsin II state (31, 33). The signal is then passed from R* to the GDP bound form of the heterotrimeric G protein, transducin (G_{Tαβγ}), by a direct binding interaction (31, 33, 34). This interaction induces a conformational switch in the G_{Tα} subunit causing the rapid dissociation of GDP and binding of GTP (6, 34, 35). This exchange causes both the rapid release of G_T from R* as well as dissociation of the active G_{Tα}-GTP from the G_{Tβγ} subunits (6, 34, 35). As each R* activates multiple transducin molecules, this initial event represents the first signal amplification stage, which account for the high gain in signal of the rod cell response mentioned earlier (19, 28, 29, 31).

Second messenger mediated signal amplification in visual signal transduction. In the next amplification step, released G_{Tα}-GTP stimulates the activity of cGMP phosphodiesterase (PDE), (Figure 1. 3), (36). Activation of PDE (PDE*) in turn causes a reduction in cytoplasmic concentrations of cGMP, the second messenger in the

phototransduction system (13, 34, 36). This decrease in cGMP levels is detected by cGMP-gated channels located in the rod cell plasma membrane and induces their closure (13, 34, 36). Closure of these channels reduces the steady inward current that is normally carried by Na^+ and Ca^{2+} ions in the dark, thus causing membrane hyperpolarization and a subsequent decreased release of the synaptic transmitter glutamate at the photoreceptor terminal (13).

Attenuation of signal trasduction by auxiliary proteins. Signal attenuation, recovery and return of the system to the dark state involves the inactivation of each of the active intermediates of the phototransduction cascade (18). To expedite attenuation, rod cells utilize additional rhodopsin regulatory proteins, namely rhodopsin kinase and arrestin (37-40). The active MII state of rhodopsin is first recognized and phosphorylated at serine and threonine residues at its C-terminal tail by rhodopsin kinase (37-40). Phosphorylated rhodopsin is subsequently recognized and bound by the protein arrestin, which effectively prevents further activation of G_T (13, 18, 37-41). Further downstream in the cascade G_T molecules are inactivated through hydrolysis of bound GTP to GDP. This in turn ends G_T stimulation of the cGMP phosphodiesterase, which brings the rate of cellular cGMP hydrolysis down to dark state levels (13). In addition, calcium ions regulate several stages of the phototrasduction pathway by modifying the activity of key Ca^{2+} binding proteins in a feed back inhibition loop detailed in Figure 1. 3 (13, 25).

The loss of the chromophore is the final step in the attenuation process, since the resulting phosphorylated opsin is incapable of binding G_T , rhodopsin kinase or arrestin (13). This occurs when the all-*trans*-retinal Schiff base linkage of MII rhodopsin is hydrolyzed and cleaved, releasing free retinal and leaving the “inactive” apoprotein,

opsin (42-44). As opposed to the processes of signal activation and subsequent signal transduction cascade, the molecular aspects of Schiff base hydrolysis and retinal release from the opsin-binding pocket are poorly understood (45). A major focus of this dissertation is to advance our understanding of the molecular details governing this important process, and these studies are discussed in chapters two, four and five.

Resetting the opsin back to the light sensitive form involves a complex series of enzymatic events, called the retinoid cycle (Figure 1. 4), (45, 46). During this cycle, the *all-trans*-retinal released following Schiff base hydrolysis is first converted to *all-trans*-retinol by NADPH-dependent *all-trans*-retinol dyhydrogenase (45, 46). The *all-trans*-retinol is then transported to the retinal pigment epithelium, where it proceeds through a number of enzyme catalyzed steps and is ultimately converted into 11-*cis*-retinal (45, 46). Thus converted, the chromophore is shuttled back to opsin, where it subsequently binds to regenerate light-sensitive rhodopsin (45). Note also that both the first step (retinal release from MII) and the last step of the retinoid cycle (regeneration of opsin with 11-*cis*-retinal) rely on the chemically similar act of either forming or hydrolyzing a retinal Schiff base linkage. Furthermore recent work indicates the some retinal diseases are caused by defects in the retinoid cycle (45, 46).

1. 3: Rhodopsin Structure.

Rhodopsin is unique among GPCRs in that its ligand (the 11-*cis*-retinal chromophore) is covalently attached to the protein through a protonated Schiff base linkage to the amino side chain of residue K296. However, rhodopsin also exhibits modifications common to most members of the GPCR super family. These include palmitoylation (at cysteine residues near the C-terminal tail at residues C322 and C323),

(27, 47), a conserved disulfide bond in the extracellular region of the protein (between C110 and C187), and glycosylation at the N-terminus (at residues N2 and N15), (4, 48, 49). In addition, as an integral membrane protein, rhodopsin appears to interact with tightly bound phospholipids, which are thought to stabilize the protein and coat the hydrophobic transmembrane regions of the protein (50, 51).

A detailed synopsis of previous rhodopsin studies and an in-depth description of the dark state crystal structure are beyond the scope of this introduction. Instead, following a brief overview of the dark state structural model, the subsequent sections of this introduction will concentrate primarily on regions of the protein relevant to the studies presented in this dissertation.

To date, rhodopsin is the only GPCR for which the structure is known to high-resolution (52). The crystal structure was initially solved to 2.8 Å and has recently been refined to 2.6 Å (52-54). Only the dark (off) state structure is known, but this structure confirmed conclusions based on years of biochemical and biophysical study, including the general arrangement of the TM helices (predicted from cryo-electron microscopy, mutagenesis and site-directed labeling studies) and residues predicted to form the retinal chromophore binding pocket (predicted from mutagenesis and photocrosslinking studies (31, 52, 55-60). A ribbon model of the rhodopsin structure is presented in Figure 1. 5A and each of its domains; extracellular, transmembrane, retinal binding pocket and intracellular, are discussed further below.

Extracellular domain. The extracellular domain of rhodopsin is comprised of the N-terminal tail and three extracellular loops (E-1, residues 101-106; E-2, residues 174-199 and E-3, residues 278-285). While previous mutagenesis studies have implicated this

domain in the folding and stability of rhodopsin, the high degree of structural complexity was somewhat of a surprise (61-65). The extracellular region seems to form a lid over the retinal-binding site and as such has been coined the “retinal plug” (66, 67). Importantly, residues on loop E-2 in this domain make extensive contacts with the retinal chromophore.

Transmembrane domain. The membrane-embedded domain consists of seven predominantly α -helical TM segments, which form a compact bundle that contains the binding site for the 11-*cis*-retinal chromophore (48, 52). These transmembrane helices account for 56% of the 348 amino acids in rhodopsin (4). The overall stability of the TM domain may be attributed in part to several hydrogen-bonded networks, which seem to constrain the helices (52, 54, 67, 68).

Retinal binding pocket. The retinal binding pocket is offset toward the extracellular region from the center of the TM domain (52), and is comprised of a mixture of both hydrophobic and polar/charged residues. A diagram illustrating residues that interact with retinal is shown in Figure 1. 5B. The retinal Schiff base linkage is protonated in the dark state due to its unusually high pK_a . Residue E113, which is in close proximity to the Schiff base attachment site, serves as the counter-ion to this internal charge in the dark state of the receptor (69-71). In addition, at least 2 water molecules are thought to reside in the retinal binding pocket near the protonated Schiff base linkage (54). The interactions between residue side chains that line the binding pocket and the retinal chromophore serve to modulate both the wavelength of photon absorption as well as the signaling state of the receptor. The wavelength modulation

process or “spectral tuning” is discussed further below as well as in chapter 2 of this dissertation.

Cytoplasmic domain. The cytoplasmic face of rhodopsin is made up of three intercellular loops (I-1, I-2 and I-3), and a short cationic amphipathic α -helix (helix 8), which extends parallel to the membrane and the C-terminal tail (52-54). This intracellular surface interacts with the cognate G-protein for rhodopsin – transducin (G_T) to initiate visual signal transduction upon receptor activation. While mutagenesis and chemical-labeling studies have implicated loops I-2 and I-3 in the binding of G_T , the location of this interface as well as the types of protein-protein interactions mediating this union are at present unknown. In addition, the signal of photon capture must be transmitted from the core of the TM bundle to the cytoplasmic surface and result in conformational changes to activate the receptor and allow interaction with and activation of G_T . Chapter six of this dissertation as well as the appendix that follows, describe site-directed fluorescence labeling experiments in conjunction with additional biochemical and biophysical studies, which explore these conformational changes.

1. 4: Rhodopsin Structure/Function Relationships.

1. 4. 1: Retinal Schiff base linkage.

Early studies on visual signal transduction implicated a “retinene” compound similar to vitamin A as the chromophore responsible for light absorption (72, 73). Wald, Morton and co-workers subsequently showed this compound was an aldehyde of vitamin A, called retinal, and proposed that it was attached to the protein via a Schiff base linkage (72-75). To account for the shifted absorption spectrum of free retinal in solution ($\lambda_{\max} = 380 \text{ nm}$) to that of rhodopsin, ($\lambda_{\max} = 500 \text{ nm}$), Hubbard and Kropf suggested that the

Schiff base linkage must be protonated (76-78). This proposal was confirmed by the work of Bownds and Akhtar (79, 80) and further supported directly by resonance Raman vibrational studies of rhodopsin by Oseroff and Callender (81).

Interestingly, the pK_a of protonation for the Schiff base in dark state rhodopsin is thought to be greater than 15, whereas the pK_a for protonation of model Schiff base compounds is approximately 7 (82-85). Studies suggest that the high pK_a of the Schiff base may be due in part to the low pK_a of the counter-ion E113 (86-88). For example, an E113Q mutation reduces the Schiff base pK_a for protonation from ~ 15 to 8 (69-71). While high in the dark state, the Schiff base pK_a must drop following light absorption during transition to the active MII state as studies suggest it is transiently deprotonated during this process (27, 88-90). This presents an interesting 2-part question; 1) Why is the pK_a of the retinal Schiff base in the dark state rhodopsin many orders of magnitude higher than for model compounds and 2) How is the pK_a drastically reduced in the MII state to account for deprotonation? A more comprehensive understanding of the interactions between the retinal Schiff base linkage and the rhodopsin protein environment that surrounds it is necessary to fully answer this question. Chapters two through five of this dissertation present studies investigating these interactions.

It has been hypothesized that the Schiff base pK_a in dark state rhodopsin is high to lower the rate of thermal isomerization of the chromophore (91-94). In fact, thermal isomerization in a single rhodopsin molecule at physiological temperature has been estimated to occur approximately once in every 470 years, well beyond the human lifetime (28). This extremely low incidence of thermal isomerization results in a very

low amount of background noise and thus the ultra-high sensitivity exhibited by rhodopsin, which is capable of detecting photons in the single digit range (28).

1. 4. 2: Spectral tuning.

In all known photoreceptors the retinal chromophore is attached to the opsin apoprotein through a Schiff base linkage (18), yet the absorption maximums of these pigments vary from the ultraviolet to the near-infrared (18, 88). The absorption maximum (λ_{\max}) of the retinal chromophore in both rhodopsin and color visual pigments are tuned as a result of interactions with the apoprotein environment to which they are bound (95). 11-*cis*-retinal free in solution exhibits a λ_{\max} centered at ~ 380 nm, and model intact protonated retinal Schiff base compounds exhibit λ_{\max} values at ~ 440 nm (48, 95, 96). Site-directed mutagenesis in combination with UV/vis spectroscopy has illustrated residues important to λ_{\max} determination between the rod and cone pigments (96-100). Mechanistically, the λ_{\max} shifts demonstrated by the visual opsins are thought to arise primarily from the electrostatic interaction of dipolar amino acid residues with both the ground-state and excited-state charge distribution of the chromophore and Schiff base site in conjunction with adjustment of the counter ion location (48, 95, 96). This mechanism, initially proposed through the use of resonance Raman vibrational spectroscopy (48, 95, 96) is supported by the crystal structures which reveal a large number of dipolar or polarizable amino acid residues lining the retinal-binding pocket (52-54).

1. 4. 3: Retinal plug.

As noted above, the extracellular domain of rhodopsin encapsulates one face of the retinal-binding site and is referred to as the “retinal plug” (66, 67). The extracellular

domain contains a highly conserved disulfide bond linking cysteine residues C110 and C187 (101). The presence of this disulfide bond seems important for the stability of the active MII signaling state, as its removal through site-directed mutagenesis results in a functional yet unstable MII intermediate (102). Initial mutagenesis studies illustrated the importance of this domain in proper protein folding, chromophore binding and cellular trafficking (62, 103, 104). Furthermore, several point mutations that result in amino acid substitutions in this domain are linked to *Autosomal Dominant Retinitis Pigmentosa* (ADRP), (20, 27, 48, 63, 105). ADRP is an inherited human disease that causes progressive retinal degeneration, loss of dim-light vision, loss of peripheral vision and eventually blindness (48, 106).

Perhaps the most interesting feature of the extracellular domain is loop E-2, which connects helices four and five (residues 174-199) and forms a twisted β -hairpin that makes extensive contacts with the retinal chromophore (52-54), (Figure 1. 5A). This novel finding – unappreciated until the advent of the dark state structure, raises a number of important questions: What role does loop E-2 play in the stability and function of rhodopsin? What types of interactions stabilize the loop E-2 structure? How do amino acids on loop E-2 affect Schiff base integrity among the receptor signaling states? These questions concerning the function of loop E-2 are explored in chapters three, four and five of this dissertation.

1. 4. 4: Rhodopsin activation / attenuation mechanism.

As detailed above the initial event in dim-light vision is the capture of photons by the 11-*cis*-retinal chromophore and isomerization to the all-*trans*-retinal configuration (107, 108). Due to the presence of the chromophore, the main signaling states and

transitions between photointermediates in the rhodopsin photocycle may be followed using absorbance spectroscopy. In the dark state, purified rhodopsin exhibits a visual λ_{\max} centered at 500 nm (Figure 1. 6). A diagram of the rhodopsin photocycle illustrating the characteristics of the photointermediates stages is presented in Figure 1. 7. Following photon capture the protein proceeds through a series of thermal relaxation intermediates that are short lived and do not result in any large scale changes of the receptor, but may be trapped at low temperatures and identified (14). The short-lived initial photospecies in turn give rise to the longer lived Metarhodopsin intermediates; MI, MII and MIII (14, 33, 109). MI (λ_{\max} centered at ~ 480 nm) is in a pH and temperature dependent equilibrium with its successor MII and is the first intermediate in which changes in the secondary structure of the protein may be detected (110). In addition, the strength of the hydrogen bond for the Schiff base proton in the MI state is significantly less than in the dark state (18, 88). Furthermore, the counter ion to the protonated Schiff base in the dark state (E113) is thought to switch to a residue on loop E-2 (E181) during formation of the MI state (111). The MI state then gives rise to the MII intermediate, the functionally active state of rhodopsin.

The MII intermediate state of rhodopsin is responsible for binding and activation of G_T – thus eliciting the visual signal transduction cascade. Transition to the MII state is accompanied by retinal Schiff base deprotonation, with residue E113 acting as the proton acceptor, in a process that results in a large shift in λ_{\max} from ~ 480 to 380 nm (Figure 1. 6), (14, 89, 112). Substantial conformational changes also accompany this transition and enable the receptor to bind to and activate G_T (31, 113, 114). Specifically, TM helix 6 has been shown to move outward from the helical bundle upon formation of the active

MII state (114-116). It is thought that movement of helix 6 exposes portions of the conserved D/ERY sequence (E134, R135 and Y136) on helix 3 for interaction with the transducin G-protein (51, 114). The importance of this movement is underscored by experiments demonstrating that inhibition of this conformational change prevents receptor activation of G_T (114, 115). Additionally, it has been suggested that this movement may open up a binding pocket for G_T (116, 117) and this hypothesis is further explored in chapter six of this dissertation.

In the context of stabilizing interactions revealed by the dark state crystal structure it has been suggested that the activation process for rhodopsin could be considered as removal of structural constraints which keep the receptor in the “off” conformation (51). Yet, not all of these constraints are currently accounted for, and others remain to be tested. Prior to the elucidation of the rhodopsin dark state structure, mutagenesis data suggested that the steric interactions between the opsin protein and the C_9 -methyl group of the retinal chromophore constrained the receptor in the dark state conformation (118-121). This in turn gave rise to the steric trigger hypothesis of rhodopsin activation (122). This theory purports a direct steric interaction between the C_9 -methyl group on the retinal chromophore and residue G121 on transmembrane helix 3 of rhodopsin that holds the receptor in the dark state. It was further suggested that the relief of this interaction as a result of retinal isomerization gives rise to the active state of the receptor. However, the crystal structure revealed that residue G121 is not close enough to the C_9 -methyl group of the retinal to make steric contact, calling the steric trigger activation theory into question. In chapter two this theory is tested using site-

directed mutagenesis to alter amino acids that contact the C₉-methyl moiety of retinal and assess their functional ramifications.

The phototransduction cycle ends with the decay of the active MII intermediate, which may occur through 2 parallel pathways (Figure 1. 8). In one pathway the MII state decays directly to free all-*trans*-retinal and the opsin apoprotein (75, 123). In the other pathway the pool of MI/MII intermediates transition through the MIII state, which subsequently decays to all-*trans*-retinal and opsin (75, 124, 125). The physiological role of the MIII intermediate is not at present certain, however it has been proposed to act as a storage form of retinal within the eye (44, 125). The MIII intermediate is thought to arise as a result of thermal isomerization of the chromophore C=N bond resulting in a all-*trans*-15-*syn* configuration – as opposed to the all-*trans* configuration of the MII intermediate (125). However, the molecular interactions leading up to and resulting in hydrolysis of the retinal Schiff base and release from the opsin-binding pocket are not entirely clear (45).

1. 4. 5: Schiff base hydrolysis and retinal release.

Ultimately, the all-*trans*-retinal must dissociate from the opsin-binding pocket of rhodopsin to enable the enzymatic recovery of the 11-*cis*-retinal chromophore via the retinoid cycle and regeneration of the dark state photoreceptor. However, the molecular details governing this process in rhodopsin are not well known. A brief review of what is known is detailed below.

Transient Schiff base linkages are utilized during catalysis by numerous enzymes, including class I aldolases and enzymes involved in amino acid transamination reactions (126). It has been suggested that the transamination reaction is subject to general acid-

base catalysis during hydrolysis of the Schiff base linkage (126), and hydrolysis of the Schiff base linkage of retinal is thought to occur in a similar manner (85). The notion of water-mediated hydrolysis was first suggested by the early studies of Kühne who observed anomalous photobleaching patterns in dehydrated retinas (127) and subsequent studies by Wald and co-workers illustrated that water is necessary for the MI \rightarrow MII transition (128). Furthermore, isotopic labeling studies show the incorporation of ^{18}O into the hydrolyzed all-trans-retinal recovered from samples photobleached in the presence of H_2^{18}O (85).

While the general chemistry of retinal Schiff base hydrolysis was initially worked out in the 1950s (72, 74, 75), a proposed mechanism for retinal Schiff base hydrolysis in rhodopsin was not put forth until the late 1980s (85). Initial deuterium solvent isotope effect experiments on the hydrolysis process of non-retinal model Schiff base compounds were interpreted mechanistically as proceeding through a protonated carbinolamine intermediate (129, 130). Subsequent resonance Raman spectroscopy experiments further implicated the presence of a carbinolamine intermediate during retinal Schiff base hydrolysis and suggested a tetrahedral configuration for this intermediate (85, 131). Incorporating the above-mentioned findings into the context of their own work, Cooper and co-workers proposed a mechanism of retinal Schiff base hydrolysis, and an adaptation of this mechanism is depicted in Figure 1. 9 (85). This mechanism suggests base catalyzed attack of an internal water molecule on the retinal Schiff base linkage and incorporates a tetrahedral carbinolamine intermediate in the transition state of the reaction. However, the model predates both the discovery of the rhodopsin counter-ion residue E113 as well as the crystallographic model of the protein in its dark state form.

As such, the model does not address which amino acids near the Schiff base site may participate in the hydrolysis mechanism. Furthermore, conformational changes, which occur in the protein during Schiff base hydrolysis, remain largely unexplored. In chapter five of this dissertation as well in the appendix, findings from studies addressing these important issues are presented.

1. 5: Dissertation Overview.

The overall objectives of this thesis project are to understand how interactions between the rhodopsin protein and the retinal chromophore stabilize the Schiff base linkage and how the integrity of this linkage relates to the signaling state of the receptor. Toward this end, I have carried out a number of studies investigating structural factors that mediate rhodopsin retinal stability, receptor activation and signaling attenuation. How these results are presented in the remaining chapters of this dissertation is outlined below.

In chapters two through five I report our investigations into understanding how the rhodopsin protein stabilizes the retinal Schiff base linkage. Chapter two details the development and application of Arrhenius analysis to understand the process of Schiff base hydrolysis and retinal release in rhodopsin mutants, and reports investigations into the rhodopsin activation process by providing experimental evidence against the steric trigger mechanism of activation. In chapter three, the assays developed in chapter two are further utilized in studies on the role of a conserved ion pair (R177/D190) on loop E-2 of rhodopsin. Chapter three shows that this ion pair is important to Schiff base stability in the dark state of the receptor and suggests that loop E-2 may function as a kinetic trap, to block retinal release as well as constrain a network of hydrogen bonds stabilizing the

Schiff base linkage site. Next, chapter four details further studies into mechanisms that regulate Schiff base stability. This work explores the effect of the counter-ion E113 on rhodopsin stability and is contrasted with studies on an ADRP causing mutation D190 that is found in loop E-2 of the protein. From this work the rhodopsin protein is proposed to stabilize the Schiff base linkage through at least three fundamentally different mechanisms. Chapter five discusses investigations into a hydrogen bond network that surrounds the retinal Schiff base linkage, and these findings are related to the stability mechanisms detailed in chapter four. These investigations on the retinal Schiff base hydrolysis mechanism are presented, and a proposed model for this process is discussed.

Chapter six returns to a discussion of studies on the molecular mechanism of rhodopsin activation. Through site-directed fluorescent labeling experiments, the binding location of the transducin α -subunit C-terminal tail onto the cytoplasmic face of rhodopsin is mapped. These studies demonstrate that this interaction is mediated in part by key hydrophobic interactions and show that this interaction is dependent on the integrity of the retinal Schiff base linkage. A summary of the conclusions from this dissertation and suggestions for possible future directions to explore is presented in chapter seven. In the appendix that follows, preliminary findings suggesting that the integrity of the retinal Schiff base linkage regulates the conformation of TM helix 6 during signaling attenuation are presented.

The main conclusions derived from this dissertation may be subdivided into three categories; retinal Schiff base stability in the dark state, mechanism and stability of receptor activation and the signal attenuation process.

Retinal Schiff base stability in the dark state.

- The rhodopsin protein mediates retinal Schiff base stability through 3 fundamentally different mechanisms – i) by affecting the hydrolysis chemistry, ii) by shielding the retinal linkage from solvent, or iii) by acting as a kinetic trap to slow retinal release.
- A conserved ion pair, R177/D190, on loop E-2 stabilizes the retinal Schiff base linkage in the dark state, possibly through a kinetic trap mechanism.
- The rhodopsin counter-ion E113 stabilizes the retinal Schiff base linkage in the dark state chemically through protonation.
- A hydrogen bond network that surrounds the retinal chromophore stabilizes the retinal Schiff base linkage in the dark state in part by shielding the linkage from the bulk solvent.

Mechanism and stability of receptor activation.

- Residues G90, E122 and A295 affect the stability of the MII state.
- Removal of steric contacts between the C₉-methyl group of retinal and amino acids contacting this site does not drastically alter rhodopsin stability or signaling, refuting the steric trigger hypothesis of activation.
- Transmembrane helix 6 movement during formation of the MII state opens up a cleft on the cytoplasmic face of rhodopsin, which binds the C-terminal tail of the transducin α -subunit.

- Key hydrophobic interactions mediate the coupling of the C-terminal tail of the transducin α -subunit to MII rhodopsin to initiate receptor signaling.

Signal attenuation processes.

- Residues T94, E113 and S186 effect the chemical process of retinal Schiff base hydrolysis during the decay of the MII state.
- The chemical event of retinal Schiff base hydrolysis seems to be the rate-limiting step in the retinal release process.
- The process of rhodopsin retinal Schiff base hydrolysis exhibits deuterium solvent isotope effects consistent with the formation of a tetrahedral carbinolamine intermediate.
- Transmembrane helix 6 moves back toward the helical bundle during MII decay in a process regulated by the integrity of the retinal Schiff base linkage (Appendix 1).

Figure 1. 1: G-protein coupled receptor mediated signal transduction. GPCRs have a central common core made of seven transmembrane α -helices connected by three intracellular (I-1, I-2, I-3) and three extracellular (E-1, E-2, E-3) loops. GPCRs respond to a wide array of ligands and initiate cellular signal transduction cascades through binding and activation of their cognate heterotrimeric G-proteins composed of α , β , and γ subunits. Ligand activated GPCRs induce the exchange of GDP for GTP in their respective G-protein α -subunits, which in turn dissociate from the receptor as well as from the β and γ subunits. Thus activated, these subunits interact with their respective effector proteins – ultimately resulting in an intracellular response to an extracellular stimulus. Figure taken from (3).

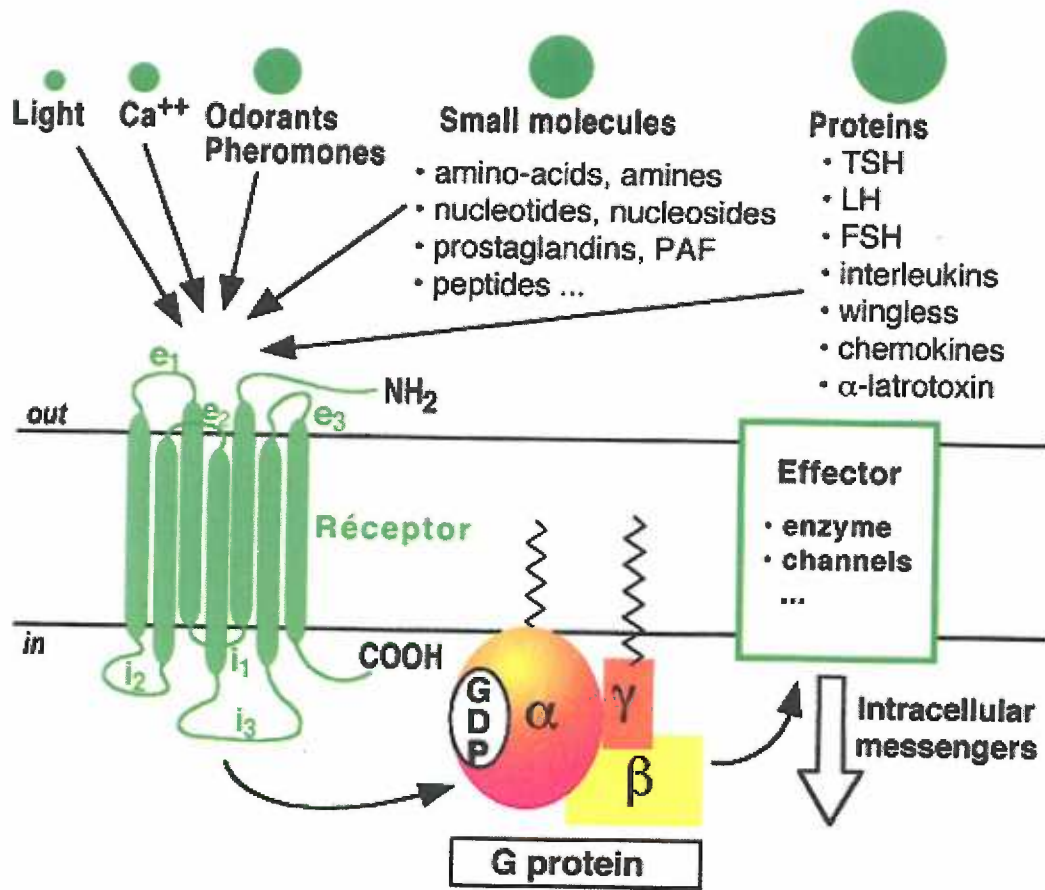


Figure 1. 2: Rod cell morphology and rhodopsin absorption. Left, schematic of a vertebrate rod cell. The outer segments consist of stacks of disc membranes containing the photoreceptor protein rhodopsin which are continually renewed by new synthesis and assembly near the inner segment of the rod cell and by shedding of older material from its tip into the retinal pigment epithelium (19, 21, 22). The disc membrane shown in expanded cross section shows the oval shapes of densely packed rhodopsin molecules that traverse the lipid bilayer. In the lower right of the figure is a cartoon of the polypeptide chain of rhodopsin as it may exist in the lipid bilayer in three dimensions. The N-terminus is modified by two oligosaccharide chains at the intradiscal surface. The cutaway view shows the 11-*cis*-retinal, which is attached to lysine 296 on TM 7 through a protonated Schiff base linkage in a pocket formed by the inside surface of the helical bundle. Figure adapted from (132).

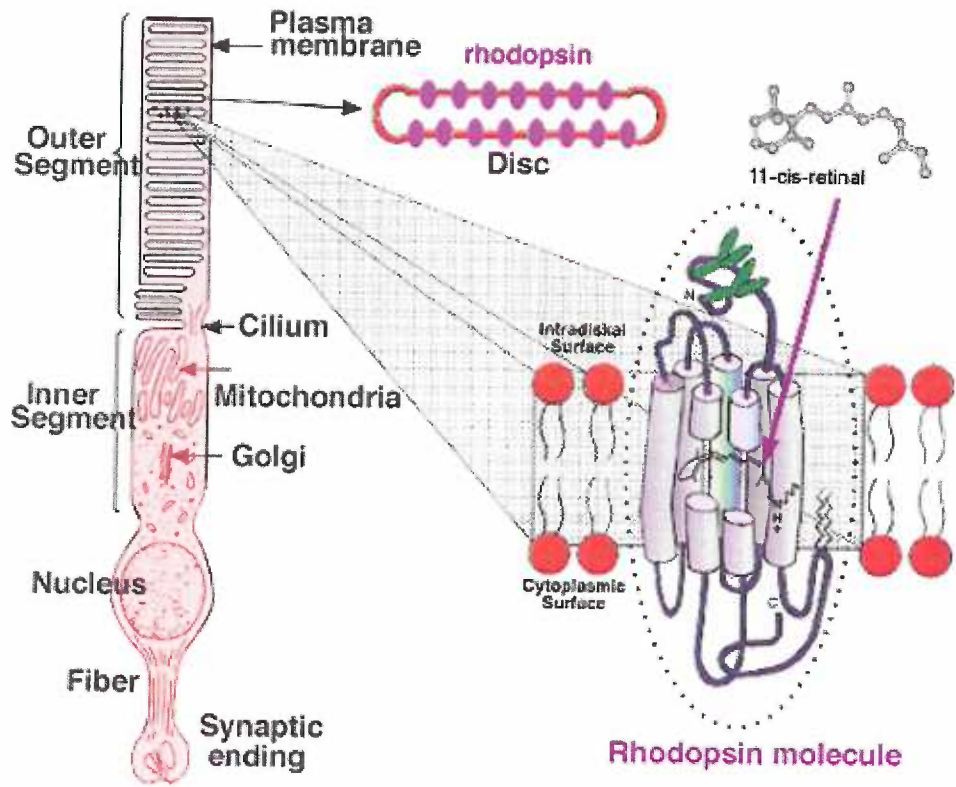


Figure 1. 3: Phototransduction cascade of the rod cell. Rhodopsin (R), the visual pigment of the rod cell, is localized specifically to a distinct portion of the cell, the outer segment. Photon absorption by the chromophore leads to its isomerization to the all-*trans*-configuration along with accompanying changes in the protein moiety to generate the active form of the receptor R*. R* is catalytically active, binding and activating a G-protein (transducin, T). In turn, T* activates the membrane-associated phosphodiesterase (PDE). Cation channels are gated by cGMP and control the influx of ions across photoreceptor plasma membranes. The hydrolysis of cGMP by PDE changes the cGMP-gated channel conformation and channels closure. Channel closure decreases the conductance of the plasma membrane to cations, resulting in hyperpolarization of the plasma membrane, inhibition of neurotransmitter release, and subsequent signaling to adjacent neurons. Ca^{2+} regulates guanylyl cyclase (GC), the enzyme that catalyzes the conversion of GTP to cGMP during dark state recovery. In the dark, the concentration of Ca^{2+} is high, and GC activity is low. Following photoactivation, channels the plasma membrane close, which reduces the influx of cations. However, the cell's $\text{Na}^+/\text{Ca}^{2+}\text{-K}^+$ exchanger continues to extrude Ca^{2+} , which causes Ca^{2+} levels to decrease. This drop causes the activation of GCs to produce cGMP and specific Ca^{2+} binding proteins – guanylate cyclase activating proteins (GCAPs), further regulating GCs activity. Figure taken from (13).

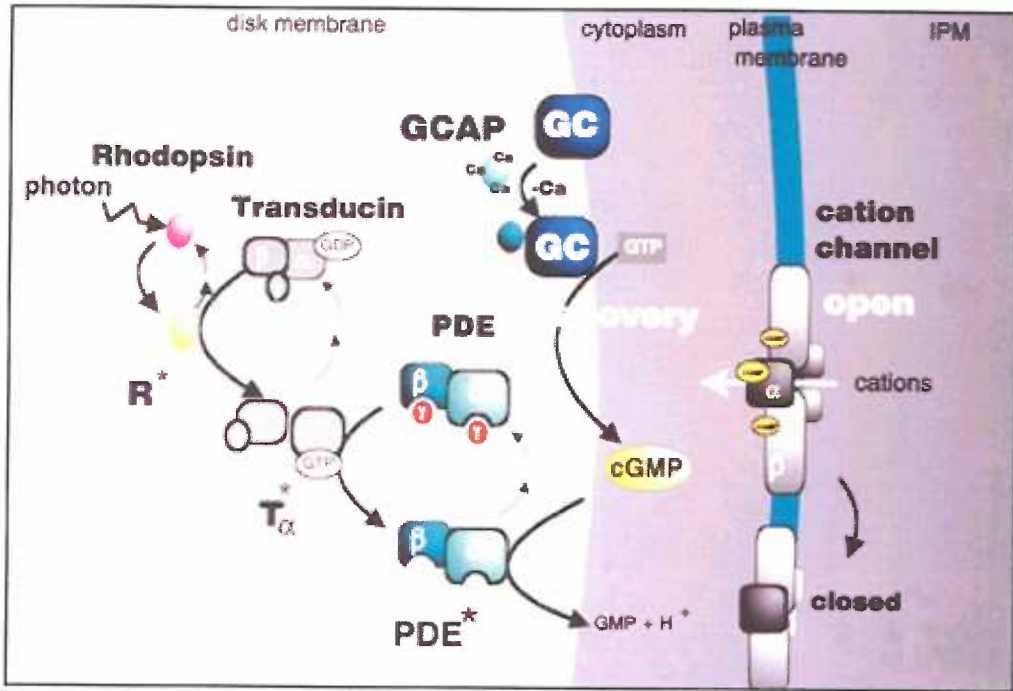
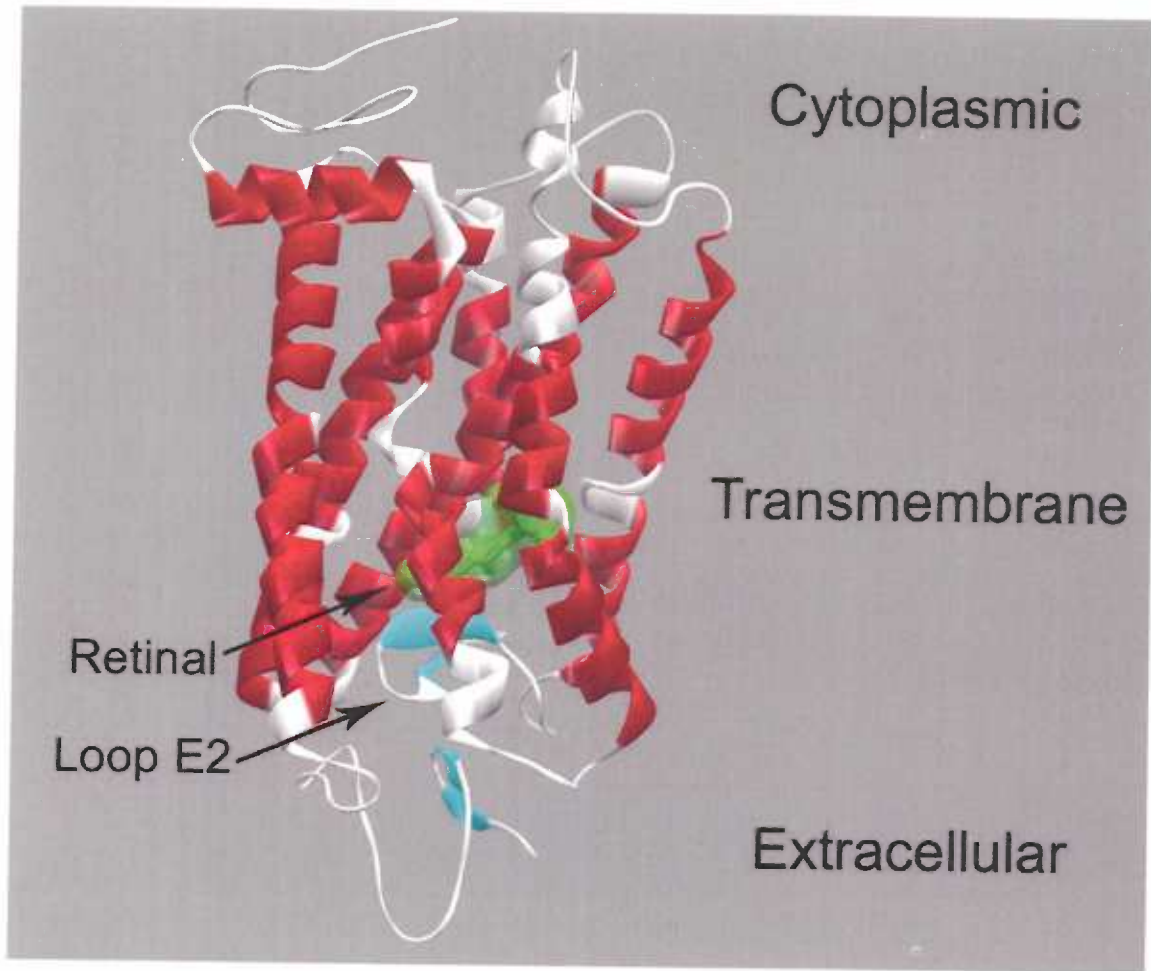


Figure 1. 4: 11-*cis*-retinal is recycled through the enzymatic processing of the retinoid cycle. Rhodopsin sits at the interface between the rhodopsin, visual signaling and retinoid cycles. Absorption of photons by dark state rhodopsin (retinal in the 11-*cis* form; Rho, red) activates the receptor (retinal in the all-*trans* form; Rho*, blue) and initiates the visual signal transduction cycle (purple). Further details regarding the signaling cycle are presented in Figure 1. 3. Following signaling Rho* is phosphorylated by rhodopsin kinase (RK), and bound by the protein arrestin (Arr). The all-*trans*-retinal (ATR-al) is released from rhodopsin following hydrolysis of the retinal Schiff base linkage. The released ATR then enters the retinoid cycle for regeneration of 11-*cis*-retinal. ATR-al is reduced to all-*trans*-retinol (ATR-ol) by the enzyme retinol dehydrogenase (RDH). ATR-al is supplied to RDH by the efforts of the ATP-driven photoreceptor specific ABC binding cassette transporter (ABCR), which rapidly removes ATR-al from the intradiscal space. During the retinoid cycle ATR-ol moves through the interphotoreceptor matrix space (IPM) to the retinal pigment epithelium (RPE) in a process mediated by the interphotoreceptor retinal binding protein (IPBP). ATR-ol is subsequently converted to 11-*cis*-retinal within the IPM through a complex process, which to date is not fully worked out. ATR-ol is possibly esterified by lecithin:retinol acyl-transferase (LRAT), it is then thought to be isomerized to the 11-*cis* form by a yet to be identified isomerohydrolase. Thus converted, 11-*cis*-retinol is oxidized to 11-*cis*-retinal by 11-*cis*-retinol dehydrogenase (11-*cis*-RDH). Finally, 11-*cis*-retinal moves to the rod photoreceptors via diffusion, or transport via IRBPs, for regeneration of dark state rhodopsin. Figure adapted from 45.

Figure 1. 5: Three-dimensional structural model of rhodopsin in the dark state and a schematic showing the residues within 4.5 Å distance from retinal chromophore.

(A) Ribbon model of the dark state rhodopsin crystal structure. The model illustrates the location of the cytoplasmic, transmembrane and extracellular domains relative to each other. The retinal chromophore is shown in green residing within the TM helical bundle and attached to K296 via a protonated Schiff base linkage. The location of extracellular loop E-2, which makes contacts with the retinal, is also denoted. The structural shape of the extracellular domain has been termed the “retinal plug”. The model was generated using the program WebLab based on the rhodopsin crystal structure coordinates (PDB # 1L9H (54)). (B) Schematic diagram of the rhodopsin retinal binding pocket representing residues within 4.5 Å distance to the retinal chromophore. The light blue lines and numbers denote the distances between the Schiff base nitrogen atom and charged or polar atoms that are within 4.5 Å. Figure 1. 5B taken from (52).

(A)



(B)

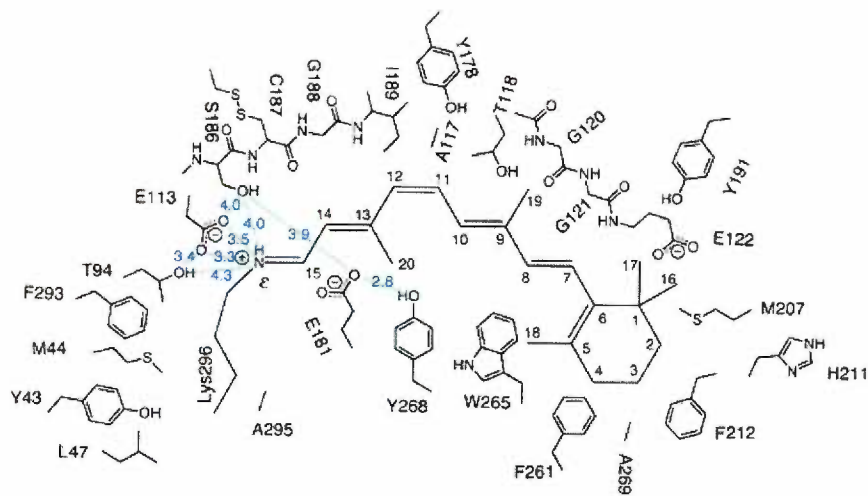


Figure 1. 6: Monitoring rhodopsin signaling states by absorption spectroscopy.

Spectra shown are for purified WT rhodopsin under standard buffer conditions (0.05% DM, 5 mM MES pH 6.0, at 20 °C). WT rhodopsin in the dark state (DS, red) exhibits a visible λ_{\max} at 500 nm corresponding to the chromophore and a UV λ_{\max} at 280 nm corresponding to the opsin protein. Properly folded purified rhodopsin that has fully bound 11-cis-retinal typically exhibits a $\lambda_{280}/\lambda_{500}$ ratio of 1.6 to 1.8. Upon photobleaching with > 495 nm light the λ_{\max} shifts to 380 nm, which is characteristic of the unprotonated active MII intermediate (+ hv, blue). The presence of an intact retinal Schiff base linkage in the MII state may be confirmed by acid denaturation of the protein to pH 1.9, which results in curve with a λ_{\max} 440 nm – characteristic of an intact retinal protonated Schiff base linkage (PSB, black).

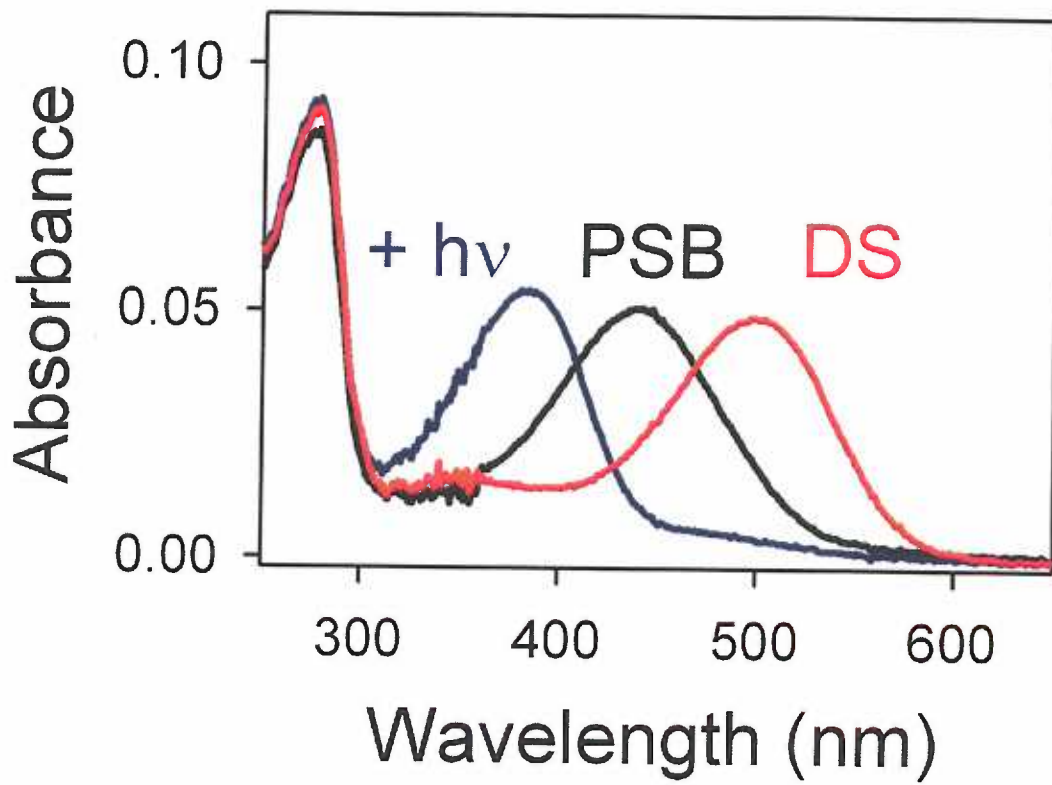


Figure 1. 7: (A) Rhodopsin photocycle indicating spectroscopically detected photointermediates. Photoisomerization of the 11-*cis* double bond occurs on a femtosecond time scale and yields the photoproduct photorhodopsin with a highly distorted 11-*trans* bond. Thermal relaxation and progressive release of the strain in the chromophore results in transition through the short-lived bathorhodopsin, blue-shifted intermediate (BSI) and lumirhodopsin intermediate species leading to the MI state. Up to the MI state the retinal Schiff base is still protonated, possibly due to the low pK_a of the stabilizing counter ion E113. Significant conformational changes in the protein accompany the transition to the active MII state, which is in equilibrium with its predecessor MI. The MII state represents the agonist-bound active conformation of the receptor capable of interaction with the G-protein transducin. Transition to the MII state is facilitated by retinal in its all-*trans* conformation, which allows efficient proton transfer to the counter ion. This proton transfer from the Schiff base to the counter ion results in a large blue-shifted value in the λ_{max} (380 nm). MII decays into the apoprotein opsin and all-*trans*-retinal as a result of irreversible hydrolysis of the Schiff base linkage. Released all-*trans*-retinal is reduced to retinol by retinol dehydrogenase and transported out of the photoreceptor cell to the adjacent retinal pigment epithelial cells, where it is enzymatically converted into 11-*cis*-retinal via the retinoid cycle. Decay of the Metarhodopsin intermediates are further detailed in Figure 1. 8. Figure adapted from (33).

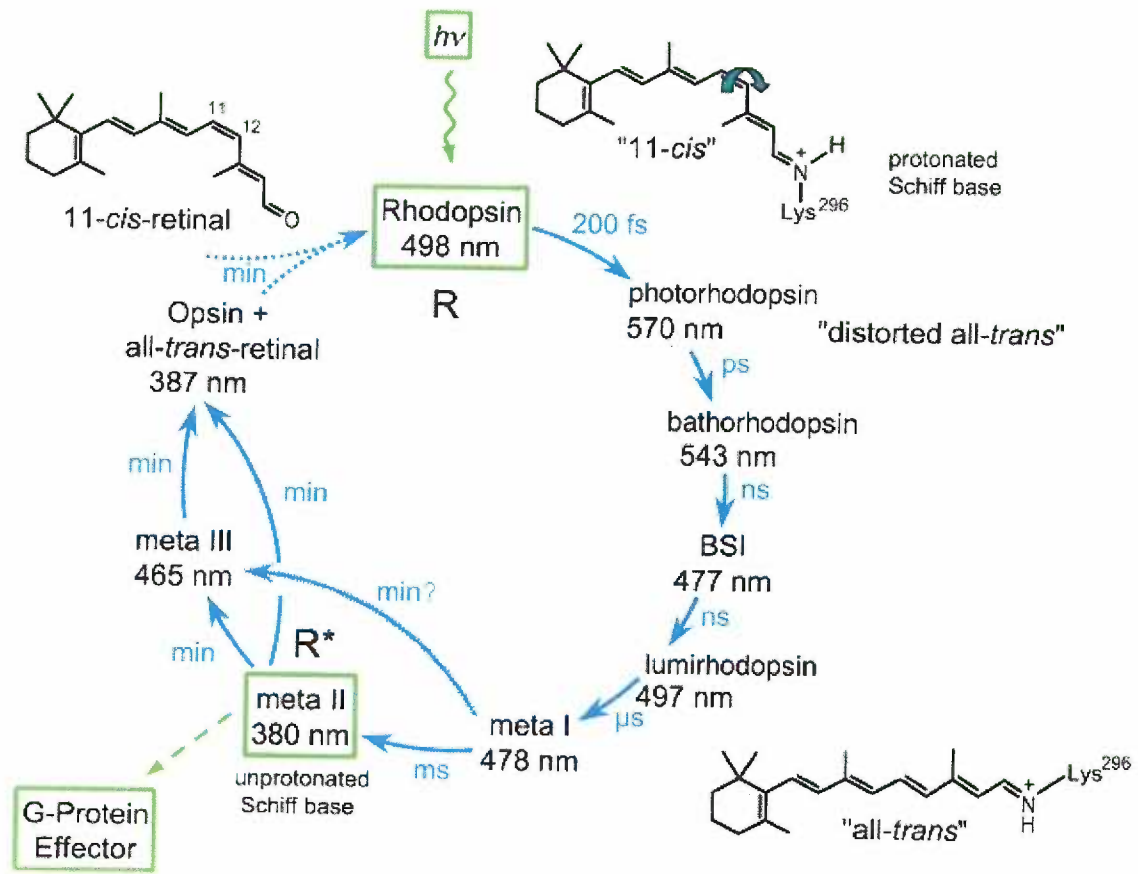


Figure 1. 8: Decay of Metarhodopsin photointermediates. Light activation of rhodopsin results in the rapid formation of an equilibrium mixture of the MI and active MII photointermediates. The MII intermediate decays directly to opsin and all-*trans*-retinal by hydrolysis of the retinal Schiff base linkage. The MIII photointermediate is thought to arise from an additional thermal isomerization of the chromophore C=N bond in the MI state, which results in an all-*trans*-15-*syn*-retinal conformation. The MIII intermediate may then decay via a back reaction into the MI/MII pool, or decay directly via slow hydrolysis of its retinal Schiff base linkage. Figure taken from (125).

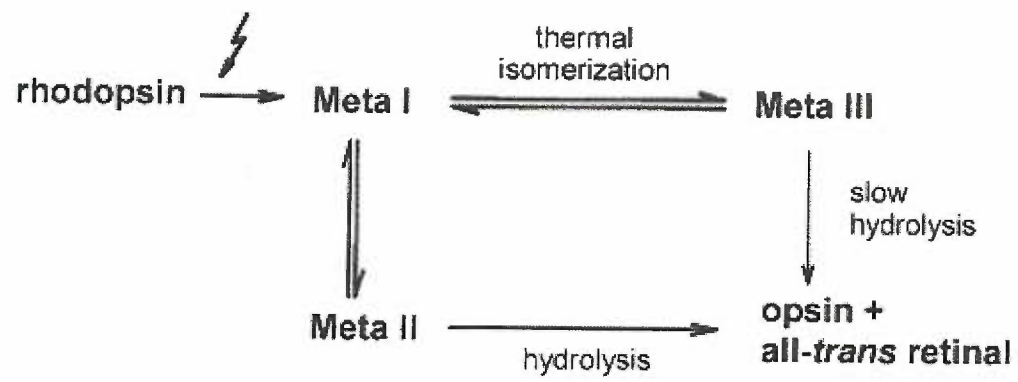
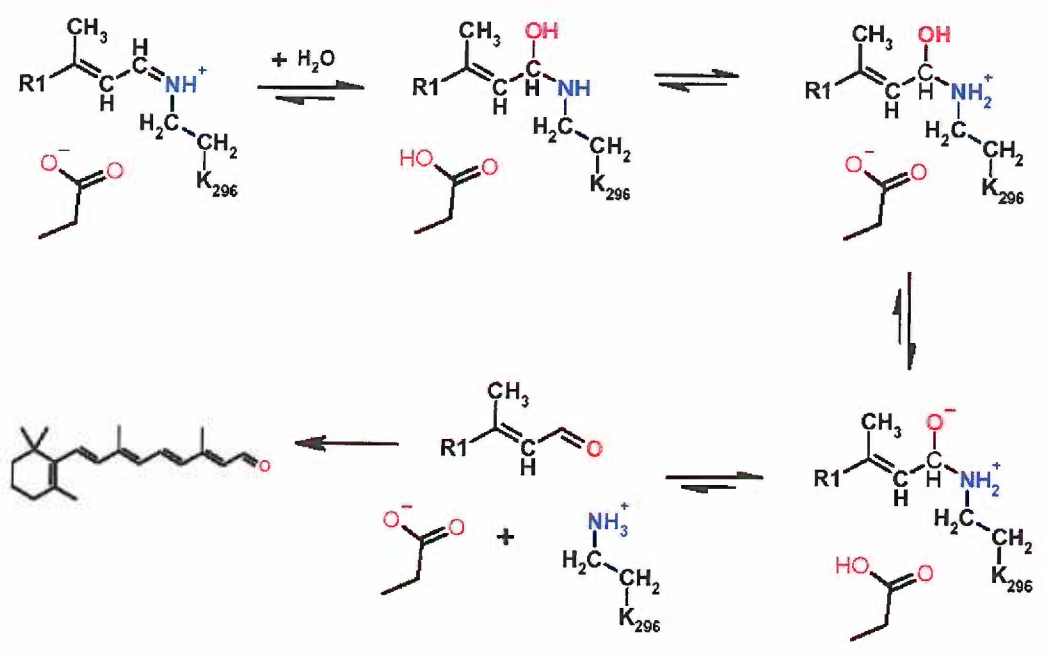


Figure 1. 9: Proposed mechanism of retinal Schiff base hydrolysis in rhodopsin. In this model, retinal Schiff base hydrolysis is initiated by the attack of a water molecule which is base catalyzed by a proximal negative point charge. This attack results in the formation of a carbinolamine intermediate, which is next protonated from the solvent. Following this event, the carbinol species is deprotonated, presumably by proton transfer to a neighboring amino acid side chain. The linkage subsequently breaks and gives rise to all-*trans*-retinal aldehyde held in place by noncovalent interactions within the opsin-binding pocket. However, this noncovalent complex is unstable presumably due to steric interference between opsin and the *trans* geometry of the retinal moiety. As such, the all-*trans*-retinal dissociates from the opsin-binding pocket to be recycled via the retinoid cycle leaving empty opsin. With the exception of the last event – retinal release, all steps in this hydrolysis pathway are reversible.



Chapter 2

Engineering a Functional Blue-Wavelength Shifted Rhodopsin Mutant.

Jay M. Janz[§] and David L. Farrens[§]

[§]Department of Biochemistry and Molecular Biology,

Oregon Health and Science University

3181 S. W. Sam Jackson Park Drive, Portland, Oregon 97239-3098

Running Title: Functional Blue-Wavelength Shifted Rhodopsin Mutants.

2. 1: SUMMARY

We report an effort to engineer a functional, maximally blue-wavelength shifted version of rhodopsin. To achieve this goal we first constructed and assayed a number of previously described mutations in the retinal binding pocket of rhodopsin, G90S, E122D, A292S and A295S. Of these mutants, we found that only mutants E122D and A2992S were wild type like. In contrast, mutant G90S showed a perturbed photobleaching spectrum, and mutant A295S showed decreased ability to activate transducin. We also identified and characterized a new blue-wavelength shifting mutation (at site T118); a residue conserved in most opsin proteins. Interestingly, although residue T118 contacts the critically important C₉-methyl group of the retinal chromophore, the T118A mutant exhibited no significant perturbation other than the blue-wavelength shift. In analyzing these mutants, we found that although several mutants showed different rates of retinal release, the activation energies of the retinal release were all ~ 20 kcal/mol, almost identical to the value found for WT rhodopsin. These latter results support the theory that chemical hydrolysis of the Schiff base is the rate-limiting step of the retinal release pathway. A combination of the functional blue-wavelength shifting mutations was then used to generate a triple mutant (T118A/E122D/A292S), which showed a large blue-wavelength shift (absorption $\lambda_{\max} = 453$ nm) while exhibiting minimal functional perturbation. Mutant T118A/E122D/A292S thus offers the possibility of a rhodopsin protein that can be worked with and studied using more ambient lighting conditions.

This chapter illustrates that Arrhenius analysis may be utilized to study the kinetics and energetics of retinal Schiff base hydrolysis and release in rhodopsin mutants, a technique used extensively in subsequent chapters of this thesis. We find that

mutations G90S, E112D and A295S all affect the stability of the MII signaling intermediate. Finally, through the characterization of new mutants T118A and I189A we provide experimental evidence that cast serious doubt on the currently accepted “steric trigger” hypothesis of photoreceptor activation.

All experiments reported in this chapter were performed by the author of this dissertation and the manuscript portion of this chapter is published in Janz, J. M., and Farrens, D. L. (2001) *Biochemistry* **40**, 7219-7227.

2. 2: INTRODUCTION

Trichromatic color vision is mediated by three types of cone cells, which contain opsin pigments that absorb maximally at three different wavelengths: blue (414 nm), green (533 nm) and red (560 nm) (99), (133), (134). In contrast, dim light vision is mediated by the rod photoreceptor rhodopsin that absorbs maximally at 500 nm. Rhodopsin is the only G-protein-coupled receptor (GPCR) with a crystal structure and is arguably the best-characterized member of this large and important family of sensory proteins (for reviews see (135), (136), (27)). All of these visual pigments are thought to share a similar, general structure of 7 TM helices (with a chromophore, 11-*cis*-retinal, attached to a lysine residue) (137), (132). The resulting color absorption by the different opsins is due to “spectral tuning” (i.e., controlling the λ_{max} of rhodopsin) through interactions of amino acids lining the chromophore binding pocket with the protonated Schiff base (PSB) (138), (96).

The mechanism of spectral tuning in opsin proteins is being elucidated by the efforts of several laboratories through a combination of mutagenesis, absorption

spectroscopy and Raman spectroscopy techniques (139-145). One of these studies has shown that substitutions of nine rhodopsin amino acids can account for ~ 80 % of the opsin shift between the blue cone pigment and rhodopsin (96), and suggested that a blue-wavelength shift may be induced by dipolar substitutions through long range electrostatic effects on the change in dipole moment of the photoexcited chromophore (96). However, complementary experiments carried out on the human blue cone pigment indicate that although mutagenesis studies on bovine rhodopsin serve well as predictive models of spectral tuning near the ring portion of the retinal, mutations near the Schiff base do not (99). In general, although these informative studies have gone far to shed light on understanding the process of spectral tuning, little work investigating the functional effects of introducing blue-wavelength shifting mutations into bovine rhodopsin has been carried out.

The goal of the present chapter is to use some of the previously identified blue-wavelength shifting mutations to engineer a maximally blue-wavelength shifted rhodopsin that retains functionality, i.e., normal stability of the MII state and ability to activate the G-protein transducin. In the process of these studies we also identified and characterized a new blue-wavelength shifting mutation at site T118, a residue conserved in most opsin proteins and found to be in contact with the C₉-methyl group of the retinal chromophore (52). In addition, while characterizing these mutants we found evidence supporting the conclusion that the rate-limiting step in retinal release is the chemical event of Schiff base hydrolysis.

2. 3: MATERIALS and METHODS

2. 3. 1: Materials.

All buffers and chemicals were purchased from either Fisher or Sigma except where noted below. Protease inhibitor cocktail tablets and GTP γ S were purchased from Boehringer Mannheim. Dodecyl maltoside (DM) was purchased from Anatrace (Maumee, OH), GBX red filters from Eastman Kodak Corp. Polystyrene columns (2-ml bed volume) were purchased from Pierce. Frozen bovine retinas were from J.A. Lawson Co. (Lincoln, NE). Transducin was purified from rod outer segments as previously described (146). Restriction endonucleases were from New England Biolabs (Beverly, MA). 11-*cis*-retinal was a generous gift from Dr. R. Crouch (Medical University of South Carolina and the National Eye Institute). The 1D4 antibody was purchased from the National Cell Culture Center (Minneapolis, MN). The nonapeptide corresponding to the C-terminus of rhodopsin was acquired from the Emory University Microchemical Facility (Atlanta, GA). Cuvettes were purchased from Uvonics (Plainview, NY). Band pass filters and long pass filters were purchased from Oriel (Stratford, CT).

2. 3. 2: Buffers.

The definitions of the buffers used in this chapter are as follows: PBSSC (0.137 M NaCl, 2.7 mM KCl, 1.5 mM KH₂PO₄, 8 mM Na₂HPO₄ (pH 7.2)), Buffer A (5 mM Tris-HCL, 2 mM EDTA, (pH7.4)), Buffer B (1% DM, PBSSC (pH 7.2)), Buffer C (2 mM ATP, 0.1% DM, 1 M NaCl, 2 mM MgCl₂ (pH 7.2)), Buffer D (0.05% DM, PBSSC (pH 7.0)), and Buffer E (0.05% DM, MES (pH 6.0)).

2. 3. 3: Construction and expression of rhodopsin mutants.

Site-directed mutagenesis was performed as described previously in the PMT4 plasmid (147), (148). Specifically, mutant T118A was generated by replacement of the fragment *XhoI* – *PvuI* in the synthetic Bovine rhodopsin gene with synthetic oligonucleotide duplexes containing the corresponding sequence GCC for ACC to generate T118A. Mutants A292S and A295S were generated in a similar manner by replacing the fragment *Apal* – *AatII* containing the corresponding sequence TCT for GCT at each site, respectively. Overlap extension PCR was used to generate *EcoRI* and *NotI* fragments containing either the G90S or the E122D mutation (149). The sequences for the primers were as follows: 5'GTCTTCGGTTTCGTTCACCACCACCCTC3' for G90S, and 5'GGGCGGTGACATTGCACTGTGGTCTCT3' for E122D. These PCR fragments were then subcloned into PMT4 using *BclI* – *XhoI* restriction sites for G90S, and *XhoI* – *SfiI* for E122D, respectively. All mutations were confirmed by the dideoxynucleotide sequencing method. The mutant rhodopsin proteins were transiently expressed in COS-1 cells using the DEAE-dextran method and cells were harvested 52-56 hours after transfection (150), (114).

2. 3. 4: Purification of rhodopsin mutants.

Prior to mutant purification the cell membranes were prepared as follows. Briefly, five 15-cm plates of transfected COS-1 cells were washed twice with 7 ml of cold PBSSC buffer, pelleted and subsequently lysed in 10 ml of cold Buffer A containing 0.5 mM (PMSF) in the presence of protease inhibitors. Cells were subsequently vortexed and spun at 45,000 X g to pellet cell membranes. The remaining steps in the procedure were in dark room conditions under filtered red light. The membranes were resuspended

in 10 ml of cold PBSSC (pH 6.5) and regenerated with 11-*cis*-retinal (10 μ l of 10 mM stock) at 4 °C for one hour as previously described (151), then an additional 5 μ l of 11-*cis*-retinal was added and regeneration allowed to proceed for an additional hour. The purification of the rhodopsin mutants proceeded essentially as the original procedure (150) except small polystyrene columns were used (116). Rhodopsin containing membranes were solubilized in 5 ml of buffer B containing 0.5 mM PMSF at 4°C for 1 h, then centrifuged at 45,000 X g. The supernatant was mixed with 200 μ l of 1D4 antibody-Sepharose beads (binding capacity ~ 1 μ g of rhodopsin/ μ g resin) in buffer C containing 0.5 mM PMSF and nutated at 4 °C for 4 - 5 h. The slurry was subsequently transferred to polystyrene columns and washed once with 50-ml buffer D followed by a 40 ml wash with buffer E by gravity filtration. During the last 5 ml of the second wash a 27 gauge 0.5-inch needle was attached to the column to decrease the flow rate. Samples were eluted in 300 μ l fractions of buffer E containing 200- μ M nonapeptide corresponding to the 1D4 antibody epitope (the last nine amino acids of the C-terminus of rhodopsin). A spectrum of each elution fraction was measured using a Shimadzu UV-1601 spectrophotometer (described below) and the purified samples were snap frozen in liquid N₂ and stored at – 80 °C.

2. 3. 5: UV/vis absorption spectroscopy.

All UV/vis absorption spectra were recorded with a Shimadzu UV-1601 spectrophotometer at 20 °C using a 2 nm bandwidth, 1 s response time, and a scan speed of 240 nm/min unless otherwise noted. For calculations, a molar extinction coefficient value (λ_{500}) for WT rhodopsin was taken to be 40,600 M⁻¹ cm⁻¹ (73). The samples were photobleached in buffer E by illuminating for 30 s (at a 6 Hz flash rate) with a Machine

Vision Strobe light source (EG&G) equipped with a wavelength > 490 nm long pass filter. This light treatment was found to be adequate for full conversion of samples, as 5 s was sufficient for full bleaching of WT rhodopsin. The blue-wavelength shifted mutants were bleached using a wavelength > 470 nm long pass filter to ensure full bleaching. The presence of a PSB in the MII state for each mutant was determined by adding H₂SO₄ to a pH of 1.9 and immediately following photobleaching measuring the absorbance spectrum (within 1 min) to look for the presence of a spectral species at 440 nm (representative of a PSB linkage that is present in the acid) (152). Rhodopsin mutants that exhibited abnormal bleaching behavior were studied further as a function of time after irradiation as described previously (153). Extinction coefficients were determined as previously described in buffer E at 15 °C (69).

2. 3. 6: Measurement of retinal release/MII decay by fluorescence spectroscopy.

The MII stability was assessed by measuring the time course of retinal release after MII on a Photon Technologies QM-1 steady state fluorescence spectrophotometer (154). Each measurement was carried out using 80 µl of a 0.25 µM mutant sample in buffer E and the sample temperatures were maintained using a water jacketed cuvette holder. After photobleaching the samples to the MII state (see above) the retinal release measurements were carried out at the appropriate temperature by exciting the sample for 3 s (excitation wavelength = 295 nm, ¼-nm bandwidth slit setting) then blocking the excitation beam for 42 s, to avoid photobleaching the samples. Tryptophan fluorescence emission was monitored at 330 nm (12-nm bandwidth slit setting), and this cycle was repeated for 90 min during each measurement. Results were analyzed manually to determine the $t_{1/2}$ values. Series of MII decay rates were obtained at 13, 20, 27, and 33

°C, and the rates applied to the Arrhenius equation $k = Ae^{-E_a/RT}$ to determine the activation energy (E_a) of each mutant rhodopsin.

2. 3. 7: Determination of transducin (G_T) activation rates.

Activation of G_T by rhodopsin was monitored using fluorescence spectroscopy at 20 °C as described previously (148), (155), (156). The excitation wavelength was 295 nm, (2-nm bandwidth), and fluorescence emission wavelength was monitored at 340 nm (12 nm bandwidth). G_T was added (final concentration of 250 nM) to the reaction mixture containing 10 mM Tris (pH 7.2), 2 mM $MgCl_2$, 100 mM NaCl, 1 mM DTT, and 0.01 % DM. The solution was stirred for 300 s to establish a baseline. Photobleached mutant rhodopsin (see above) was then added to the mixture to a final concentration of 5 nM, and allowed to stir 300 s to equilibrate. $GTP\gamma S$ was added to the reaction mixture to a final concentration of 5 μM , and the increase in fluorescence was followed for an additional 2000 s. To calculate the activation rates, the slopes of the initial fluorescence increase after $GTP\gamma S$ addition were determined through the data points covering the first 60 s.

2. 4: RESULTS

2. 4. 1: Sites selected for mutagenesis in bovine rhodopsin.

Amino acids G90, E122, A292, and A295 were selected for mutagenesis based on previous work indicating that substitutions at these sites confer a blue-shift (60, 96, 155, 157, 158), . While other blue-wavelength shift mutants have been previously reported (for example W265 and F268) we did not pursue mutations of these residues because substitutions at these sites either perturbs the ability of opsin to bind retinal or results in a

nonfunctional mutant pigment (60), (159). The rationale for studying the amino acids we chose is as follows: A serine residue at the equivalent of position 292 causes the blue-wavelength shift in the dolphin long-wavelength sensitive cone photopigment (158). Mutations G90S, E122D, and A295S were previously observed to confer blue shifts in λ_{\max} when introduced into bovine rhodopsin, (96), (60). We investigated a previously unidentified site, position T118, because it is conserved in most opsins and is located approximately one turn above the counter-ion (E113) and thus might be expected to perturb the location of the counter-ion, resulting in a blue-wavelength shift (95). The locations of these residues relative to 11-*cis*-retinal are shown in Figure 2. 1.

2. 4. 2: Spectral characterization of rhodopsin mutants.

In general, yields of purified mutant protein were comparable to WT rhodopsin ($\sim 10 \mu\text{g}/15 \text{ cm}$ plate). All mutants formed characteristic rhodopsin-like chromophores after purification with spectral ratios ($A_{280}/A(\lambda_{\max})$) between 1.6 and 1.8 (Figure 2. 2). All of the mutants (except G90S) exhibited normal bleaching behavior with respect to formation of a λ_{\max} 380-nm species, characteristic of the MII intermediate (137). Acidification of these photobleached samples generated a λ_{\max} 440-nm species, indicating the presence of a protonated retinal Schiff base (152). An example of normal photobleaching behavior is shown for mutant T118A (Figure 2. 3A), and these results are compiled in Table 2. 1. In contrast, mutant G90S, while being capable of forming both a MII species and a PSB, exhibited abnormal bleaching behavior (Figure 2. 3B). Following illumination, a residual species with a $\lambda_{\max} \sim 480 \text{ nm}$ persisted in the G90S mutant. This species was followed as a function of time after irradiation, and even 10 h after illumination a residual amount of $\lambda_{\max} \sim 480 \text{ nm}$ species could be detected (Figure

2. 3B). To test whether this ~ 480 nm species is representative of the MI photointermediate, bleaching was performed in the presence of transducin. Transducin binding should shift the MI/MII equilibrium to the MII state (160-162). The presence of transducin (1 μ M) was observed to have no effect on G90S bleaching behavior (data not shown), suggesting the ~ 480 nm species in G90S is not a normal MI like photoproduct.

2. 4. 3: Retinal release rates of wavelength shifted single mutants.

The rate of retinal release from the MII state was measured using a fluorescence based assay (154) at 20 °C. Under the conditions used for bleaching, the $t_{1/2}$ for retinal release for WT rhodopsin buffer E was 15 min. The corresponding $t_{1/2}$ values for the wavelength-shifted single mutants ranged from 4.8 to 26 min (Table 2. 1). Only mutant A295S showed a strikingly accelerated retinal release rate ($t_{1/2} = 4.8$ min). In contrast, mutant E112D exhibited a slower rate of retinal release ($t_{1/2} = 26$ min). The observed twofold decrease in retinal release for E122D relative to WT is in agreement with the slowed MII decay rate for this mutant obtained by low-temperature time-resolved spectroscopy (163). The values for each of the mutants are compiled in Table 2. 1.

2. 4. 4: Transducin activation by wavelength shifted mutants.

The blue-wavelength shifted mutants were next tested for their ability to activate transducin using a fluorescence based assay which measures the increase in tryptophan fluorescence of the $G_{T\alpha}$ -GTP γ S species (156), (164). The results are shown in Figure 2. 4B as initial rates of fluorescence increase relative to WT rhodopsin. An example representative of data collected is shown in Figure 2. 4A. Mutants G90S, T118A, E122D, and A292S show rates of fluorescence increase that are similar to that of WT

rhodopsin. Mutant A295S was much less able to activate transducin as judged from its initial rate of fluorescence increase. These results are summarized in Table 2. 2.

2. 4. 5: Activation energy for Meta II decay measured by fluorescence increase.

The rate of fluorescence increase from photobleached WT rhodopsin and blue-wavelength shifted mutants was measured in buffer E at four different temperatures (13, 20, 27 and 33 °C). The rate of fluorescent increase in all cases was temperature-dependent, and Arrhenius plots of these measurements indicate a temperature dependent linear relationship for all mutants (Figure 2. 5). From these plots an activation energy (E_a) of 20.1 kcal/mol was obtained for WT rhodopsin, in good agreement with the previous reported value of 20.2 kcal/mol (154). Interestingly, although several of the blue-wavelength shifted mutants showed different rates of retinal release (see Table 2. 1), an Arrhenius plot of the retinal release rates measured at different temperatures showed nearly E_a values for the mutants (Figure 2. 5, Table 2. 2). For example, mutants G90S, T118A, and A292S had retinal release rates slightly faster than that of WT at any given temperature, yet the Arrhenius plot of these measurements yielded E_a values that were very similar for each (Table 2. 2). The most extreme difference in retinal release rates were found for mutant A295S (exhibited a 3 fold increased rate in retinal release; 4.5 min) and mutant E122D (exhibited a ~ 2 fold decreased rate in retinal release; 26 min).

2. 4. 6: Construction of a substantially blue-wavelength shifted mutant with minimal spectral perturbation.

The spectral characterization of rhodopsin blue-wavelength shifted point mutants indicated two of the mutations (G90S and A295S) are structurally and/or functionally perturbing when introduced into bovine rhodopsin (see Figures 2. 3B, 2. 4B, Table 2. 1

and Table 2. 2). G90S exhibits abnormal photobleaching properties, whereas, mutant A295S exhibits an accelerated MII decay rate, suggesting it is not stable. In contrast, the other three blue-wavelength shifted mutants (T118A, E122D, and A292S) exhibit wild type like behavior, and thus were subsequently combined into a single mutant and further characterized, described below.

2. 4. 7: Spectral characterization of mutant T118A/E122D/A292S.

The triple point mutant T118A/E122D/A292S expressed at levels similar to WT (~ 10 µg/15 cm plate) and formed a rhodopsin-like chromophore with a spectral ratio ($A_{280}/A(\lambda_{\max})$) of 1.7 (Table 2. 3). Mutant T118A/E122D/A292S exhibits a 47-nm blue shift relative to WT rhodopsin with a λ_{\max} at 453 nm (Table 2. 3 and Figure 2. 6). The slight narrowing of the spectral curve can be attributed to the E122D mutation (60). The effects that individual mutations have upon λ_{\max} of the pigment appears to be additive (Table 2. 1 and Table 2. 3). Photobleaching analysis indicates that the engineered opsin is capable of forming a MII species (λ_{\max} 380 nm), and upon acidification forms a PSB (λ_{\max} 440 nm) (Figure 2. 6A). The retinal release rate of the engineered opsin exhibits a $t_{1/2}$ value of 11.1 min. The spectral characteristics of T118A/E122D/A292S are compiled in Table 2. 3. Additionally, T118A/E122D/A292S is functionally active. The engineered opsin is able to activate transducin with a relative initial rate of activation ~ 50 % of WT rhodopsin (Table 2. 3).

2. 5: DISCUSSION

In this chapter we systematically investigated the structural and functional consequences of introducing blue wavelength shifting mutations into the retinal binding

pocket of bovine rhodopsin. Our goal was to develop a mutant rhodopsin that exhibits maximal blue-wavelength shift yet remains stable in terms of structure and function for future use in biophysical studies. To achieve this goal, we engineered a series of five point mutations based on their ability to confer a blue-wavelength shift. Amino acids at positions 90, 122, 292, and 295 were chosen for mutation since these residues had been shown in earlier studies to affect the λ_{\max} of the mutant pigment (96), (155), (157), (60). In our hands, all of these mutants showed expression levels similar to WT rhodopsin, ($\sim 10 \mu\text{g}/15 \text{ cm plate}$) and could be purified to homogeneity forming rhodopsin-like chromophores, with spectral ratios ($A_{280}/A(\lambda_{\max})$) between 1.6 and 1.8 (Figure 2. 2, Table 2. 1). In the present work we also characterize a mutation at a new position, T118, where a threonine exists in almost all known opsin proteins. We find that a T118A mutation affects the λ_{\max} of the mutant pigment (Figure 2. 3A). The effects of the various wavelength shifting mutations are discussed further below.

2. 5. 1: Photobleaching behavior of blue-wavelength shifted mutants.

All of the blue-wavelength shifted mutants exhibited normal photobleaching behavior (for example see Figure 2. 3A), except for mutant G90S, which showed a slow decaying species at $\sim 480 \text{ nm}$ (Figure 2. 3B). Note also that a mutation at G90 (G90D) previously has been shown to exhibit abnormalities in photobleaching behavior (157), (165). Since the λ_{\max} of the residual decay species is $\sim 480 \text{ nm}$ it is possible that this mutation disrupts the MI/MII equilibrium (166). To see if the species represents a transient MI like species we bleached it in the presence of transducin ($1 \mu\text{M}$), but no absorbance shift was observed, arguing against the residual $\sim 480 \text{ nm}$ species being a transitional MI intermediate (data not shown). Because the G90S mutant is capable of

activating transducin upon light activation (see Figure 2 .4B), and forms a PSB upon acidification (data not shown) we surmise that the ~ 480 nm species represents an active, MII-like intermediate containing a PSB, as was suggested for the mutant G90D (157), (165). Additionally, G90S exhibits a slightly faster rate of retinal release compared to WT (~ 50 % faster, Table 2. 1) but not as fast as that reported for G90D which, (by a different assay), was found to have a PSB decay rate ~ 75 % that of WT (165).

Interestingly, the recent crystal structure of WT rhodopsin models the G90 residue more than 4.5 \AA away from the Schiff base attachment site (52), too far away for direct hydrogen bonding interactions. This fact suggests other factors contribute to the mechanism of wavelength shifting by mutations at the G90 site. One possibility is that mutations at this site disrupt bridging water molecules, which could also account for the perturbed photobleaching and activation properties exhibited by this mutant. Indeed, previous results investigating mechanisms of spectral tuning in the human blue cone pigment have shown that although substitutions in the ring portion of the retinal binding pocket of bovine rhodopsin can be predictive based on the analogous residues in the human blue cone pigment, mutations near the Schiff base are not necessarily complementary (99).

2. 5. 2: Transducin activation.

With the exception of mutant A295S, most of the mutants tested were able to activate transducin with initial rates similar to WT (Figure 2. 4B). The fact that mutant T118A was able to activate transducin so well was surprising: the recent crystal structure of bovine rhodopsin reveals that this site is found to contact the C₉-methyl group of the retinal chromophore (52). The local steric interaction between the retinal C₉-methyl with

amino acids in the chromophore-binding pocket has led to the “steric trigger” model of rhodopsin activation (122). Experimental support for this model demonstrates that regeneration of opsin with a 9-demethyl-retinal analogue results in reduced ability of the artificial pigment to activate transducin (167). Furthermore, the C₉-methyl group is proposed to act as a scaffold for opsin to adjust key donor and acceptor side chains for the proton transfer reactions that stabilize the active signaling state (168), and is thought to impact the MI/MII equilibrium upon photoactivation (166).

Thus, we expected that a T118A mutation might be functionally similar to an artificial pigment regenerated with 9-demethyl-retinal, however this was not observed. To our surprise, while the T118A mutation clearly effects the spectral tuning of the mutant pigment, it essentially conferred no other structural or functional perturbations that we could detect. However, mutations at this site may confer constitutive activity of the receptor in the dark state, and future experiments should address this possibility.

The wavelength shift caused by the T118A mutation may be due to perturbation of the secondary structure of TM helix 3, and potentially causes the repositioning of the E113 counter-ion, or water molecules within the chromophore binding pocket and/or neighboring amino acids, leading to the observed blue-wavelength shift (96), (55), (169). Further it is also possible that the methyl group of the alanine substitutions is sufficient to interact with the C₉-methyl of 11-*cis*-retinal, thus accounting for WT like function, or that water molecules may compensate for the lost OH hydrogen bond interactions as well as fill the steric void caused by the alanine mutation. While we are not sure of the precise mechanism of the blue-shift caused by T118A, future studies using a combination of site-directed mutagenesis at this residue in conjunction with Resonance Raman and/or retinal

analogues may prove helpful in understanding the cause of the blue shift in this region. Our results do not resolve the issue of the role that C₉-methyl group plays in receptor activation, nor the potential roles for amino acids that interact with this important moiety. However, our results suggest that future experiments might incorporate sterically small residues such as glycine or bulky amino acid side chain groups at 118 to test the proposed “steric trigger” mechanism (see Supplementary Material at the end of this chapter). Additionally, a serine substitution at this site may provide insight to the role of the hydroxyl residue at 118 in signal transduction.

Mutant A295S had a 4-fold lower initial rate of transducin activation compared to WT (Figure 2. 4). Our interpretation of this result is as follows: Mutant A295S showed rapid retinal release rates, approximately 3-fold faster at 20 °C than WT (Table 2. 1). During bleaching of the samples (prior to incubation with the transducin mixture in the cuvette) the faster initial retinal release rate of A295S reduces the population that can activate transducin, leading to the decreased rate of transducin activation in the G-protein activation assay. Taking into account the parameters of the assay and the MII decay rate for A295S (4.75 min) we calculate that there is less than half of the active sample present during the assay (data not shown). The rapid A295S MII decay might be due to the fact it is positioned adjacent to the retinal Schiff base attachment site (L296). This may be important because one model of rhodopsin retinal Schiff base hydrolysis involves a tetrahedral carbinolamine intermediate in the MI/MII transition preceding Schiff base hydrolysis (85). Thus it is possible that the serine substitution at A295 acts either to stabilize this intermediate and/or provide general acid catalysis (by activating a water

molecule involved in the attack) to this mechanism. Either scenario would serve to expedite the Schiff base hydrolysis reaction.

2. 5. 3: Thermodynamic parameters and activation energies of retinal release.

The rate limiting step for retinal release from the chromophore binding pocket may be either 1) the chemical process of Schiff base hydrolysis or 2) unfavorable steric interactions between all-*trans*-retinal and amino acids forming the binding pocket (shown in brackets in scheme 2. 1 below).



In the above scheme, rhodopsin forms MII (indicated by presence of PSB) following illumination. The MII state next converts to opsin with all-*trans*-retinal still in the binding pocket. In the final stage (which is irreversible), free retinal leaves the chromophore-binding pocket. Although some of the retinal release rates differ from WT, the largest difference was only a ~ 3 fold rate increase. While we cannot unequivocally rule out the possibility that these residues play a direct role, these finding suggests that none of the residues described in the present work play a direct catalytic role in the Schiff base hydrolysis, (if so, one would have expected the rates to differ 10 to 100 fold or greater). Further, all of the mutants in this study exhibit retinal release E_a values that are quite similar. It is possible that the introduced mutations structurally perturb the protein enough to expedite retinal release (A295S) or slow it down (E122D). The Arrhenius plots of retinal release rates illustrate that the slopes for most of the mutants are similar to WT, while their intercepts differ (Figure 2. 5). We interpret this to mean that the slight structural perturbations that these mutants confer are generally entropic in nature (170).

The exception is E122D which, judged by its slightly different slope, has enthalpic contributions as well. Additionally, since the rates of MII decay (which monitors Schiff base hydrolysis) differ among the various mutants, the E_a values for the overall process of retinal release are relatively similar. This data supports the theory that chemical hydrolysis is the rate limiting step in the retinal release pathway.

2. 5. 4: Functional blue-wavelength shifted mutant.

The information gleaned from the characterization and analysis of the individual blue-wavelength shifting point mutations was used to construct a triple point mutant, T118A/E122D/A292S. In designing this mutant we omitted mutant G90S (because of the perturbed photobleaching properties) and mutant A295S (because of the faster retinal release rate and minimal transducin activation). Our results suggest mutant T118A/E122D/A292S confers a substantial blue-wavelength shift while retaining most of its structural stability and ability to activate transducin (note the normal photobleaching properties (Figure 2. 6A) and ability to activate transducin (Table 2. 3)). We propose mutant T118A/E122D/A292S will be useful in biophysical studies since the 47 nm blue-shift allows the protein to tolerate yellow-orange light (~ 560 nm) at higher intensity than WT, which offer a practical advantage when handling the protein for techniques such as NMR and X-ray crystallography. Additionally, we have begun to use the T118A/E122D/A292S mutant in fluorescent spectroscopic studies. One of the difficulties of using fluorescent probes to study rhodopsin is the amount of spectral overlap of the fluorescent probes' emission with the dark and MII state of rhodopsin. While fluorescent probes that have little spectral overlap with rhodopsin exist, they are all large and bulky, potentially perturbing the protein domains into which they are

introduced. The substantial blue-wavelength shift of mutant T118A/E122D/A292S will facilitate site-directed fluorescence labeling (SDFL) studies of rhodopsin by allowing for the use of small fluorescent probes, such as those previously described (116). Studies of this nature are concurrently under way in our laboratory.

2. 6: ACKNOWLEDGMENTS

The authors wish to thank Dr. J. Denu and Dr. H.P. Bächinger for helpful discussions regarding kinetics and thermodynamic analysis, and T. Dunham, S. Mansoor and Dr. B. Nauert for critical reading of this manuscript.

Table 2. 1: Functional Characterization of Wavelength-shifted Single Point Mutants (Spectral Ratio, Absorption Maxima, Absorption Shift, Extinction Coefficient, $t_{1/2}$ of Retinal Release Rates).

Mutant	$A_{280}/A(\lambda_{\max})$	λ_{\max}	λ -Shift (nm)	ϵ ($M^{-1}\cdot\text{cm}^{-1}$) ^a	MII decay $T_{1/2}$ (min) ^b
WT	1.8	500	-	40,600 ^c	15
G90S	1.8	487 ^d	13	39,000	10.3
T118A	1.8	484	16	41,000	10.6
E122D	1.6	477 ^e	23	45,000 ^f	26
A292S	1.7	489.5 ^d	9.5	40,500	10.5
A295S	1.6	498	2	45,000	4.75

^a Extinction coefficients determined in buffer E at 15 °C, for further details see Materials and Methods.

^b MII decay assays performed in buffer E at 20 °C as described in Materials and Methods.

^c The extinction coefficient for WT was assumed to be 40,600 $M^{-1}\cdot\text{cm}^{-1}$ (27).

^d λ_{\max} similar to (35).

^e λ_{\max} similar to (10).

^f Extinction coefficient similar to (30).

**Table 2. 2: Relative Transducin Activation Rates
and Activation Parameters of Retinal Release^a.**

Mutant	Relative Transducin Activation	E _a (kcal/mol)
WT	1.00	20.1
G90S	0.74	19.6
T118A	0.84	19.7
E122D	0.76	16.3
A292S	0.77	19.2
A295S	0.25	21.1

^a All experiments performed in buffer E as described in Materials and Methods.

Table 2. 3: Functional Properties of Mutant T118A/E122D/A292S in Comparison With WT Rhodopsin. (Spectral Ratio, Absorption Maxima, Extinction Coefficient, $t_{1/2}$ of Retinal Release Rates, Relative Transducin Activation Rates and Activation Parameters of Retinal Release).

Mutant	$A_{280}/A(\lambda_{\max})$	λ_{\max} (nm)	ϵ ($M^{-1}\cdot\text{cm}^{-1}$) ^a	MII decay $t_{1/2}$ (min)	Relative Rate of G_T Activation	E_a of Retinal Release (Kcal/mol)
WT	1.8	500	40,600 ^b	15	1.0	20.1
T/E/A	1.7	453	40,000	10	0.51	21.1

^a Extinction coefficients determined in buffer E at 15 °C, for further details see Materials and Methods. All values were rounded to the nearest 500 $M^{-1}\cdot\text{cm}^{-1}$.

^b The extinction coefficient for WT was assumed to be 40,600 $M^{-1}\cdot\text{cm}^{-1}$ (27).

Figure 2. 1: Models of bovine rhodopsin indicating sites for introducing blue-wavelength shifting mutations. (A) Suggested two-dimensional model of rhodopsin. Individual amino acids mutated in this study are shown in bold, cysteine residues involved in a disulfide bond are shaded gray. K296 the retinal Schiff base attachment site and E113 the counterion are boxed. The cytoplasmic side is on the top in this rendition, with labels A-G referring to the TM helices below. **(B)** Three dimensional model of the retinal binding pocket of rhodopsin adapted from the bovine opsin crystal structure (52). Sites mutated in this study are shown respective to the retinal chromophore.

Figure 2. 2: UV/vis absorption spectra of WT and mutant rhodopsin pigments in the dark state. The respective blue shifts in λ_{max} are indicated. The spectra were recorded in buffer E at 20 °C. For display purposes, the WT and A292S spectra were divided by 1.4 to allow for comparison with the other spectra.

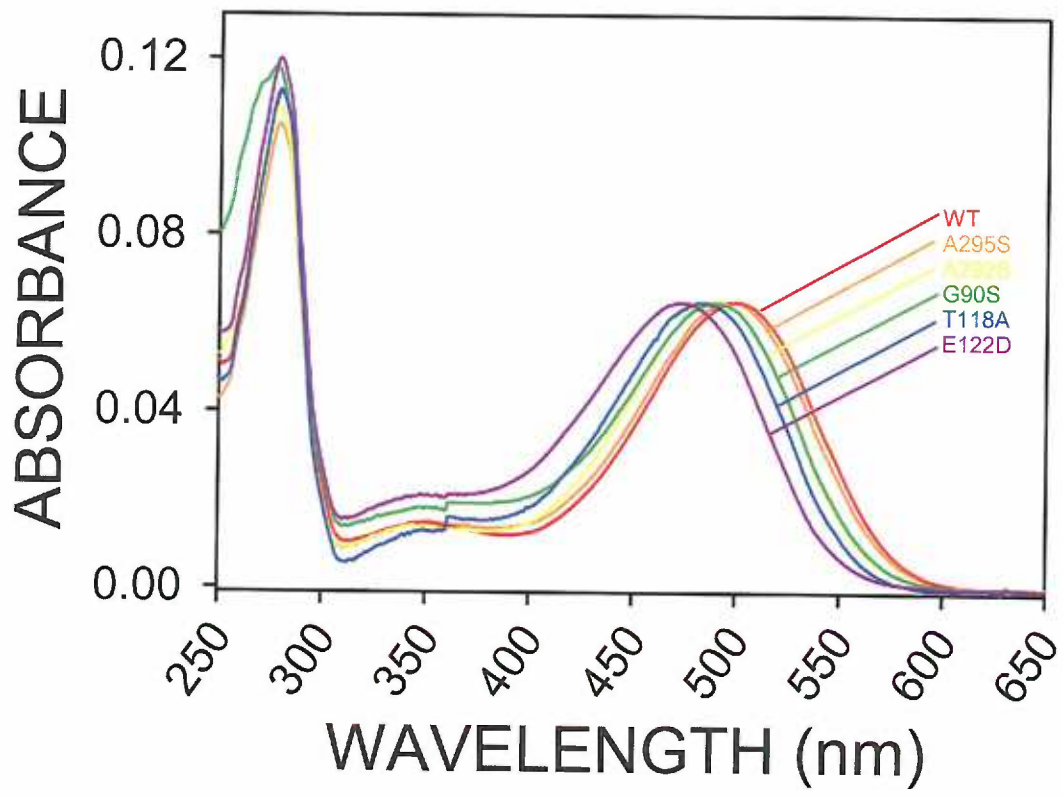
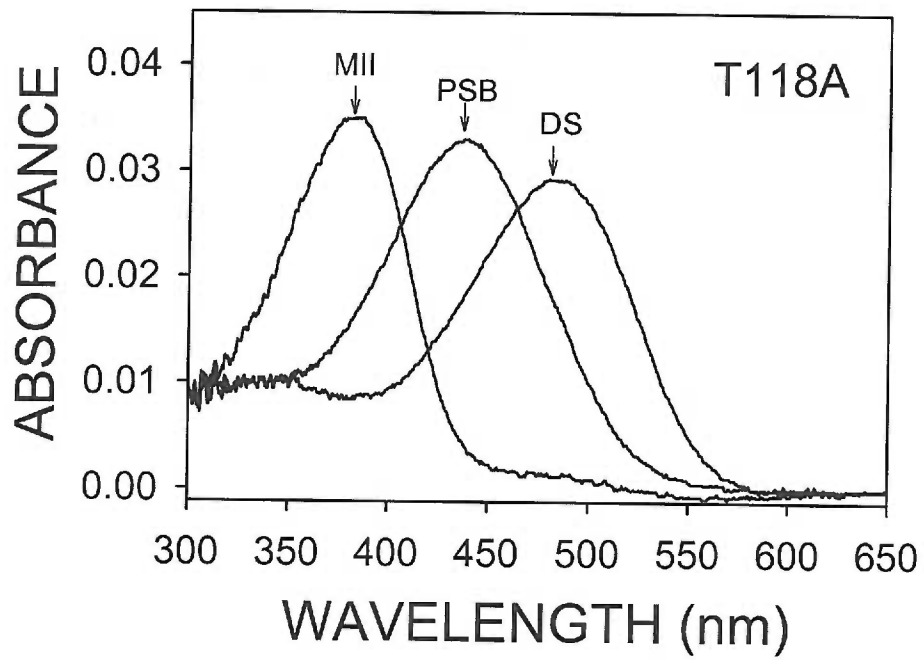


Figure 2. 3: UV/vis spectral properties of select blue-wavelength shifted rhodopsin mutants. (A) Photobleaching properties of T118A. DS, dark state; MII, Meta II state; PSB, protonated Schiff base (at pH 1.9). **(B)** Photobleaching properties of G90S. Following illumination ($\lambda > 470$ nm) for 30 s a residual species remains with a $\lambda_{\text{max}} \sim 480$ nm. This species was followed as a function of time as indicated.

(A)



(B)

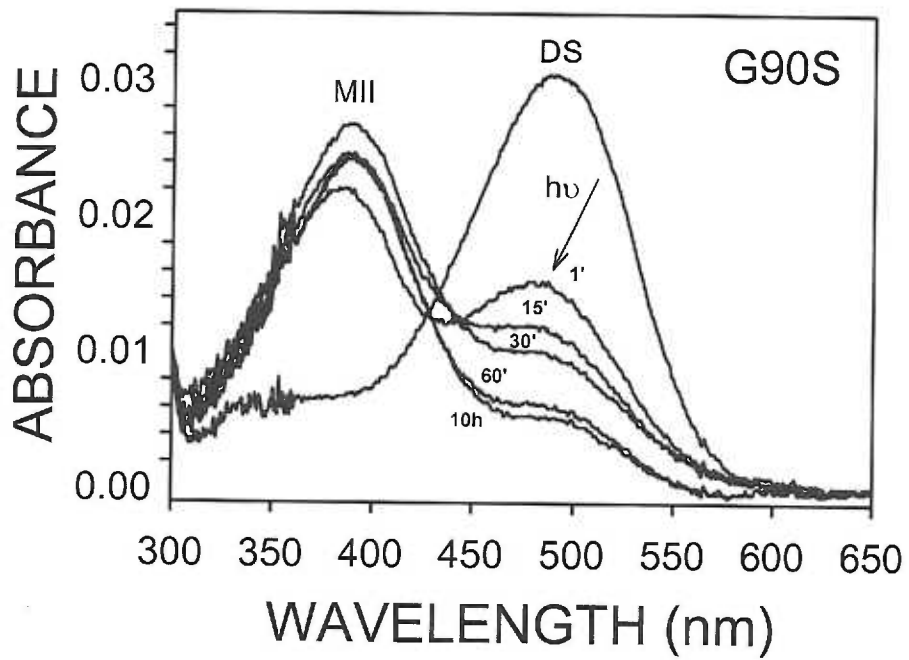
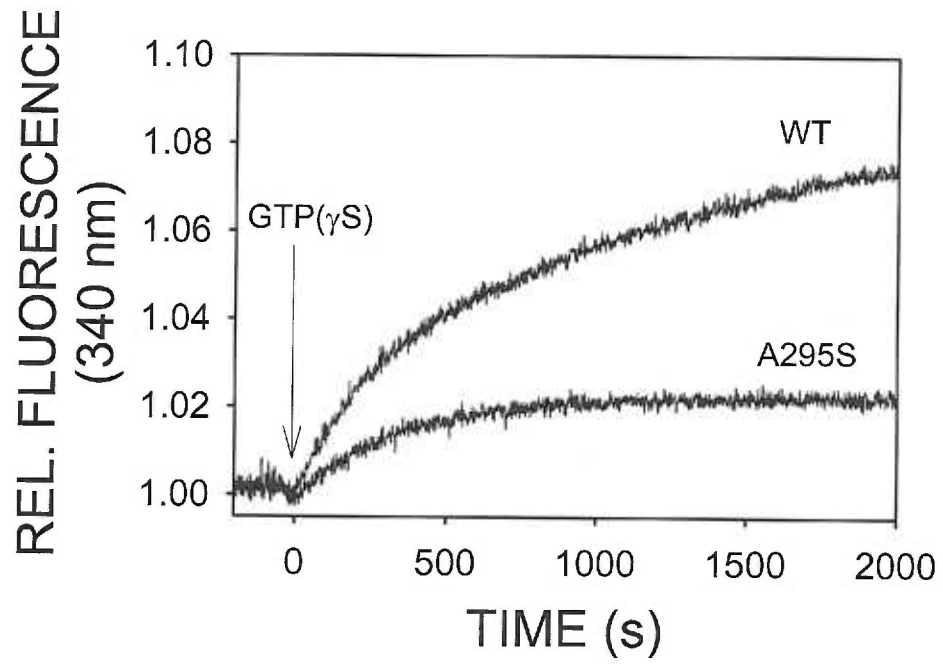


Figure 2. 4: Transducin activation by blue-wavelength shifted rhodopsin mutants.

(A) Example of transducin activation as measured by the fluorescence assay. The assay directly monitors transducin activation by measuring increase in $G_{T\alpha}$ tryptophan fluorescence that occurs upon formation of the $G_{T\alpha}$ -GTP γ S complex when GTP γ S is added (arrow). For assay conditions and further details see Materials and Methods. **(B)** Comparison of the initial rates for transducin activation by wavelength shifted rhodopsin mutants. The rate in the first minute after GTP γ S addition relative to wild type rhodopsin is shown for each mutant.

(A)



(B)

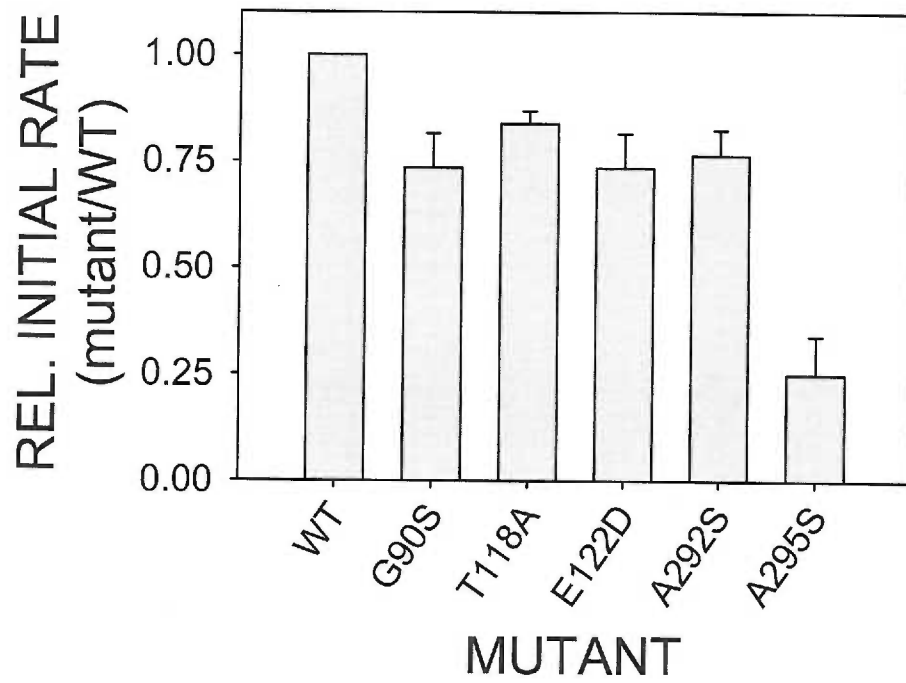


Figure 2. 5: Arrhenius plot of the retinal release rates from photobleached WT and mutant rhodopsins. The rate constants were obtained from traces of the retinal release assay (see Materials and Methods) performed in buffer E, with temperatures ranging from 13 to 33 °C. The activation energy (E_a) of this process for WT and all mutants are given in Table 2. 2.

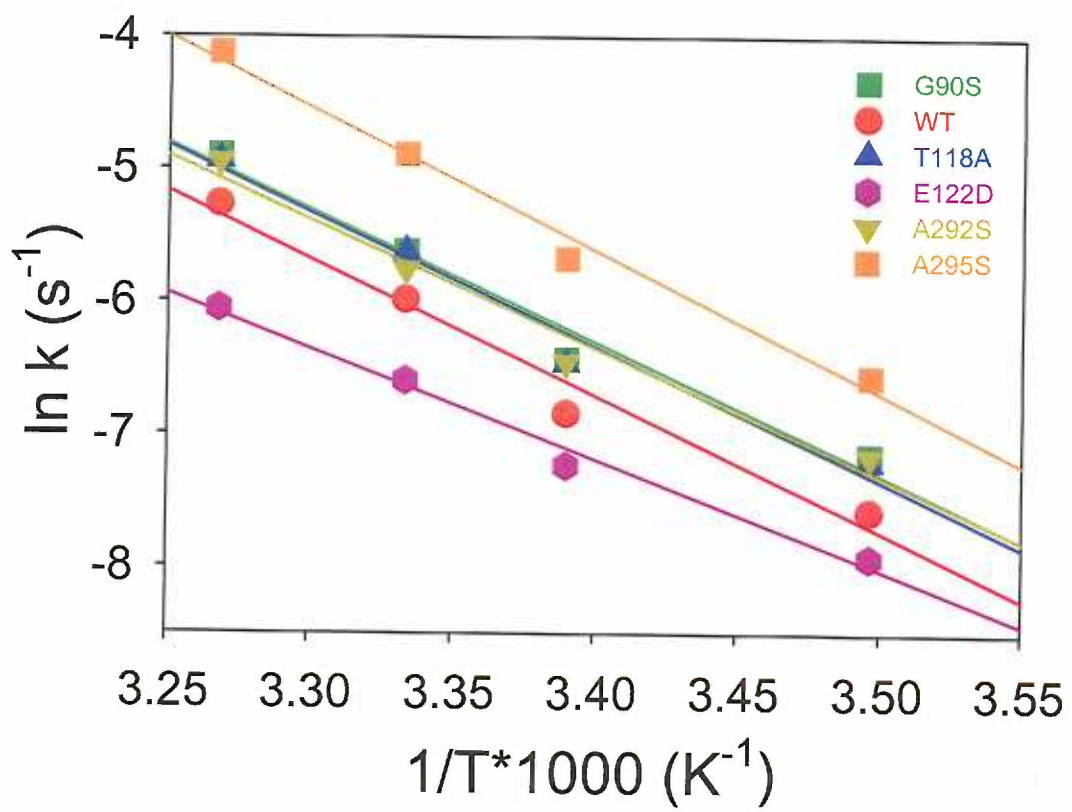
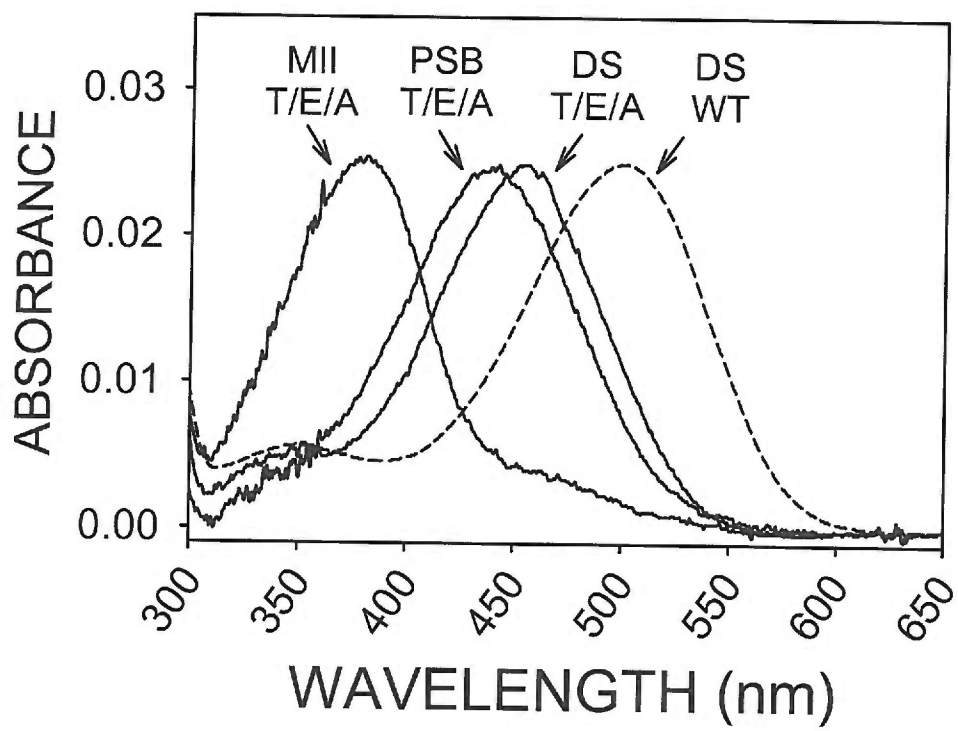


Figure 2. 6: UV/VIS spectral properties of rhodopsin mutant T118A/E122D/A292S (T/E/A) relative to WT. Mutant T/E/A exhibits a 47 nm blue-wavelength shift relative to WT in the dark state (DS). Following illumination ($\lambda > 470$ nm) for 30s, T/E/A adopts the MII state. Upon acidification (to pH 1.9) the absorbance maximum of the T/E/A MII species changes to 440 nm, of a protonated Schiff base (PSB). The dark state (DS) spectrum of a WT sample is included for comparison purposes (dashed line).



2. 7: SUPPLEMENTARY MATERIAL

2. 7. 1: Steric trigger hypothesis for rhodopsin activation.

Interactions between 11-*cis*-retinal and amino acid side chains of the retinal binding pocket spectrally tune the chromophore, maintain the stability of the Schiff base linkage and regulate photocycle intermediates initiated by *cis-trans* isomerization of the retinal during receptor activation (4, 14, 27, 48). In particular the C₉-methyl group is proposed to act as a scaffold for opsin to adjust key donor and acceptor side chains for the proton transfer reactions that stabilize the active signaling state (168), and is thought to impact the MI/MII equilibrium upon photoactivation (166). Evidence for scaffolding was provided by experiments on rhodopsin in which the native 11-*cis*-retinal chromophore was replaced with a 9-demethyl-retinal analogue (lacking the C₉-methyl group), these artificial pigment were shown to have reduced ability to activate transducin (167). Based in part on rhodopsin models that predate the crystal structure a “steric trigger” model of rhodopsin activation was proposed (122). This model suggests that steric interactions between amino acid side chains of rhodopsin and the C₉-methyl group of retinal regulate receptor signaling by maintaining the protein in the dark state. However, this theory was based in part on mutagenesis data of residues that do not make steric contact (come within van der Waals contact distance) with the C₉-methyl group (118-121).

To directly test this theory we have mutated residues that do make steric contact (defined as being within 4 Å) with the C₉-methyl group of rhodopsin – namely, T118 and I189 and characterized their effects (see above and Figure 2. S1). We generated alanine mutations that would presumably disrupt the steric interactions between the retinal and

these residues, T118A and I189A. As presented above the results for mutant T118A suggest abolishing steric interactions provided by the threonine residue results in no drastic effects on rhodopsin stability, photocycle intermediates or signaling (Figures 2. 3A, 2. 4B, 2. 5). Consistent with these results we also find that mutant I189A stably binds 11-*cis*-retinal, photobleaches properly and does not perturb the MI/MII transition (Figure 2. S2). Furthermore, we find that mutant I189A forms a stable MII intermediate that is functional to near WT levels (Figure 2. S3). Taken together, our studies on residues T118 and I189 are not consistent with the “steric trigger” hypothesis.

While it is possible that compensatory mechanisms such as interactions by water molecules or alterations in the protein fold provide alternate steric contacts to the retinal C₉-methyl group our results indicate that simple localized steric interactions between the C₉-methyl group of retinal and rhodopsin do not seem to play a significant causal role in mediated signal transduction. Our findings do not rule out the possibility the mutants T118A and I189A exhibit some level of constitutive activity. Further, our conclusions do not account for any residues that may interact with the C₉-methyl group as a result of possible conformational changes occurring in the transition to the active MII state, as structural details of this intermediated are not at present available.

Figure 2. S1: Three-dimensional model of rhodopsin residues making steric contact with the C₉ methyl of 11-*cis*-retinal. Both residues T118 and I189 are within 4 Å of the C₉ methyl side chain of 11-*cis*-retinal (shown in green). The model was generated using the program Weblab using coordinates from the crystal structure (PDB# 1F88, (52)).

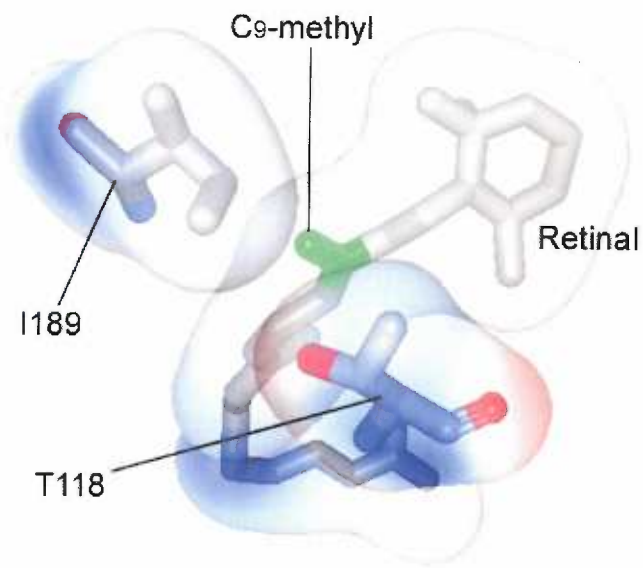


Figure 2. S2: Photobleaching characteristics of rhodopsin mutant I189A. (A)

Absorbance scans of I189A in the dark state (DS), after bleaching to the MII state with > 495 nm light for 30 s (MII) and following acid denaturation of the photobleached product to pH 1.9 to confirm the presence of a protonated Schiff base (PSB). **(B)** Spectral properties of I189A following bleaching. The sample was scanned in the dark state (black) then following 30 s photobleaching (red) and subsequently scanned as indicated. Following a brief initial rise in λ_{480} nm absorbance (arrow) the spectra reveal no anomalous photointermediates arise during decay of the MII state. All spectra recorded in buffer E, pH 6.0 at 20 °C.

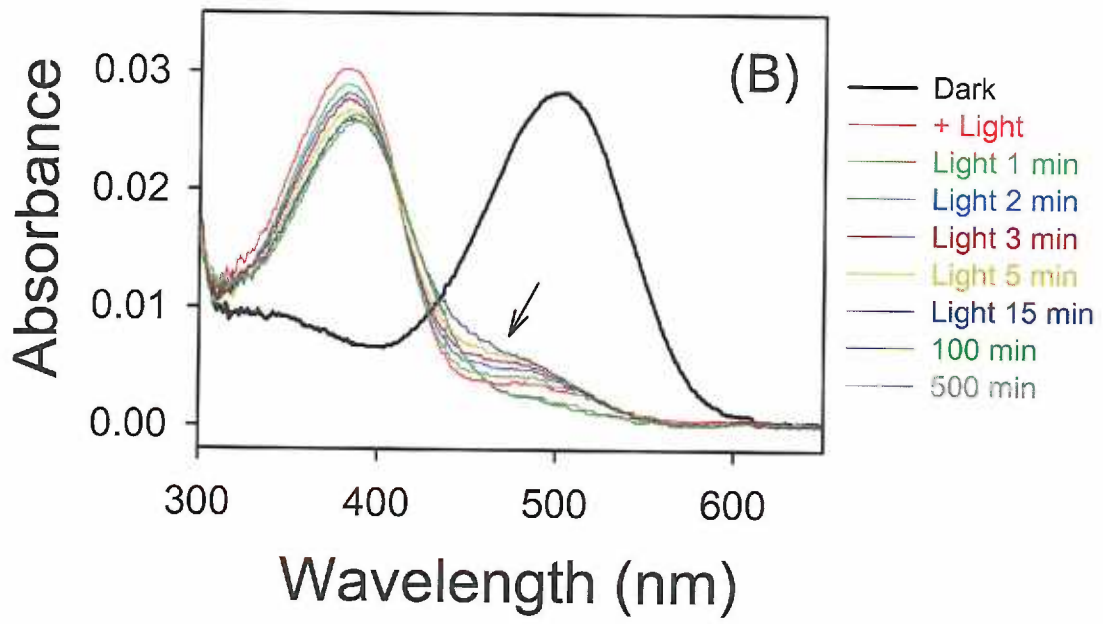
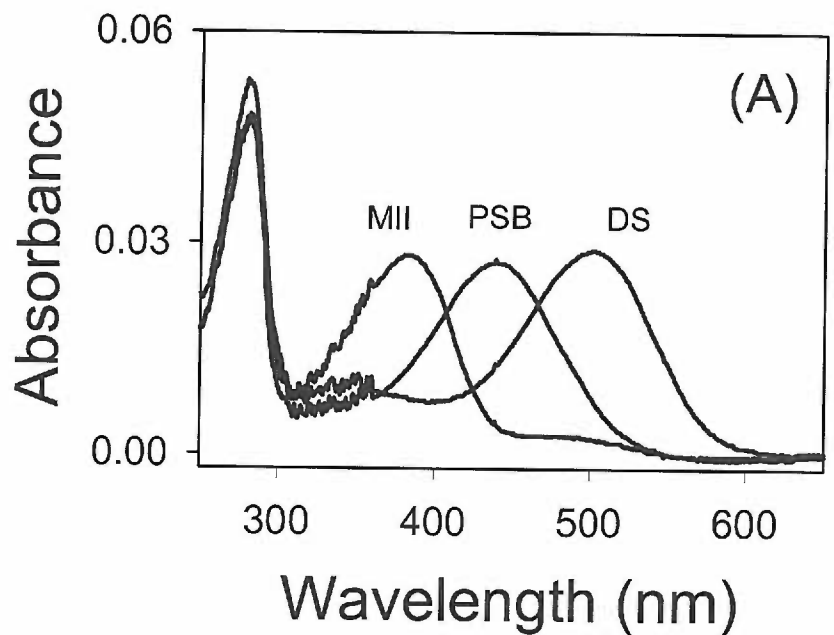
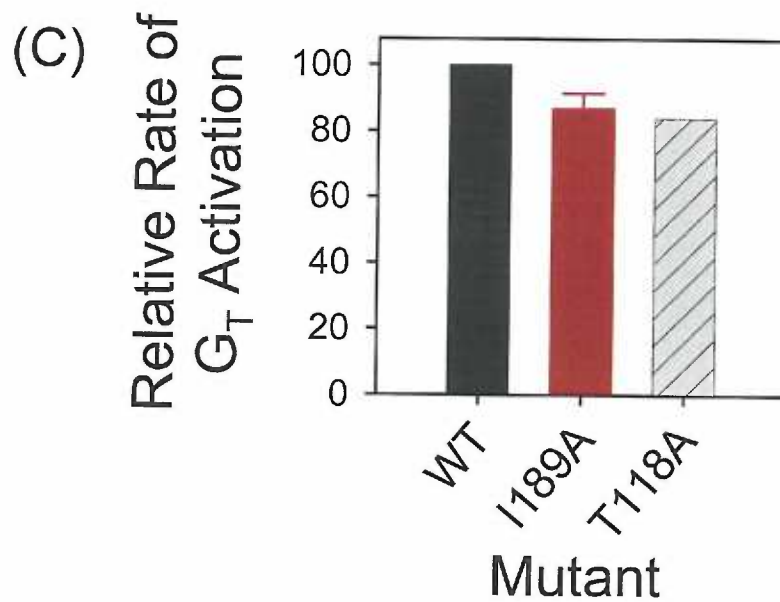
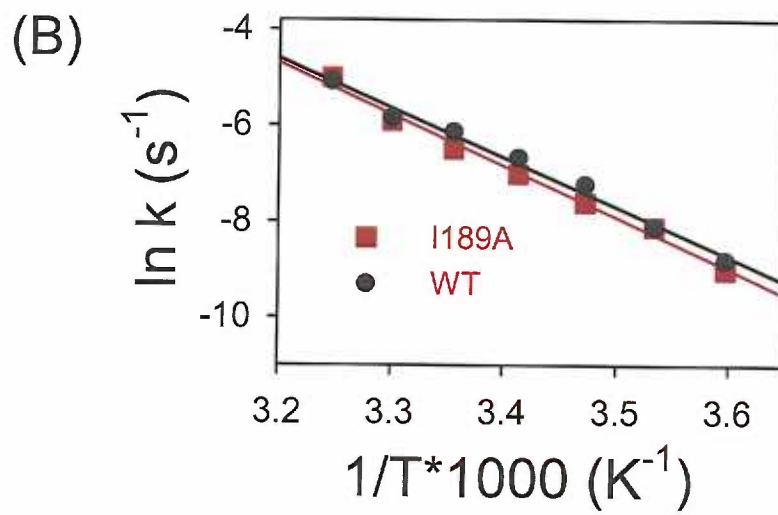
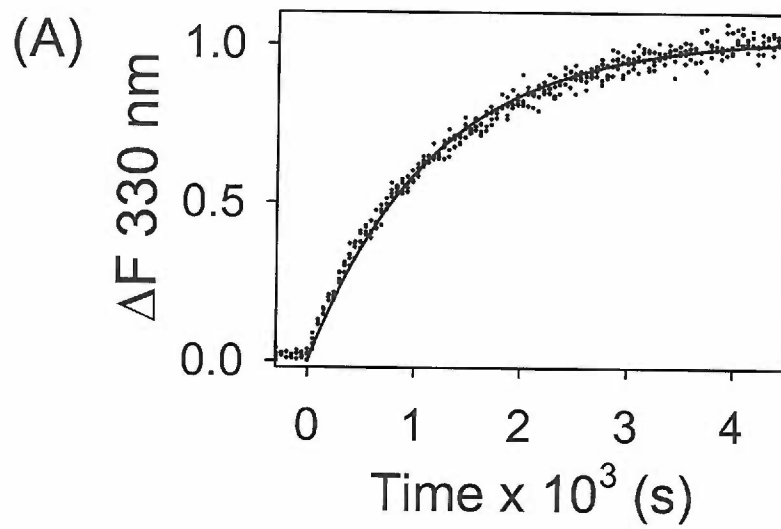


Figure 2. S3: Characterization of the MII signaling state for mutant I189A. (A) Mutant I189A exhibits a WT-like MII decay in buffer E at 20 °C, with a $t_{1/2} = 13.3$ min. **(B)** Arrhenius plot of the rate constants for the MII decay of mutant I189A in buffer E over temperatures ranging from 5 to 35 °C. The plot yields E_a values of 21 kcal/mol for I189A and 20.1 kcal/mol for WT rhodopsin. **(C)** Relative rates of transducin activation for mutant T118A, I189A relative to WT rhodopsin. Results for mutant T118A appear above in Figures 2. 3 – 2. 5 and Tables 2. 1 and 2. 2.



Chapter 3

Stability of Dark-State Rhodopsin is Mediated By a Conserved Ion-Pair in Intradiscal Loop E-2.

Jay M. Janz[§], Jonathan F. Fay[§] and David L. Farrens[§]

[§]Department of Biochemistry and Molecular Biology,

Oregon Health and Science University

3181 S. W. Sam Jackson Park Drive, Portland, Oregon 97201-3098

Running Title: Intradiscal Ion-pair Mediates Thermal Stability of Rhodopsin.

3. 1: SUMMARY

The rhodopsin crystal structure reveals that intradiscal loop E-2 forms a structure that covers the 11-*cis*-retinal, creating a sort of “retinal plug”. During examination of the structure we recently noticed the ends of loop E-2 are linked by an ion-pair formed between residues R177 and D190. This ion-pair is conserved among most vertebrate opsins, and D190 mutations are found in some *retinitis pigmentosa* patients, thus we decided to assess its role through structure/function studies. Our studies indicate the R177/D190 ion-pair is important for the folding and stability of dark state rhodopsin. Ion-pair mutants either do not regenerate with 11-*cis*-retinal, or if they do, are functionally and spectrally wild type like yet thermally unstable in their dark-state form because of rapid retinal Schiff base hydrolysis and retinal release. Interestingly, Arrhenius analysis indicates the activation energies for hydrolysis are almost identical to wild-type rhodopsin and that the R177/D190 ion-pair is almost as important as the conserved C110/C187 disulfide bond for maintaining rhodopsin dark state stability. Surprisingly, we find ion-pair mutations do not increase the mutants’ reactivity to hydroxylamine, suggesting the increased rate of retinal hydrolysis is due to some effect on the stability of the Schiff base linkage other than increased exposure to bulk solvent.

All experiments reported in this chapter we performed by the author of this dissertation with the exception of the western blots shown in Figure 3 - which were performed by Jon Fay. In addition, Jon Fay provided technical assistance in the expression of recombinant rhodopsin mutants used in this chapter as well as initial transducin activation assays on rhodopsin mutants. Portions of this chapter have

previously been published: Janz, J. M., Fay, J. F., and Farrens, D. L. (2003) *Journal of Biological Chemistry* **278**, 16982-16991.

3. 2: INTRODUCTION

Rhodopsin, the dim light photoreceptor of rod cells, is the best-characterized member of the superfamily of G-protein coupled receptors (GPCRs), (14, 18, 48, 51, 52, 67, 135, 171). Rhodopsin consists of a chain of 348 amino acids, approximately half of which form a cluster of seven membrane-spanning helices located within the membrane (Figure 3. 1). The rhodopsin chromophore, 11-*cis*-retinal, resides in the middle of these helices attached to lysine-296 through a protonated Schiff base linkage (132, 137).

Interactions of amino acid side chains, as well as water molecules within the chromophore-binding pocket with the retinal result in the 500 nm absorbance maxima for dark-state rhodopsin (95, 140). Dim light vision begins when the 11-*cis*-retinal chromophore in rhodopsin absorbs a photon and is converted to all-*trans*-retinal. This change in retinal configuration initiates a series of photo-intermediates and conformational changes in the protein, culminating in a 380 nm absorbing species called metarhodopsin II (MII), the “active conformation” which is able to bind and activate the G-protein transducin (48, 67, 172).

Recently, high-resolution crystal structures of rhodopsin have been obtained (52-54). These structures confirm some of the previous hypotheses about the rhodopsin structure, such as the general arrangement of the transmembrane helices, the locations of the disulfide bond, and glycosylation sites (57, 58, 61, 101, 173, 174). However, they also revealed several surprises. One of the most intriguing aspects was the high degree of

order in the intradiscal loops (the equivalent to the extracellular loops in other GPCRs and hereby denoted as such). Especially intriguing is loop E-2, which connects helices 4 and 5 and forms a twisted β -hairpin that lies alongside the retinal chromophore, potentially forming a “lid” or “plug” across the retinal-binding pocket (52-54), (Figure 3. 1). This unexpected finding has led to a number of new questions. What role does the structure of loop E-2 play in the stability and function of rhodopsin? Does it help provide a place for retinal to bind, or does retinal binding induce structure in loop E-2? If the loop E-2 structure is present in the apoprotein (opsin), how does retinal get into and out of the binding pocket?

We have recently begun to address some of these questions, and in the process noticed an ion-pair, R177/D190, is present on the ends of loop E-2 (Figure 3. 1B). This ion-pair, (R177/D190), is conserved in almost all vertebrate opsins¹ and may also be present in other GPCRs (Figure 3. 2). Furthermore, the potentially important functional role of this ion-pair is suggested by the fact that mutations at residue D190 in rhodopsin are found in patients with Autosomal Dominant Retinitis Pigmentosa (ADRP) (63, 71, 175-177).

In this chapter we report our investigations into the structural and functional role of the R177/D190 ion-pair. Our primary finding is that the ion-pair helps stabilize the dark state rhodopsin structure. We find that mutations to the ion-pair either result in opsin proteins that do not regenerate with 11-*cis*-retinal, or if they do regenerate, undergo rapid retinal Schiff base hydrolysis in the dark-state. Surprisingly, the active MII

¹ Vertebrate rhodopsin alignments were carried out using ExpASy (Expert Protein Analysis System) proteomics server of the Swiss institute of Bioinformatics (us.expasy.org). The sole exception was sheep rhodopsin which contains a leucine residue at site 190 (L190) and interestingly, a glutamine residue at site 181 (Q181).

signaling state and MII decay processes are not affected by mutations at the ion-pair. We also find that the ion-pair mutations do not increase the susceptibility of Schiff base attack by the bulk solvent (as judged by hydroxylamine reactivity assays), nor affect the activation energy barrier for Schiff-base hydrolysis. These results illustrate the importance of loop E-2 in retinal binding, rhodopsin stability, and retinal release processes.

3. 3: MATERIALS and METHODS

3. 3. 1: Materials.

Except where noted below, all buffers and chemicals were purchased from either Fisher (Pittsburgh, PA) or Sigma (St. Louis, MO). Protease inhibitor tablets and GTP γ S were purchased from Boehringer Mannheim (Indianapolis, ID). Dodecyl maltoside (DM) was purchased from Anatrace (Maumee, OH), and GBX red light filters were from Eastman Kodak Corp (Rochester, NY). Polystyrene columns (2 mL bed volume) were purchased from Pierce (Rockford, IL). Frozen bovine retinas were from J. A. Lawson Co. (Lincoln, NE). Transducin was purified from rod outer segments as previously described (146). DNA oligos were purchased from Qiagen/Operon (Alameda, CA). Restriction endonucleases were from New England Biolabs (Beverly, MA). 11-*cis*-retinal was a generous gift from Dr. R. Crouch (Medical University of South Carolina and National Eye Institute). The rho1D4 antibody was purchased from the National Cell Culture Center (Minneapolis, MN). The nonapeptide corresponding to the C-terminus of rhodopsin was acquired from the Emory University Microchemical Facility (Atlanta, GA). Cuvettes were purchased from Uvonics (Plainview, NY). Band-pass filters and long-pass filters were purchased from Oriel (Stratford, CT). The 30%

acrylamide/bisacrylamide solution (37.5:1) was purchased from Bio-Rad. Goat anti-Mouse (H+L) conjugated with peroxidase and SuperSignal West Pico Luminol/Enhancer Solution were obtained from Pierce (Rockford, IL).

3. 3. 2: Buffers.

The definitions of the buffers used are as follows: PBSSC [0.137 M NaCl, 2.7 mM KCl, 1.5 mM KH₂PO₄, and 8 mM Na₂HPO₄ (pH 7.2)], buffer A [1% DM and PBSSC (pH 7.2)], buffer B [2 mM ATP, 0.1% DM, 1 M NaCl, and 2 mM MgCl₂ (pH 7.2)], buffer C [0.05% DM and PBSSC (pH 7.0)], and buffer D [0.05% DM and 5 mM MES (pH 6.0)], buffer E [5 mM Tris-HCL, 2 mM EDTA, (pH 7.2)], buffer F [20 mM Tris-HCL, pH 7.4, 5 mM MgCl₂ & 1 mM EDTA (pH 7.2)].

3. 3. 3: Construction and expression of rhodopsin mutants.

Site-directed mutagenesis was performed using a cassette-based strategy as described previously in the pMT4 plasmid (147, 148), as well as overlap extension PCR (149) to generate *EcoRI* and *NotI* fragments containing either the R177C/K/Q or D190C/E/N mutations in the synthetic bovine rhodopsin gene (147). The sequences for the primers were as follows:

R177C, 5'CGTCGGCTGGTCTTGCTACATCCCGGAG3';

R177K, 5'GCTCGTCGGCTGGTCTAAGTACATCCCGGAGGGGCATGCAGTGC3';

R177Q, 5'GCTCGTCGGCTGGTCTCAGTACATCCCGGAGGGGCATGCAGTGC3';

D190C, 5'CTCGTGCGGGATCTGCTACTACACGCCG3';

D190E, 5'GGAGGGCATGCAGTGCTCGTGCGGGATCGAGTACTACACGCCG3';

D190N, 5'GGAGGGCATGCAGTGCTCGTGCGGGATCAACTACTACACGCCG3'.

Subsequent to PCR mutagenesis, the PCR fragments were subcloned into the pMT4

vector containing the synthetic gene of rhodopsin using *XhoI* and *PstI* restriction sites, double mutants were constructed using the *BsrI* restriction site. Cysteine mutants were subcloned into the pMT4 plasmid theta, a synthetic gene of rhodopsin in which the potentially reactive background cysteine residues 140, 316, 322 and 323 were replaced with serines (162, 178). All mutations were confirmed by the dideoxynucleotide sequencing method. The mutant rhodopsin proteins were transiently expressed in COS-1 cells using the DEAE-dextran method, and cells were harvested 56 to 72 h after transfection as previously described (150, 179).

3. 3. 4: Purification of rhodopsin mutants.

For rhodopsin purification please refer to section 2. 3. 4 in chapter 2.

3. 3. 5: Immunoblot analysis of rhodopsin mutant cell membranes.

COS cells expressing rhodopsin mutants were pelleted and resuspended in 1 ml/plate of buffer E and homogenized on ice. The homogenates were then centrifuged at 40,000 x g for 45 min at 4°C, and the pellets were washed with 5 ml of buffer F and subsequently resuspended via douncing in buffer F. Protein concentrations of the resuspended membrane pellets were determined by a modified Dc protein Assay from Bio-Rad Laboratories (Hercules, CA). Manufactures instructions were followed except for the addition 1.45% SDS to each well. Aliquots of the membrane preparation were snap frozen and stored at -80 °C until use. SDS/PAGE was performed according to Laemmli (180), using a 5% stacking gel and a 10% resolving gel. The protein bands were electrotransferred onto Immobilon-P transfer membranes (Millipore), and detected using the rho1D4 monoclonal antibody as previously described (61). Protein expression

levels were determined using a Bio-Rad Phosphoimager, and pixel densities were determined using a GS-525 Molecular imaging system using supplied software.

3. 3. 6: UV/vis absorption spectroscopy.

For UV/vis absorption spectroscopy please refer to section 2. 3. 5 in chapter 2.

3. 3. 7: Thermal bleaching of rhodopsin samples.

Absorbance Measurements: Thermal decay rates were followed by UV/vis spectroscopy in buffer D. Specific temperatures were maintained using water-jacketed cuvette holders connected to a circulating water bath. Temperature was monitored through emersion of a digital thermometer into the sample chamber, with an accuracy of approximately ± 0.2 °C. Thermal stability of the mutants was determined by first measuring the samples from 650 nm to 250 nm at 1 minute intervals at a given temperature. Thermal decay rates were then measured by monitoring the decrease of the 500 nm absorbing dark state species from these measurements over time (102, 181, 182). Baseline drift was corrected for by normalizing all spectra to an absorbance of zero at 650 nm.

Fluorescence measurements: Thermal decay rates were also measured by monitoring the increase in tryptophan fluorescence at 330 nm, caused by the release of retinal from the chromophore-binding pocket (154). The experimental setup was similar to that of the retinal release assay (described below) except that the samples were not photobleached. All thermal decay data was analyzed using mono-exponential decay (absorbance experiments) or mono-exponential rise to maxima (fluorescence experiments) fitting algorithms in Sigma Plot (Jandel Scientific Software).

3. 3. 8: Thermodynamic calculations of thermal decay rates.

Activation energies (E_a) were determined by applying rate data to the Arrhenius equation: $k = Ae^{-E_a/(RT)}$. Thermodynamic parameters ΔH^\ddagger , ΔG^\ddagger , and $\Delta\Delta G^\ddagger$ were calculated from the rate data as previously described (102, 183). Briefly, the following thermodynamic equations were used:

$$\Delta G^\ddagger = -(2.3) RT \log (k_1 h / k_B T) \quad (\text{Eq 3. 1})$$

$$E_a = \Delta H^\ddagger - T \Delta S^\ddagger \quad (\text{Eq 3. 2})$$

$$\Delta G^\ddagger = \Delta H^\ddagger - T\Delta S^\ddagger \quad (\text{Eq 3. 3})$$

Where R is the universal gas constant, T is the temperature, k_1 is the thermal decay rate, h is Planck's constant, and k_B is the Boltzmann constant.

3. 3. 9: Measurement of the rate of retinal release and/or MII decay by fluorescence spectroscopy.

The MII stability was assessed by measuring the time course of retinal release occurring after MII formation using a Photon Technologies QM-1 steady state fluorescence spectrophotometer (154). Each measurement was carried out using 100 μL of a 0.25 μM mutant sample in buffer D, and sample temperature was maintained as described above. After the samples were photobleached to the MII state (see above), the retinal release measurements were carried out at the appropriate temperature by exciting the sample for 3 s (excitation wavelength = 295 nm, $1/4$ nm bandwidth slit setting) and then blocking the excitation beam for 42 s, to avoid further photobleaching the samples. Tryptophan fluorescence emission was monitored at 330 nm (12-nm bandwidth slit

setting), and this cycle was repeated for up to 100 min during each measurement. To determine the $t_{1/2}$ values for retinal release, experimental data was analyzed using a mono-exponential rise to maxima fit in Sigma Plot (Jandel Scientific Software). In this manner series of MII decay rates were obtained at 5, 10, 15, 20, 25, 30, and 35 °C, and their rates were applied to the Arrhenius equation, $k = Ae^{-E_a/(RT)}$, to determine the activation energy (E_a) of the retinal release process for each mutant rhodopsin.

3. 3. 10: Determination of transducin (G_T) activation rates.

For determination of G_T activation rates please refer to section 2. 3. 7 in chapter 2.

3. 3. 11: Hydroxylamine reactivity.

Hydroxylamine reactivity of the dark state was determined for purified rhodopsins by monitoring the rate of 500 nm absorbance decrease after the addition of hydroxylamine (pH 6.0) to the samples in buffer D to a final concentration of 50 mM at the indicated temperatures (184). Baseline drift was corrected as described above (see Thermal bleaching of rhodopsin samples).

3. 3. 12: Effect of R117Q thermal decay on ability to activate transducin.

Activation of G_T by rhodopsin was monitored as described above. Activation assays were first performed on freshly thawed WT and R177Q stocks. The stocks were next incubated in the dark at 37 °C to facilitate thermal decay of the 500 nm absorbing species and aliquots were withdrawn at the indicated time points and assayed for G_T activation.

3. 4: RESULTS

3. 4. 1: Rational for choice of Loop E-2 ion-pair mutations.

Amino acid mutations were constructed based on their ability to disrupt or potentially restore the ion-pair charge interaction, while introducing minimal steric perturbation. Thus, residue R177 was mutated to R177K (conserved charge), and R177Q (neutral substitution). Residue D190 was mutated to D190E (conserved charge), and D190N (ADRP mutation, neutral charge). Mutants R177C, and D190C were constructed to enable chemical modification of the single cysteine residues. We did not analyze other ADRP associated point mutations at site D190 (D190A, D190G, D190Y), because previous reports suggest these mutations are defective in folding, trafficking, and/or chromophore binding (63, 175, 176).

3. 4. 2: Characterization of rhodopsin mutants.

Expressed ion-pair mutant rhodopsins were analyzed for expression levels, proper post-translational modifications, ability to bind 11-*cis*-retinal and photobleaching properties. Immunoblot analysis of mutants expressed from transfected COS cells indicates all mutants expressed to similar levels comparable to that of wild-type rhodopsin (Figure 3. 3A). Mutants R177C, D190C and D190E did not regenerate in our hands, and were therefore not further characterized. These mutants also had abnormal glycosylation patterns in comparison to WT rhodopsin in that they did not exhibit the characteristic glycosylation smear pattern when expressed in COS cells (Figure 3. 3A). Furthermore, mutants defective in chromophore binding tended to form large molecular weight aggregates relative to both WT and other mutants (Figure 3. 3A).

Immunoblot analysis of recombinant rhodopsins purified using the rho1D4 monoclonal antibody reveal a band pattern similar to that of wild-type rhodopsin, with an apparent molecular mass of ~ 40 kDa and the characteristic heterogeneous glycosylation smear due to over expression in a COS cell system (Figure 3. 3B), (185). Mutants capable of regenerating with 11-*cis*-retinal formed characteristic rhodopsin-like pigments and could be purified to obtain spectral ratios (A_{280}/A_{500}) between 1.6 and 1.8. The R177 and D190 single point mutants exhibited normal photobleaching behavior with respect to formation of a blue-shifted $\lambda_{\max} \approx 380$ nm species (characteristic of the MII intermediate), (137).

Acidification of these photobleached samples generated a $\lambda_{\max} = 440$ nm species, indicating the presence of a protonated retinal Schiff base (PSB), (152). These results are compiled in Table 1, and a representative example of the photobleaching behavior is shown for mutants R177Q and D190N (Figure 3. 4A). Similar to the single mutants R177Q and D190N, the R177Q/D190N double mutant shows wild-type behavior in terms of expression levels, post-translational modifications and chromophore binding.

However, it did exhibit perturbed photobleaching properties. Although capable of forming both a spectral MII species and a PSB, following illumination a residual species with a λ_{\max} of ~ 480 nm persists up to 10 h after illumination (See Supplementary Material below). The cause of this is not known, although similar effects have been reported for other rhodopsin point mutations such as G90S and L226C (70, 148, 179).

3. 4. 3: Retinal release rates and activation energies for Meta II decay measured by fluorescence spectroscopy.

To determine potential effects the ion-pair mutations may have on the stability of the MII active signaling species of rhodopsin, the activation energies for retinal release

were determined. The rate of retinal release occurring during the decay of the MII species was measured using a fluorescence-based assay at 20 °C (154). Under the conditions used for this assay the $t_{1/2}$ of retinal release for WT rhodopsin at 20 °C in buffer D was 13 ± 0.5 min ($n = 3$), comparable to the 13 – 15 min values previously reported for both ROS purified and COS expressed rhodopsin (114, 179, 182, 186). Somewhat unexpectedly, the corresponding $t_{1/2}$ values for the ion-pair mutant rhodopsins were similar to that of WT rhodopsin. The values for each of the mutants are compiled in Table 3. 1. The activation energy for the Meta II decay process was obtained by monitoring the rate of fluorescence increase in buffer D at seven different temperatures (5, 10, 15, 20, 25, 30 and 35 °C). The rate of fluorescence increase in all cases was temperature-dependent, and Arrhenius plots of these measurements indicate a temperature-dependent linear relationship for all mutants (Figure 3. 4B). From these plots an activation energy (E_a) of 20.2 kcal/mol was obtained for purified WT rhodopsin in DM, in good agreement with previously reported values (154, 179, 187). Arrhenius plots of the retinal release rates for the ion-pair mutants show nearly equal E_a values (Figure 3. 4B and Table 3. 1).

3. 4. 4: Transducin activation by ion-pair mutants.

To assess the potential functional effects, the ion-pair mutants were tested for their ability to activate transducin using a fluorescence-based assay which measures the increase in tryptophan fluorescence of the $G_{T\alpha}$ -GTP γ S species (114, 156, 164). All ion-pair mutations that regenerated with retinal are functionally active, and representative examples are presented in Figure 3. 4C. The results for transducin activation are compiled in Table 3. 1 as initial rates of fluorescence increase relative to WT rhodopsin.

3. 4. 5: Thermal stability in the dark state.

The most dramatic perturbation induced by the ion-pair mutations was on the stability of the dark-state structure. Thermal stabilities of dark state WT and ion-pair mutant rhodopsins were determined by measuring the loss of the 500 nm absorbing species over time as described in Materials and Methods. An example of this assay is depicted for mutant R177Q at 37 °C in figure 3. 5A. The loss of the 500 nm species directly correlates with a loss of ability to activate transducin (Figures 3. 5B and 3. 5C). Additionally, the decrease in absorbance at 500 nm reflects a loss of the chromophore Schiff base linkage as judged by decay of the acid denatured 440 nm species over the duration of the thermal decay assay (Figures 3. 5D and 3. 5E). Furthermore, we conclude the retinal is leaving the chromophore binding pocket after the hydrolysis because the rate of the loss of the 500 nm absorbing species correlates with the rate of tryptophan fluorescence increase, and irradiation of the sample with light following a plateau in signal does not cause a further fluorescence increase (Figure 3. 5F), (154).

All of the ion-pair mutants showed significantly expedited rates of thermal decay in comparison to WT rhodopsin as judged by their loss in absorbance at 500 nm and increase in fluorescence at 330 nm (Table 3. 2). A comparison of the thermal decay rates at 55 °C monitored by absorbance is shown in Figure 3. 6. Note that the thermal decay rate of ROS purified rhodopsin was similar to that of WT recombinant rhodopsin purified from COS cells (38.5 ± 3.0 and 37 min at 55 °C, respectively). The activation energies for the thermal absorbance decay processes were determined by monitoring the loss of the 500 nm absorbing species over time at 7 different temperatures (37, 41, 45, 47.5, 50, 52.5 and 55 °C). In all cases, the rate of loss in 500 nm absorbance was temperature-

dependent, and Arrhenius plots indicate a similar temperature-dependent relationship for all mutants (Figure 3. 7). The Arrhenius plots are clearly concave, suggesting at least 2 different rate-limiting processes may occur during the temperature dependent absorbance decay. With this in mind, two linear regressions were used to approximate the activation energies for the two apparent processes (55 - 47.5 °C and 47.5 - 37 °C, respectively). From this analysis, the E_a for WT rhodopsin was determined to be approximately 16 kcal/mol at 37 °C, and 103 kcal/mol at 55 °C. The thermodynamic parameters E_a , ΔG^\ddagger , ΔH^\ddagger and $\Delta\Delta G^\ddagger$ were estimated from the rate data for WT and mutant rhodopsins using previously described equations (see Table 3. 2), (102, 183).

3. 4. 6: Hydroxylamine reactivity.

Hydroxylamine reactivity experiments showed that the ion-pair mutants were not more susceptible to hydroxylamine in the dark-state. These assays were carried out for purified ROS rhodopsin and each mutant sample, and the decay of the dark state 500 nm absorbing species was monitored in buffer D at either 20, 37 or 50 °C over time following the addition of hydroxylamine (pH 6.0) to a final concentration of 50 mM. WT rhodopsin purified from retinal sources and from expressed COS cells, was found to be inert to hydroxylamine in the dark-state, as previously described (184). Intriguingly, none of the ion-pair mutants exhibited any increased reactivity toward hydroxylamine treatment in the dark state at 20, 37 and 50 °C (Figure 3. 8).

3. 5: DISCUSSION

Early studies by Khorana and others led to the hypothesis that the rhodopsin intradiscal domain plays a crucial role in maintaining proper protein folding, correct post-

translational modifications, trafficking, and 11-*cis*-retinal binding (62, 64, 65, 103, 185, 188). Consistent with this theory, a number of point mutations that naturally occur in this region result in Autosomal Dominate Retinitis Pigmentosa (ADRP), an inherited human disease causing retina degradation (63, 106, 175, 176, 189, 190). As noted in the introduction, the rhodopsin crystal structures reveal a high degree of order and structure in the intradiscal region. This region of the protein is proposed to be structurally critical for maintaining the electrostatic and hydrogen-bonded network surrounding the retinal chromophore (54). Most notably, loop E-2 forms a twisted β -sheet which lies across the retinal chromophore (52-54). Through analysis of the loop E-2 region we noticed an ion-pair R177/D190 is present on either end of this loop structure. Additionally, we noticed that residue R177 is hydrogen bonded to the backbone carbonyl of residue P7, a residue found at the turn of loop E-1 in the proteins N-terminus. The fact that residues R177 and D190 interact with many residues within the intradiscal region of rhodopsin suggests that the ion-pair may play a significant role in maintaining the structural integrity of the “retinal plug” domain. The published rhodopsin crystal structures show very little difference in the region around the R177/D190 ion-pair (analysis of all three structures using the program Swiss-PDB Viewer shows that the 87 amino acid side-chains within 16 Å of R177 show an RMS deviation of 1.0 Å or less (52-54)). However, we do notice a difference in the placement of residue N200, which exhibits a different rotameric flip between structures 1HZX, 1L9H and 1F88, and thus exhibits alternate hydrogen bonding to residue D190 in the different structures (52-54). The present report details our studies on the structural and functional effects caused by disrupting the R177/D190 intradiscal ion-pair located on either end of loop E-2 (Figure 3. 1B).

3. 5. 1: General characteristics of mutants.

The majority of the single ion-pair mutants we created expressed to similar levels comparable to WT rhodopsin, underwent proper glycosylation (as judged by whole cell lysate immunoblotting, Figure 3. 3), and regenerated with 11-*cis*-retinal. Additionally, with the exceptions of mutants R177C, D190C, and D190E, the mutants were properly folded, as judged by their ability to bind the 11-*cis*-retinal chromophore and produce a wild type like A_{280}/A_{500} ratio (Table 3. 1). The fact that most of the D190 mutations were unable to bind retinal is in agreement with previous reports of other D190 mutations, which also were found to be defective in retinal binding (63, 64, 175). One possible reason for the sensitivity of this site to mutations may be that residue D190 is partially buried and makes contacts with several residues (I189, Y191), which form part of the retinal binding pocket (Figure 3. 1B), (52, 54, 186). Abrogation of these contacts by mutations to residue D190 may thus distort the retinal-binding pocket thereby making it inaccessible or sterically unfavorable for proper binding of 11-*cis*-retinal. Additionally, it is also possible that the R177C and D190C mutants are not able to regenerate with 11-*cis*-retinal because improper disulfide bonds are formed in the final folded structure, as these residues are in close proximity to the conserved C110-C187 disulfide pair, as well as residue C185 (Figure 3. 1B). This explanation is supported by recent findings, which shows that improper disulfide bonds form as a result of mutations to this region (191-193). Furthermore, the fact that the glycosylation patterns of whole cell lysate immunoblots of mutants R177C, D190C and D190E are different suggests the misfolding may have already occurred by the time the protein reached the ER, and thus the lack of regeneration is not simply due to an ultra-fast rate of retinal hydrolysis after regeneration

(Figure 3. 3A). These three mutants also tend to form high molecular weight aggregates when analyzed on SDS gels and such aggregation has been suggested to result in proteins that eventually become degraded in the ER rather than proceeding through the Golgi to the plasma membrane (176, 194).

The spectral behaviors for the mutants that did regenerate with 11-*cis*-retinal were WT-like in their ability to form a MII absorbing species and a PSB upon acid denaturation (Figure 3. 4A). One exception was the double mutant R177Q/D190N, which although WT like in its MII and PSB characteristics, demonstrated a residual absorbing species with a λ_{\max} of ~ 480 nm following illumination (see Supplementary Material below). This ~ 480 nm absorbing species may be a MII-like intermediate containing a PSB, as was suggested for mutations at site G90 (157, 165, 179), or it may be a MIII intermediate, due to an altered equilibrium between the MII and MIII states (124, 195). However, why the double mutation shows this characteristic when the single mutants do not is unknown.

3. 5. 2: The R177/D190 ion-pair is not required for MII formation, signaling, or stability.

We were surprised to find that the R177/D190 ion-pair does not appear critical for the formation or maintaining the stability of the MII state. All ion-pair mutants show retinal release rates similar to that of WT rhodopsin in buffer D at 20 °C (13 ± 0.5 min, Table 3. 1), and activation energies (E_a) for retinal release from MII almost identical to the 20.2 kcal/mol obtained for WT rhodopsin (Figure 4B, Table 1) (154, 179, 187). These results are in contrast to our previous findings on mutations within the chromophore-binding pocket, which increased the retinal release rate from MII (although

the activation energy for retinal release were unaffected (179)). Notably, disruption of the C110/C187 disulfide bond in the intradiscal region of rhodopsin dramatically disrupts MII decay and stability (102). In contrast, the regenerated ion-pair mutants all show normal MII function and decay, suggesting they must still contain a normal C110/C187 disulfide bond. Furthermore, the ion-pair mutants are functionally active, as they could activate the G-protein transducin, though not quite to the full extent of WT rhodopsin (Figure 3. 4C, Table 3. 1). Taken together, these results suggest that the intradiscal ion-pair is not critical for the formation or stability of the active signaling MII state.

3. 5. 3: R177/D190 ion-pair helps stabilize the dark state rhodopsin structure.

The most dramatic effect exhibited by the ion-pair mutants was a sharp decrease in the stability of their dark state structures in comparison to WT rhodopsin. Recent studies have begun to carefully address the thermodynamics of rhodopsin protein stability (182, 196, 197). In the present work, our conclusions about rhodopsin thermal stability are primarily based on monitoring the stability of the retinal Schiff base, which we measure as the loss of absorbance at 500 nm. We feel confident that these measurements report on Schiff base hydrolysis and release of retinal from the binding pocket, for the following reasons. The loss in absorbance at 500 nm correlates with both the loss of the PSB (as observed by a decrease in the acid denatured 440 nm species over time) as well as the increase in tryptophan fluorescence at 330 nm (Figure 3. 5 and Table 3. 2). Furthermore, the loss of absorbance at 500 nm also correlates with the loss in ability of the protein to activate transducin (Figure 3. 5C). Taken together these results indicate that during the thermal decay of the dark-state structure the Schiff base is hydrolyzed and the retinal leaves the chromophore-binding pocket.

3. 5. 4: Arrhenius analysis indicates the thermal decay in rhodopsin may occur through more than one pathway.

Interestingly, the Arrhenius analysis of the thermal decay rates shows a concave plot, with all of the mutants decaying much faster than WT rhodopsin. To our knowledge, this behavior has not previously been reported for rhodopsin. Concave Arrhenius plots can be attributed to several factors; although the most common interpretation is that at least two different rate-limiting steps are involved (198). With this interpretation in mind, we fit our WT rhodopsin data assuming two different activation energies may be present, and find E_a values of ~ 16 kcal/mol for the lower temperature range (37 – 47.5 °C), and ~ 103 kcal/mol for the higher temperature range (47.5 - 55 °C). As shown in Table 3. 2, the ion-pair mutants all showed similar E_a values ranging from 17 to 31 kcal/mol for the lower temperature range, and 94 to 107 kcal/mol for the higher temperature range. Finally, thermodynamic analysis of the Arrhenius data show that the ion-pair and WT rhodopsins have similar ΔH^\ddagger values (see Table 3. 2), suggesting the perturbation caused by the mutations are generally entropic in nature (102, 170, 179).

It is informative to compare the thermal decay activation energies from this study with previous findings. For example, our E_a of 103 kcal/mol for WT rhodopsin (at the higher temperatures) is in excellent agreement with the 102.1 ± 5.8 kcal/mol value previously reported by the Khorana laboratory for WT using a similar experimental set up (102). Furthermore, the E_a value of 16 kcal/mol we observe at the lower temperatures is similar to the 20.2 kcal/mol value obtained for the retinal release process that occurs

during MII decay (154, 179), and to the E_a of hydrolysis for model Schiff-base retinal compounds (85), as well as the E_a for retinal binding in rhodopsin (199).

What might be the cause of the different E_a values obtained for the Arrhenius analysis at different temperatures? The higher activation energy barriers at higher temperatures may reflect the less favorable conditions for hydrolysis of the Schiff base linkage present in the interior of unfolded rhodopsin. In other words, thermal denaturation of the protein occurs, which may reposition key amino acids involved in Schiff base formation and hydrolysis, thereby increasing the E_a observed at the higher temperatures. Alternatively, the lower E_a observed at the lower temperatures suggests that at these temperatures another process also contributes to Schiff base hydrolysis, one which occurs more efficiently at lower temperatures (such as proton tunneling) than the process which dominates at higher temperatures. Another possibility is that the pre-exponential factor in the Arrhenius analysis has changed – the pre-exponential factor is related to steric factors and/or the efficiency with which the collisions lead to a productive reaction (198).

3. 5. 5: Thermodynamic significance of the R177/D190 ion-pair.

The $\Delta\Delta G^\ddagger$ values for the ion-pair mutants are approximately -1.5 to -2.4 kcal/mol, similar to the -2.9 ± 1.2 kcal/mol reported for the C110A/C187A mutation of the critical rhodopsin disulfide bond (102). Thus, in terms of dark state stability, abrogation of the ion-pair results in free energy changes comparable to those observed for the loss of the C110/C187 disulfide bond. This is perhaps not surprising, since the R177/D190 ion-pair is in close proximity to the intradiscal C110/C187 disulfide bond (Figure 3. 1B). However, it is important to note that the ion-pair mutations we report here apparently

have little effect on the stability of the MII structure, in contrast to the disulfide bond which appears crucial for MII stability (102). This later point is of interest — to the best of our knowledge, the R177/D190 ion-pair mutants represent a previously unidentified class of rhodopsin mutants which alter the stability and structure of the dark state yet have little to no effect on the stability of the MII state. One explanation for this phenomena may be that the loop E-2 region changes structure during MII formation and the ion-pair is no longer present in the MII state - thus the stability of MII would not be affected by mutations to the R177/D190 ion-pair. We note that while the R177 and D190 residues point away from the helical bundle, it is also possible that mutations to this ion-pair may effect the positioning or orientation of helices 5 and 6. However, there is some precedence for conformational changes in loop E-2, as Ridge and co-workers have previously shown residue C185 becomes accessible to chemical labeling only in the MII state (200).

3. 5. 6: Disrupting the R177/D190 ion-pair does not appear to increase the exposure of the retinal Schiff base to bulk solvent.

We initially interpreted our results to mean that disrupting the R177/D190 ion-pair causes a loosening of the loop E-2 structure, and thus hypothesized the increased rate of Schiff base hydrolysis was due its increased exposure to external solvent. However, to our surprise, we found that the presence of 50 mM hydroxylamine had no effect on any of the mutants tested, even when tested at three different temperatures (Figure 3. 8) ². The lack of increased hydroxylamine sensitivity argues against the hypothesis that the

² Normally, if solvent accessible, a retinal Schiff base is rapidly cleaved by hydroxylamine, and this property has frequently been used as a measure of accessibility of the retinal Schiff-base linkage in rhodopsin (102, 165, 181, 186, 197).

thermal instability induced in the ion-pair mutants is due to a structural perturbation that renders their Schiff base more susceptible to attack by the bulk solvent. Rather, the hydroxylamine data suggest that the R177/D190 ion-pair in the intradiscal domain of rhodopsin mediates thermal stability of the dark-state structure through some other mechanism.

3. 5. 7: Speculation on the role of R177/D190 in stabilizing rhodopsin.

Previous chemical models of the retinal-binding and release pathways have speculated that the protonated retinal Schiff base linkage can spontaneously hydrolyze and thus is in dynamic equilibrium with retinal covalently bound to rhodopsin (85, 201). One interpretation of our data may be that the ion-pair stabilizes the “retinal plug” structure. If the “retinal plug” functions to block the release of free 11-cis-retinal produced through spontaneous hydrolysis (through a steric mechanism which confines the transiently hydrolyzed retinal to the chromophore binding pocket), disruption of this structure might lead to an apparent increase in Schiff base hydrolysis rates. In this scenario the function of the “retinal plug” is to effectively force the transiently formed free 11-cis-retinal to remain in the binding pocket and reform a Schiff base linkage with rhodopsin. Alternately, the ion-pair may enhance rhodopsin stability by constraining the conformation of a network of water molecules and residues attached to loop E-2 (E181-S186-C187) that directly link loop E-2 with the retinal Schiff base through residue E113 (54, 186). Restraining the flexibility of this region may thus make rhodopsin more stable by inhibiting transient formation of the tetrahedral carbinolamine intermediate thought to be involved in the transition state of Schiff base hydrolysis (85, 202). We are presently carrying out further experiments to test these hypotheses.

3. 5. 8: Conclusions.

The R177/D190 ion-pair located on either end of intradiscal loop E-2 appears to be important for maintaining dark state rhodopsin stability, although it does not appear to play a critical role in formation or stability of the active MII species. These results illustrate the importance of the rhodopsin structure revealed by X-ray crystallography (52-54). With the structure of rhodopsin in hand, it is now possible to assess the heretofore-unappreciated functional role of interactions that occur within the protein to provide receptor stability and allow receptor activation and attenuation.

3. 6: ACKNOWLEDGMENTS

This research was supported in part by Grants EY12095-01 to D.L.F. and T32-EY07123-09 to J.M.J. from the National Institutes of Health. We are grateful to Dr. John Denu (Oregon Health and Science University), Dr. Mark Krebs (Illinois State University), and numerous members of the 10th International Conference on Retinal Proteins for helpful discussions.

Table 3. 1: Functional Characterization (Absorption Maxima, Spectral Ratio, Extinction Coefficient, $t_{1/2}$ of Retinal Release, Activation Energy of Retinal Release, Relative Rate of Transducin Activation) of ion-pair mutants.

	λ_{\max} (nm) ^a		A_{280}/A_{500}	ϵ ($M^{-1}cm^{-1}$) ^b	MII Decay 20 °C $t_{1/2}$ (min) ^c	E_a Retinal Release (kcal/mol)	Relative G_T Activation Rate ^d
	dark	light					
WT	500	381	1.6	40600 ^e	13.0 ± 0.5	20.2	1.0
R177C ^f	nd ^g	nd	nd	nd	nd	nd	nd
R177K	500	385	1.6	40000	12.5 ± 0.8	20.3	0.93
R177Q	501	385	1.8	41000	12.8 ± 0.3	20.8	0.73
D190C ^f	nd	nd	nd	nd	nd	nd	nd
D190N	497	385	1.8	31500	11.6 ± 0.4	20.8	0.85
D190E ^f	nd	nd	nd	nd	nd	nd	nd
R177Q/ D190N	497	380	1.8	38000	10.5 ± 0.3	20.8	0.64

^a All λ_{\max} values are determined from the 1st derivative of the raw spectral data and estimated to within ± 1 nm. ^b Extinction coefficients determined in buffer D at 15 °C; for further details see Materials and Methods. ^c MII decay assays performed in buffer D as described in Materials and Methods. Values from three independent experiments are presented as the mean ± SEM. ^d The relative initial rate of G_T activation is represented by the rate of fluorescence increase obtained from the slope of the fluorescence measurements in the first 60 s after addition of GTP γ S relative to that of WT rhodopsin. ^e The extinction coefficient for WT was assumed to be 40600 $M^{-1}cm^{-1}$ (73). ^f Mutants R177C, D190C, and D190E did not bind 11-*cis*-retinal to form a stable pigment. ^g nd = not determined.

Table 3. 2: Thermodynamic Parameters for the Dark State Thermal Decay of Wild Type and Ion-Pair Mutant Rhodopsins^a.

37 °C						
	500 nm Decay $t_{1/2}$ ^b (min)	E_a Thermal Decay ^c (kcal/mol)	ΔG^\ddagger (kcal/mol)	$\Delta\Delta G^\ddagger$	ΔH^\ddagger (kcal/mol)	
WT	3100 ± 45	16.1	25.7	-	15.5	
R177Q	165 ± 10	30.6	24.0	- 1.7	30.0	
R177K	230 ± 15	26.2	24.2	- 1.5	25.6	
D190N	224 ± 15	17.2	24.2	- 1.5	16.6	
R177Q/D190N	219 ± 17	nd ^d	nd	nd	nd	
55 °C						
	500 nm Decay $t_{1/2}$ ^b (min)	Fluorescence Increase $t_{1/2}$ ^e (min)	E_a Thermal Decay ^c (kcal/mol)	ΔG^\ddagger (kcal/mol)	$\Delta\Delta G^\ddagger$	ΔH^\ddagger (kcal/mol)
WT	38.5 ± 3.0	38	103	24.5	-	102.3
R177Q	0.9 ± 0.2	2.1	115.5	22.1	- 2.4	114.8
R177K	2.5 ± 0.2	3.3	94.1	22.7	- 1.8	93.4
D190N	2.4 ± 0.4	3.3	106.9	22.8	- 1.7	106.2
R177Q/D190N	1.4 ± 0.4	2.7	nd	nd	nd	nd

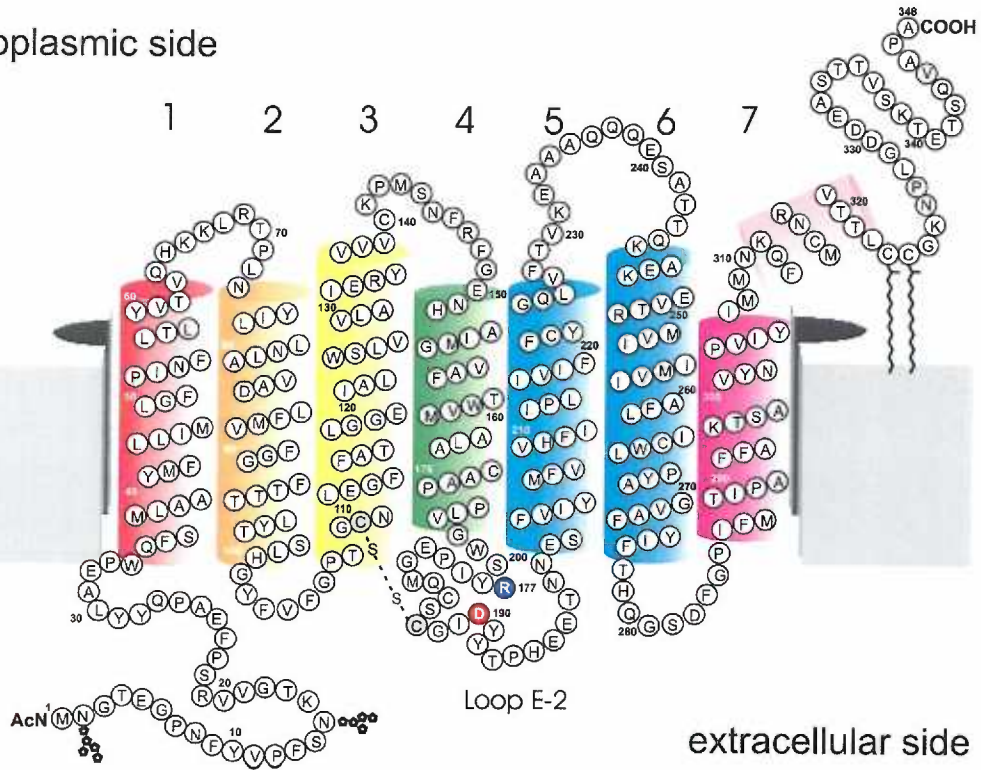
^a All experiments performed in buffer D as described in Materials and Methods.

^b Dark-state thermal decay rates obtained from absorbance measurements at respective temperatures. Values from three independent experiments are presented as the mean ± SEM. ^c Activation energies (E_a) and thermodynamic parameters (ΔG^\ddagger , $\Delta\Delta G^\ddagger$, ΔH^\ddagger) obtained from linear regression of Arrhenius plots (Figure 3. 7), for further details see Discussion. ^d nd = not determined. ^e Increase in tryptophan fluorescence monitored once at 330 nm to monitor dark-state thermal decay rates.

Figure 3. 1: (A) Two-dimensional model of rhodopsin adapted from (52). Intradiscal ion-pair residues R177 and D190 in loop E-2 are colored blue and red, respectively. Residues C110 and C187 that form a disulfide bond in the intradiscal region are shaded gray. (B) Three-dimensional model of the rhodopsin intradiscal domain showing the ion-pair formed by residues R177 and D190 on either end of loop E-2. The figure also indicates the carbonyl backbone of residue P7 is hydrogen bound to R177, as well as the 11-*cis*-retinal chromophore, and the disulfide bond between cysteine residues C110 and C187 in loop E-2. These same features are present in all three rhodopsin crystal structures (52-54). The model shown was prepared using coordinates from 1L9H (54) using the program WebLab.

(A)

cytoplasmic side



(B)

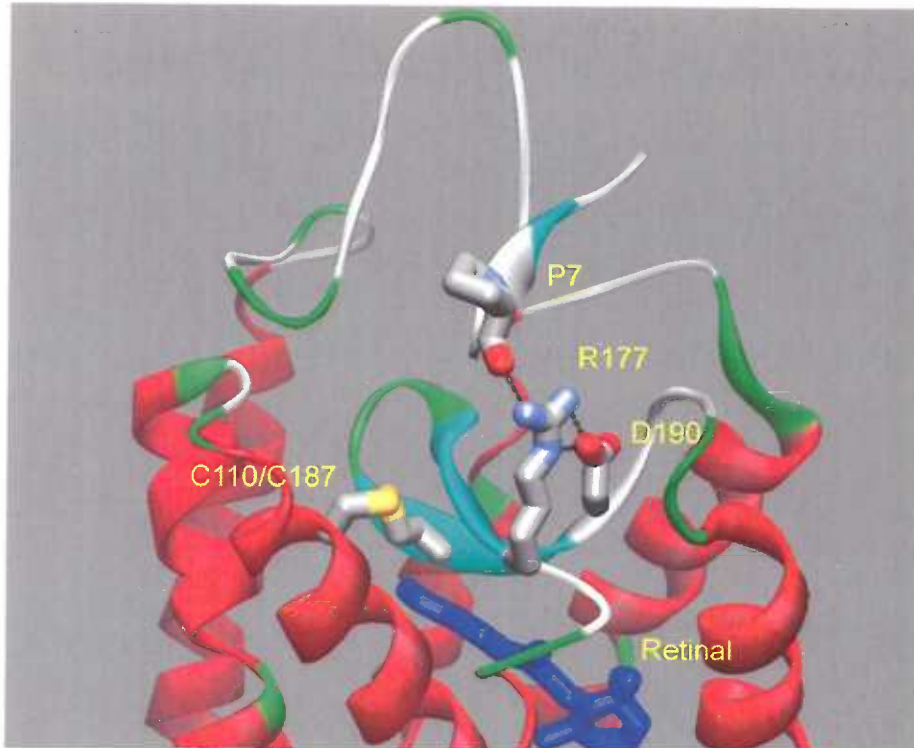
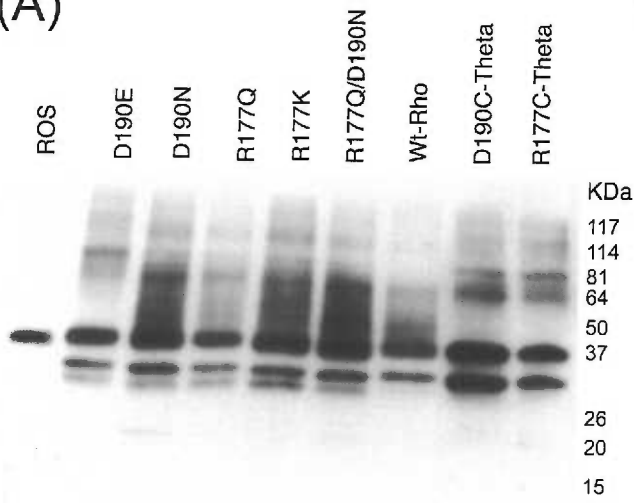


Figure 3. 2: Sequence alignment of loop E-2 for rhodopsin, β -2 adrenergic and CB1 cannabinoid receptors. Notice that the charged residues found in rhodopsin at R177 and D190 are mirrored in β AR and CB1. For comparison purposes conserved proline, tryptophan and cysteine residues are also highlighted.

RHO_bovine: PLVG-WSRYIPEGMQCSCGIDYYTPHE
RHO_mouse: PLVG-WSRYIPEGMQCSCGIDYTLKPEVNN
RHO_human: PFAG-WSRYIPEGLQCSCGIDYYTLKP
 β AR_mouse: PIQMHWRATHKKAIDCYTEETCCDFE
 β AR_human: PIQNGWRATHQEAINCYANETCCDFE
CB1_mouse: PLLGWNCKKLQSVCSDFPLIDETYLMEFW
CB1_human: PLLGWNCEKQLQSVCSDFPHIDETYLMEFW

Figure 3. 3: Immunoblot analysis of mutant rhodopsins. (A) Immunoblot of COS cell membrane fractions expressing mutant rhodopsin proteins, probed using the rho1D4 antibody. The full length ROS, COS expressed WT, and ion-pair mutants run at molecular weight values of ~38 kDa. The lower molecular weight bands most likely reflect under or unglycosylated opsins (61). (B) Immunoblot of purified ion-pair rhodopsin mutants. Purified recombinant rhodopsin mutants were prepared as described in Materials and Methods and probed using the rho1D4 antibody. ROS purified rhodopsin was included as a control. Notice that purification removes the lower weight species.

(A)



(B)

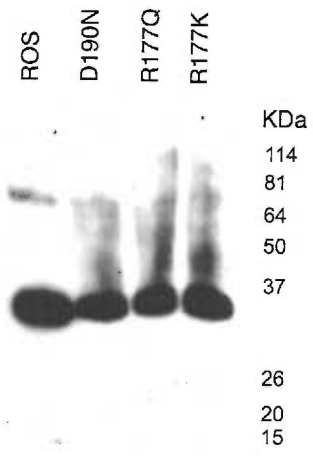


Figure 3. 4: Disrupting the R177/D190 ion-pair does not impair MII stability or function in mutants that regenerate with 11-*cis*-retinal. Left panels show representative results for mutant R177Q, right panels for mutant D190N. **(A)** Characterization of ion-pair mutants by UV/vis spectroscopy: DS, dark-state; $h\nu$, photobleached Meta II state; PSB, protonated Schiff base (at pH 1.9). Spectral property values are reported in Table 3. 1. **(B)** Arrhenius plots of retinal release rates from the MII state of ion-pair mutant rhodopsins. The rate constants were obtained from the retinal release assays (see Materials and Methods) performed in buffer D at pH 6.0, with temperatures ranging from 5 to 35 °C. For comparison, values obtained for wild-type rhodopsin are overlaid in black open circles fit with black lines. The activation energy (E_a) values determined from these assays are reported in Table 3. 1. **(C)** Example of transducin activation by ion-pair mutants. Transducin activation was measured by monitoring the increase in $G_{T\alpha}$ tryptophan fluorescence that occurs upon MII stimulation of the $G_{T\alpha}$ -GTP γ S complex formation. The arrow indicates the time of GTP γ S addition. The relative rates of transducin activation of the mutants compared to WT rhodopsin are reported in Table 3. 1.

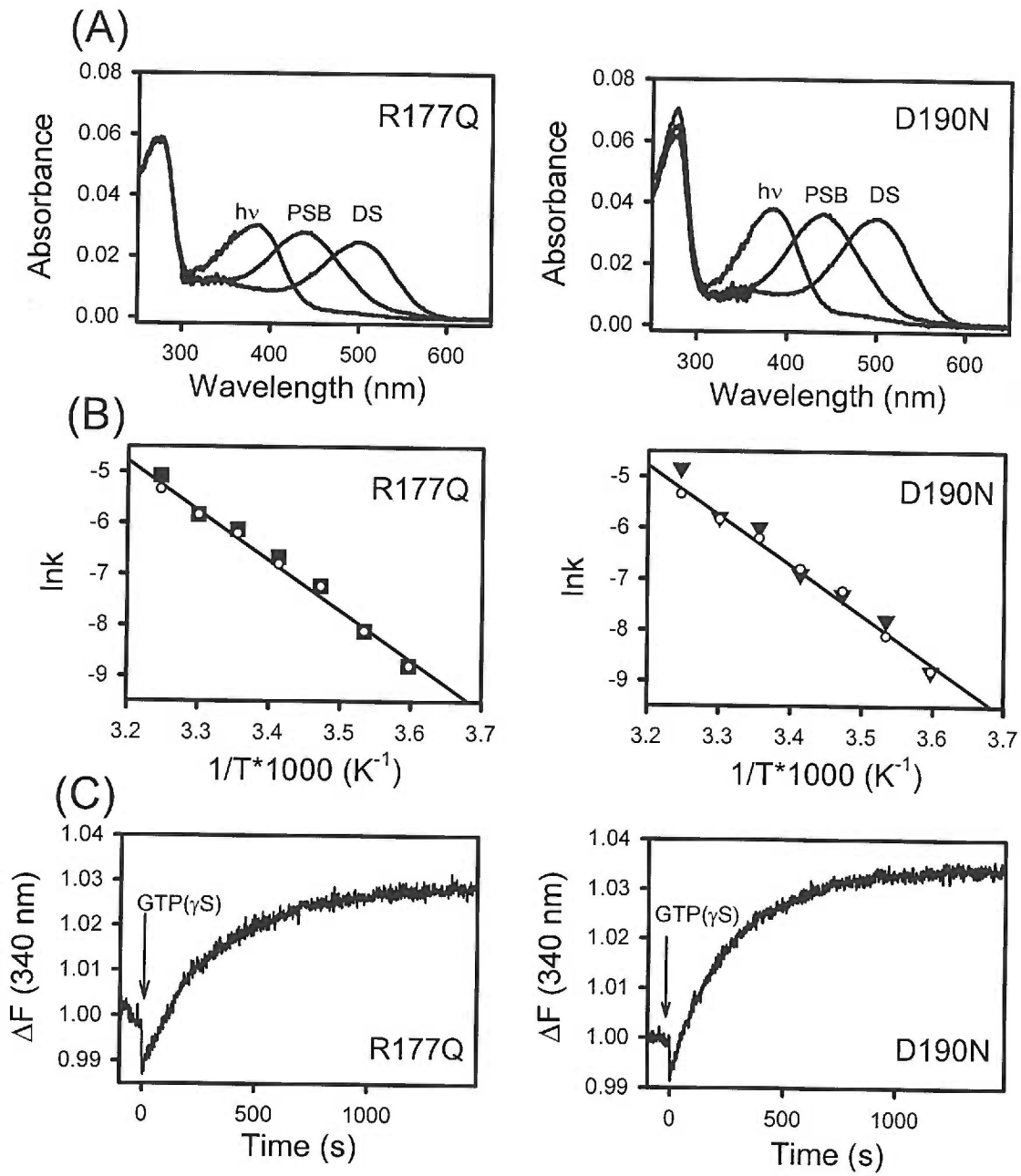


Figure 3. 5: Rapid thermal decay of R177Q mutant correlates with loss of functional ability, loss of Schiff base linkage, and release of chromophore. Top panels: Rapid loss of 500 nm absorbance for R177Q mutant correlates with loss in ability to activate transducin. **(A)** Representative spectra of mutant R177Q depicting loss of 500 nm absorbing species and gain in 380 nm species over time at 37 °C in buffer D. Spectra are plotted in 30 m intervals, with $t = 0$ as a darker line. **(B)** Transducin activation assays performed on mutant R177Q incubated in the dark at 37 °C and assayed at the indicated time points. The arrow indicates the time of GTP γ S addition. **(C)** Loss of 500 nm absorbing species (black circles) correlates with loss of functional activity. The relative rates of transducin activation of mutant R177Q following thermal decay at 37 °C for 0, 5 or 14 h, is plotted (open triangles) as the percent of initial R177Q activity. Bottom panels: Loss of 500 nm absorbance in R177Q mutant is due to retinal Schiff base hydrolysis and release of retinal from the chromophore-binding pocket. **(D)** The initial ($t = 0$ h) dark-state absorbance spectra (solid line) and acid denaturing spectra (dashed line) of mutant R177Q, at 37 °C shows the presence of protonated Schiff base. **(E)** After 14 hours and loss of 500 nm absorbance species (solid line), no protonated Schiff base is obtained upon acidification (dashed line), indicating retinal linkage has been hydrolyzed. **(F)** Thermal decay of the 500 nm absorbing species ($t_{1/2} = 198$ min see Figure 5C) correlates with the rate of retinal release from the chromophore-binding pocket, as monitored by increase in fluorescence at 330 nm from dark state species ($t_{1/2} = 187$ min). At the end of the experiment the sample was photobleached with white light, with no noticeable increase in tryptophan fluorescence suggesting the retinal has completely left the binding-pocket.

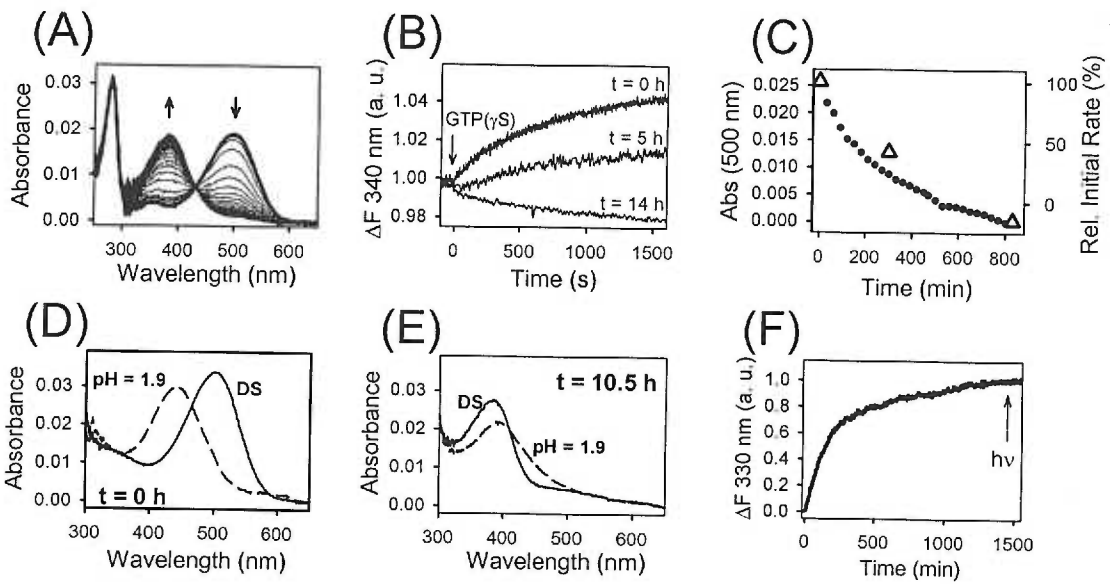


Figure 3. 6: Ion-pair mutants show much faster rates of thermal decay than wild type rhodopsin. Plot shows the loss of 500 nm absorbance at 55 °C as a function of time for WT rhodopsin and ion-pair mutants (WT, filled circles; R177K, filled diamonds; R177Q, open squares; D190N, open triangles; R177Q/D190N, filled hexagons). Data were fitted to a monoexponential decay function (see Materials and Methods) and the $t_{1/2}$ value for the process was determined for each mutant over a range of different temperatures. The values are given in Table 3. 2.

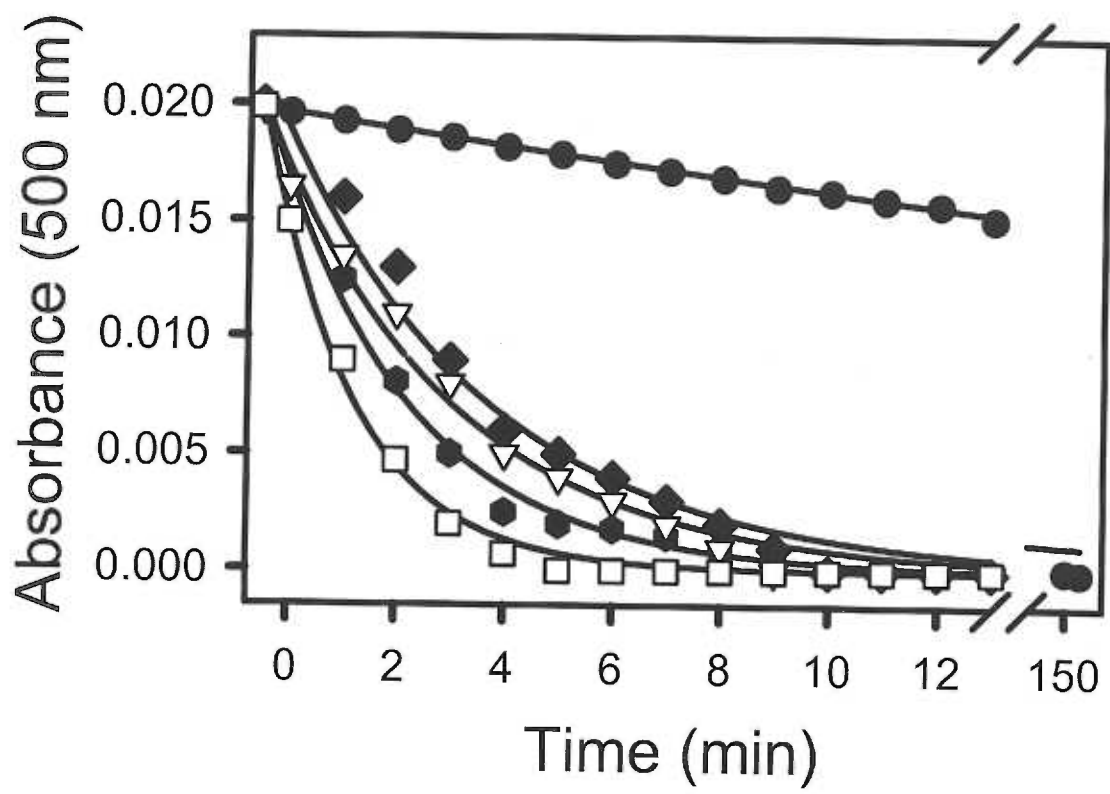


Figure 3. 7: Arrhenius plots of dark state thermal decay rates show ion-pair mutants have similar activation energies for retinal hydrolysis yet faster rates than wild type rhodopsin. The rate constants were obtained from the dark state thermal absorbance decay experiments (see Figure 3. 6), performed in buffer D, with the temperatures ranging from 37 to 55 °C (WT, filled circles; R177K, filled diamonds; R177Q, open squares; D190N, open triangles). The concave plot suggests two different processes may lead to thermal decay. The activation energy (E_a) and thermodynamic values approximated for these processes are presented in Table 3. 2.

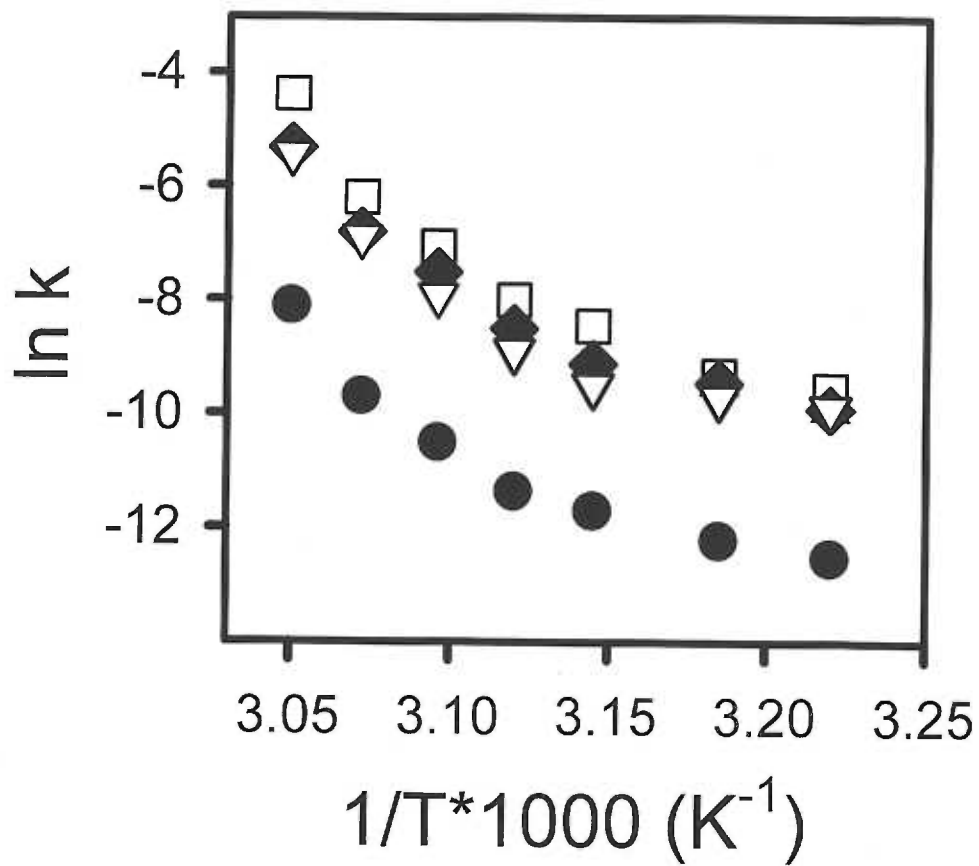
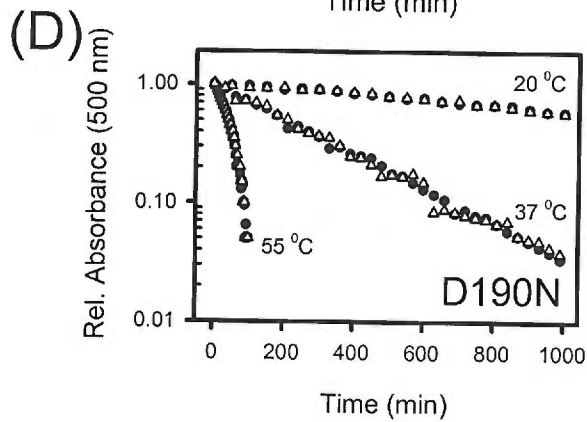
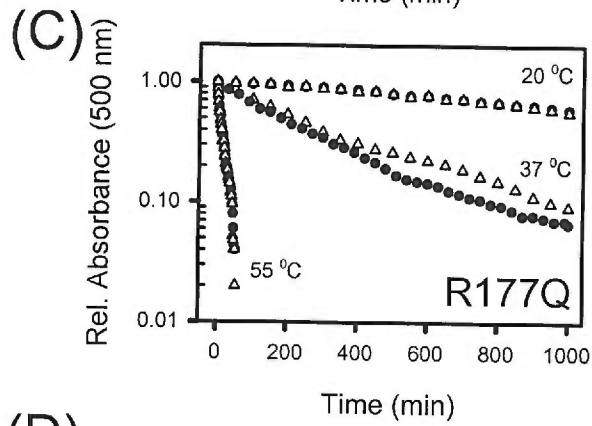
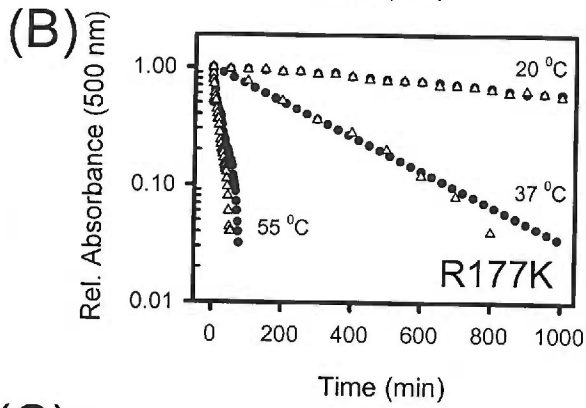
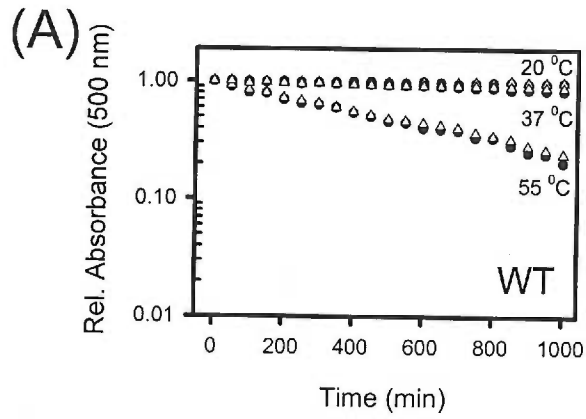


Figure 3. 8: Ion-pair mutants do not show increased susceptibility to hydroxylamine. The rate of thermal decay of (A) WT, or ion-pair disrupting mutant rhodopsins; (B) R177K, (C) R177Q, (D) D190N, is not increased in the presence of 50 mM hydroxylamine. Loss of λ_{500} nm absorbing species was monitored as a function of time in the presence (open triangles) or absence (filled circles) of 50 mM hydroxylamine, pH 6.0, in buffer D at 20, 37, and 50 °C. The initial λ_{500} nm absorbance of the samples was ~ 0.025 for comparison purposes, the data are plotted on a logarithmic scale with initial absorbance data normalized to 1.0.



3. 7: SUPPLEMENTAL MATERIAL

3. 7. 1: Comments on the photobleaching properties of R177Q/D190N.

As noted above, bleaching of the double mutant R177Q/D190N gives rise to a spectra with a primary absorption centered at 380 nm and a secondary shoulder centered at ~ 480 nm (Figure 3. S1). It is not know what the ~ 480 nm species represents, it may be either the MI or the MIII intermediate which both absorbs at this wavelength.

3. 7. 2: Salt effects on the thermal decay process.

The effect of salt on process of thermal decay was measured for rhodopsin mutant D190N. The rhodopsin structure contains multiple ion-pairs, which are thought to stabilize the dark state conformation (4, 51, 182, 197). Recent reports suggest that the presence of high concentrations of salt disrupts the MI \leftrightarrow MII equilibrium, yet may have a stabilizing effect on the conformation of decayed opsin (182, 197). These effects were most pronounced only at high concentrations of NaCl (greater than 2 M) and were interpreted as effecting the multiple ionic interactions that take place to stabilize the rhodopsin structure. We tested the possible effect that physiological levels of NaCl have on the decay process of representative ion-pair mutant D190N (Figure 3. S2). Under these conditions only a minor effect on the rate was observed; the $t_{1/2}$ without NaCl = 224 min, with NaCl = 205 min. Due to the multiple ionic interactions taking place within rhodopsin noted above, the effects of higher salt concentrations were not test as interpretation of their results would be difficult.

Figure 3. S1: Photobleaching properties of rhodopsin mutant R177Q/D190N.

Bleaching of dark state (DS) R177Q/D190N (red) for 30 s with >495 nm light ($h\nu$) gives rise to an intermediate with a primary λ_{max} at 380 nm and a secondary shoulder at ~ 480 nm (arrow).

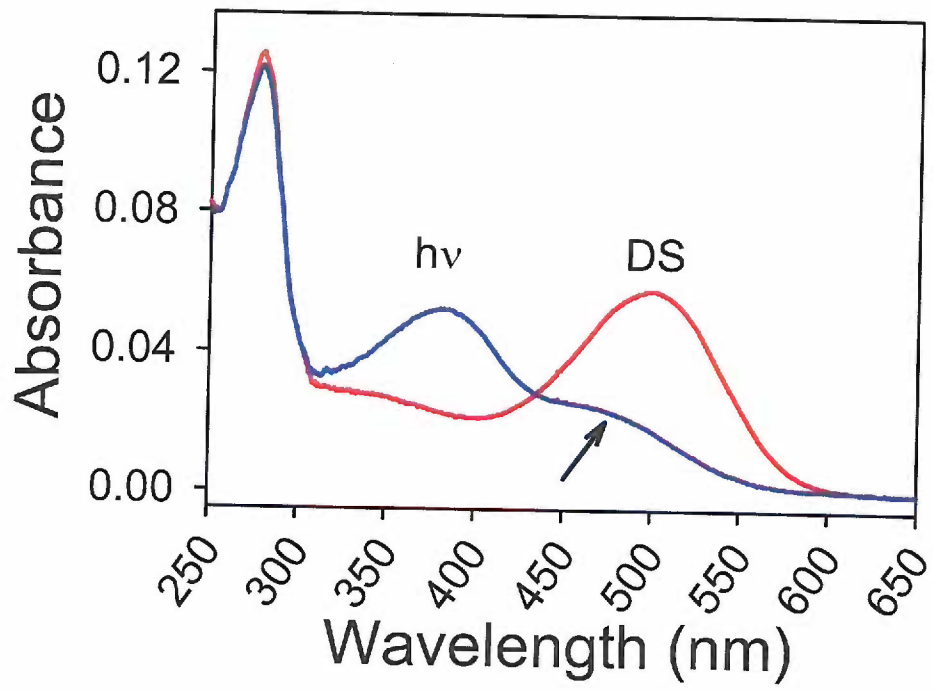
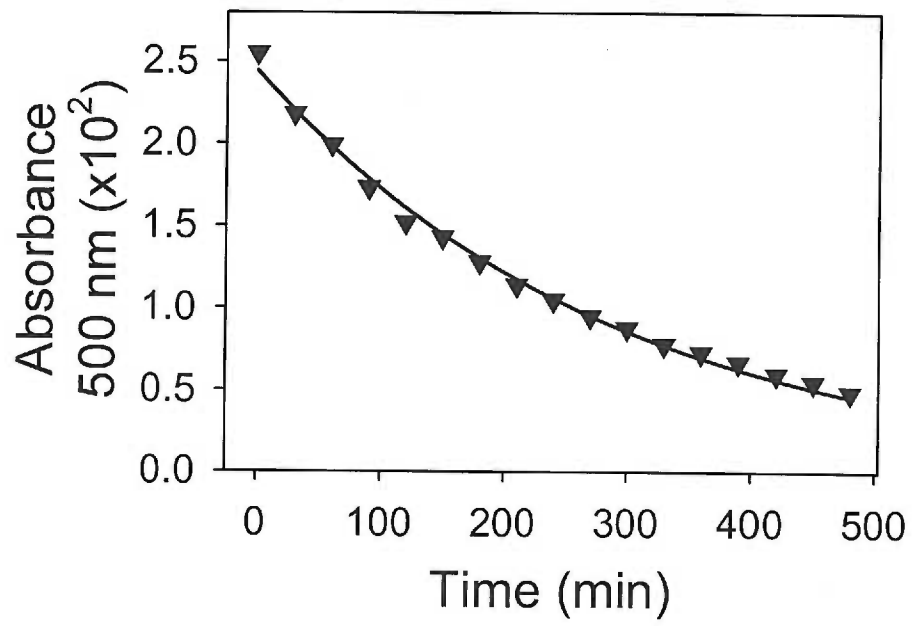


Figure 3. S2: Effects of 140 mM NaCl on the thermal decay process of rhodopsin mutant D190N. Thermal decay of ADRP mutant D190N in the presence of physiological levels of NaCl (140 mM). The decay process was measured as describe in Figure 3. 5A, under identical conditions but in the presence of NaCl. The NaCl did not drastically effect the rate of the 500 nm absorbance decay process, $t_{1/2} = 205$ min.



Chapter 4

Assessing Structural Elements That Influence Schiff Base Stability:

Mutants E113Q and D190N Destabilize Rhodopsin

Through Different Mechanisms.

Jay M. Janz[§] and David L. Farrens[§]

[§]Department of Biochemistry and Molecular Biology,

Oregon Health and Science University

3181 S. W. Sam Jackson Park Drive, Portland, Oregon 97239-3098

Running Title: Structural Mechanisms of Rhodopsin Schiff Base Stability.

4. 1: SUMMARY

This chapter reports our efforts to understand how interactions between the opsin apoprotein and its bound ligand, 11-*cis*-retinal, stabilize the Schiff base linkage which unites them into the functional rhodopsin photoreceptor. Utilizing techniques developed in the preceding chapters we investigate the process by which the counter-ion E113 influences Schiff base stability.

The stability of the retinal chromophore attachment varies between different visual pigments and may factor in some retinal disease states. Opsin appears to stabilize this Schiff base linkage by: i) affecting the hydrolysis chemistry, ii) shielding the retinal linkage from solvent, or iii) acting as a kinetic trap to slow retinal release. Here we describe methods to determine Schiff base stability in rhodopsin, present examples of dark state and MII rhodopsin stability differences, and show that studies of mutants E113Q and D190N demonstrate different parts of rhodopsin influence Schiff base stability in different ways.

All experiments reported in this chapter we performed by the author of this dissertation and portions of this chapter have previously been published: Janz, J. M., and Farrens, D. L. (2003) *Vision Research* **43**, 2991-3002.

4. 2: INTRODUCTION

Rhodopsin, the dim light photoreceptor of Rod cells, initiates a signal transduction cascade after light induces isomerization of its 11-*cis*-retinal ligand into the all trans-retinal configuration, thus converting rhodopsin into the active, signaling Metarhodopsin MII (MII) state (137). Signaling by the MII form may be attenuated or

“turned off” through different yet concomitant pathways. In one pathway, the MII form is recognized and phosphorylated by a rhodopsin kinase and then bound by the protein arrestin, thereby occluding further interaction of MII with its signaling G-protein transducin. Through a parallel pathway, the *all-trans* retinal Schiff base linkage of MII may be hydrolyzed and cleaved, releasing free retinal and leaving the “inactive” apoprotein, opsin (42-44).

Resetting the opsin back to the light sensitive form involves a complex series of events, called the retinoid cycle. During this cycle, the *all-trans* retinal released from MII is transported to the retinal pigment epithelium where it is enzymatically converted into an *11-cis* retinal form, then shuttled back to opsin, where it subsequently re-binds to regenerate light-sensitive rhodopsin (45). In recent years it has become apparent that some retinal diseases are caused by defects in this cycle. Note that both the first step (retinal release from MII) and the last step of the retinoid cycle (regeneration of opsin with *11-cis* retinal) rely on the chemically similar act of either forming or hydrolyzing a retinal Schiff base linkage.

What factors control Schiff base hydrolysis in rhodopsin? The basic chemistry of retinal Schiff base formation and hydrolysis was established years ago (74, 75), and more recently detailed information about the reaction has come from further studies of rhodopsin and model retinal Schiff base compounds in solution (85, 203). In the model compound studies, it has been found that Schiff base hydrolysis is rapid ($t_{1/2}$ of ~ 1 min at pH 6), and occurs even faster at lower pH values, presumably due to protonation of the retinal Schiff base (85). However, in the context of the whole protein, the model compound studies present an interesting paradox regarding the observed differences in

the stability between dark state and MII rhodopsin. Schiff base hydrolysis in dark state rhodopsin is very slow ($t_{1/2}$ on the order of days), even though the Schiff base is protonated, due to its unusually high pKa (83). In contrast, Schiff base hydrolysis in MII occurs within minutes, even though the Schiff base in MII is deprotonated (131) through a complex process (204). The literature presents conflicting theories regarding these observations. Some experts propose the high pKa of the retinal Schiff base linkage acts to suppress thermal isomerization, while others feel it blocks the spontaneous hydrolysis of the chromophore. Whatever the explanation, significant alterations in the Schiff base environment clearly must occur between the dark and MII states of rhodopsin.

Furthermore, Schiff base stability appears to vary for different types of opsin proteins (18). For example, the Schiff base linkage in cone opsins is much less stable than rhodopsin (98, 205, 206), and the cone cells seem to accommodate for this by undergoing rapid regeneration during continuous illumination, thus extending their activity by recycling (205). Taken together, the above examples indicate that structural factors in rhodopsin play a major role in controlling the stability of the retinal Schiff base linkage.

What are these structural factors? We feel the rhodopsin structure imparts stability to the retinal Schiff base linkage in three different ways; i) by affecting the chemistry of Schiff base hydrolysis, ii) by limiting the accessibility of the Schiff base to solvent, and iii) by acting as a "kinetic trap" that inhibits the release of transiently hydrolyzed retinal, thus encouraging re-binding and reformation of the Schiff base linkage. Cartoon representations of these three concepts are shown in Figure 4. 1.

We have begun to try and determine the relative contribution each of these factors makes to Schiff base stability (179, 207). Our approach is to mutate key residues

suggested by the rhodopsin crystal structures (52-54), and then assess their role in stability, using a combination of spectroscopic and kinetic analysis methods.

Essentially, it is possible to think of Schiff base hydrolysis in enzymatic terms, and begin to probe and define the reaction pathway using traditional enzymological methods. In the present paper, we describe how we are using these approaches to define the kinetics and energetics of Schiff base hydrolysis in wild-type rhodopsin, and we present examples of how these rates are altered in different ways by two destabilizing mutations, E113Q and D190N. As seen in Figure 4. 2, these residues are located at different distances in relation to the Schiff base. Mutation E113Q is located at the site of the Schiff base “counter-ion”, and mutation D190N is located in a highly conserved ion-pair at the ends of loop E-2 (207), and interestingly is also an Autosomal Dominant Retinitis Pigmentosa (ADRP) mutation (63, 175). We show here that the retinal Schiff base stability is altered in both of these mutants, apparently through substantially different mechanisms.

4. 3: MATERIALS and METHODS

4. 3. 1: Materials

Except where noted below, all buffers and chemicals were purchased from either Fisher (Pittsburgh, PA) or Sigma (St. Louis, MO). Dodecyl maltoside (DM) was purchased from Anatrace (Maumee, OH). Frozen bovine retinas were from J. A. Lawson Co. (Lincoln, NE). DNA oligos were purchased from Invitrogen (Carlsbad, CA). Restriction endonucleases were from New England Biolabs (Beverly, MA). 11-*cis* retinal was a generous gift from Dr. R. Crouch (Medical University of South Carolina and National Eye Institute). The rho1D4 antibody was purchased from the National Cell

Culture Center (Minneapolis, MN). The nonapeptide corresponding to the C-terminus of rhodopsin was acquired from the Emory University Microchemical Facility (Atlanta, GA). The definitions of the buffers used are as follows: PBSSC [0.137 M NaCl, 2.7 mM KCl, 1.5 mM KH₂PO₄, and 8 mM Na₂HPO₄ (pH 7.2)], buffer A [1% DM and PBSSC (pH 7.2)], buffer B [2 mM ATP, 0.1% DM, 1 M NaCl, and 2 mM MgCl₂ (pH 7.2)], buffer C [0.05% DM and PBSSC (pH 7.0)], buffer D [0.05% DM and 5 mM 2-(N-Morpholino)-ethanesulfonic acid Monohydrate (MES) (pH 6.0)].

4. 3. 2: Construction, expression and purification of rhodopsin and recombinant rhodopsins

For construction, expression and purification of rhodopsin mutants please refer to section 2. 3. 3 and 2. 3. 4 in chapter 2.

4. 3. 3: UV/vis Absorption Spectroscopy.

For UV/vis absorption spectroscopy please refer to section 2. 3. 5 in chapter 2.

4. 3. 4: Thermal Bleaching of Rhodopsin Samples.

Thermal hydrolysis rates were measured by UV/vis spectroscopy in buffer D as previously described (207). Specific temperatures were maintained using water-jacketed cuvette holders connected to a circulating water bath. Thermal stability of the mutants was determined by first measuring the samples from 650 nm to 250 nm at various intervals at a given temperature. Thermal hydrolysis rates were subsequently measured by monitoring the decrease of the 500 nm absorbing dark-state species from these measurements over time (102, 181, 197, 207). Baseline drift was corrected for by normalizing all spectra to an absorbance of zero at 650. Dark state thermal hydrolysis rates for mutant E113Q were measured by monitoring the increase in tryptophan

fluorescence at 330 nm, caused by the release of retinal from the chromophore-binding pocket (154). The experimental setup was as previously described and similar to that of the retinal release assay (described below) except that the samples were not photobleached, and excitation band pass settings of $\frac{1}{4}$ nm were used to minimize sample bleaching as previously described (207). We have previously shown that dark state hydrolysis rates obtained in this manner are similar or equal to rates obtained using the absorbance assay (207). A control experiment (using WT rhodopsin at pH 6, 37 °C, over 13 hours) using our described instrumental conditions shows less than 3% bleaching by the excitation beam (not shown). All thermal decay data was analyzed using mono-exponential decay (absorbance experiments) or mono-exponential rise to maxima (fluorescence experiments) fitting algorithms in Sigma Plot (Jandel Scientific Software).

To monitor the pH dependence of WT and mutant E113Q hydrolysis rates the measurements were performed in Buffer D as described above with the following modifications: Adjustment of pH to 5.0 or 7.5 was performed by adding a small aliquot (~10 μ L) of either 500 mM MES pH 5.0, or 500 mM, 2-amino-2-hydroxymethyl-1,3-propanediol (Tris) pH 7.5 to the purified sample. The buffering pH was confirmed using pH paper strips, and subsequent measurements using a small Corning pH microelectrode indicated the reported values are correct to within ~ 0.1 pH units. In this manner the correct assay pH was obtained with little perturbation to the protein and only slight alterations of the buffering conditions.

4. 3. 5: Measurement of the Rate of Retinal Release and/or MII Decay by Fluorescence Spectroscopy.

The MII stability was assessed as previously described (154), using a Photon Technologies QM-1 steady state fluorescence spectrophotometer. Briefly, the assays involved measuring the increase in fluorescence that occurs over time as the retinal is released from opsin during MII hydrolysis/decay. The studies were carried out using 100 μ L of a 250 μ M mutant sample in buffer D unless otherwise noted; the sample temperature was maintained as described above. After the samples were photobleached to the MII state (see above), the retinal release measurements were carried out at the appropriate temperature by exciting the sample for 3 s (excitation wavelength = 295 nm, $\frac{1}{4}$ nm bandwidth slit setting) and then blocking the excitation beam for 42 s, to avoid further photobleaching the samples. Tryptophan fluorescence emission was monitored at 330 nm (12-nm bandwidth slit setting), and this cycle was repeated during the course of each measurement. To determine the $t_{1/2}$ values for retinal release, experimental data was analyzed using a mono-exponential rise to maxima fit in Sigma Plot (Jandel Scientific Software). In this manner a series of MII hydrolysis rates were obtained at 5, 10, 15, 20, 25, 30, and 35 $^{\circ}$ C, and their rates were applied to the Arrhenius equation, $k = Ae^{-E_a/(RT)}$, to determine the activation energy (E_a) of the retinal release process for each mutant rhodopsin. Although we also measured MII decay rates at 40 and 45 $^{\circ}$ C for WT rhodopsin at the different pH values and include them in Figure 3 for visual reference, these values were not used in calculating the activation energies, since they could not be well fit to a single rate. Lower temperature rate experiments (5, 10, and 15 $^{\circ}$ C) were omitted for mutant E113Q at pH 6.0 and pH 7.5 due to its greatly decreased retinal

release rates. The pH dependence of retinal release for mutant E113Q was monitored as described above (see 2. 3. 4: Thermal Bleaching of Rhodopsin Samples).

4. 3. 6: Hydroxylamine Reactivity.

For hydroxylamine reactivity please refer to section 3. 3. 11 in chapter 3.

4. 4: RESULTS

4. 4. 1: Retinal Schiff base hydrolysis can be monitored using spectroscopic methods.

The integrity of the rhodopsin protein and the retinal linkage can be assessed by analysis of absorbance spectra, as shown in Figure 4. 3A. The figure shows the differences in dark state (DS) absorbance at 500 nm, MII absorbance at 380 nm, and the absorbance at 440 nm which occurs after acidifying DS rhodopsin to produce a protonated Schiff base (PSB). The simplest indirect way to monitor Schiff base hydrolysis rates in DS rhodopsin is to follow the loss of 500 nm absorbance and increase in 380 nm absorbance that occurs as the Schiff base linkage is hydrolyzed, as shown in Figure 4. 3B. Unfortunately, monitoring the rate of Schiff base hydrolysis during MII decay by absorbance spectroscopy is difficult because free retinal ($\lambda_{\max} = 385$ nm) and MII ($\lambda_{\max} = 380$ nm) have similar spectral properties (compare Figure 4. 3B with Figure 3A). One can measure rates of MII decay by acidifying aliquots of sample at different time points to detect the amount of remaining (protonated) Schiff base that absorbs at 440 nm (the PSB shown in Figure 4. 3A). An easier way to measure MII decay is to monitor the increase in opsin fluorescence at 330 nm that occurs as retinal leaves the binding pocket (44, 154). As shown in Figure 4. 3C, rates determined using this fluorescence

approach exactly mirror the rates determined using the more laborious acid protonation method, and the fluorescence assays require much less sample (an important point when studying mutant rhodopsin proteins).

Using these approaches we have previously measured the rate of Schiff base hydrolysis from both DS and MII rhodopsin at different temperatures, and show these results in Figure 4. 3D in the form of a classic Arrhenius plot. Two things are especially noteworthy about these plots. First, at each of the pH values we tested (pH 5.0, 6.0 and 7.5), the plot for dark state rhodopsin (circles) is not linear; rather it shows a concave Arrhenius plot. Second, at the lower, more physiologically relevant temperatures (from 37° C to 47° C), the rates for dark state and MII (triangles) hydrolysis differ by orders of magnitude, yet show similar energetics for hydrolysis (the slopes of the plots, and thus calculated E_a 's are similar). The implication of these observations is explored further in the Discussion. Below we present examples of how rhodopsin mutants can be used to explore the cause and implication of these unusual Arrhenius plots.

4. 4. 2: Spectral properties of mutants E113Q and D190N.

Figure 4 shows the spectral properties of mutants E113Q and D190N. The absorbance spectrum of the counter-ion mutant E113Q is highly pH sensitive, as shown in Figure 4. 4A. At higher pH, the 500 nm absorbance completely disappears, whereas at pH 5 the protein is fully in a 500 nm absorbing form. By titrating this unusual pH dependent absorbance effect, Oprian and colleagues have recently shown the Schiff base pKa for E113Q is 6.4 (208) compared to the pKa > 16 for wild-type rhodopsin (83). Figure 4. 4B shows an example of photoproperties of E113Q at pH 6.0. Bleaching this sample with >495 nm light results in full conversion of the residual 500 nm absorbing

form to the 380 nm absorbing MII species, and acidification results in a protonated Schiff base (PSB) which absorbs at 440 nm. Figure 4. 4C shows the spectral properties of mutant D190N. D190N shows a normal 500 nm absorbance in the dark state form which converts to a 380 nm MII form upon irradiation with >495 nm light, and as for wild type, acidification results in a 440 nm protonated Schiff base (compare Figure 4. 4C with Figure 4. 3A). Thus, although the Schiff base in mutant D190N is destabilized (discussed below), its spectral properties are almost identical to wild type rhodopsin.

4. 4. 3: Arrhenius analysis of mutants E113Q and D190N indicates the retinal Schiff base linkage can be destabilized in fundamentally different ways.

Figure 4. 5 shows how the DS and MII Schiff base stability varies widely between WT rhodopsin, mutant E113Q and mutant D190N. Analysis of these plots reveals several interesting points. For example, the dark state hydrolysis of the counter-ion mutant E113Q is dramatically faster than WT rhodopsin, and does not exhibit a concave Arrhenius plot (Figure 4. 5A). Note that because E113Q has a complicated absorbance spectrum at different pH values, (see Figure 4. 4A), for this mutant we measured the rates of hydrolysis using the fluorescence assay that monitors the increase in opsin fluorescence as retinal leaves the protein-binding pocket (see (207) for more details). As can be seen in the plots, the energetics and rates of Schiff base hydrolysis for mutant E113Q in the dark state are pH sensitive – as the pH is increased from 5 to 7.5; the slope (and thus E_a) increases from ~20 kcal/mol to ~39 kcal/mol (see Table 4. 1). In contrast, the rate of Schiff base hydrolysis in the MII form of E113Q is substantially slower than that observed for WT rhodopsin, and shows a steeper slope (and thus higher E_a) for hydrolysis. Interestingly, we find the rates for hydrolysis in MII are similar for pH 6.0

and pH 7.5, whereas at pH 5 the rates (and thus slope and E_a values) are much more like WT rhodopsin. One complication with the pH 5 studies is that at the higher temperatures, both mutant E113Q and wild type rhodopsin began to exhibit both a fast component and a fraction of a slower component to the fluorescence increase. For the data shown here in Figure 4. 5B, only the faster components at pH 5 were plotted.

In contrast, mutant D190N, a mutation associated with ADRP (63, 175), shows faster DS hydrolysis yet retains the concave Arrhenius plot seen for WT (Figure 4. 5C). Since the slopes of the plots are identical, it indicates the activation energies are not affected by the D190N mutation, only the kinetics. Surprisingly, in the MII state the decay rates for D190N are not affected, indicating the retinal linkage stability in the active state of this mutant is not affected (Figure 4. 5D). Similar results were found for other mutations in the conserved R177/D190 ion pair (207). Clearly, these results indicate mutations can affect the stability of the retinal linkage in different ways and in a state-dependent manner. One way to probe the mechanisms responsible for these phenomena is to measure the susceptibility of the Schiff base linkage to exogenously added agents, as described below.

4. 4. 4: Differences in hydroxylamine reactivity indicate the retinal Schiff base linkage can be destabilized in fundamentally different ways.

An approach that has long been used to measure the solvent accessibility of retinal in studies on rhodopsin and bacteriorhodopsin is to use the small molecule hydroxylamine (NH_2OH), which rapidly cleaves retinal Schiff base linkages. As shown in Figure 6, top panel, 50 mM hydroxylamine has no effect on the hydrolysis rate of dark state WT rhodopsin. In contrast, the counter-ion mutant E113Q is very susceptible to

hydroxylamine as shown in Figure 4. 6, middle panel. Again, due to the complicated pH dependent absorbance spectrum of E113Q (see Figure 4. 4A), these experiments were carried out using the fluorescence assay to monitor retinal release after Schiff base hydrolysis. Curiously, although dark state decay in mutant D190N is much faster than WT rhodopsin, it is not affected by hydroxylamine, even at 50 mM. The results of the above analysis are compiled in Table 4. 1.

4. 5: DISCUSSION

4. 5. 1: Overview of Chapter.

In all known visual pigments, the retinal chromophore attaches to the apoprotein through a Schiff base linkage. The stability of this linkage varies widely between different opsins, and may factor in some retinal disease states (207-211). Unfortunately, the factors that control retinal Schiff base linkage stability in bovine rhodopsin are not well understood, thus, we are trying to define and establish the key factors involved. Towards this goal we are developing methods to determine to what extent individual parts of the rhodopsin structure influence Schiff base stability. Our working assumption is that the protein influences Schiff base stability in three fundamentally different ways: i) by affecting the hydrolysis chemistry through the involvement of residues near the Schiff base, ii) by shielding the retinal linkage from solvent, and/or iii) by acting as a kinetic trap to slow the rate of retinal release.

Earlier in this paper, we described methods we are using to study retinal Schiff base stability in rhodopsin, and showed how these methods indicate clear differences between DS and MII stability in wild type rhodopsin, as well as between two unstable

rhodopsin mutants, E113Q and D190N. In the following section, we describe how the analysis of these results clearly indicates different elements in the rhodopsin structure influence Schiff base stability in different ways.

4. 5. 2: Wild-type rhodopsin exhibits an unusual Arrhenius plot for dark state hydrolysis.

We noted earlier that analysis of Schiff base hydrolysis in dark state wild-type rhodopsin shows a non-linear, concave Arrhenius plot (207). What is the implication of this finding? The most common explanation for concave Arrhenius plots is that two or more different rate-limiting steps are involved (198). With this possibility in mind, the WT rhodopsin data can be fit assuming two different activation energies, one with an E_a value of ~ 16 kcal/mol (for 37 – 47.5 °C), and another with an E_a value of ~ 103 kcal/mol (for the 47.5 – 55 °C temperature range).

What could cause the different E_a values? The higher activation energy barrier observed at the higher temperature range may be due to rhodopsin being thermally denatured and thus causing a repositioning of key amino acids involved in Schiff-base formation, hydrolysis and stabilization. This repositioning would then retard hydrolysis and thus increase the activation energy required (E_a). The lower E_a suggests that at more physiologically relevant temperatures the rhodopsin structure ensures that the energetics required for hydrolysis are not large, and thus the hydrolysis can occur more efficiently. The lower E_a also suggests a process may occur more efficiently at low temperatures (such as proton tunneling) than the process(es) that occur more efficiently at higher temperatures. Alternately, the concave plots may indicate that the pre-exponential factor

in the Arrhenius analysis has changed (the pre-exponential factor is related to steric factors and/or the efficiency with which the collisions lead to a productive reaction (198))

The higher E_a value (~ 103 kcal/mol) has previously been observed in other rhodopsin thermal stability studies (102), and recent studies are beginning to carefully address factors that influence the thermodynamics of rhodopsin protein stability (196, 197, 212). However, to the best of our knowledge the lower E_a value we describe here for Schiff base hydrolysis (and in (207)) has not previously been reported. This lower E_a value has interesting implications - it indicates the activation energy barrier for hydrolysis of dark state rhodopsin is actually similar (and in fact is lower) than the energy barrier for hydrolysis in the MII state (compare WT values of 16.1 kcal/mol for DS vs. 20.2 kcal/mol for MII, Table 4. 1). Thus, at physiologically relevant temperatures, the greater stability for the Schiff base linkage in DS vs. MII state is not simply due to a higher E_a . In other words, although the hydrolysis rate is much faster in MII, the E_a is not much greater than for the DS rhodopsin at lower temperatures. Taken together, these data suggest that a major way that the opsin protein affects Schiff base stability is by altering the kinetic rate of Schiff base hydrolysis, not the activation energy for bond hydrolysis.

As described above, Arrhenius analysis of Schiff base stability can help dissect the relative contribution of different factors to Schiff base hydrolysis. Below, we discuss how applying this approach to study key rhodopsin mutants can be used to address the relative contribution of each factor to Schiff base stability.

4. 5. 3: Mutation E113Q dramatically alters the stability of the retinal Schiff base in MII rhodopsin, in a pH dependent fashion.

Prior to the rhodopsin crystal structure, mutagenesis studies identified residue E113 as the counter-ion to the protonated Schiff base, and showed this residue plays a key role in controlling the absorbance spectrum of dark state rhodopsin (69, 70, 184). Early on, it was also noticed the rate of MII decay in mutant E113Q is dramatically slowed, with a $t_{1/2}$ of ~ 150 min at pH 6.0 (69, 186), in contrast to the usual rate of ~ 15 min for WT rhodopsin (154). We have re-explored this phenomenon and report here the slow rate of MII decay in E113Q is likely due to the fact that it has a larger activation energy for hydrolysis; at pH 6.0 and pH 7.5 the E_a is ~ 39 kcal/mol instead of the E_a of ~ 20.2 kcal/mol observed for WT rhodopsin MII hydrolysis rhodopsin. Interestingly, MII hydrolysis in E113Q is also pH dependent – at pH 5.0 the rates are dramatically faster and the E_a becomes ~ 19 kcal/mole, more like WT rhodopsin. (Note that at higher temperatures, for both WT and E113Q at pH 5 we observed a second, slower component in the MII fluorescence increase data). We are in the process of studying this observation but do not yet have an explanation for its origin. These results again suggest protonation of the Schiff base is rate-limiting step for hydrolysis.

4. 5. 4: Mutation E113Q dramatically reduces Schiff base linkage stability in dark state rhodopsin in a pH dependent fashion.

We find mutant E113Q is very unstable in the dark state, exhibiting a rapid rate of Schiff base hydrolysis (see Figure 4. 5A and Table 4. 1). For example, at 37°C the $t_{1/2}$ for DS hydrolysis in WT rhodopsin is $\sim 3,100$ min, whereas at the same pH and temperature the $t_{1/2}$ for DS hydrolysis in mutant E113Q is ~ 29 min, two orders of magnitude

difference. This point may explain why this mutant often appears to have poor expression - it may in fact express well, but rapidly falls apart during purification or storage.

The rate of Schiff base hydrolysis in DS E113Q is clearly pH dependent and seems to correlate with protonation of the Schiff base linkage (see the Absorbance spectrum in Figure 4. 4A). Again, these data indicate a critical role for Schiff base protonation in the overall process of hydrolysis at physiologically relevant temperatures. Furthermore, we find lowering the pH and thus protonating the Schiff base in E113Q (going from pH 7.5 to 5.0) both increases the rate and lowers the E_a barrier for hydrolysis. Note that we are safe in assuming that lowering the pH to 5.0 results in a predominantly protonated Schiff base for mutant E113Q, as the Oprian laboratory has recently shown the pK_a for E113Q is 6.4 (208). These observations are noteworthy in light of previous work on model retinal Schiff base studies that proposed Schiff base protonation is the rate-limiting step in hydrolysis (85), and recent results that show mutant E113Q exhibits a slower rate of Schiff base formation, consistent with the role this residue may play as the general base in Schiff base formation (211). Taken together, studies on mutant E113Q clearly indicate an example of the opsin protein structure affecting the “chemistry” of Schiff base hydrolysis. Our results do not completely rule out the possibility that a different group (linked to the Schiff base through a hydrogen bond network) may actually be the residue protonated at the lower pH values. Note also that some of the behavior of mutant E113Q may be due to other factors as well, such as the cognate partner in the Schiff base counter ion, K296, being left without a counter-stabilizing charge or the perturbation of a water molecule(s) near the Schiff base that

could be intimately involved in Schiff base formation/hydrolysis (213). It will be interesting to see how different anions, which can change the Schiff base pK_a in WT rhodopsin (214), will affect the rates of Schiff base hydrolysis in E113Q.

4.5.5: Mutant E113Q is highly susceptible to hydroxylamine.

We find mutant E113Q is highly susceptible to hydroxylamine, as previously reported (69, 186). There are at least two possible causes for this increased reactivity - the E113Q mutation may increase the accessibility of the Schiff base to external solvent, perhaps by disrupting the network of hydrogen bonds connecting loop E-2 with the Schiff base (54, 111), or the E113Q mutation may increase the reactivity of the Schiff base to hydroxylamine. At present it is difficult to ascertain which effect is dominant, although we are in the process of elucidating the preferred mechanism.

4.5.6: Mutation D190N (in the conserved R177/D190 ion pair) dramatically alters the stability of the retinal Schiff base in dark state rhodopsin but does not affect the MII state.

Mutant D190N provides a clear example of a situation in which the Schiff base linkage is destabilized through a process that does not affect the activation energy barrier to hydrolysis. Studies of this mutant have forced us to consider a “kinetic trap” hypothesis for the role of loop E-2 in rhodopsin, as described below. Recently, we noticed the ends of loop E-2 in rhodopsin appear to be held together by an ion-pair, R177/D190 (see Figure 4. 2). Through characterizing the effect of mutations at this site, it became clear this ion-pair is important for stabilizing DS rhodopsin, but has no effect on MII stability. We find this point intriguing – the fact that MII decay in the ion-pair mutants is not affected suggests the R177/D190 ion-pair is not present in MII rhodopsin,

perhaps due to some structural change in this region during MII formation (200). In the present paper our discussion is focused on mutant D190N, since *in vitro* this mutation is wild type like in its ability to bind retinal and activate transducin (207), yet is observed in some patients with ADRP (63, 175).

As mentioned above, Arrhenius analysis indicates mutant D190N is destabilized through an effect on the kinetics, not the energetics of Schiff base hydrolysis. As shown in Figure 4. 5, hydrolysis in D190N still has a concave Arrhenius plot, indicating the E_a for hydrolysis has not changed, although the rates of hydrolysis are clearly faster (see Table 4. 1). Furthermore, mutation D190N also does not change the susceptibility to hydroxylamine, a most surprising result. Taken together, we interpret these results as follows: the ion-pair helps loop E-2 to act as a “kinetic trap”, blocking release of transiently hydrolyzed retinal in dark state rhodopsin. This would be consistent with the data indicating the kinetic rates of hydrolysis are affected, but neither the energetics of stability (Fig. 4. 3), nor the accessibility to exogenous reagents (Figure 4. 4).

4. 5. 7: Summary of mutant’s behavior vs. WT rhodopsin.

Although mutations E113Q and D190N both increase the rate of Schiff base hydrolysis, and thus appear to destabilize retinal Schiff base stability, they do so through significantly different mechanisms. The E113Q mutation affects the energetics of hydrolysis process, whereas the D190N mutation does not. Mutant E113Q (inside the protein, near the Schiff base) shows an increased reactivity (and by inference, accessibility) to hydroxylamine. In contrast, mutation D190N (on the outside of loop E-2) destabilizes the Schiff base yet appears to do so without affecting the energetics of hydrolysis, and without increasing the susceptibility/reactivity of the Schiff base to

hydroxylamine (see Figure 4. 5C, and Figure 4. 6, bottom panel, and (207)). This latter finding has sparked our interest in the possibility of a “kinetic trap” role for loop E-2, and raises the possibility that this loop in other GPCRs may play a general role for slowing the off rate of ligands, since loop E-2 may adopt a similar structure in other GPCRs (215)

4. 5. 8: Summary.

Our goal in this chapter was to provide an overview of ways that the rhodopsin structure can lend stability to the retinal Schiff base linkage. How the recently proposed secondary retinal binding site(s) in rhodopsin (216) affect retinal stability perhaps by influencing the kinetics of retinal release remains to be determined. Our future studies will focus on examining the role of a network of hydrogen bonded residues and water molecules that together link loop E-2 to the retinal Schiff base, as well as assessing how the dynamics of loop E-2 effect Schiff base stability. It will also be interesting to use the approaches outlined here to assess what structural factors affect Schiff base stability in other retinal proteins, such as the cone and invertebrate opsins.

4. 6: ACKNOWLEDGMENTS

This research was supported in part by grants EY12095 and DA14896 to D. L. Farrens and T32-EY07123-09 to J. M. Janz from the National Institutes of Health. The authors wish to thank Dr. John Denu and Dr. Ujwal Shinde for helpful discussion. A preliminary version of this data was presented at the 7th Annual Vision Research Conference: The Retinoid Cycle and Retina Disease, Fort Lauderdale, FL, 2003.

Table 4. 1: Schiff Base Hydrolysis Characteristics for WT Rhodopsin and Mutants E113Q and D190N^a.

Mutant	pH	DS hydrolysis $t_{1/2}$ 37 °C (min) ^b	DS hydrolysis E_a 37 °C (kcal/mol) ^c	DS hydrolysis E_a 55 °C (kcal/mol) ^c	MII hydrolysis $t_{1/2}$ 20 °C (min) ^d	MII hydrolysis E_a (kcal/mol) ^e	Hydroxylamine reactivity $t_{1/2}$ (min) ^e
WT	5.0	2110	19.0	89	12	19.8	nd ^g
WT ^f	6.0	3100 ± 45	16.1	103	13.2	20.2	3100
WT	7.5	2410	19.2	92	11.8	19.6	nd
E113Q	5.0	7.7	22.2	22.2	6.1	19.5	nd
E113Q	6.0	29	32.1	32.1	125	39.2	4.8
E113Q	7.5	150	54.8	54.8	198	39.1	nd
D190N ^f	6.0	224 ± 15	17.2	107	11.6	20.8	215

^a All experiments performed in buffer D, pH adjustments performed as described in Materials and Methods.

^b Dark-state thermal hydrolysis rates obtained from absorbance measurements (WT and D190N) or fluorescent measurements (E113Q) at respective temperatures.

^c Activation energies (E_a) obtained from linear regression of Arrhenius plots (Figures 4. 4. 4. 5). For further details see Discussion.

^d MII hydrolysis assays performed as described in Materials and Methods.

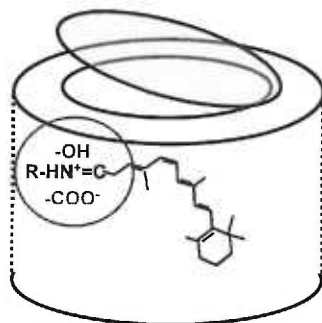
^e Hydroxylamine reactivity rates determined from mono-exponential fits of dark state thermal hydrolysis experiments performed at pH 6.0, 37 °C in the presence of 50 mM pH buffered hydroxylamine. For further details see Materials and Methods.

^f Values for WT at pH 6.0 and mutant D190N taken from (207).

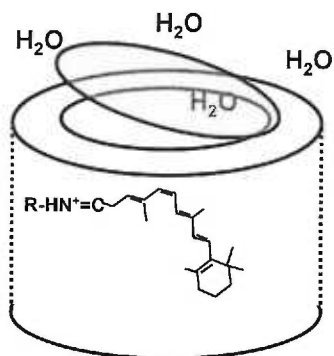
^g nd = not determined.

Figure 4. 1: Cartoon representation of three different ways the rhodopsin structure might affect stability of retinal Schiff base linkage, by: i) affecting the “chemistry” of the hydrolysis reaction through nearby residues, ii) shielding the retinal linkage from solvent, or iii) acting as a kinetic trap to slow retinal release.

Hydrolysis reaction



Solvent Accessibility



Kinetic Trap

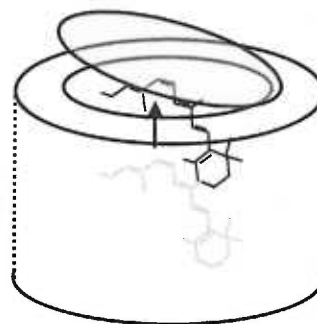


Figure 4. 2: Three-dimensional model of the rhodopsin intradiscal domain. The model shows the location of retinal, the retinal Schiff base linkage to Lysine 296, and residue E113 (note that part of the structure has been omitted for clarity). The figure also shows residue D190, which forms part of a highly conserved salt bridge with residue R177, and appears to stabilize intradiscal loop E-2. The model was prepared using coordinates from PDB file 1HZX (53), using the program WebLab.

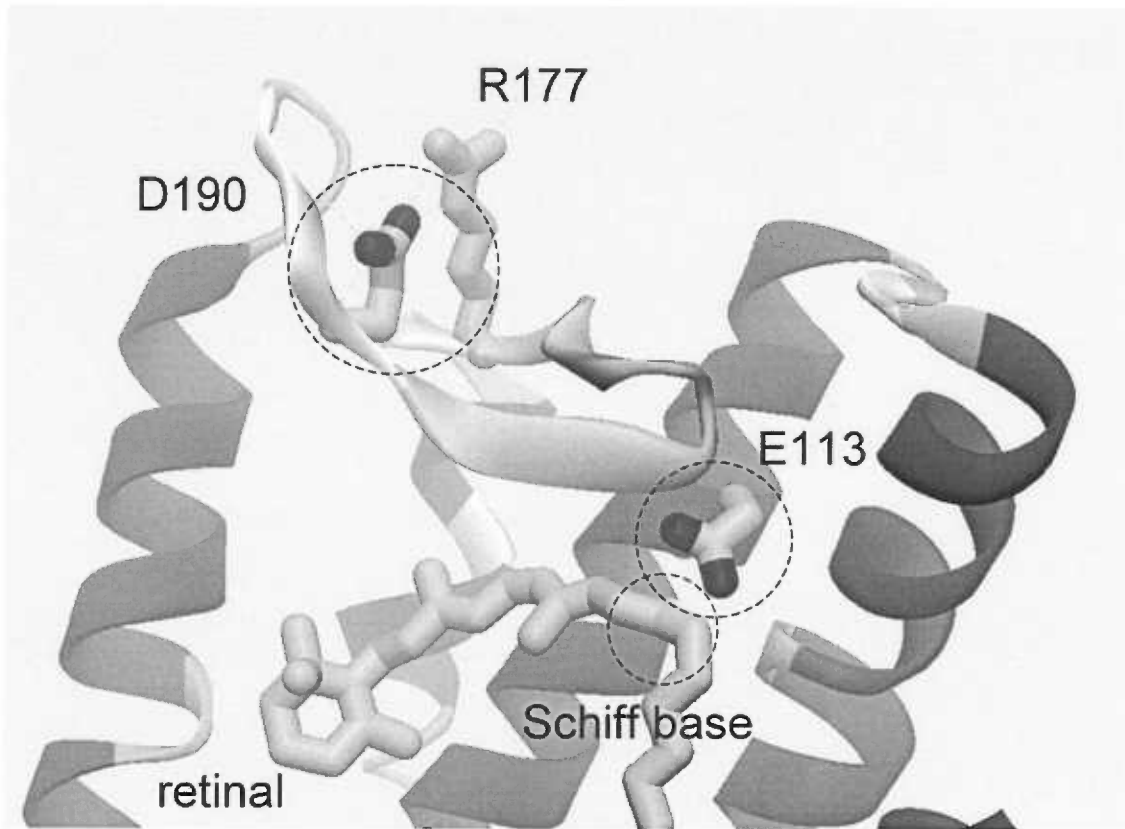


Figure 4. 3: Monitoring retinal Schiff base stability in dark state and MII rhodopsin. (A) WT rhodopsin UV/visible absorbance photobleaching properties in buffer D: DS, dark state; PSB, protonated Schiff base (at pH 1.9, an intact protonated Schiff base absorbs at 440 nm); MII, photobleached Metarhodopsin II state. (B) Example of loss of wild type rhodopsin absorbance thermal decay depicting the loss of the 500 nm absorbing species and gain in 380 nm absorbing species over time at 45 °C in buffer D. Spectra are plotted in 30 minute intervals with the initial $t = 0$ spectrum as a darker line. (C) MII decay of rhodopsin determined by monitoring the increase in intrinsic rhodopsin tryptophan fluorescence (330 nm) as the retinal leaves the binding pocket. The rate of fluorescence increase (330 nm, open triangles) correlates with the loss of the retinal Schiff base linkage, as determined by carrying out acid protonation studies (filled circles) to quantify the amount of remaining protonated Schiff base (from (154)). (D) Arrhenius plots of the dark state hydrolysis (large filled circles) and MII hydrolysis rates (large filled triangles) for WT rhodopsin at pH 6.0. The plots indicate that energetics and rates of Schiff base hydrolysis are different for the dark state and MII state. The non-linear concave plots for dark state rhodopsin hydrolysis indicate complex kinetics and suggest that multiple events may be involved in the hydrolysis process. Altering the pH to either 5.0 (small open circles) or 7.5 (small dotted circles) has essentially no effect on WT dark state hydrolysis. Similarly, changing the to either 5.0 (small open triangles) or 7.5 (small dotted triangles) does not effect the MII Schiff base hydrolysis process. The rate constants were obtained from dark state absorbance decay assays and fluorescent retinal release experiments (see Materials and Methods).

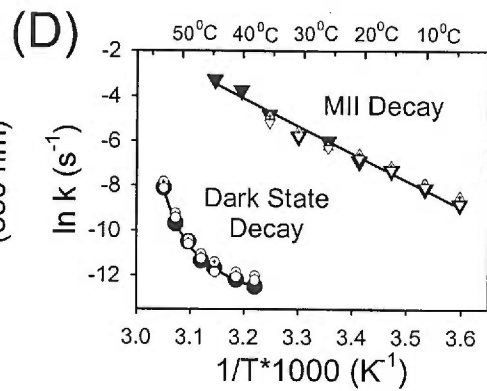
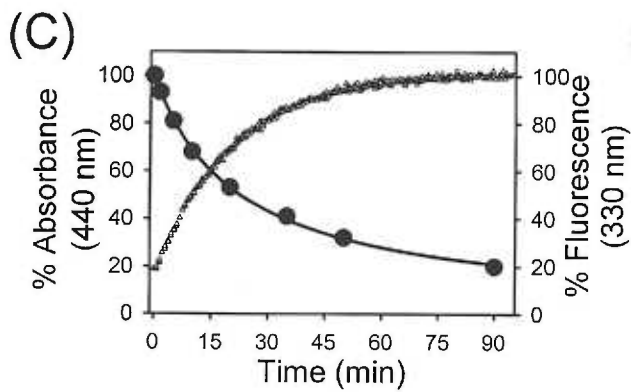
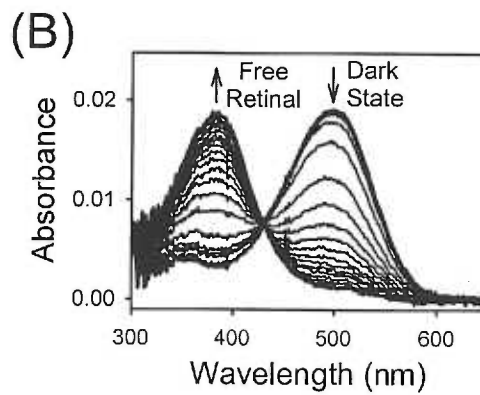
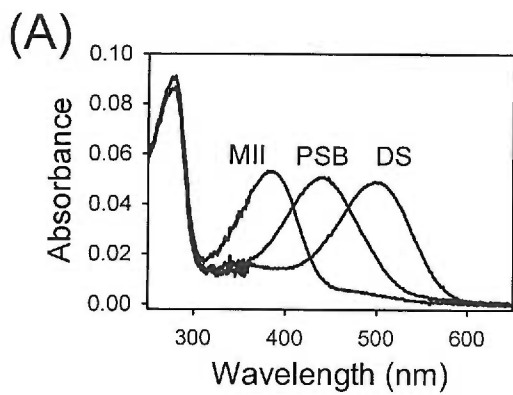


Figure 4. 4: Spectral properties of two different rhodopsin mutants with perturbed Schiff base stabilities. (A) Photobleaching properties for counter-ion mutant E113Q at pH 5.0, pH 6.0 and pH 7.5. Notice that the 500 nm absorbance is dramatically affected by pH, due to protonation of the Schiff base. (B) Photobleaching properties of mutant E113Q at pH 6.0, in buffer D. Upon irradiation with >495 nm light, the residual 500 nm species is converted to a 380 nm MII form (dotted line). Mutant E113Q mutant has an intact Schiff base as evident from the 440 nm absorbing species present in the acid denatured state (PSB), (dashed line). (C) Photobleaching properties of ion-pair mutant D190N are similar to those of WT (see Figure 4. 3A). Data for D190N is from (207).

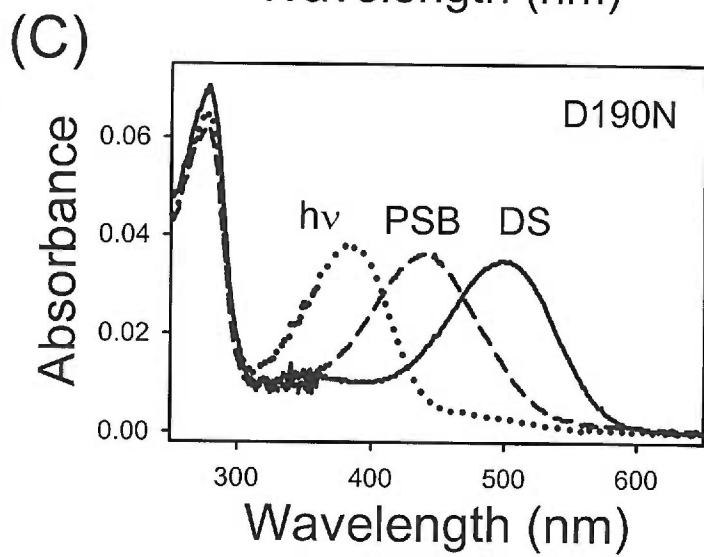
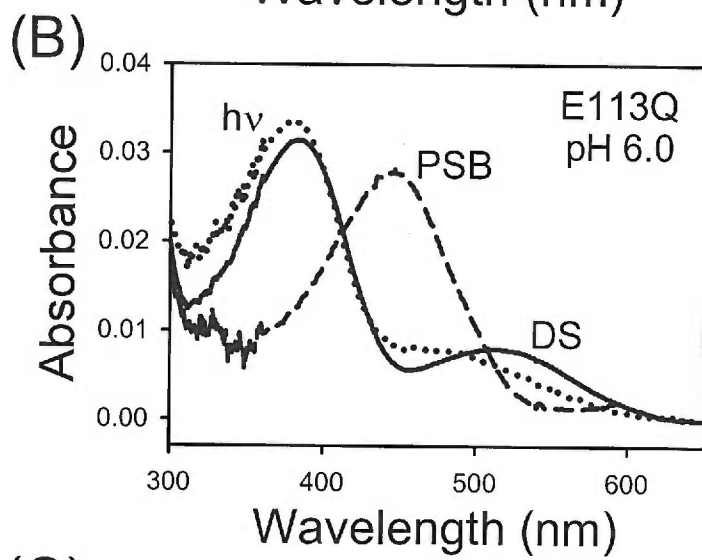
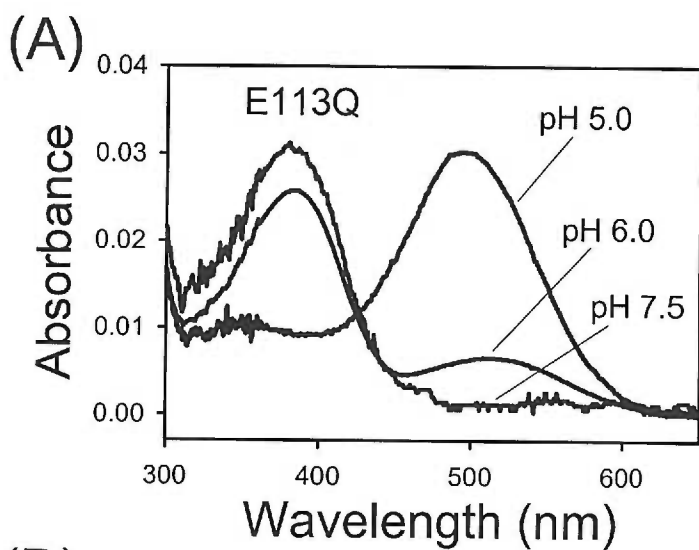


Figure 4. 5: Mutations can alter the retinal Schiff base stability in rhodopsin in fundamentally different ways. (A) Arrhenius plot of the dark state thermal decay rates for E113Q obtained from fluorescence spectroscopy. Mutant E113Q shows greatly accelerated rates of dark state hydrolysis. Furthermore, the pH dependence of the stability is $\text{pH } 5.0 < \text{pH } 6.0 < 7.5$. Unlike WT, the Arrhenius plot for E113Q is linear, and also pH dependent. **(B)** Arrhenius plot of E113Q MII decay rates carried out at different temperatures. Again the process shows pH dependence (compare pH 5.0, pH 6.0, and pH 7.5). However, in contrast to its diminished dark state stability the Schiff base linkage of mutant E113Q at higher pH values is much more stable than WT in the MII state, yet at pH 5.0 appears to be more like WT rhodopsin. **(C)** Arrhenius analysis of ion-pair mutant D190N (open diamonds) indicates this mutant has faster dark state decay rates compared to WT rhodopsin, yet retains the non-linear concave shape of the plot, suggesting the D190N mutation effects the kinetics of the reaction more than the energetics. **(D)** Interestingly, mutant D190N shows no observable change in the stability of its MII state compared to WT rhodopsin, in contrast to its altered dark state stability. Data for D190N is from (207).

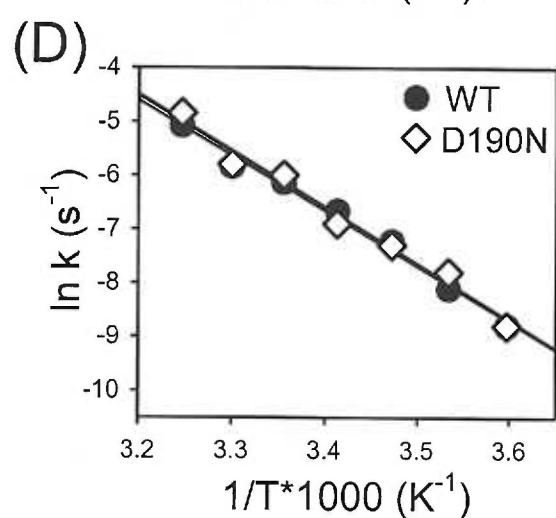
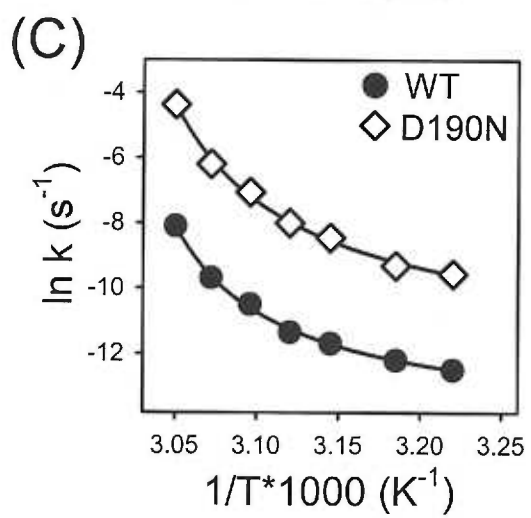
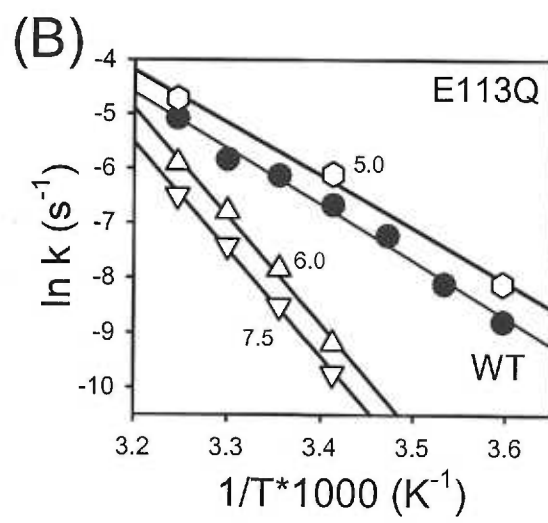
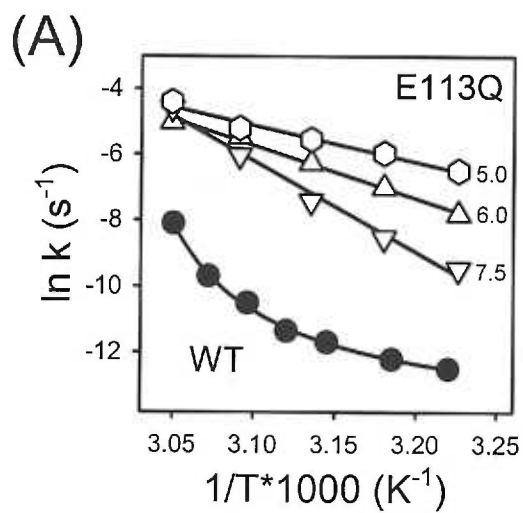
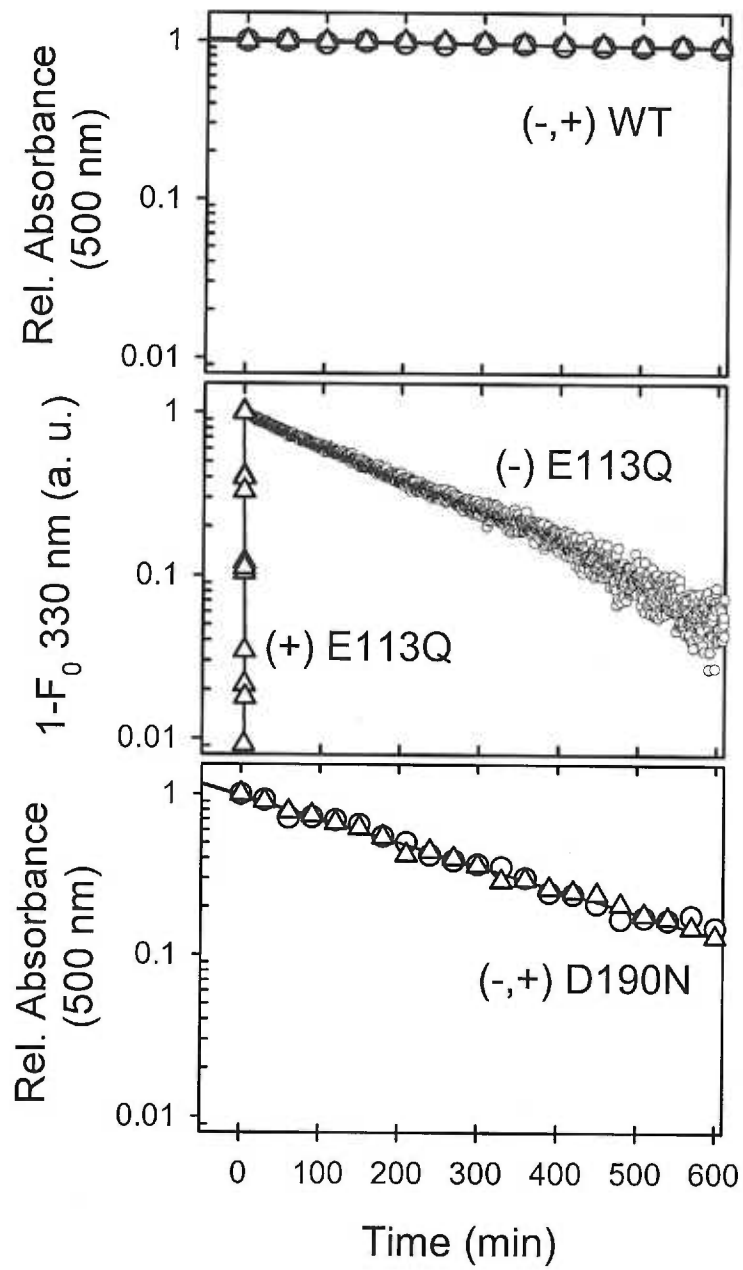


Figure 4. 6: Hydroxylamine sensitivity indicates fundamental differences between mutants that exhibit altered Schiff base stability. For example, counter-ion mutant E113Q shows dramatically increased susceptibility to hydroxylamine while ion-pair mutant D190N is largely unaffected. The rates of dark state thermal decay rates were measured for each purified mutant (500 nM) in the absence (-) and presence (+) of 50 mM buffered hydroxylamine in buffer D, pH 6.0 at 37 °C. Rates were determined using the absorbance decay assay (WT and D190N) or the fluorescence assay (E113Q), for further details see Materials and Methods. For comparison purposes the data are plotted on a logarithmic scale with the initial absorbance or fluorescence data normalized to 1.0. Top, WT rhodopsin is not accessible to attack by hydroxylamine (-, open circles; + open triangles). Middle, hydroxylamine greatly accelerates the rate of dark state Schiff base hydrolysis in mutant E113Q (-, open circles; +, open triangles). Bottom, hydroxylamine does not increase the rate of dark state Schiff base hydrolysis in mutant D190N (-, filled circles; +, open triangles). The differing degrees of hydroxylamine reactivity observed for WT, E113Q and D190N suggests significant alterations or the Schiff base environment in these rhodopsins in their dark state. Data for D190N is from (207).



4. 7: SUPPLEMENTAL MATERIAL

4. 7. 1: pH effects on the thermal decay process of mutant D190N.

The effect of pH on the process of thermal decay was measured for rhodopsin mutant D190N. The rhodopsin structure contains multiple ion-pairs, which are thought to stabilize the dark state conformation (4, 51, 182, 197). We tested the possible effect that alteration of the pH from 6.0 to either 5.0 or 7.5 has on the decay process of ion-pair mutant D190N (Figure 4. S1). Thermal decay rates were determined for each pH at three different temperatures (55, 47.5 and 37 °C), and the rates plotted according to the Arrhenius Equation. As can be seen from Figure 4. S1, the rates tested at these temperatures appear unaffected over the pH range tested and the concave shape of the plot appears to be retained. Taken together these results suggest that for the range tested pH does not have a drastic effect on either the thermodynamics or kinetics of dark state decay for mutant D190N.

4. 7. 2: pH effects on the MII decay process of mutant D190N.

Possible pH effects on the process of MII decay and retinal release for rhodopsin mutant D190N were also tested. Retinal release rates were determined for D190N (as describe in section 4. 3. 5 above) at pH 5.0, and 7.5 and these rates were plotted over results from the same experiment conducted at pH 6.0. Rates were determined at 30, 20 and 10 °C and values plotted according to the Arrhenius Equation. As can be seen from Figure 4. S2, the rates tested at these temperatures appear unaffected over the pH range tested and the slope (and therefore the E_a) of the process is unchanged. Taken together these results suggest that for the range tested pH does not have a drastic effect on either the kinetics or thermodynamics of MII decay and retinal release for mutant D190N.

Figure 4. S1: Effects of pH on the thermal decay process of rhodopsin mutant

D190N. Arrhenius analysis of ion-pair mutant D190N (diamonds) thermal decay rates at pH 7.5 (red) and 5.0 (blue) relative to pH 6.0 (black). At these pH values D190N shows faster dark state decay rates compared to WT rhodopsin (also see Figure 4. 5). Alteration of the pH to either 5.0 or 7.5 does not drastically affect the rate of D190N thermal decay relative to pH 6.0.

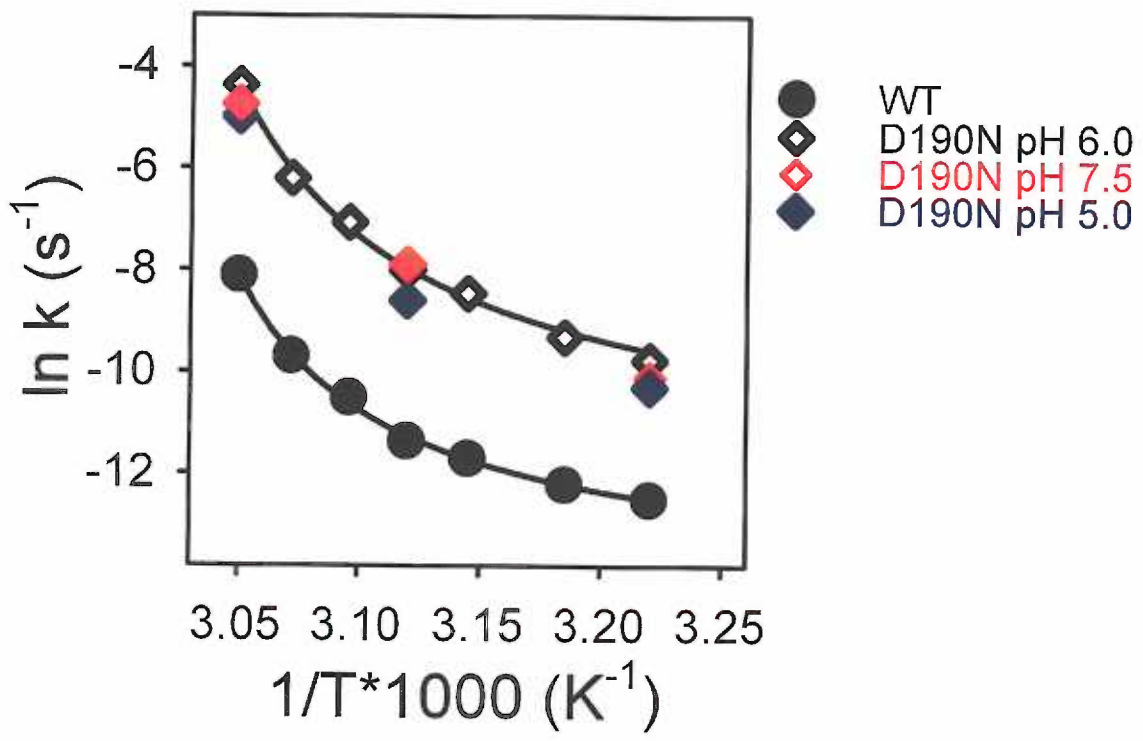
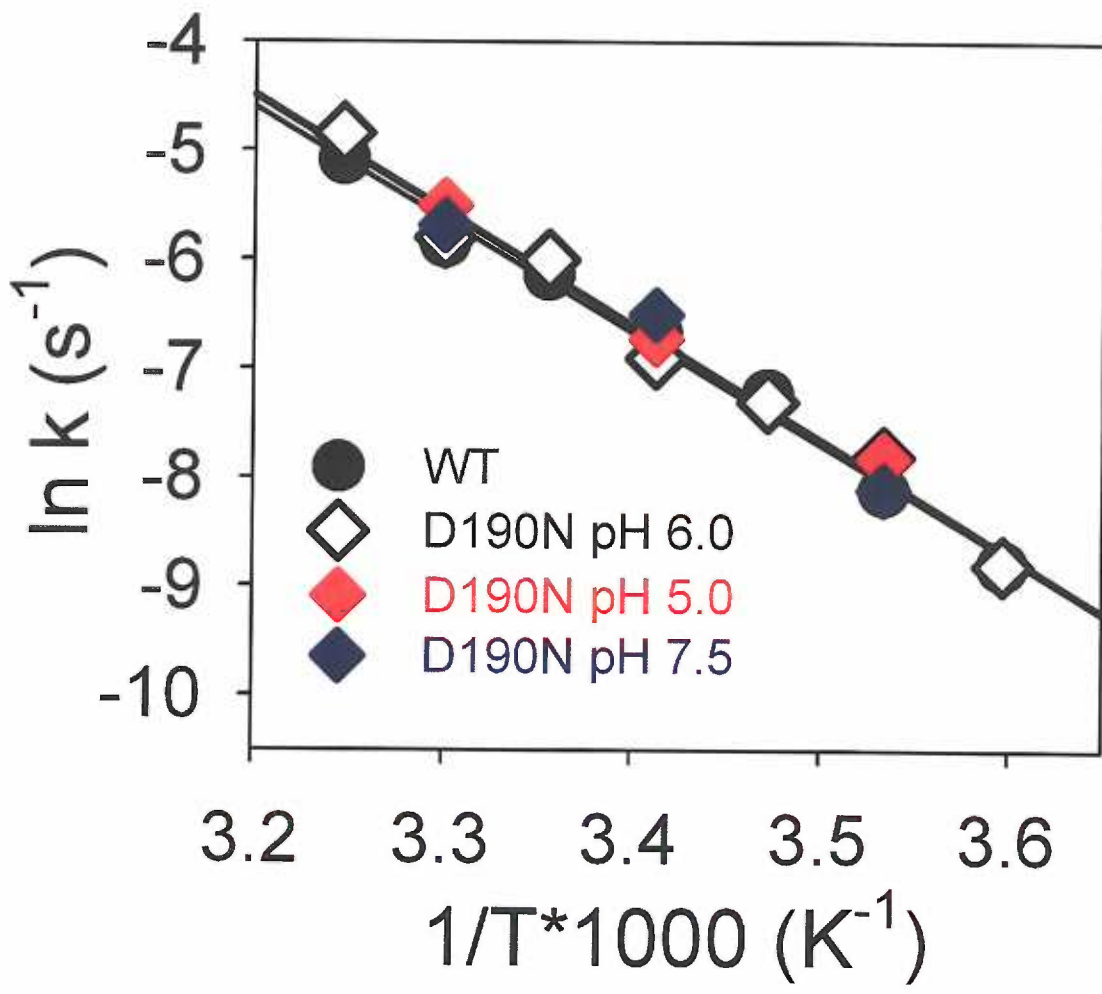


Figure 4. S2: Effects of pH on the process of MII decay and retinal release on rhodopsin mutant D190N. Alteration of the pH from 6.0 (black) to either 7.5 (blue) or 5.0 (red) does not greatly alter the stability of the retinal Schiff base in the MII state, as measured by the rate of retinal release. All three pH values exhibit similar rate values.



Chapter 5

Role of Retinal Hydrogen Bond Network in Schiff Base Stability and Hydrolysis.

Jay M. Janz[§] and David L. Farrens[§]

[§]Department of Biochemistry and Molecular Biology,

Oregon Health and Science University

3181 S. W. Sam Jackson Park Drive, Portland, Oregon 97239-3098

Running Title: Hydrogen Bond Network Stabilizes the Rhodopsin Schiff Base
Linkage.

5. 1: SUMMARY

This chapter reports our investigation into the role the retinal hydrogen bond network in relation to the retinal Schiff base linkage. Through site-directed mutagenesis we find that disruption of this network results in compromised stability of the Schiff base linkage in the dark state. Hydroxylamine reactive assays suggest that this compromised stability may be due to increased exposure to the bulk solvent. In addition, we find that mutation of this network also affects Schiff base stability in the MII state, but does so in a location dependent manner. These sites, (T94, E113 and S186) appear to act as participants in Schiff base hydrolysis and the retinal release process. We also provide evidence that multiple proton transfer events occur during the process of Schiff base hydrolysis and subsequent retinal release. The findings support a retinal Schiff base hydrolysis mechanism where the process precedes through a carbinolamine intermediate and we present a proposed reaction mechanism for this process. Taken together, our results demonstrate the importance of the retinal hydrogen bond network in maintaining Schiff base integrity as well as catalyzing Schiff base hydrolysis and retinal release. The author of this dissertation performed all experiments reported in this chapter.

5. 2: INTRODUCTION

Rhodopsin, the dim light photoreceptor of rod cells is arguably the best-characterized member of the class A superfamily of G-protein coupled receptors (GPCRs), (14, 18, 31, 48, 49, 51, 52, 67). A transmembrane receptor, it has evolved into an efficient photoreceptor by covalently binding its chromophore, 11-*cis*-retinal, to lysine-296 via a protonated Schiff-base linkage within the helical bundle (47, 137) . Dim

light vision begins when the 11-*cis*-retinal chromophore absorbs a photon and isomerizes to the all-*trans*-retinal form. This change in retinal configuration initiates a series of photo-intermediates and conformational changes in the protein, resulting in the formation of metarhodopsin II (MII), the active conformation of rhodopsin that is able to bind and activate the G-protein transducin.

Rhodopsin is also the intermediary between two important enzymatic processes; phototransduction / recovery and the retinoid cycle (45, 217). Following activation and signal transduction, the all-*trans*-retinal Schiff base linkage is hydrolyzed and retinal is released from the binding pocket. Recycling the receptor and returning it to a photosensitive conformational state complete recovery. The retinoid cycle accomplishes this task by converting the released all-*trans*-retinal back to 11-*cis* conformation through a series of enzymatic reactions – ultimately resulting in the reformation of the retinal Schiff base linkage and regeneration of the photosensitive receptor (45, 46). While extensive research into Schiff base formation and the retinoid cycle has resulted in a wealth of knowledge (45, 46), little is known about the molecular mechanism of Schiff base hydrolysis and the subsequent retinal release both in the dark state and, importantly, during the decay of the functional MII state (45, 217).

Both rod and cone visual signaling proteins bind their retinal chromophores through a Schiff base linkage (18, 218). Notably, this linkage is less stable in cone cells than rod cells and, as a result, the turnover and regeneration rates for cone cells are significantly faster (97, 98, 163, 205, 206). Furthermore, while the retinal Schiff base linkage is quite stable in dark state rhodopsin, it is hydrolyzed quickly from the active MII signaling state of the protein (18, 83, 85, 131), suggesting that conformational

changes must occur in the vicinity of the Schiff base attachment site to account for this disparity. Clearly the apoprotein plays a significant role in stabilizing the retinal Schiff base linkage.

Recently, a high resolution structure of rhodopsin suggested the presence of a hydrogen bond network encompassing the retinal Schiff base attachment site near extracellular loop E-2 and the “retinal plug” domain (54). This network consists of both the carbonyl backbone and side chains of amino acids lining the retinal binding pocket as well as water molecules within the pocket that surround the retinal Schiff base linkage. This network was recently demonstrated to play a key role in the protonated Schiff base counter ion switch mechanism proposed to occur upon formation of the MI photointermediate subsequent to light activation (111). However, the role of this retinal hydrogen bond network plays in stabilizing the retinal Schiff base and in potentially participating in the mechanism of Schiff base hydrolysis remains as yet unexplored.

In this chapter we report our investigation into the role the retinal hydrogen bond network in relation to the retinal Schiff base linkage. Through site-directed mutagenesis we find that disruption of this network results in compromised stability of the Schiff base linkage in the dark state – possibly due to increased exposure to the bulk solvent. In addition, we find that mutation of this network also affects Schiff base stability in the MII state, but only at some sites. These sites, (T94, E113 and S186) appear to act as participants in Schiff base hydrolysis and retinal release process. Finally, we provide evidence that multiple proton transfer events occur during the process of Schiff base hydrolysis and subsequent retinal release and that this process precedes through a carbinolamine intermediate. Taken together, our results demonstrate the

importance of the retinal hydrogen bond network in maintaining Schiff base integrity as well as catalyzing Schiff base hydrolysis and retinal release.

5. 3: MATERIALS and METHODS

5. 3. 1: Materials.

Except where noted, all buffers and chemicals were purchased from either Fisher (Pittsburgh, PA) or Sigma (St. Louis, MO) and similar to section 3. 3. 1 in chapter 3. Deuterium oxide was purchased from Cambridge Isotope Laboratories, Inc. (Andover, MA). Centrifugal filter devices were purchased from Millipore (Billerica, MA), 0.5 μ M volume, 10 kDa cut off.

5. 3. 2: Buffers.

The definitions of the buffers used are as follows: Unless otherwise noted, all experiments were performed in buffer A [0.05% DM and 5 mM MES (pH 6.0)].

5. 3. 3: Construction, expression and purification of rhodopsin mutants.

For construction, expression and purification of rhodopsin mutants please refer to section 3. 3. 3 in chapter 3.

5. 3. 4: UV/vis absorption spectroscopy.

For UV/vis absorption spectroscopy please refer to section 2. 3. 5 in chapter 2.

5. 3. 5: Determination of transducin (G_T) activation rates.

For transductin activation procedure please refer to section 2. 3. 7 in chapter 2.

5. 3. 6: Thermal bleaching of rhodopsin samples.

For thermal bleaching of rhodopsin samples please refer to section 3. 3. 7 in chapter 3.

5. 3. 7: Measurement of the rate of retinal release and/or MII decay by fluorescence spectroscopy.

For MII decay procedures please refer to section 3. 3. 9 in chapter 3.

5. 3. 8: Hydroxylamine reactivity.

For hydroxylamine reactivity assays please refer to section 3. 3. 11 in chapter 3.

5. 3. 9: Solvent isotope effects on MII decay rates.

Prior to starting a 10 % DM stock and a 500 mM MES pH 6.0 stock buffer were made fresh in deuterium oxide (D₂O) and were then used to make a 0.05% DM, 5 mM MES pH 6.0 D₂O exchange buffer. The pH for the deuterium buffer is expected to be off by - 0.4 pH units. However, as the process of MII decay has been shown to be independent over a pH range of 5.0 to 8.0 (219), this slight pH change should not alter interpretation of the results. Using a concentrated stock of purified rhodopsin (to use a small volume for dilution) 2 equal molar stocks of both D₂O and H₂O rhodopsin were prepared. These samples (500 nM) were then buffer exchanged using Millipore Ultrafree 0.5 centrifugal filter devices at low spin speeds. The D₂O sample was washed 6 times with 500 μL of D₂O buffer, while the H₂O sample was washed in the exact same method using H₂O buffer. In this manner any concentration of detergent that may have taken place during the exchange would be equal for both samples. The samples were then assayed for MII decay rates as described above at 20 °C. The procedure was repeated and values obtained from 3 separate experiments from 2 different stock preparations.

5. 3. 10: Proton inventory studies on MII decay/retinal release rates.

The stock solutions were prepared as described above and combined in various proportions to give different mole fractions (n) of deuterium ranging from 0 to 1.0. The

MII decay rate of WT rhodopsin was monitored at 20 °C as described above over the range of different mole fractions of D₂O. Data was analyzed by plotting the ratio of k_n/k_H versus the mole fraction of D₂O, where k_n is the rate in the molar fraction of D₂O and k_H is the rate in 100% H₂O.

5. 4: RESULTS

5. 4. 1: Rational for choice of mutants.

The site-directed rhodopsin mutants analyzed in this study were generated to assess their individual roles in maintaining retinal Schiff base integrity. Specifically, mutants were investigated to evaluate their role in the proposed retinal hydrogen bond network, which is based on crystallographic data (54), functional studies (69, 111, 186, 208, 210, 211, 219) as well as molecular modeling. Mutants were designed to disrupt the hydrogen bond capability of the individual residue, yet preserve the size of the amino acid side chain. Toward this end, the following series of retinal binding pocket mutants were made and analyzed: T94I, E113Q, E181Q, S186A, Y192F, Y268F (Figure 5. 1). In addition to being part of this hydrogen bonding network, mutant T94I is associated with the disease *Congenital Night Blindness* (CNB) (208, 210, 211) and mutant E113Q alters the role of the “counter-ion” (69, 70).

5. 4. 2: Characterization of rhodopsin mutants.

All mutants expressed to levels similar to WT rhodopsin in a COS cell expression system, were capable of binding the chromophore 11-*cis*-retinal and could be purified following standard procedures to homogeneity. All mutants exhibited spectral ratios ($\lambda_{280}/\lambda_{max}$) between 1.6 and 1.8, with the exception of the counter ion-mutant E113Q,

which shows a pH dependence in its absorbance profile (69, 70, 184). Many of the mutants exhibited shifted dark state absorption maximum values (λ_{max}), (Figure 5. 2). Mutant T94I, which is in close proximity to the counter-ion residue E113, showed a λ_{max} of 478 nm in agreement with previous results (208, 210, 211). Additionally, mutant E181Q showed a slight red-shift in its absorbance profile (186), while the dark state λ_{max} of mutant S186A is similar to that of WT rhodopsin (111). Notably, mutation of tyrosine residues to phenylalanine at residues 192 and 268 resulted in blue-shifted λ_{max} values in the dark state of 491 and 495 nm, respectively.

Photobleaching experiments were subsequently carried out on the purified hydrogen bond network mutants. All mutants could form a MII-like photointermediate upon illumination with λ_{max} values not deviating substantially from that of WT rhodopsin ($\lambda_{\text{max}} = 381$ nm, see Table 5. 1.). In addition, acid denaturation of this species confirmed the presence of an intact protonated retinal Schiff base linkage ($\lambda_{\text{max}} = 440$ nm), (Fig. 5. 2). However, while capable of forming a MII-like intermediate containing a PSB upon acid treatment, mutant Y268F and to a lesser extent Y192F also were observed to exhibit a “shoulder” species centered at ~ 480 nm immediately following illumination (Figure 5. 2). Interestingly, this species decays slightly over time, but is still present up to 500 min following bleaching (Figure 5. 3). While the cause of this is not currently known similar results have been reported previously for other rhodopsin point mutants including G90S and L226C (148, 179, 207, 220). Spectral properties for all mutants are presented in Table 5. 1.

5. 4. 3: Effects on retinal Schiff base integrity in the dark state.

The stability of retinal Schiff base linkage in the dark state was assessed by measuring the dark state thermal decay rates for all of the mutants. All of the mutants tested showed significantly expedited rates of thermal decay in comparison to WT rhodopsin as judged by their loss rate in absorbance at 500 nm, or in the case of mutant E113Q, the increase in fluorescence at 330 nm, over a range of temperatures (for rate details see Table 5. 2). To obtain activation energy (E_a) values for this process thermal decay assays were conducted at a variety of different temperatures and the rate data was analyzed using Arrhenius analysis essentially as previously described (207, 219). As can be seen from these plots, the rates of loss in 500 nm absorbance (or gain in fluorescence at 330 nm) illustrate a temperature-dependent relationship for all mutants (Figure 5. 4). All of the mutants have significantly expedited rates of thermal decay in comparison to WT rhodopsin. Interestingly, while the Arrhenius plot of WT rhodopsin is concave, all of the mutants tested exhibit linear plots (Figure 5. 4). Taken together these data suggest that mutations of the retinal hydrogen bond network residues effect both the kinetics and energetics of the dark state thermal decay process. Data from the dark state thermal decay experiments are presented in Table 5. 2.

5. 4. 4: Effects on retinal Schiff base integrity in the MII state.

The effect of the mutations on the stability of the MII active signaling species was also assessed by determining the kinetic rates and activation energies for retinal release (179, 207). Under our conditions the $t_{1/2}$ of retinal release for WT rhodopsin was 13.5 min at 20 °C in buffer A, comparable to values previously reported for both ROS purified and COS expressed rhodopsin (114, 179, 182, 186). Relative to WT rhodopsin, mutants

E181Q, Y192F and Y268F show slightly increased rates of retinal release during MII decay (see Table 5. 2). In contrast, mutants T94I, E113Q and S186A all show dramatically decreased rates of retinal release (Table 5. 2).

The activation energy values for MII Schiff base hydrolysis and retinal release was determined for each mutant by monitoring the rate of fluorescence increase in buffer A at seven different temperatures (5, 10, 15, 20, 25, 30 and 35 °C). Arrhenius plots of these measurements indicate a temperature-dependent linear relationship for all mutants tested (Figure 5. 5). Interestingly, mutants E181Q, Y192F and Y268F show little effect on the process of Schiff base hydrolysis and retinal release during decay of the MII state (Figure 5. 5A). Conversely, the retinal Schiff base linkage in the MII state for mutants T94I, E113Q and S186A are all substantially more stable than WT rhodopsin (Figure 5. 5B). Schiff base hydrolysis and retinal release rates and E_a values for WT and rhodopsin mutants are presented in Table 5. 2.

5. 4. 5: Solvent accessibility.

The small molecule hydroxylamine (NH_2OH) has long been used to measure the solvent accessibility of retinal in studies on rhodopsin as it rapidly cleaves retinal Schiff base linkages. While WT rhodopsin is effectively non-reactive to NH_2OH in the dark state at 37 °C (207, 219), it is highly reactive in the MII state. As a result, dark state hydroxylamine reactivity may be used to probe the solvent accessibility of the retinal Schiff base in rhodopsin mutants. Hydroxylamine reactivity experiments illustrate that relative to WT rhodopsin all of the mutants are more susceptible to hydroxylamine cleavage of the retinal Schiff base in the dark-state. Kinetic parameters for dark state hydroxylamine reactivity are presented in Table 5. 2.

5. 4. 6: Transducin activation by hydrogen bond network mutants.

Mutants were tested for their ability to catalytically activate transducin using a fluorescence-based assay that measures the increase in tryptophan fluorescence of the $G_{T\alpha}$ -GTP γ S species (114, 156, 164). The slight decreases in initial rates for mutants T94I and E181Q were in agreement with values previously reported (186, 208). We found that the relative rate of G_T activation for counter-ion mutant E113Q is 45% of WT rhodopsin. Moreover, we found that the ability of mutants S186A, Y192F and Y268F to activate transducin are all greatly diminished relative to WT rhodopsin. The results for transducin activation are compiled in Table 5. 1 as initial rates of fluorescence increase relative to WT rhodopsin.

5. 4. 7: Deuterium isotope effect on MII Schiff base hydrolysis.

To investigate the role of protons and water molecules in the chemical process of retinal Schiff base hydrolysis in the MII state deuterium isotope exchange experiments were conducted on WT rhodopsin. Retinal release assays were performed following D_2O buffer exchange and rate values compared to samples prepared in an identical fashion using H_2O buffers. The rate of Schiff base hydrolysis and subsequent retinal release at 20 °C is substantially slower in deuterium buffer ($k_{H_2O} = 15.3 \pm 0.4$ min, $k_{D_2O} = 38.6 \pm 0.3$ min, $n = 3$ for both), exhibiting a solvent isotope effect of 2.5 (Figure 5. 6A). Proton inventory analysis of these reactions results in a nonlinear plot (Figure 5. 6B). The interpretation of this finding is discussed further below.

5. 5: DISCUSSION

The initial crystal structure model of rhodopsin revealed that extracellular loop E-2 folds back into the core of the protein and forms a plug surrounding the retinal binding pocket (52). Numerous amino acid side chains positioned on loop E-2 make contact with the retinal and may be important for both Schiff base stability as well as signal transduction (111, 186, 207). Recently, a higher resolution model was reported (54) which suggested the location of water molecules within the retinal binding pocket, in agreement with previous suggestions of their presence (169, 221). The authors also detailed a hydrogen bond network that surrounds the retinal Schiff base linkage (54). The present report details the structural and functional implications this retinal hydrogen bond network has on the stability of the retinal Schiff base as well as rhodopsin signaling.

5. 5. 1: General characteristics of hydrogen bond network mutants.

All of the mutants examined in this study express to WT levels in a COS cell system (typical yields of 10 to 15 $\mu\text{g}/15\text{ cm plate}$). In addition, most of the mutants were properly folded and shown to bind 11-*cis*-retinal (Figure 5. 2). The notable exception is the counter-ion mutant E113Q which has been previously shown to exhibit a pH dependence in its absorbance profile most likely reflecting its protonation state (69, 70, 184, 208, 222). As all of the mutants generated for this study are part of, or in close proximity to, the retinal binding pocket it is perhaps not surprising that they effect the dark state λ_{max} values. Consistent with prior reports we find that mutant T94I results in a large blue-shift presumably due to the loss of stabilizing effects on the protonated Schiff base linkage provided by the counter-ion E113, which is in proximity (208, 210, 211). In addition, we find mutant E181Q shows a slight red-shift in its absorbance profile (186),

while that of S186A is similar to WT rhodopsin (111). Interestingly, we find that two new mutants Y192F and Y268F result in dark state blue-shifts (Figure 5. 2, Table 5. 1). The small shift ($\lambda_{\text{max}} = 495 \text{ nm}$) shown for Y268F may be do to slight alterations in its interaction with the retinal, which it makes contact with, or possibly through disruption of the retinal hydrogen bond network as Y268 appears to be holding residue E181 in place (54, 111). This later reason seems applicable to mutant Y192F ($\lambda_{\text{max}} = 491 \text{ nm}$), as it too appears to align residue E181.

The spectral behaviors for most of the mutants were WT-like as all of the mutants could form a MII absorbing species and exhibit a PSB upon acid denaturation (Figure 5. 2). However, mutant Y268F and to a lesser extent Y192F demonstrate a residual absorbing species with a λ_{max} of $\sim 480 \text{ nm}$ following illumination (Figure 5. 2). This photoproduct was followed as a function of time for mutant Y268F and shown to slightly decay over time yet still retain some residual $\sim 480 \text{ nm}$ absorbance (Figure 5. 3A). In contrast, at this pH the behavior of WT rhodopsin under identical conditions exhibits only a slow increase in $\sim 480 \text{ nm}$ absorbance, presumably due to the formation of the MIII storage intermediate (124, 172). While the exact nature of the photoproduct in mutant Y268F is unknown it is possible to speculate its composition in light of the recently proposed counter-ion switch mechanism of rhodopsin activation (111). According to this theory the counter-ion to the charged retinal PSB linkage in rhodopsin switches from residue E113 in the dark state to residue E181 in the MI state. This transfer is mediated via a hydrogen-bonding network of residue side chains and water molecules within the retinal binding pocket in conjunction with retinal isomerization and slight conformational changes by rhodopsin itself. It is therefore possible that mutations Y192F and Y268F

result in improper alignment of residue E181 thereby resulting in inefficient counter-ion transfer and the possible build-up of the preliminary bleaching intermediates. However, it is also possible that these residues trap the MI or MIII states upon illumination and further studies, particularly FTIR may help shed light on the identity of this species.

The ability of each of the hydrogen bond network mutants to activate transducin varied. In agreement with previous results we find that mutants T94I and E181Q do not drastically effect initial rates of transducin activation (69, 186, 208, 210, 223). In contrast, mutations S186A, Y192F and Y268F all show significantly reduced initial rates of transducin activation (Table 5. 2). In our hands, mutation E113Q impairs transducin activation. However, previous studies showed that this mutant activates transducin to levels similar to WT rhodopsin (69). While we are presently unsure of the cause of this discrepancy it is possible that the sample tested in the present report had undergone some dark state thermal decay, which may account for the decrease levels observed in this study.

5. 5. 2: Hydrogen bond network helps stabilize the dark state rhodopsin structure and contributes to the concave Arrhenius plot.

All of the hydrogen bond mutants tested exhibit dark state thermal decay rates significantly faster than WT rhodopsin (Table 5. 2). In addition, Arrhenius plots of these thermal decay rates over a range of temperatures are linear for all mutants – in contrast to the concave plot shown for WT rhodopsin (Figure 5. 4). Previously we have suggested that the concave Arrhenius plot exhibited by WT rhodopsin may be attributed to the presence of at least 2 different rate limiting steps occurring during dark state decay (207, 219). With this interpretation in mind, the data suggest that mutations to the retinal

hydrogen bond network result in dark state decay processes that are dependent upon only one rate limiting step. At physiological temperatures (37 °) the activation energies (E_a) for hydrolysis is significantly higher for the mutants than for WT rhodopsin (Table 5. 2). One possibility is that at lower temperatures an event (such as proton tunneling) may occur more efficiently in WT rhodopsin and this process is abrogated in the hydrogen bond network mutants, thereby accounting for the differences observed (207). In contrast, the E_a values calculated at higher temperatures, 55 °C for WT are larger than those of the mutants (Table 5 .2). It is possible that at higher temperatures some denaturation of the protein occurs which may reposition key amino acids involved in Schiff-base hydrolysis, thereby increasing the observed E_a value for WT (207). Mutation of the retinal hydrogen bond network may have already altered these key regions and, as a result, the higher temperature differences in E_a observed for these mutants are of less magnitude than those of WT rhodopsin. These results establish that the hydrogen bond network mutants all effect both the kinetics and energetics of dark state Schiff base hydrolysis.

Hydroxylamine reactivity assays were performed to determine if the loss of retinal Schiff base stability observed for the hydrogen bond network mutations may be due in part to increased exposure to the bulk solvent. As illustrated in Table 5. 2, all of the mutants show increased reactivity with hydroxylamine respective to both WT rhodopsin, as well as to their rates of dark state decay under identical conditions in the absence of hydroxylamine. Previously, we had suggested the opsin apoprotein may stabilize the retinal Schiff base linkage through three fundamental mechanisms; i) by affecting the chemistry of Schiff base hydrolysis, ii) by limiting the accessibility of the

Schiff base to solvent, and iii) by acting as a "kinetic trap" that inhibits the release of transiently hydrolyzed retinal, thus encouraging re-binding and reformation of the Schiff base linkage (219). With these interpretations in mind the spectral, thermal decay and hydroxylamine data suggest the hydrogen bond network serves to stabilize the retinal Schiff base in the dark state. It does this both by affecting the chemistry of Schiff base hydrolysis and by limiting the accessibility of the Schiff base linkage to solvent.

5. 5. 3: Location dependent effects on MII Schiff base stability.

Previously, we have found that Arrhenius analysis of MII Schiff base hydrolysis and retinal release can help define the role of individual rhodopsin mutations (179, 207). The rates of retinal release at 20 °C for mutants E181Q, Y192F and Y28F are slightly faster than WT rhodopsin, Table 5. 1. In contrast, the rates of T94I, E113Q and S186A are all substantially slower with respect to the WT rate, Table 5. 1. Arrhenius analysis of these rates at different temperatures indicates that residues E181Q, Y192F and Y268F have only minor effects on MII Schiff base hydrolysis, as they exhibit E_a values similar to WT (Figure 5. 5A). The slope of Y192F is slightly altered which corresponds to the slight decrease in the E_a value reported for this mutant, Table 5. 2. In contrast, the plots of mutants T94I, E113Q and S186A deviate considerably from that of WT rhodopsin (Figure 5. 5B). These mutants also show greatly attenuated rates and E_a values, which are all much greater than the 20.5 kcal/mol value determined for WT rhodopsin, Table 5. 2.

Why are the $t_{1/2}$ values and E_a of MII Schiff base hydrolysis and retinal release so much greater for mutants T94I, E113Q and S186A? The fluorescence retinal release assay measures the rate of retinal leaving the opsin-binding pocket following the

chemical event of Schiff base hydrolysis. The decreased rate observed for these three mutants can thus be attributed to affecting either the chemistry of hydrolysis or the steric properties of opsin associated with retinal release from the binding pocket. Given the proximity of these residues to the Schiff base attachment site as well as to internal water molecules within the binding pocket, it seems reasonable to suggest these residues are at least partially involved in the chemical event of Schiff base hydrolysis. Previously proposed models of rhodopsin retinal Schiff base hydrolysis suggest that base catalyzed water molecules may initiate hydrolysis in a process that proceeds through a tetrahedral carbinolamine intermediate (85). In the absence of structural data on the retinal binding pocket in the MII state of rhodopsin it is difficult to discern the precise role of individual residues and water molecules that may catalyze Schiff base hydrolysis. However, the results of the present study seem to rule out the direct effects of residues E181Q, Y192F and Y268F on this process. Furthermore, our results suggest that residue T94, E113 and S186 are important to this process, potentially acting in catalysis as water activators or proton donors/acceptors. It is also possible that the hydrogen bond network confines the geometry of the Schiff base site so as to prevent the spontaneous formation of the carbinolamine transition state proposed to form during Schiff base hydrolysis (85).

5. 5. 4: Solvent isotope effect on MII Schiff base hydrolysis.

To gain further insight into the chemical process of Schiff base hydrolysis deuterium isotope exchange experiments were performed. These experiments were conducted to investigate the possible role(s) of proton transfer during catalysis. As illustrated in Figure 5. 6A the rate of retinal release in WT rhodopsin, pH 6.0 at 20 °C is substantially slower in D₂O than H₂O, yielding a solvent isotope effect of 2.5 for this

process. Combined with our mutagenesis data, these results suggest the involvement of proton exchange occurring during the rate limiting step of MII Schiff base hydrolysis. In addition, they also support the theory that the rate limiting step in the retinal release process is the chemical event of Schiff base hydrolysis (179). The solvent isotope effect of 2.5 we observe is very similar to the solvent isotope effect of 2.3 reported from earlier studies for hydrolysis of model Schiff base compounds (129, 130). These prior studies interpreted the effects mechanistically as the transition state of the hydrolysis reaction bearing a close resemblance to a protonated carbinolamine intermediate. The solvent isotope effect value of 2.5 we find for WT rhodopsin lends further support that this proposed transition state mechanism occurs in rhodopsin. Furthermore, we find the proton inventory studies on solvent isotope effect of retinal Schiff base hydrolysis exhibit a non-linear relationship between the rate ratio and molar ratio of D₂O (Figure 5. 6B). This non-linear plot suggests that more than one time of flight proton is involved in the rate-limiting step of the hydrolysis reaction (224). This is perhaps not surprising given the estimated complexity of the MII retinal Schiff base hydrolysis reaction (85). If the assumption is made that one or more H₂O molecules are exchanged with D₂O in the retinal binding pocket then one can postulate several proton transfers occurring between the D₂O(s), the amino acid side chains and the retinal itself. This assumption is validated by previous Raman and FTIR experiments, which illustrated that the Schiff base proton itself undergoes D→H exchange (81). The data fit best to a cubic equation ($R^2 = 0.995$), which may suggest 3 protonation events occur during the reaction (224). This is interesting as there are three residues that show an effect on this process when they are mutated.

5. 5. 5: Proposed mechanism of retinal Schiff base hydrolysis.

Interpretation of the results presented here in conjunction with previous studies enable us to present an updated mechanistic scheme for rhodopsin retinal Schiff base hydrolysis (Figure 5. 7). The absence of structural data on the MII intermediate of rhodopsin makes it impossible to delineate the exact role of amino acid side chains participating in the hydrolysis reaction. Previous resonance Raman and FTIR studies show that the Schiff base is not protonated in the MII state. However, for the hydrolysis reaction to efficiently proceed, Schiff base protonation, (occurring either from the solvent or neighboring amino acids – possibly involving orientation by S186), would be necessary. It is possible that a small population of MII rhodopsin exists in the protonated form that is not resolved by the above-mentioned techniques, which would allow initiation of the hydrolysis reaction.

In the reaction mechanism presented in Figure 5. 7 a water molecule within the binding pocket initiates hydrolysis by attacking the Schiff base linkage. It is reasonable to speculate that the initial water activation step may be mediated by base catalysis from residue E113 and is properly orientated in part by T94 (Figure 5. 7, step 1). This attack would give rise to the tetrahedral carbinolamine intermediate and results in reorientation of the active site contacts to allow protonation of the basic carbinolamine either from the solvent or perhaps residue E113 (step 2). The carbinol species is subsequently deprotonated, again either by the solvent or a neighboring amino acid side chain (step 3). The linkage then breaks leaving the all-*trans*-retinal aldehyde and the free amino group of residue K296 (step 4). The noncovalent complex of the retinal and the opsin-binding

pocket is unstable due to the sterically unfavorable *trans*-configuration of the retinal and it irreversibly dissociates from opsin, leaving the binding pocket empty (step 5).

5. 5. 6: Conclusions.

In the present work we have shown that a hydrogen bond network provided by the surrounding amino acid side chains helps stabilize and maintain the retinal protonated Schiff base linkage in rhodopsin. In the dark state, these residues stabilize this linkage at least in part by limiting its accessibility to the bulk solvent. In contrast, in the active MII state, only three residues (T94, E113 and S186) appear to be intimately involved in the process of Schiff base hydrolysis. Interestingly, these residues appear to help accelerate retinal release in MII rhodopsin, most likely by playing a role in the multiple proton transfer events occurring during retinal Schiff base hydrolysis in the MII state. We speculate the inability to accelerate/promote Schiff base hydrolysis could be a causative role in CNB for T94I, as suggested by others (208, 210).

5. 6: ACKNOWLEDGMENTS

We are grateful to Dr. Mike Jackson and Dr. John Denu for helpful discussions regarding kinetics and isotope experiments.

Table 5. 1: Spectral and Functional Properties of Hydrogen Bond Network Mutants (absorbance maxima, $t_{1/2}$ of retinal release, transducin activation).

Mutant	Dark State λ_{\max} (nm) ^a	MII State λ_{\max} (nm) ^a	MII Decay $t_{1/2}$ (min) ^b	G _T activation rate (%) ^c
WT	500	381	13.5	100
T94I	478	381	95.4	89
E113Q	385/495 ^d	378	126.2	45
E181Q	508	381	6.8	71
S186A	500	384	51.4	36
Y192F	491	386	5.8	35
Y268F	495	386	6.8	26

^a All λ_{\max} values are determined from the 1st derivative of the raw spectral data and estimated to within ± 1 nm.

^b MII decay (retinal release) assays performed at 20 °C in buffer A as described in Materials and Methods.

^c The relative initial rate of G_T activation is represented by the rate of fluorescence increase obtained from the slope of the fluorescence measurements in the first 60 s after addition of GTP γ S relative to that of WT rhodopsin. The averages of $n = 2$ experiments are shown.

^d The λ_{\max} of mutant E113Q is pH dependent (see Results).

Table 5. 2: Kinetic and Thermodynamic Parameters of Schiff Base Stability Studies on Hydrogen Bond Network Rhodopsin Mutants.

Mutant	DS ^a hydrolysis $t_{1/2}$ 37 °C (min)	DS ^b hydrolysis E_a 37 °C (kcal/mol)	DS ^a hydrolysis $t_{1/2}$ 55 °C (min)	DS ^b hydrolysis E_a 55 °C (kcal/mol)	MII hydrolysis $t_{1/2}$ 20 °C (min)	MII ^b hydrolysis E_a (kcal/mol)	Hydroxyl- amine reactivity $t_{1/2}$ 37 °C ^c (min)
WT	3100 ± 45	16.1	38.5	103	13.5	20.5	3100
T94I	103	53.5	0.9	53.5	96	25.4	19.5
E113Q	29	32.1	1.8	32.1	125	39.3	4.8
E181Q	2150	58.5	12.1	58.8	6.8	21.7	58
S186A	1032	49.5	2.4	49.5	70.8	33.4	14.9
Y192F	958	51.2	10.5	51.2	5.8	14.7	21
Y268F	1152	80.8	1.1	80.8	6.8	21.7	13.9

^a Dark state thermal decay rates obtained from mono-exponential fits of dark state

thermal hydrolysis absorbance measurements at respective temperatures.

^b Activation energies (E_a) obtained from linear regression of Arrhenius plots.

^c Hydroxylamine reactivity rates determined from mono-exponential fits of dark state thermal hydrolysis experiments performed at pH 6.0, 37 °C in the presence of 50 mM pH buffered hydroxylamine. For further details see Materials and Methods.

Figure 5. 1: Residues involved in a hydrogen bond network around the retinal Schiff base linkage in rhodopsin. Individual amino acids are labeled and waters are shown as blue spheres. The retinal Schiff base attachment site to K296 is shown in blue. The backbone of residue C187 also participates in this network (not shown). Portions of the protein surrounding the retinal binding pocket have been removed for clarity. The model is based on the rhodopsin crystal structure (Protein Data Bank accession #: 1L9H, (54)) and generated using the program Weblab.

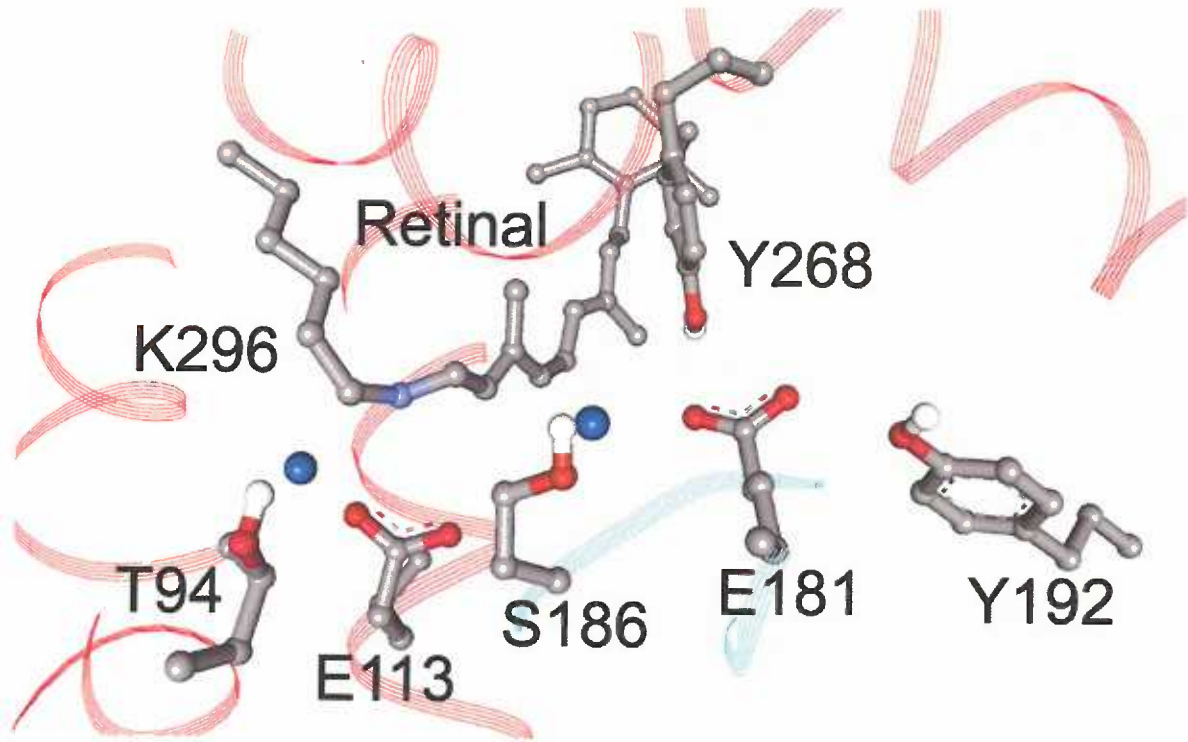


Figure 5. 2: UV/vis absorption profiles of purified rhodopsin hydrogen bond network mutants. Photobleaching properties are shown for each mutant relative to WT: dark state (red), following 30 s bleaching (Meta II state - blue), and immediately following acid denaturation of the photobleached species to a pH 1.9 (black). All spectra recorded in buffer A, pH 6.0 at 20 °C. The ~ 480 nm shoulder species present in mutant Y268F following photobleaching is followed as a function of time in Fig. 5. 3. Absorbance values are presented in Table 5. 1.

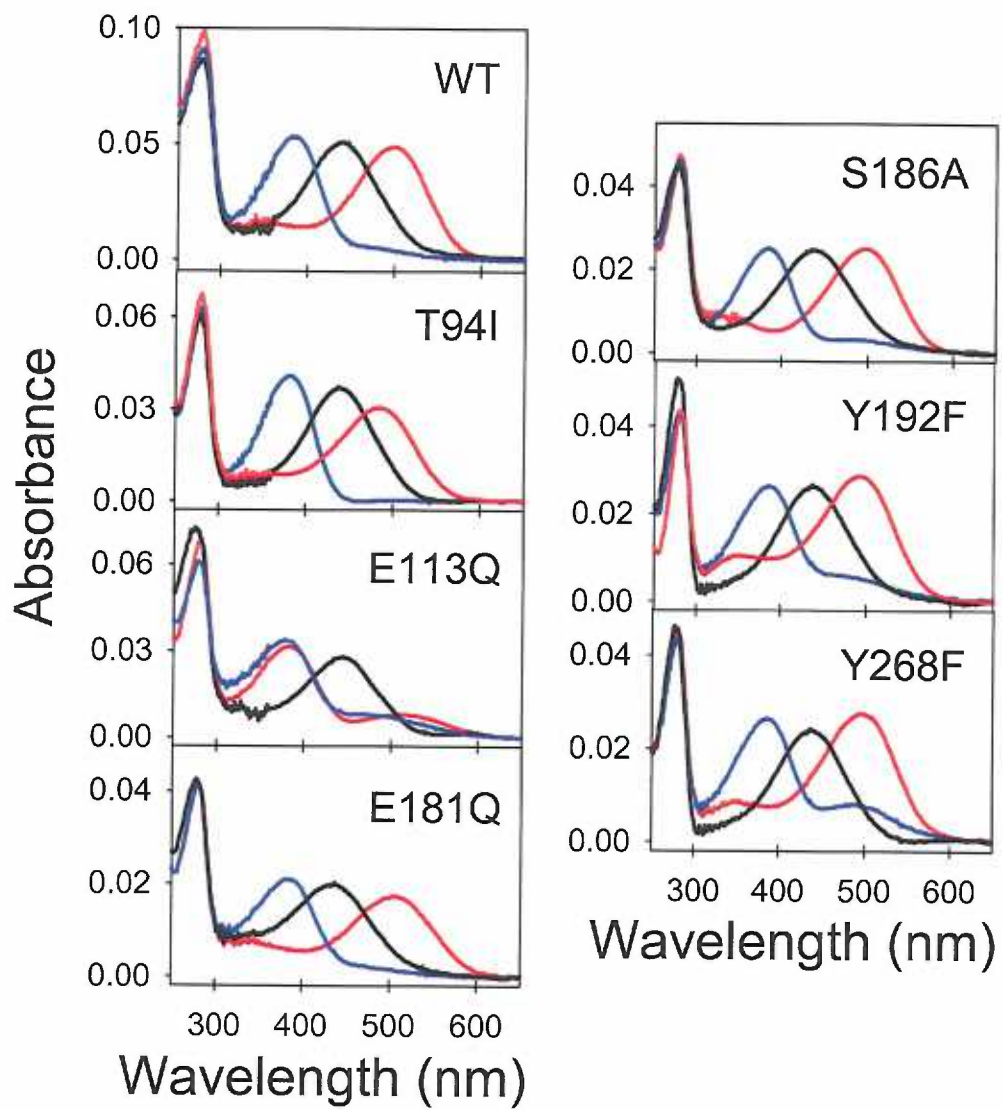


Figure 5. 3: Spectral properties of mutant Y268F in comparison with WT following illumination. Samples were photobleached for 15 s in buffer A, pH 6.0 at 20 °C. Upon illumination, Y268F (top panel) exhibits a spectral shoulder centered around ~ 480 nm. This species persists even 500 min post-illumination. In contrast, WT rhodopsin (bottom panel) exhibits no ~ 480 nm species immediately following photobleaching. The arrow in the lower panel indicates a slow rise over time of a 480 nm species – the MIII intermediate.

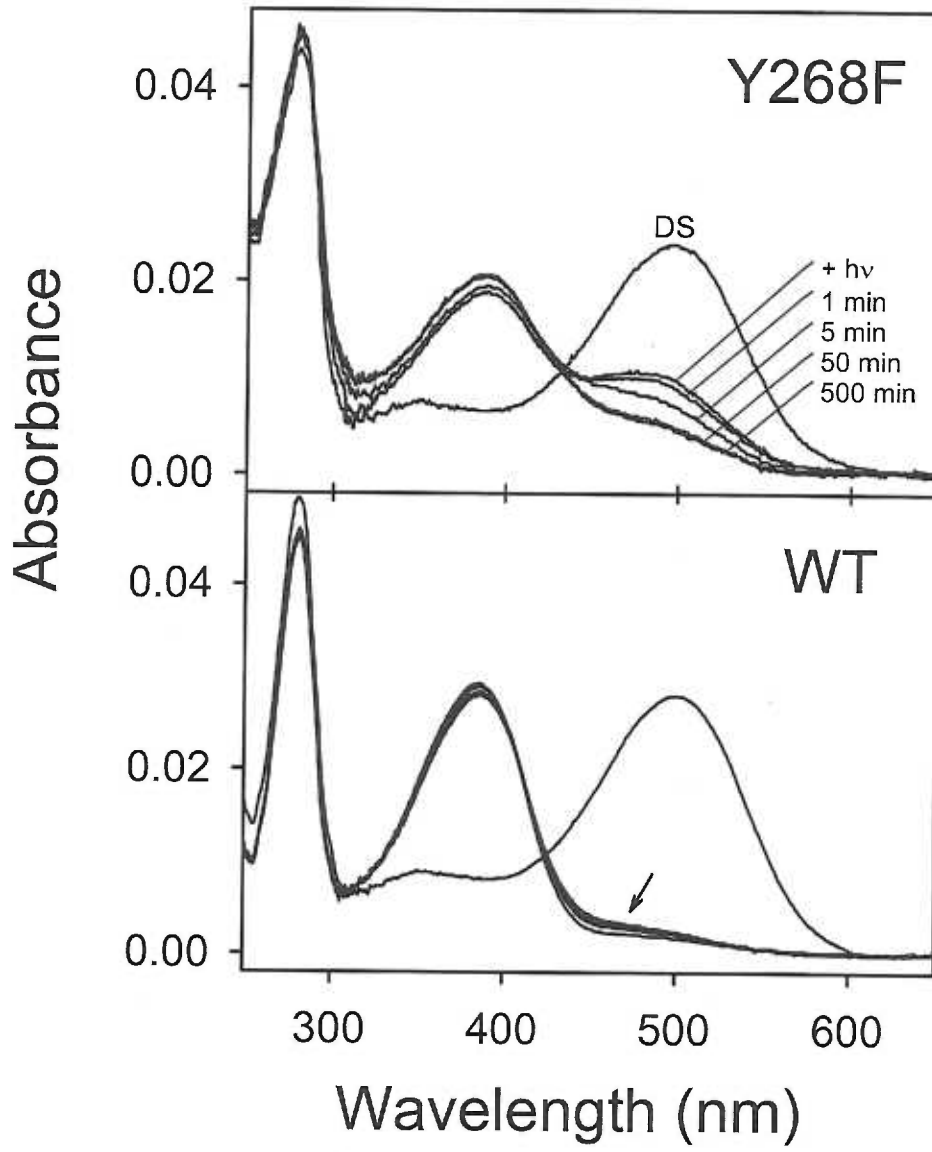


Figure 5. 4: Arrhenius plots of dark state thermal decay rates. Rates were obtained from absorbance decay or fluorescence retinal release assays. All mutations show accelerated rates of dark state decay suggesting a kinetic effect. Additionally, all of the mutants show linear plots (contrast to the concave plot WT) suggesting the reaction energetics have changed as well. All measurements were carried out in buffer A at pH 6.0 over a temperature range of 36 to 55 °C. Kinetic and thermodynamic parameters provided in Table 5. 2.

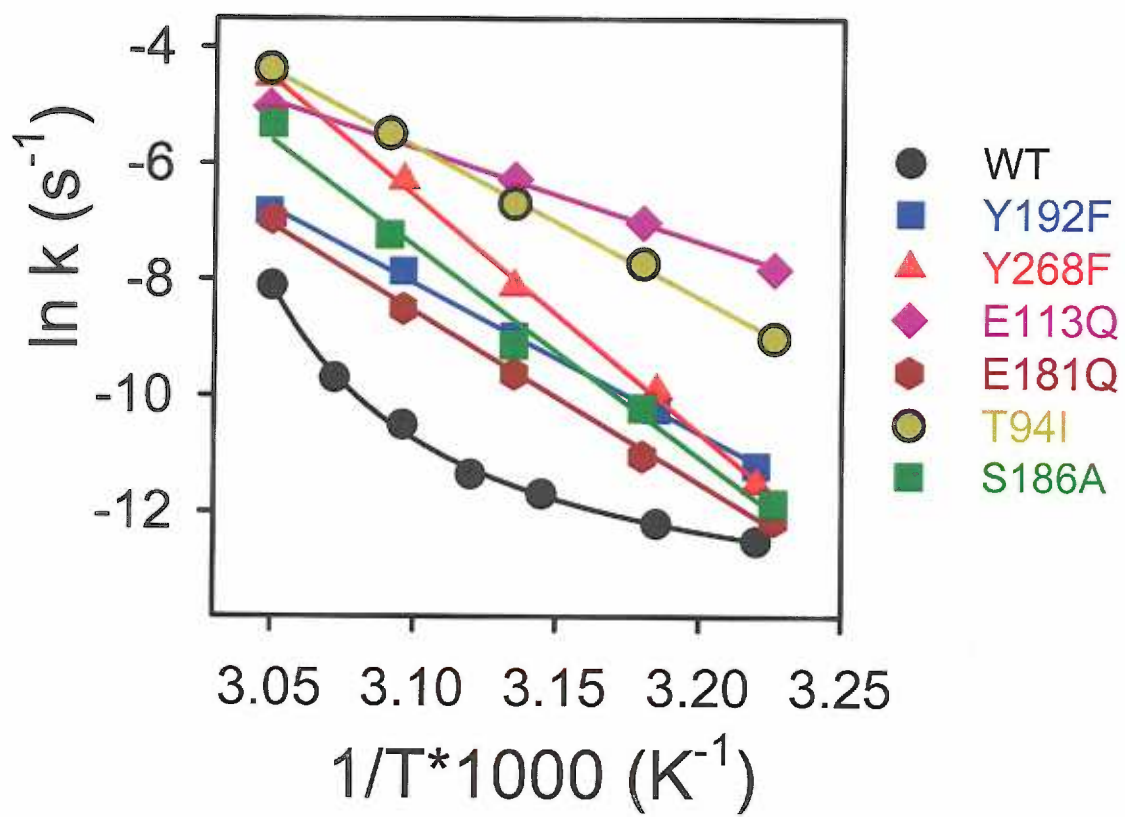


Figure 5. 5: Hydrogen bond network rhodopsin mutations show location dependent effects on Schiff base stability in the MII state. Arrhenius plots of retinal release rates for hydrogen bond network mutations in buffer A at pH 6.0 over a temperature range of 5 to 35 °C. **(A)** Mutants E181Q, Y192F and Y268F show no dramatic effect on MII Schiff base linkage stability compared to other hydrogen bond network mutation sites. **(B)** In contrast to their diminished dark state stabilities in the MII state (see Fig. 5. 4) the Schiff base linkage of mutants T94I, E113Q and S186A are all significantly more stable than WT rhodopsin. Kinetic and thermodynamic parameters provided in Table 5. 2.

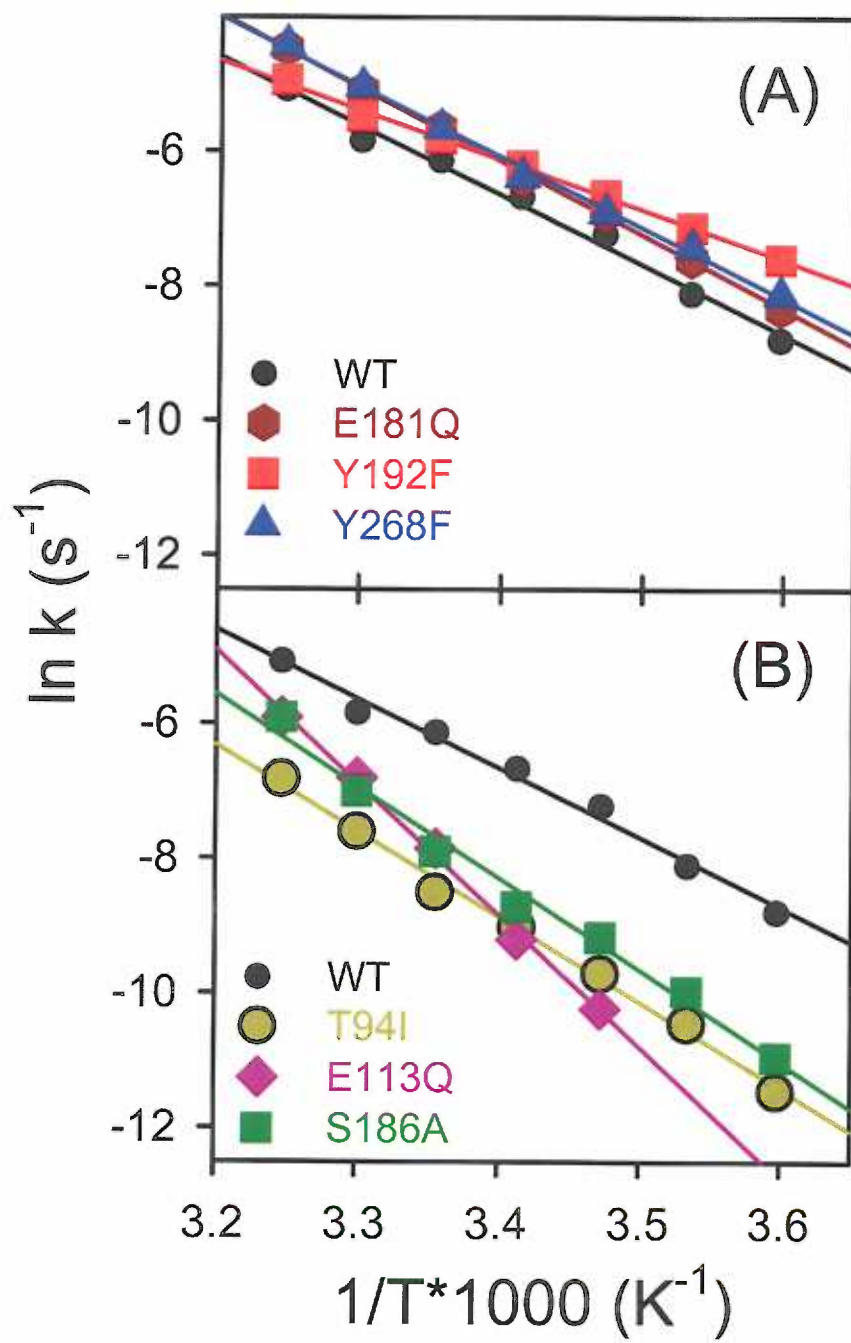
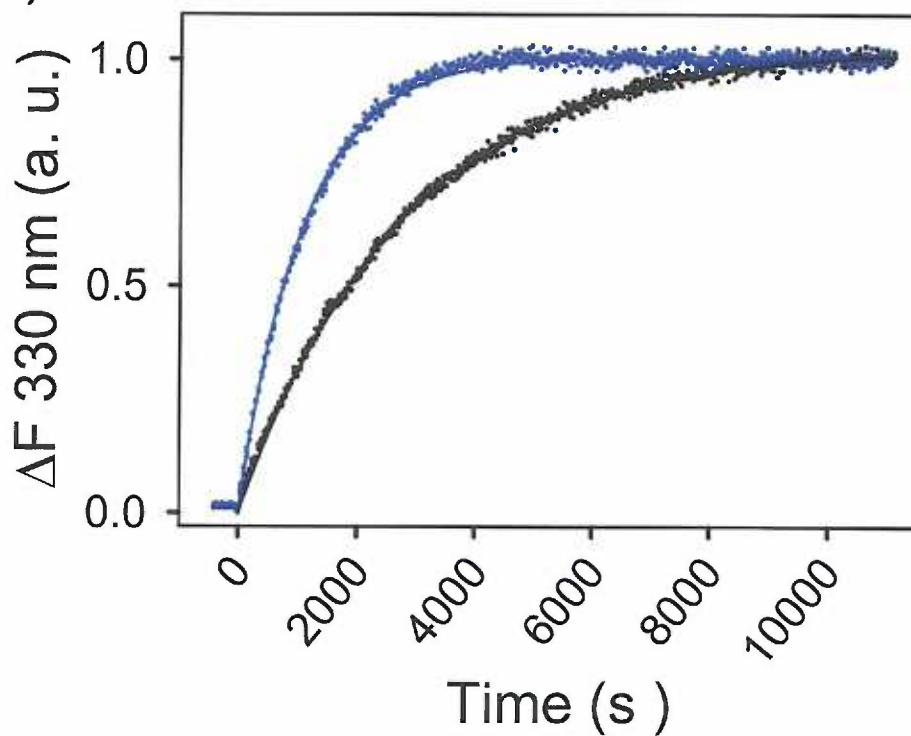


Figure 5. 6: Kinetic isotope effects of retinal Schiff base hydrolysis and retinal release. (A) Retinal release assay on WT rhodopsin at 20 °C, pH 6.0, in buffer A prepared in either H₂O (blue) or D₂O (black). (B) Proton inventory of deuterium solvent isotope effect on retinal release process. The data fit best to a cubic equation (solid line), the linear fit is shown as a dashed line. For further details see Materials and Methods and Discussion.

(A)



(B)

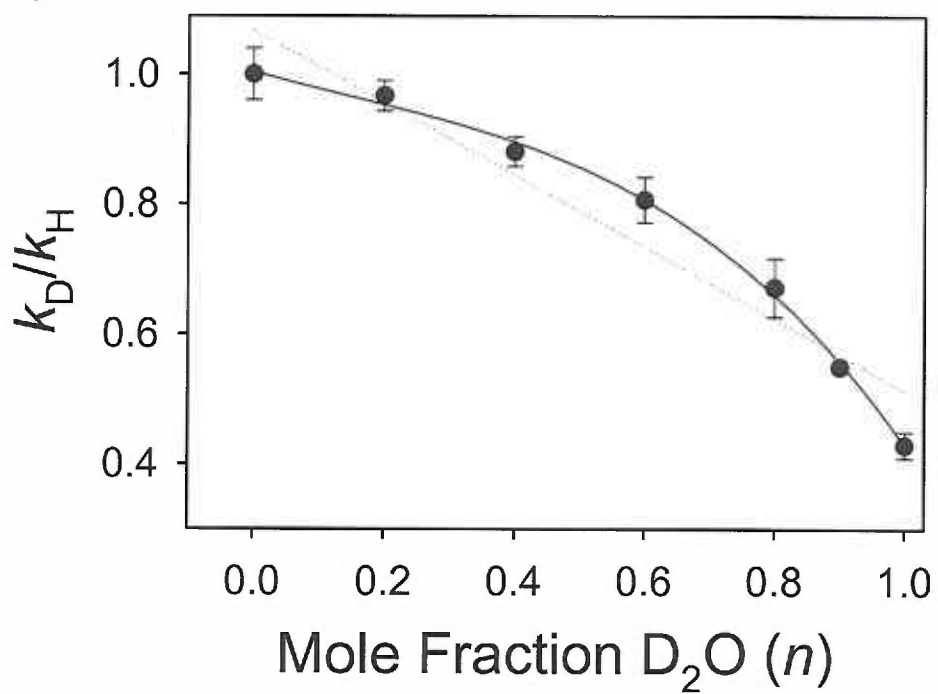
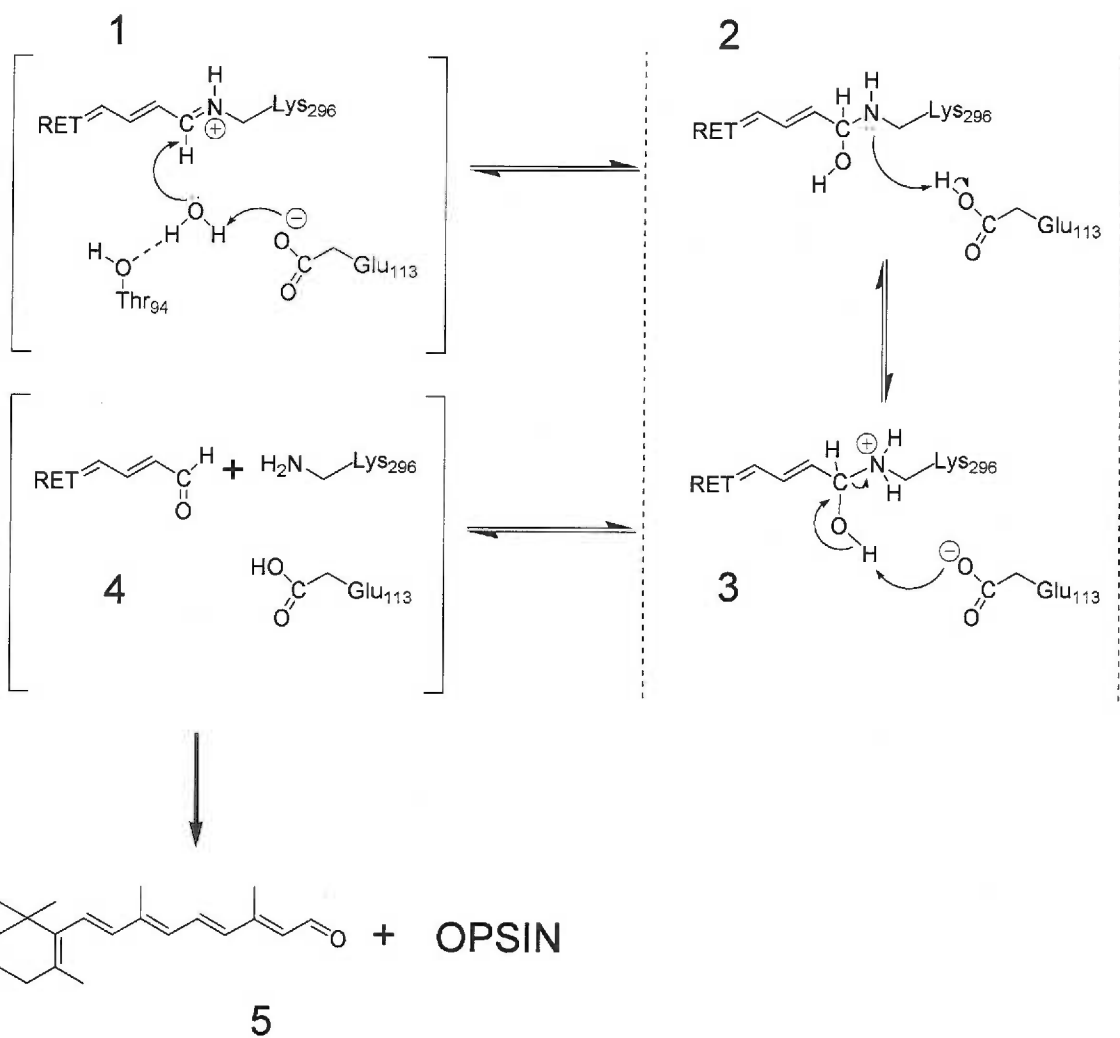


Figure 5. 7: Proposed mechanism for retinal Schiff base hydrolysis from rhodopsin.

During decay of the MII species all-*trans*-retinal is hydrolyzed and leaves the opsin-binding pocket. A water molecule within the binding pocket, possibly orientated by T94 and base catalyzed by E113, initiates hydrolysis by attacking the Schiff base linkage (step 1). This gives rise to the tetrahedral carbinolamine intermediate and results in reorientation of the active site contacts to allow protonation of the basic carbinolamine either from the solvent or perhaps residue E113 (step 2). The carbinol species is subsequently deprotonated, again either by the solvent or a neighboring amino acid side chain (step 3). The linkage then breaks and gives rise to the all-*trans*-retinal aldehyde and the free amino group of K296 (step 4). The noncovalent complex of the retinal and the opsin-binding pocket is unstable due to the sterically unfavorable *trans*-configuration of the retinal and it irreversibly dissociates from opsin, leaving the binding pocket (step 5). With the exception of the last process all steps in the mechanism are potentially reversible.



Chapter 6

Rhodopsin Activation Exposes a Key Hydrophobic Binding Site For the Transducin α -subunit C-terminus.

Jay M. Janz[§] and David L. Farrens[§]

[§]Department of Biochemistry and Molecular Biology,

Oregon Health and Science University

3181 S. W. Sam Jackson Park Drive, Portland, Oregon 97239-3098

Running Title: Mapping Rhodopsin - Transducin Interactions by Fluorescence
Spectroscopy.

6. 1: SUMMARY

Conformational changes enable the photoreceptor rhodopsin to couple with and activate the G-protein transducin. Here we demonstrate a key interaction between these proteins occurs between the C-terminus of the transducin alpha-subunit ($G_{T\alpha}$) and a hydrophobic cleft in the rhodopsin cytoplasmic face exposed during receptor activation. We mapped this interaction by labeling rhodopsin mutants with the fluorescent probe bimane, and then assessed how binding of a peptide analogue of the $G_{T\alpha}$ C-terminus (containing a Tryptophan quenching group) affected their fluorescence. From these and other assays, we conclude the $G_{T\alpha}$ C-terminal tail binds to the inner face of helix 6. Further, we find that a "hydrophobic patch" comprising key residues in the exposed cleft is required for transducin binding/activation as it enhances the binding affinity for the $G_{T\alpha}$ C-terminal tail, contributing up to 3 kcal/mole for this interaction. We speculate the hydrophobic interactions identified here may be important in other GPCR signaling systems, and our Trp/bimane fluorescence methodology may be generally useful for mapping sites of protein-protein interaction.

All experiments reported in this chapter we performed by the author of this dissertation and portions of this chapter have been accepted for publication: Janz, J. M., and Farrens, D. L. (2004) *Journal of Biological Chemistry* – *In Press*.

6. 2: INTRODUCTION

Visual signal transduction begins with light induced structural changes in the photoreceptor rhodopsin. These changes convert this model G-protein coupled receptor

(GPCR) into an active form (called MII), which couples with and activates the G-protein transducin, thus initiating the biochemical cascade that results in vision (14, 31, 34, 51).

A key step in MII formation involves an outward movement of transmembrane helix 6 in the rhodopsin cytoplasmic face (114). This movement increases the exposure of residues on the inner face of this helix (113, 116, 225), (Figure 6. 1) and is needed for transducin (G_T) activation (114, 115). A similar movement appears to occur in ligand activated GPCRs (8, 226-228), suggesting helix 6 movement represents a conserved event in GPCR signaling (7).

How might this movement enable coupling with transducin? We and others have hypothesized helix 6 movement opens a cleft that provides a binding site for the transducin α subunit C-terminal tail ($G_{T\alpha}$ C-terminus) (66, 116, 117) (Figure 6. 1). Several lines of evidence show that the rhodopsin cytoplasmic face directly interacts with the $G_{T\alpha}$ C-terminus. For example, peptides and peptide analogues corresponding to the $G_{T\alpha}$ C-terminus can bind and stabilize MII rhodopsin (229-231), and binding induces structure in these peptides (232-235). Rhodopsin mutagenesis studies show residues in intracellular loops I2 and I3 are important in this interaction (236, 237), and a photocrosslinking probe on loop I3 at residue 240 on rhodopsin crosslinks to this region of $G_{T\alpha}$ (238). However, direct evidence for where and how the $G_{T\alpha}$ C-terminus and rhodopsin interact is lacking.

In the present manuscript we set out to test whether the $G_{T\alpha}$ C-terminus binds to the cleft formed during rhodopsin activation, through use of a combination of site-directed labeling and fluorescence methods. Using these approaches, we were able to map where these regions interact by monitoring the tryptophan quenching of bimane

fluorescence from modified cysteine residues on rhodopsin. Our results indicate the $G_{T\alpha}$ C-terminal tail does indeed bind to the inner face of helix 6, and we obtained evidence that critical hydrophobic contacts in this region control the affinity of the rhodopsin-transducin interaction, with key residues contributing up to 3 kcal/mole binding energy. We propose the lack of these contacts are the underlying defect in several mutant rhodopsin proteins and speculate that the activation mechanism described and hydrophobic interactions identified here may be universally important in other GPCR signaling systems.

6. 3: MATERIALS and METHODS

6. 3. 1: Materials and nomenclature.

Definitions for the buffers used are as follows: PBSSC [0.137 M NaCl, 2.7 mM KCl, 1.5 mM KH_2PO_4 , and 8 mM Na_2HPO_4 (pH 7.2)], buffer A [1% DM and PBSSC (pH 7.2)], buffer B [2 mM ATP, 0.1% DM, 1 M NaCl, and 2 mM $MgCl_2$ (pH 7.2)], buffer C [0.05% DM and PBSSC (pH 7.0)], buffer D [0.05% DM and 5 mM MES (pH 6.0)].

The peptides used in this study are variants of the high affinity analogues of $G_{T\alpha}$ C-terminal 11 residues 340-350 originally developed by Hamm and colleagues (230, 231). All peptides contain free N and C termini, and were synthesized by the Emory Microchemical Facility (Atlanta, GA) and analyzed by Micro HPLC analysis and MALDI Mass Spectrometric Analysis. The name and amino acid sequences for each peptide are as follows: 23S; $NH_2VLEDLKSCGLF_{COOH}$, and W23SV $NH_2WVLEDLKSIVGLF_{COOH}$. All peptides were prepared in Buffer D at pH 6.0. The

sulfhydryl-reactive fluorescent probes 1-(2-maleimidylethyl)-4-(5-(4-methoxyphenyl)oxazol-2-yl)pyridinium methanesulfonate (PyMPO maleimide), and (2-Pyridyl)dithiobimane (PDT-bimane) were purchased from Molecular Probes (Eugene, OR) and Toronto Research Chemicals (North York, ON Canada) respectively. All remaining materials used in this study are similar to those previously described (207).

6. 3. 2: Construction, expression and purification of rhodopsin mutants.

The construction and characterization of cysteine rhodopsin mutants θ , C140, K141C, E150C, F228C, V248C, V250C and C316 used herein have been previously described (148, 153, 239, 240). Rhodopsin mutants K141C, K141C/L226A, K141C/T229A and K141C/V230A used in this study were constructed using overlap extension PCR (149) in the pMT4 plasmid θ , (in which the native cysteine residues C140, C316, C322 and C323 are replaced with serines (162, 178). All mutations were confirmed by sequencing. The mutant rhodopsin proteins were transiently expressed in COS-1 cells using the DEAE-dextran method, and cells were harvested 56 to 72 h after transfection as previously described (207). After harvesting, the samples were regenerated with 11-*cis*-retinal and purified using immunoaffinity chromatography essentially as described previously (151, 179, 207).

6. 3. 3: PDT-bimane labeling of rhodopsin mutants, and determination of labeling efficiency.

Labeling of samples with PDT-bimane and subsequent purification was carried out while the protein was bound to the 1D4 matrix as previously described for monobromobimane (See Scheme 6. 1), (116). After elution from the immunoaffinity column, a spectrum of each elution fraction was recorded (described below), and the

purified samples were either used immediately or snap frozen in liquid N₂ and stored at -80 °C. The amount of PDT-bimane label incorporation, and the presence of unreacted free label were determined as follows. Labeling efficiency was determined by incubating the samples in the presence of 50 μM TCEP reducing agent at 4 °C for 10 minutes in buffer D followed by addition of 10% TCA to each sample to precipitate the protein. The samples were incubated at 4 °C for 15 minutes in this mixture, then centrifuged at 100,000 X g for 30 minutes and fluorescence emission scans were carried out on both sets of supernatants using 380 nm excitation and monitoring emission from 410 - 605 nm. This data was then used to determine the concentration of PDT-bimane in each sample by comparison to a standard curve generated from serial dilutions of stock PDT-bimane. To determine the amount of free, unreacted label, the above procedure was carried out except the protein was first precipitated by addition TCA, and any remaining signal was attributed to label not attached to the protein.

6. 3. 4: UV/vis absorption spectroscopy.

All UV/vis absorption spectra were recorded with a Shimadzu UV-1601 spectrophotometer at 20 °C using a bandwidth of 2 nm, a response time of 1 s, and a scan speed of 500 nm/min unless otherwise noted. Concentration of protein was calculated using a molar extinction coefficient value (ϵ_{500}) for WT rhodopsin of 40 600 M⁻¹ cm⁻¹ (73), and the molar extinction coefficient (ϵ_{380}) of PDT-bimane was 5000 M⁻¹ cm⁻¹. The samples were photobleached in buffer D by illumination for 30 s (at a 6 Hz flash rate) with a Machine Vision Strobe light source (EG&G) equipped with a wavelength > 495 nm long-pass filter. This light treatment was found to be adequate for full conversion of all samples to the MII state.

6. 3. 5: Measurement of the rate of retinal release and/or MII decay by fluorescence spectroscopy.

The MII stability of the PDT-bimane labeled mutants was assessed by monitoring the fluorescence increase of opsin during retinal release using a Photon Technologies QM-1 steady state fluorescence spectrophotometer and standard instrument settings (154, 179). For further detail please refer to section 3. 3. 9 in chapter 3.

6. 3. 6: Peptide inhibition of MIII formation.

The ability to inhibit MIII formation was used to monitor peptide binding to each mutant rhodopsin. In these assays, samples were incubated in the presence or absence of 100 μ M peptide W23SV (in buffer D, pH 6.0) on ice for 10 minutes, and UV/vis spectra were recorded every 5 minutes from 650 nm to 250 nm at 10 °C. Following an initial dark state scan, samples were photobleached to the MII state and effect of the peptide on MIII formation was monitored at 460 nm over time (see Fig. 6. 2A). Instrument baseline drift was corrected for by setting absorbance of all spectra to zero at 650 nm. For comparison purposes duplicate experiments were performed on each sample in the absence of peptide (see Fig. 6. 2B, 6. 3A).

6. 3. 7: Peptide blocking of rhodopsin mutant V250C.

The reactivity of rhodopsin mutant V250C towards the sulfhydryl-specific probe PyMPO-maleimide was carried out as previously described (116). Briefly, 3 μ g of mutant rhodopsin was reacted with 25-fold excess PyMPO for 1 minute in Buffer F (pH 7.2) at 4 °C in either the dark state or following photobleaching (30 seconds) to the MII state. To test the ability of peptide W23SV to block PyMPO labeling of mutant V250C the sample was pre-incubated with 100-fold excess of peptide prior to photobleaching

and to the addition of PyMPO. All reactions were quenched by the addition of L-cysteine to a 1 mM final concentration. Samples were subsequently resolved by SDS-polyacrylamide gel electrophoresis and label incorporation was visualized using a Bio-Rad Gel Documentation Instrument. The background mutant θ (which contains no reactive cysteine residues) was used as a control to show PyMPO labeling specificity. Following label visualization, gels were subjected to Coomassie staining to assure equal distribution of protein in each of the sample wells.

6. 3. 8: KI Fluorescence quenching measurements.

Steady-state fluorescence quenching measurements of V250B were carried out as previously described (116). Briefly, 125 μ l of a 250 nM sample was excited at 380 nm (1/4 nm bandpass setting) and emission monitored from 405 nm to 605 nm (12 nm bandpass setting). Five separate samples with KI concentrations ranging from 0 to 25 mM were measured in both the dark state and in the MII state following illumination with >490 nm for 30 s. Separate samples were also measured in a similar manner following pre-incubation (10 min on ice) with 100 μ M peptide W23SV. The salt concentration of each sample was kept constant at 25 mM by the addition of a corresponding amount of KCl, and $\text{Na}_2\text{S}_2\text{O}_3$ was added to 0.10 mM to inhibit the formation of I_3^- . The resulting data were plotted as fluorescence intensity at 466 nm *versus* concentration of quenching agent (KI), to calculate the Stern-Volmer quenching constant, K_{SV} , according to equation 6. 1 below.

$$\frac{F_0}{F} = 1 + K_{SV} \cdot [Q] \quad (\text{Eq. 6. 1})$$

6. 3. 9: Fluorescence Quenching of PDT-bimane labeled rhodopsin samples by peptide W23SV.

Unless noted otherwise, the steady-state fluorescence measurements of PDT-bimane labeled rhodopsin mutants were carried out at 10 °C using 500 nM sample in buffer D, pH 6.0. All spectra were buffer subtracted and corrected for sample dilution when necessary. Fluorescence emission spectra were recorded from 405 nm to 610 nm (15 nm band pass) while being excited at 380 nm (¼ nm band pass). Dark state spectra were recorded first, followed by photobleaching the sample to the MII state. Note that conversion to the MII state results in a large increase in fluorescence intensity from the labeled samples due to the shift in rhodopsin absorbance from 500 nm to 380 nm, which removes spectral overlap with PDT-bimane fluorescence, thereby relieving the quenching due to energy transfer from the bimane to retinal. Peptide quenching experiments were performed by the addition of peptide in buffer D (pH 6.0) to MII rhodopsin to the desired concentration. In control experiments we find that the fluorescence intensity of the labeled samples in the MII state remains relatively constant throughout the short time-course of the peptide quenching assays (data not shown). Additionally, less than 8 % of the MII photointermediate decays over the time-course of the assay. Data were acquired using the program Felix (Photon Technologies Inc.) and plotted using Sigma Plot (Jandel Scientific Software).

6. 3. 10: Determination of transducin (G_T) activation rates.

Activation of G_T by rhodopsin was monitored using fluorescence spectroscopy at 10 °C, using previously described conditions (114, 155, 156, 179). Briefly, this involved exciting the samples at 295 nm (2 nm bandwidth), and monitoring fluorescence emission

at 340 nm (12 nm bandwidth). Photobleached mutant rhodopsin (see above) was added to a concentration of 5 nM to the reaction mixture consisting of 250 nM G_T in 10 mM Tris (pH 7.2), 2 mM MgCl₂, 100 mM NaCl, 1 mM DTT, and 0.01% DM, and the mixture allowed to stir for 300 s. The reaction was then initiated by adding GTP γ S to a final concentration of 5 μ M, and fluorescence increase monitored for 2000 s. To calculate the initial activation rates, the slopes of the initial fluorescence increase following GTP γ S addition were determined through the data points covering the first 60 s.

6. 3. 11: Peptide titration assays and calculation of EC₅₀ and $\Delta\Delta G^\ddagger$ values.

The EC₅₀ values for quenching of PDT-bimane labeled mutant rhodopsin samples by W23SV were determined by titrating the samples with increasing amounts of peptide. All experiments were performed at 10 °C to minimize decay of the MII species. It was necessary to account for the decay of the MII species ($t_{1/2} \approx 38$ min at 10 °C, see Table 2) during the time course of the assay. Thus, the titration experiments were performed by splitting the samples in two, and titrating each sample separately with different concentrations of peptide. In this manner dose response curves were generated in less than 10 min, in which time less than 8 % of the MII species had decayed. These peptide quenching data were combined and analyzed using nonlinear regression by fitting the data to a sigmoidal dose-response (variable slope) equation (four-parameter logistic equation), see equation 6. 2 below (231).

$$Y = \text{minimum} + (\text{maximum} - \text{minimum}) / (1 + 10^{((\log EC_{50} - x) * \text{Hillslope})}) \quad (\text{Eq. 6 .2})$$

In equation 2, “minimum” is the Y value for fluorescence at the bottom plateau (fully quenched) and “maximum” is the Y value for fluorescence at the top plateau (not quenched). LogEC_{50} is the logarithm of the EC_{50} , the concentration that gives a response halfway between maximum and minimum. The $\Delta\Delta G^\ddagger$ values for mutants K141B/226A, K141B/229A and K141B/230A were calculated using the EC_{50} values to reflect binding K_{eq} , and thus the $\Delta\Delta G^\ddagger$ values were calculated according to equation 6. 3 below.

$$\Delta G^\ddagger = -RT \ln K_{\text{eq}} \quad (\text{Eq. 6. 3})$$

In equation 3, R is the universal gas constant, T is the temperature and K_{eq} is the EC_{50} for peptide quenching.

6. 4: RESULTS

6. 4. 1: Peptide W23SV binding protects V250C on the inner face of helix 6.

Previously, we established that helix 6 movement in rhodopsin can be detected by two simple methods; through monitoring an increased reactivity of a cysteine residue introduced into the inner face of this helix at site V250, and by monitoring the increased solvent accessibility of a fluorescent probe attached at this site (116). Here we used these methods to probe the proposed $G_{T\alpha}$ C-terminus binding site in conjunction with a high affinity peptide analogue of the $G_{T\alpha}$ C-terminus. This peptide, W23SV (sequence: WVLEDLKSIVGLF), is a derivative of a peptide originally constructed by Hamm and colleagues (called 23S (230, 231)), in which we added a tryptophan residue (Trp) to the N-terminus to act as a quenching group. We also exchanged the reactive cysteine residue with a valine (231), to ensure it would not react with, or complicate the cysteine studies.

At the start of these experiments, we established that peptide W23SV binds rhodopsin mutant V250C, by monitoring its ability to inhibit formation of a 460 nm photoproduct, called MIII, which normally occurs as the MII species decays to its inactive forms (44, 125) (see Figure 6. 2A). In addition, MII stabilization studies carried out by monitoring “extra MII” in digitonin (232) indicated both peptide 23S and W23SV were able to bind to light activated rhodopsin (see supplemental Figure 6S. 1).

As seen in Fig. 6. 2B, binding of peptide W23SV completely blocks the reactivity of V250C in the MII state towards the cysteine labeling agent PyMPO maleimide (Figure 6. 2B). Similar results were obtained using peptide 23S (data not shown). However, due to possible cross reactivity of the cysteine in peptide 23S with the fluorescent probes, the remaining work was performed using peptide W23SV. Binding of peptide W23SV reduces the solvent accessibility of a fluorescent probe (bimane) attached at site 250. As indicated from the Stern-Volmer plot (Figure 6. 2C), the W23SV peptide shields the fluorescent probe from quenching by KI only in the MII state. Taken together, these results provide compelling evidence that the $G_{T\alpha}$ C-terminus binds to the cleft formed during rhodopsin activation. However, they do not formally rule out the possibility that the results described above are due to an indirect effect on the environment surrounding site V250B (where “B” indicates PDT-bimane label) caused by the peptide binding. To alleviate this potential concern, we turned to a novel approach, described below.

6. 4. 2: Mapping rhodopsin/ $G_{T\alpha}$ C-terminal interactions.

To more directly map where the $G_{T\alpha}$ C-terminus binds on the face of rhodopsin, we turned to a novel method we have recently developed for mapping protein-protein

interactions. This approach exploits the fact that a Trp residue substantially quenches the fluorescence of a bimane label only when the two are essentially within contact distance (241). Since bimane is a small probe (similar in size to a Trp residue), this new method clearly defines localized sites of interaction, since substantial quenching only occurs if the Trp and bimane are able to contact one another during the excited state of the bimane fluorophore.

The goal in these experiments was to see if the Trp residue in peptide W23SV could quench the fluorescence of bimane labels attached at different sites on the cytoplasmic face of rhodopsin (Figure 6. 1). We carried out this experiment using rhodopsin mutants containing single reactive cysteine residues introduced at sites 140, 141, 150, 228, 248, 250 and 316 in a non-reactive background mutant (called Theta (148, 178)). As can be seen in Figure 6. 1, these sites are distributed throughout the rhodopsin cytoplasmic face. These mutants were expressed, purified, and labeled with bimane at a 1:1 label to protein ratio. Photobleaching and MII decay assays confirmed that the bimane label did not perturb the structure or stability of these samples. The labeling and functional characterization of these bimane labeled rhodopsin mutants are presented in Table 6. 1.

Before carrying out the mapping experiments we first established that 100 μ M peptide W23SV could bind to all of the bimane labeled mutants, as demonstrated by its ability to block MIII formation (Figure 6. 3A). We next assessed the effect that the Trp quenching group on peptide W232SV has on the fluorescent properties of the individually bimane labeled rhodopsin mutants. We found that most of the mutants showed no fluorescence change upon peptide W23SV binding (Figure 6. 3B). Only two

mutants, C140B and K141B (where “B” indicates PDT-bimane label) showed a substantial and reproducible fluorescence decrease, with one mutant, F228B, showing a small decrease as well. As seen in Figure 6. 3C, the quenching observed for C140B, K141B and F228B occurred in a dose-dependent fashion, with peptide quenching exhibiting a titration of effect. The data from these experiments is summarized in graphical form in Figure 6. 4.

Importantly, we find that the W23SV induced quenching is reversible, since addition of an excess of peptide without the tryptophan residue (peptide 23S) can fully displace W23SV quenching (Figure 6. 5A). Furthermore, the quenching is specific for the MII form of rhodopsin, since it does not occur if peptide W23SV is added following the complete decay of the MII species (Figure 6. 5B), or following cleavage of the retinal Schiff base with hydroxylamine (NH₂OH) as shown in Figure 6. 5C. Finally, we find that peptide W23SV does not bind to dark state rhodopsin (data not shown). Taken together, these results suggest peptide W23SV binds to the cleft formed in MII rhodopsin in an orientation which places its N-terminal tryptophan within near contact distance of the bimane probe located at positions C140, K141, and to a much lesser extent, F228 (see Figure 6. 1A).

6. 4. 3: Hydrophobic interactions govern rhodopsin/G_{Tα} C-terminus affinity.

Interestingly, the rhodopsin crystal structure shows that sites which exhibit Trp/bimane quenching (C140B, K141B, and F228B) are near several residues (L226, T229 and V230, see Figure 6. 1B) previously identified by cysteine-scanning studies to be important for transducin activation (148). We hypothesized these residues may form an unappreciated “hydrophobic patch” that is required for rhodopsin/transducin

interactions. To test this theory, we measured the contribution of these residues to $G_{T\alpha}$ C-terminal binding, using the above-mentioned peptide-quenching assay. First, we substituted alanines at positions L226, T229 and V230 into the K141C mutant, and then reacted the cysteine at site 141 with the PDT-bimane label. Characterization of these labeled mutants, K141B/L226A, K141B/T229A and K141B/V230A indicated they were all similar to WT in terms of expression, chromophore binding and rates of retinal release, (see Table 6. 2).

When these mutants were assayed for their ability to stimulate $GTP\gamma S$ exchange in the whole transducin protein, all were found to be severely impaired in comparison to K141B alone or WT rhodopsin (Figure 6. 6A, Table 6. 3). However, the peptide quenching assays indicate these mutants were all able to bind peptide W23SV, but with greatly reduced affinities. As seen in Figure 6. 6B and Table III, substantially more peptide was required to see the quenching effect, resulting in EC_{50} values for “hydrophobic patch” mutants more than 160 times greater than that of K141B alone (200 nM vs. 32 μ M), Table 6. 3.

6. 5: DISCUSSION

A growing body of evidence suggests an outward movement of transmembrane helix 6 on the cytoplasmic face of the rhodopsin is a key step in receptor activation. This movement may be the only large-scale conformational change required for receptor activation (242) and may occur in all GPCRs (7). We and others have proposed that the role of this movement may be to open up a cleft that provides a binding site for the transducin α -subunit C-terminal tail as well as expose other important binding sites in

rhodopsin (68, 243). The major aim of the present work has been to directly test this hypothesis.

Using variants of a high affinity peptide analogue of the $G_{T\alpha}$ C-terminus we obtained evidence that the $G_{T\alpha}$ C-terminus binds to MII rhodopsin in a manner which occludes residue V250C, consistent with the hypothesis that the $G_{T\alpha}$ C-terminal tail is binding into the cleft formed by Helix 6 movement during rhodopsin activation. Our mapping studies suggest peptide W23SV binds in a position that places the N-terminal Trp residue near the bimane label on residues C140B, K141B and to a lesser extent F228B, although our results do not indicate how deeply into rhodopsin the $G_{T\alpha}$ C-terminus penetrates upon binding. Interestingly, site V248B shows no quenching interaction, yet the dark state structures of rhodopsin show it to be in close proximity to residues C140, K141 and F228 (52-54). These findings are consistent with the proposed movement of helix 6 during receptor activation, which would alter the location of site V248 further away from the sites that show quenching near helix 3.

In addition, our results illustrate that all of the sites labeled with bimane were able to bind the $G_{T\alpha}$ C-terminus peptide analogue (Figure 6. 3A). This suggests that none of the labeled residues participate in, or at least are required for, providing the direct binding interface between the receptor and $G_{T\alpha}$ C-terminal peptide. We have chosen not to model the exact nature of this binding, as we feel our data do not yet warrant doing so. However, our results do provide an additional constraint to the rhodopsin $G_{T\alpha}$ C-terminus interaction that will facilitate future more detailed modeling studies.

Importantly, our studies show the $G_{T\alpha}$ C-terminus binding is specific for the MII state, and that the presence of the retinal Schiff-base linkage is required to maintain the exposure of the cleft required for interaction with the C-terminal tail of $G_{T\alpha}$. Interactions between the i3 loop of rhodopsin and the C-terminus of transducin have previously been implicated in conferring efficient and specific coupling and activation (244, 245). Our results show residues L226, T229 and V230, which lie in this region, play a key role by imparting high affinity binding for the transducin $G_{T\alpha}$ C-terminal tail with each of these “hydrophobic patch” residues contributing upwards of 2.6 kcal/mol to the binding energy (Table 6. 3). Note that formally our data do not clarify whether this interaction is required for binding of $G_{T\alpha}$, or is required for some other function, such as inducing GDP/GTP exchange. Regardless, the binding energy contributed by these residues appears critical for rhodopsin/transducin interactions, since residues L226 and V230 are completely conserved in all type-1 vertebrate rhodopsins (5). Interactions between these receptor side chains with the C-terminal region of G-protein α -subunits may also aid in conferring G-protein subtype specificity.

In summary, our results suggest that the role of helix 6 movement during MII formation is to provide a binding site on the cytoplasmic face of rhodopsin for the $G_{T\alpha}$ C-terminus. This movement appears to open a cleft and expose a hydrophobic patch, which directly interacts with the $G_{T\alpha}$ C-terminus and increases the affinity of transducin binding. Our results also suggest hydrophobic interactions between rhodopsin and transducin may play a heretofore unappreciated but key role in the coupling of these two proteins, as has been suggested for other protein-protein complexes (246). Finally, we speculate that the approach we have described here may prove useful for assessing the

role of other movements that occur during activation of rhodopsin and its interaction with other proteins (225, 247-249).

6. 6: ACKNOWLEDGMENTS

We are grateful to Dr. Richard Brennan, Dr. Arthur Glasfeld, and Dr. John Denu for helpful discussions and to Dr. John Adelman, Dr. Michael Forte, Dr. Richard Goodman, Dr. Kevin Ridge, Dr. Mark Krebs and Dr. Jack Kaplan for critical reading of this manuscript.

Table 6. 1: PDT-bimane Labeling Characteristics of Single Rhodopsin Mutants
(spectral ratio, labeling ratio, % free label and $t_{1/2}$ of retinal release).

Sample ^a	A_{280}/A_{500} ^b	Labeling Ratio ^c	% Free label ^d	MII decay 10 °C $t_{1/2}$ (min) ^e
C140B	1.6	1.2 ± 0.1	4.7 ± 1.5	38.4
K141B	1.7	1.2 ± 0.1	4.3 ± 1.0	38.5
E150B	1.7	1.4 ± 0.2	3.4 ± 1.1	32.2
F228B	1.6	1.1 ± 0.1	3.6 ± 0.6	34.5
K248B	1.7	1.2 ± 0.1	3.4 ± 1.0	36.2
V250B	1.7	0.7 ± 0.1	4.2 ± 1.3	36.5
C316B	1.8	1.2 ± 0.1	4.7 ± 1.8	37.0
Theta-B	1.6	0.2 ± 0.1	3.7 ± 1.1	38.3

^a All samples are rhodopsin cysteine mutants generated in the theta background and labeled specifically at the introduced cysteine residue with the PDT-bimane probe.

^b Pure rhodopsin typically exhibits a protein (A_{280} nm) to chromophore (A_{500} nm) absorbance ratio of 1.6 to 1.8.

^c The amount of PDT-bimane label incorporated into the rhodopsin single cysteine mutants are presented as the number of labels per rhodopsin mutant (label/sample). Error values are standard error of the mean ($n = 2$).

^d The amount of free label remaining in each sample following labeling and purification is presented as a percentage of the total sample (for further details see Materials and Methods).

^e The MII decay rate of the labeled samples was determined in buffer D as described under Materials and Methods at 10 °C. Under these identical conditions the MII decay $t_{1/2}$ for unlabeled WT rhodopsin is 37.5 min.

Table 6. 2: PDT-bimane Labeling Characteristics of Rhodopsin Hydrophobic Patch Mutants (spectral ratio, labeling ratio, % free label and $t_{1/2}$ of retinal release).

Sample ^a	A_{280}/A_{500} ^b	Labeling Ratio ^c	% Free label ^d	MII decay 10 °C $t_{1/2}$ (min) ^e
K141B-226A	1.8	1.2	5.8	33.5
K141B-229A	1.9	1.5	5.7	35.0
K141B-230A	1.8	1.1	6.0	38.5

^a All samples contain a single alanine substitution generated in the K141C background and labeled specifically at the introduced cysteine residue with the PDT-bimane probe.

^b Pure rhodopsin typically exhibits a protein (A_{280} nm) to chromophore (A_{500} nm) absorbance ratio of 1.6 to 1.8.

^c The amount of PDT-bimane label incorporated into the rhodopsin mutants are presented as the number of labels per rhodopsin mutant (label/sample).

^d The amount of free label remaining in each sample following labeling and purification is presented as a percentage of the total sample (for further details see Materials and Methods).

^e The MII decay rate of the labeled samples was determined in buffer D as described under Materials and Methods at 10 °C. Under these identical conditions the MII decay $t_{1/2}$ for unlabeled WT rhodopsin is 37.5 min.

Table 6. 3: Activation and Peptide Quenching Characteristics of Rhodopsin Hydrophobic Patch Mutants (G_T activation, peptide quenching and $\Delta\Delta G^\ddagger$).

Sample ^a	Relative G_T Activation Rate (%) ^b	Peptide Quenching EC_{50} (μM) ^c	Binding $\Delta\Delta G^\ddagger$ (kcal/mol) ^d
K141B	91	0.2	-
K141B\L226A	1	32.3	2.9
K141B\T229A	2	19.4	2.6
K141B\V230A	10	24.4	2.7

^a All samples contain a single alanine substitution generated in the K141C background and labeled specifically at the introduced cysteine residue with the PDT-bimane probe.

^b The relative initial rate of G_T activation is represented by the rate of fluorescence increase obtained from the slope of the fluorescence measurements in the first 60 s after addition of $GTP\gamma S$ relative to that of WT rhodopsin (100 %).

^c Peptide quenching EC_{50} values were calculated from dose response curves generated for the combined peptide quenching data.

^d $\Delta\Delta G^\ddagger$ values were calculated by comparing the quenching EC_{50} data from the alanine containing K141B mutants with that of K141B.

Scheme 6. 1: Reaction of PDT-bimane with cysteine residues incorporated into rhodopsin. The label is attached through a reversible disulfide bond.

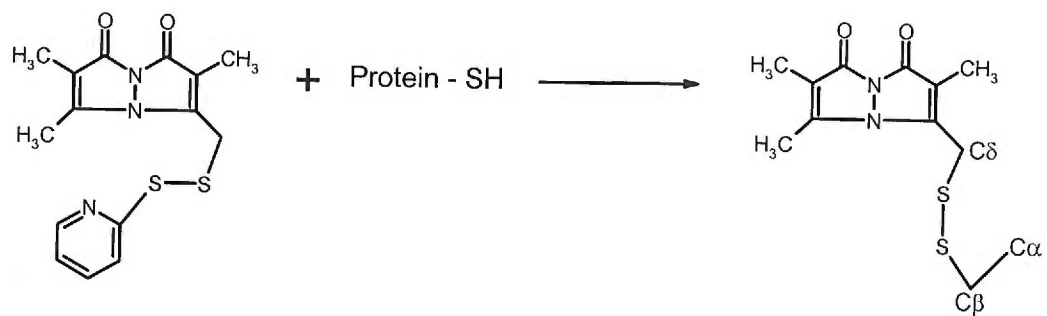
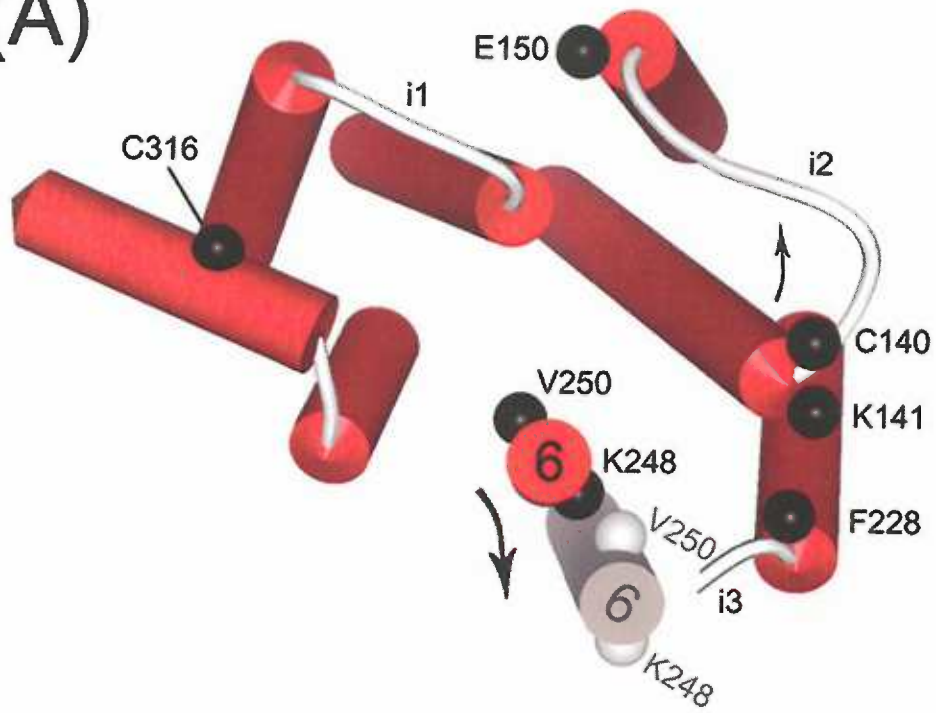


FIGURE 6. 1: Light activation of rhodopsin opens a cleft to enable binding of the $G_{T\alpha}$ C-terminus. (A) Model of the rhodopsin cytoplasmic face based on the rhodopsin crystal structure (53). The black spheres indicate the α -carbon site for each cysteine residue used in the present study. The proposed outward helix 6 movement during rhodopsin activation is shown as a gray helix, and is based on EPR derived distance constraints (114). (B) Proposed model of the hydrophobic cleft formed by rhodopsin activation. A model of the peptide used in the present studies, peptide W23SV, is based on NMR structural coordinates of a undecapeptide corresponding to residues (340-350) of the $G_{T\alpha}$ C-terminus in its MII bound state (233). The Trp residue in this peptide is shown for visualization purposes. Residues shown to be important for transducin activation (L226, T229 and V230) are shown in gray. In both models the rhodopsin extracellular domain and a portion of cytoplasmic loop i3 have been removed for clarity

(A)



(B)

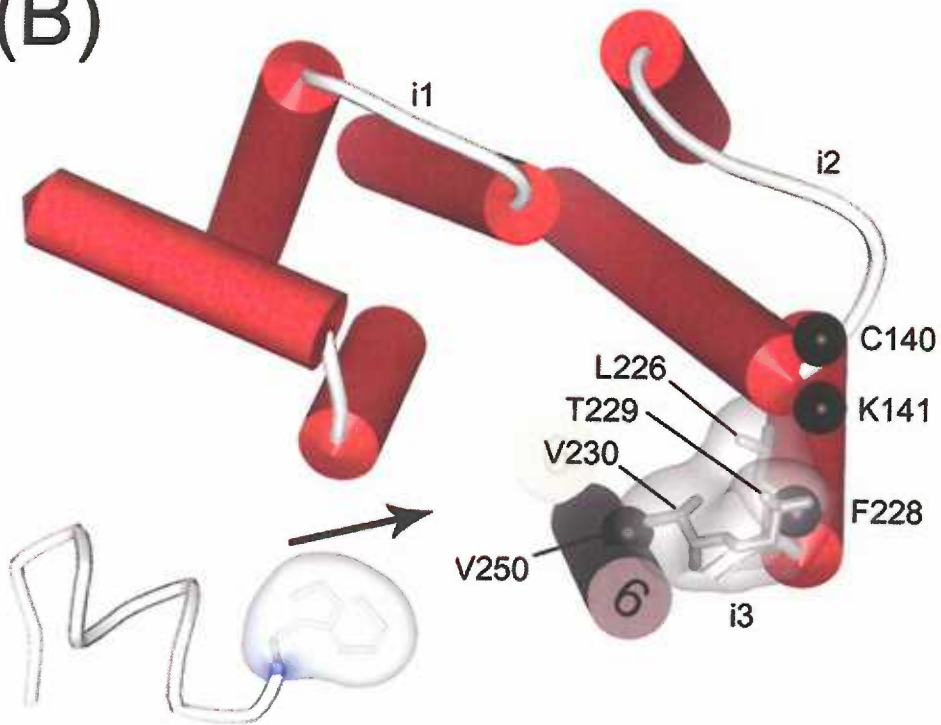


FIGURE 6. 2: Peptide W23SV binding occludes site V250C. (A) Peptide W23SV binds to light activated rhodopsin as indicated by its ability to inhibit conversion of MII rhodopsin into the λ_{460} nm absorbing MIII photoproduct. UV/vis absorption spectrum of rhodopsin mutant V250C in the absence (left, -), and presence (right, +) of 100 μ M peptide W23SV. Spectra are plotted in the dark state (DS) and in 5-minute intervals for 90 minutes following photobleaching (+hv). (B) Binding of peptide W23SV blocks labeling of mutant V250C by PyMPO-maleimide. Top, lanes 1 and 2 in the UV irradiated gel demonstrate the “cysless” background mutant θ shows no PyMPO labeling under either dark or light conditions. Mutant V250C shows essentially no PyMPO labeling in the dark state (lane 3), but shows strong labeling in the MII state (lane 4). This labeling of V250C in MII is blocked in the presence of peptide W23SV (compare lanes 7 and 8). Bottom, Coomassie staining of the same gel illustrating equal amounts of protein are present in each lane. (C) Peptide W23SV binding shields a fluorescent label (bimane) at site V250C from the fluorescence-quenching agent KI. Stern-Volmer analysis shows the label at V250C in the dark state (\bullet , $K_{SV} = 2.7 \text{ M}^{-1}$) becomes more accessible to KI quenching in the MII state (\circ , $K_{SV} = 70.5 \text{ M}^{-1}$). However, binding of peptide W23SV (100 μ M) protects the label from collisions with KI in the MII state (\square , $K_{SV} = 19.4 \text{ M}^{-1}$), although it has no effect on the dark state (\blacksquare , $K_{SV} = 2.5 \text{ M}^{-1}$).

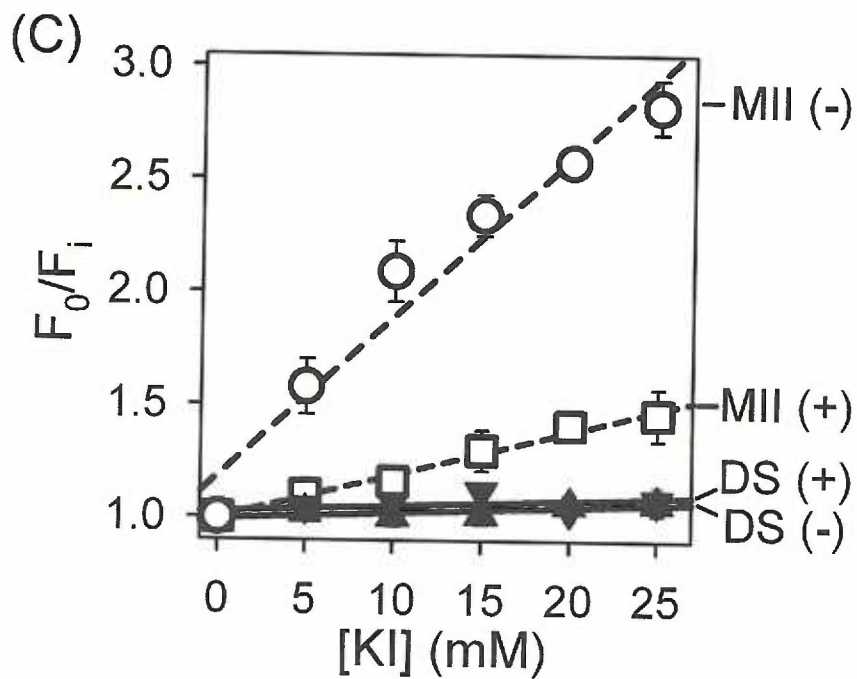
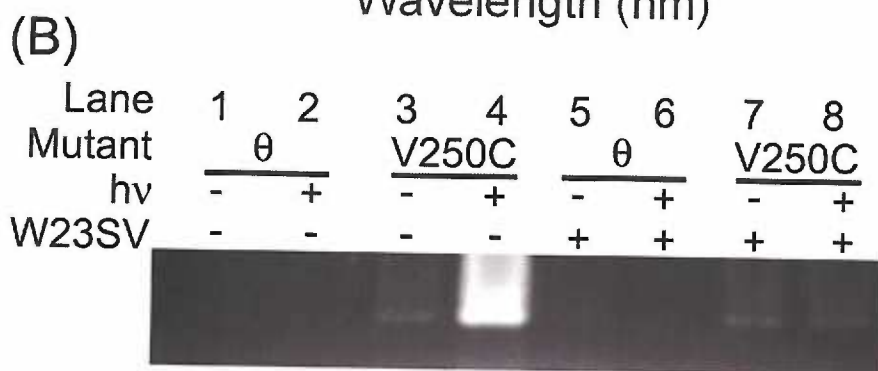
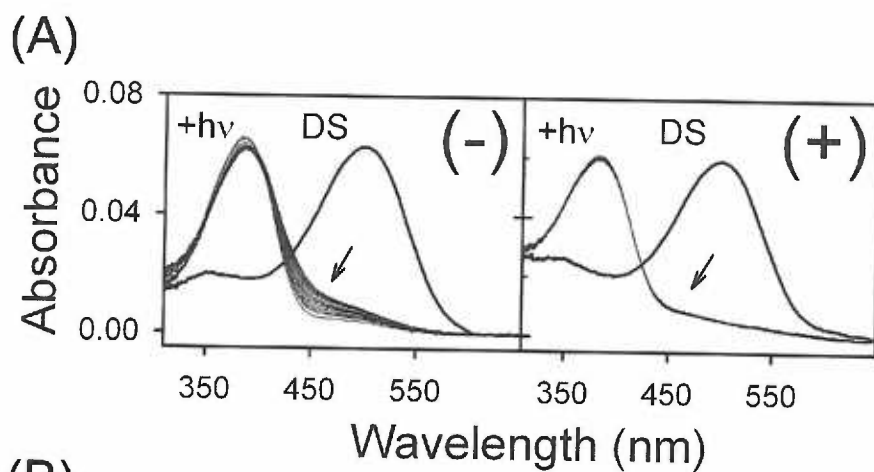


FIGURE 6. 3: Peptide W23SV binding and quenching properties of PDT-bimane labeled rhodopsin mutants. (A) Peptide W23SV can bind to all PDT-bimane labeled samples as indicated by its ability to inhibit MIII photoproduct. In the absence of peptide, the PDT-bimane labeled mutants accumulates increasing amounts of the MIII photoproduct (460 nm) during decay of the active MII species (●), whereas pre-incubation of the samples with 100 μ M W23SV peptide inhibits this process (Δ). (B) Steady-state fluorescence emission spectra of MII PDT-bimane labeled rhodopsin mutants in the absence (black) and presence (blue) of 100 μ M peptide W23SV. Notice the decrease in fluorescence intensity for C140B, K141B and to a lesser extent F228B upon addition of peptide W23SV. (C) Titration of MII PDT-bimane labeled rhodopsin mutants with increasing amounts of peptide W23SV. Mutants C140B, K141B and F228B exhibit dose-dependent saturation of PDT-bimane quenching, while no quenching is observed for the other mutants.

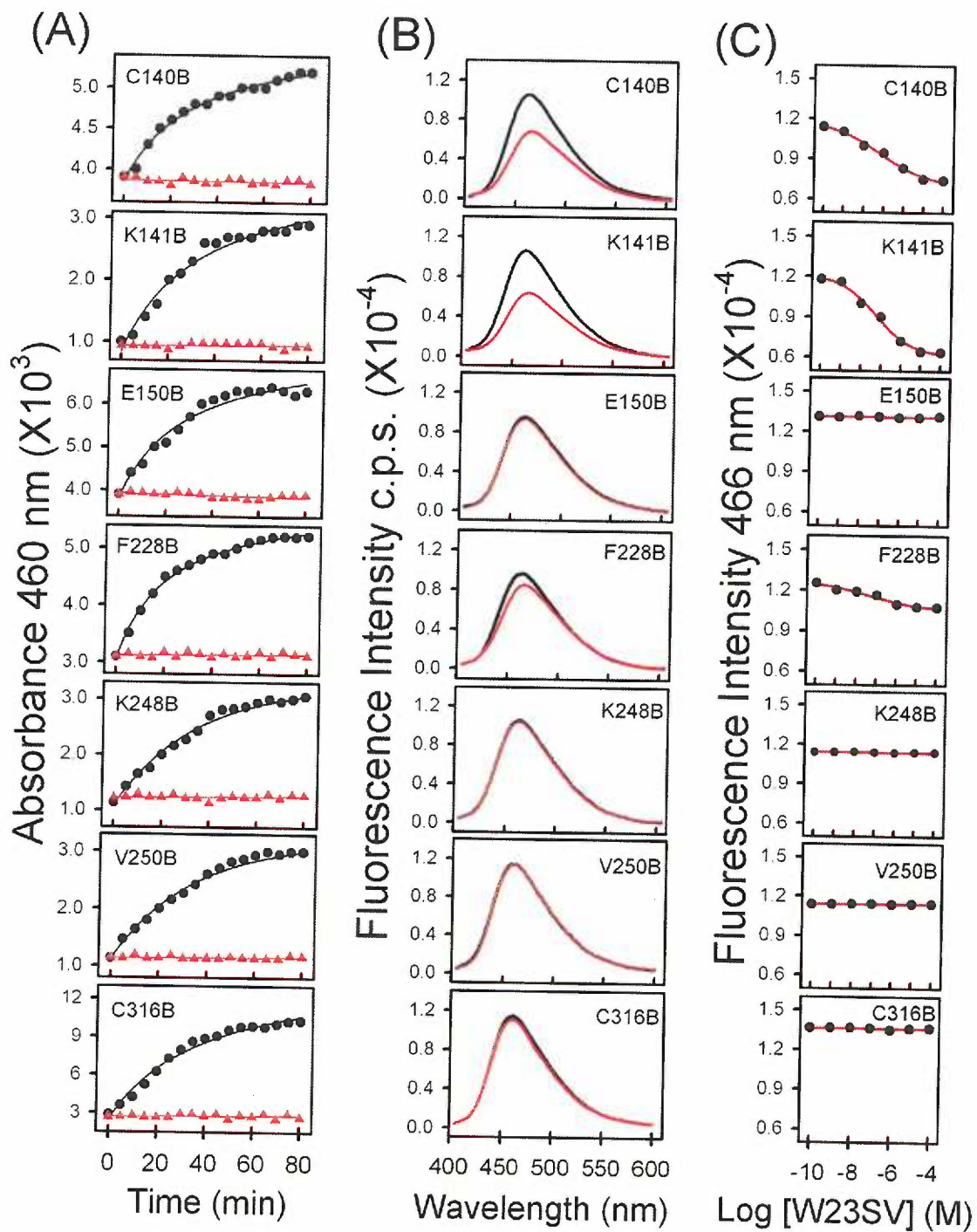


FIGURE 6. 4: Peptide W23SV binds to rhodopsin near residues C140, K141 and F228. Effect of W23SV binding on the bimane fluorescence emission of 500 nM of seven different individually labeled rhodopsin mutants in the MII state. Black bars show the emission intensity of the mutants in the absence of peptide; grey bars indicate the intensity following the addition of 100 μ M peptide W23SV. Note that only labeled positions C140B, K141B and to a lesser extent F228B exhibit a reproducible decrease in fluorescence, although all the mutants bind peptide (Fig. 6. 3). The fluorescence of the cystless background mutant θ (\sim 15% of the labeled samples) does not change upon addition of peptide (not shown). Error bars reflect S.E.M. for three separate experiments. Labeling characteristics of the samples are presented in Table 6. 1.

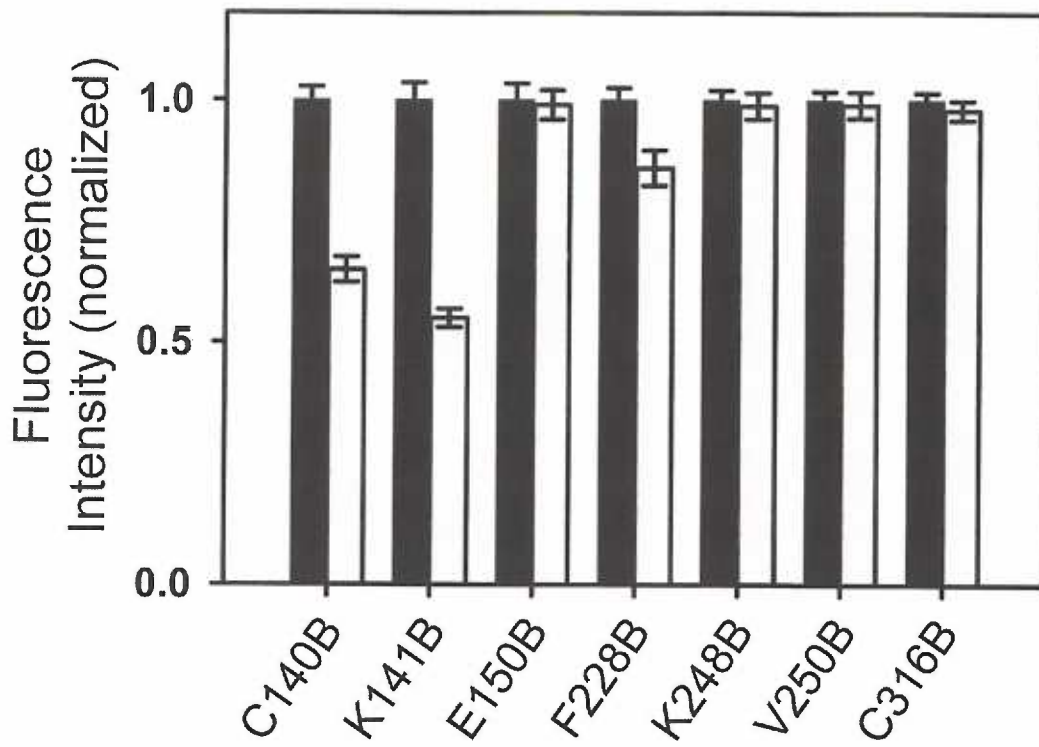


FIGURE 6. 5: Peptide W23SV binding to K141B is specific, requires the MII state, and requires an intact protonated Schiff-base linkage. (A) Quenching of mutant K141B by peptide W23SV can be competed away using a non-Trp containing peptide. Bimane emission of K141B in the MII state (1, black), following the addition of 1 μ M W23SV (2, gray). Note that the quenching is relieved following the addition of 100 μ M peptide 23S (3, dashed). W23SV quenching is not observed for dark state K141B (data not shown). **(B)** K141B emission in the photobleached MII state (1, black, $t = 0$ min) and following the addition of 5 μ M peptide W23SV after the full decay of the MII state (2, gray, $t = 300$ min). **(C)** Upon photobleaching to the MII state in the presence of 5 μ M peptide W23SV the level of fluorescence increases to levels typical of quenching (1, gray). Treatment of the quenched sample with 50 mM hydroxylamine (which cleaves the retinal Schiff base) returns the fluorescence intensity back to that of an unquenched sample (2, dashed). All experiments performed in buffer D, pH 6.0 at 10 °C.

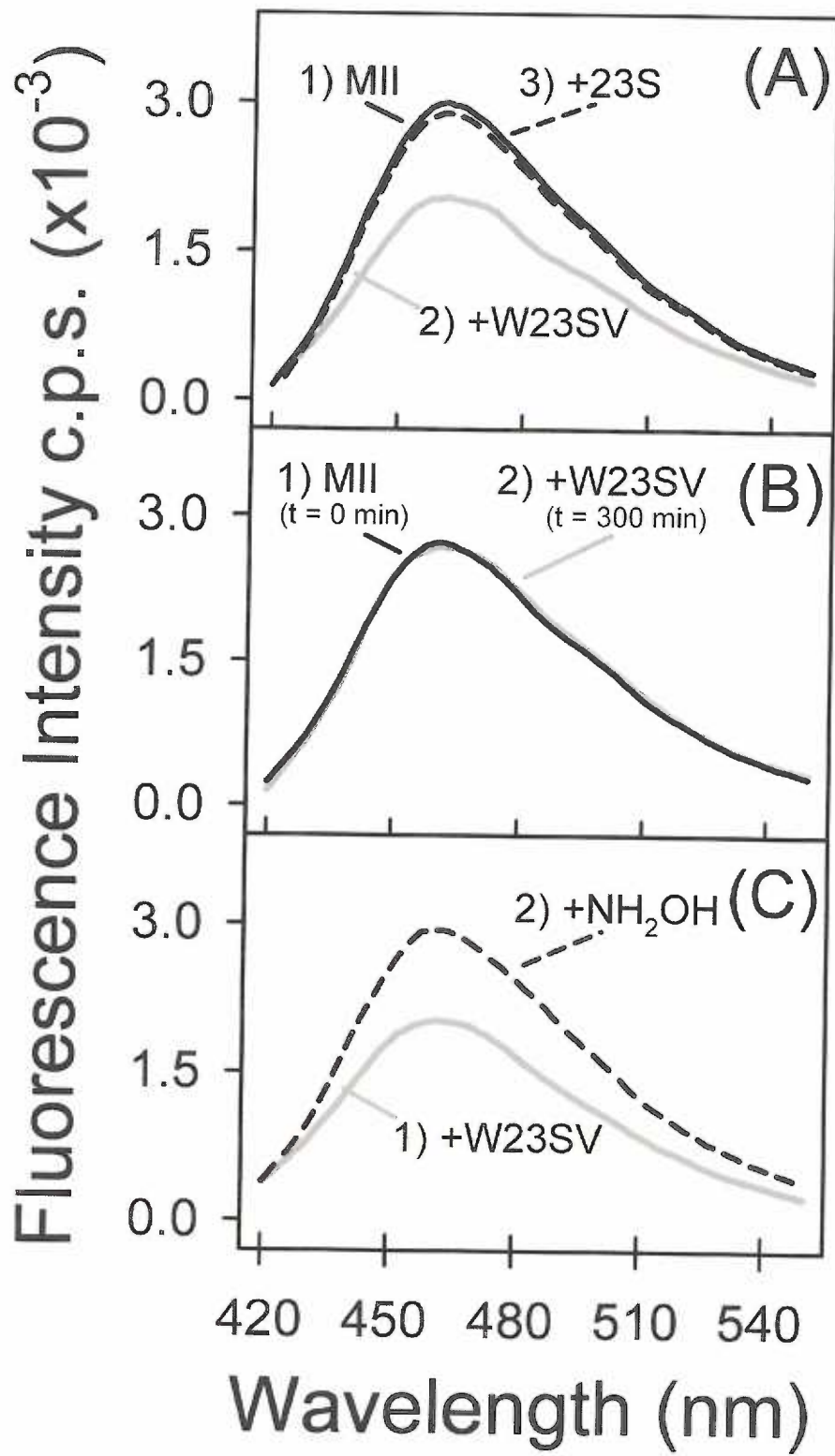
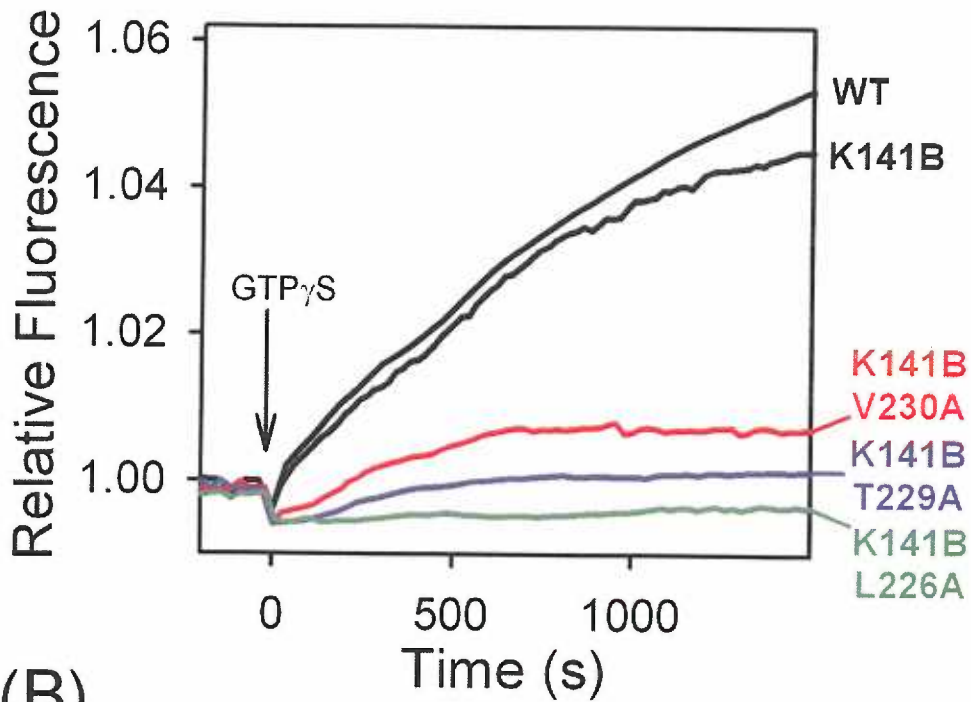
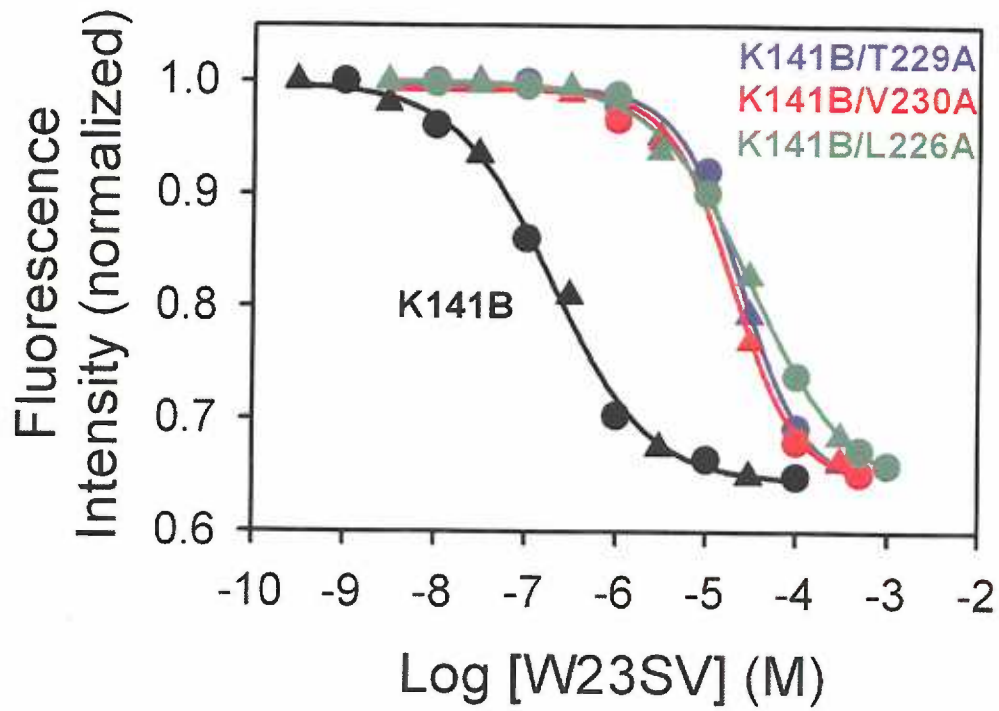


FIGURE 6. 6: Mutations in a “hydrophobic patch” on rhodopsin reduce but do not abolish peptide W23SV binding affinity. (A) Transducin activation of PDT-bimane labeled mutants in comparison to WT. Labeled mutant K141B shows near WT levels of transducin activation. In contrast, equivalent amounts of hydrophobic patch mutants K141B-L226A, K141B-T229A, and K141B-V230A all show greatly reduced abilities to activate transducin. **(B)** Monitoring the bimane quenching of these labeled mutants upon titration with W23SV indicates the mutants can bind the C-terminal tail of $G_T\alpha$, but do so with greatly reduced affinity. The plots show two separate titrations (\blacktriangle, \bullet) and the values are given in Table 6. 3.

(A)



(B)



6. 7: SUPPLEMENTARY MATERIAL

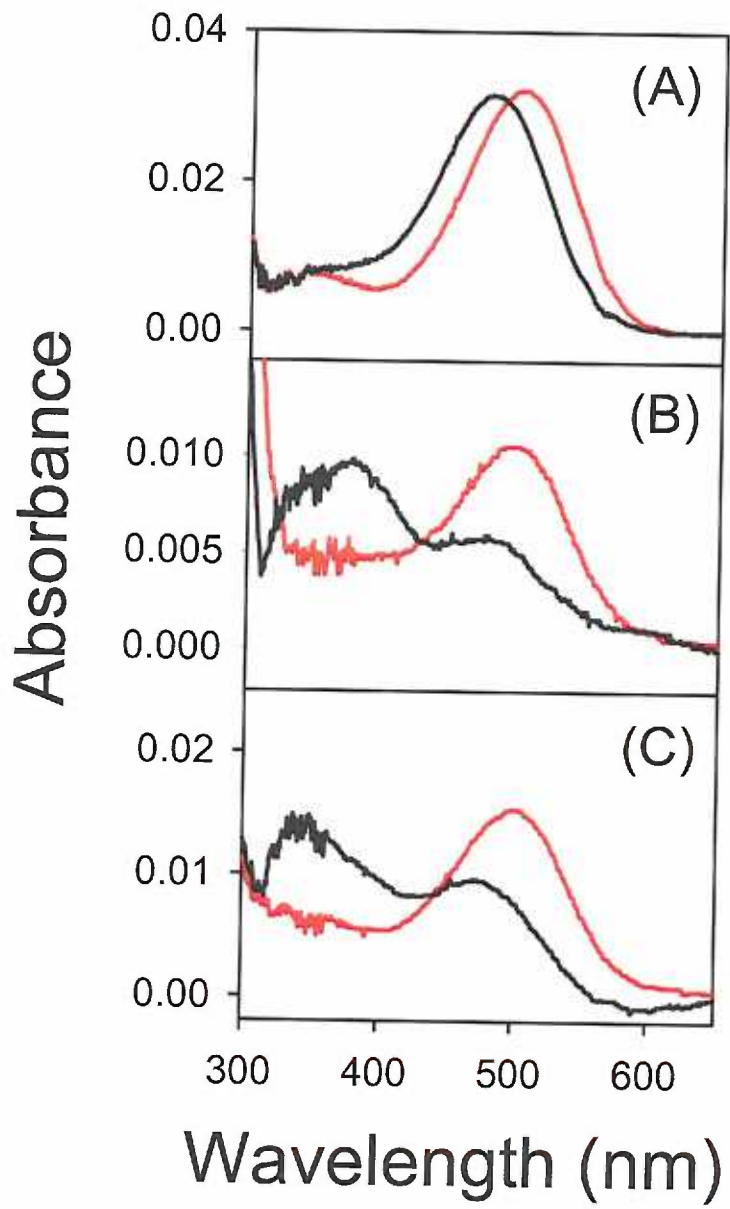
6. 7. 1: $G_{T\alpha}$ C-terminal peptide analogues stabilize the rhodopsin MII intermediate.

Following bleaching, the MI and MII photointermediates reach equilibrium between each other and it is possible to stabilize either intermediate Using different detergents. While DM primarily stabilizes the MII intermediate ($\lambda_{\max} = 380$ nm), the more ridged detergent digitonin is well known to trap the MI intermediate at lower temperatures ($\lambda_{\max} = 480$ nm), (31, 162, 229, 232, 250-254). Transducin stabilizes the MII intermediate and as a result its binding photobleached rhodopsin in digitonin shifts the equilibrium to the MII state, which may be followed as an increase in MII absorbance ($\lambda_{\max} = 480$ nm), (162, 232). Hamm and colleagues have shown that peptides corresponding to the $G_{T\alpha}$ C-terminal tail also stabilize the MII state and developed an “extra-MII” assay based on the absorbance shift accompanying the change in equilibrium (229-232). Using this assay we further confirm the ability of peptides 23S and W23SV to bind to and stabilize the MII state of rhodopsin (Figure 6. S1).

Figure 6. S1: Stabilization of MII state by $G_{T\alpha}$ C-terminal tail peptide analogues.

(A) Photobleaching dark state rhodopsin purified in digitonin (red line) stabilizes the MI photointermediate with a characteristic absorbance at ~ 480 nm (black line).

Photobleaching rhodopsin in the presence of 25 μ M peptide 23S (B), or peptide W23SV (C), shifts the MI \leftrightarrow MII equilibrium to the MII state, further indicating that both peptides bind and stabilize the rhodopsin MII intermediate. The peptides tested do not fully shift the MI/MII pool completely to the MII state, in agreement with previous studies (229, 231). It is possible that additional binding contacts between rhodopsin and the whole G_T heterotrimer are necessary to fully stabilize the MII intermediate. All experiments performed in 0.02 % digitonin, 5 mM MES, pH 6.0, 5 $^{\circ}$ C. To prevent condensation the sample chamber was continually purged with dry air during the course of the assays.



Chapter 7

Summary and Conclusions

In this dissertation I have presented our studies investigating how interactions between the rhodopsin protein and its retinal chromophore stabilize the Schiff base linkage that unites the two. I also report our studies regarding how the integrity of this linkage relates to the signaling state of the receptor. These findings provide insight into the stabilization of the retinal Schiff base in the dark state of the receptor, the mechanism of receptor activation and the stabilization of this signaling state, as well as the processes of Schiff base hydrolysis, retinal release and signal attenuation. The main conclusions are summarized according to these subjects below.

7. 1: Stabilization of the retinal Schiff base linkage in the dark state of rhodopsin.

Our studies indicate that the rhodopsin protein stabilizes the dark or “off” state of the receptor through at least three fundamentally different mechanisms; i) through an effect on the hydrolysis chemistry, ii) by shielding the retinal linkage from solvent, or iii) by acting as a kinetic trap to slow retinal release. We have shown that the rhodopsin counter-ion E113 imparts stability by affecting the chemistry of Schiff base hydrolysis through its effect on the protonation state of this linkage (219). We have also demonstrated that a hydrogen bond network that surrounds the Schiff base site stabilizes the linkage in part by constraining the opsin-binding pocket, thereby shielding the retinal linkage from the bulk solvent. In addition, we discovered a conserved ion pair (R177/D190) in visual receptors and find that this pair is important in the stabilization of the retinal plug in the extracellular domain, which we find may act as a kinetic trap to prevent the release of spontaneously hydrolyzed retinal (207). These stabilizing interactions work in concert to help maintain the dark state species of the receptor and aid

in maintaining the very low signaling background of the rod cell phototransduction system.

7. 2: Mechanism of rhodopsin activation.

Light induced isomerization of the retinal chromophore induces conformational changes in rhodopsin culminating in the formation of the active MII signaling intermediate. Our site-directed mutagenesis studies on residues T118A and I189A demonstrate that mitigation of steric interactions between rhodopsin and the C₉-methyl group of the retinal moiety neither inhibit the formation of a MII intermediate nor effect transducin activation (179). These findings do not support the proposed steric trigger theory of rhodopsin activation which suggests steric interactions with the C₉-methyl group of retinal hold the receptor in the dark state and are necessary for the proper formation of the MII intermediate (122).

7. 3: Mechanism of rhodopsin interaction with transducin.

The high resolution structures of dark state rhodopsin and heterotrimeric transducin have been solved (52, 54, 255, 256). While these structures have contributed to a substantial body of knowledge regarding signal transduction, static structures alone cannot elucidate the dynamics of receptor activation or rhodopsin – transducin interactions. To investigate the structural dynamics of rhodopsin signaling we employed site-directed fluorescence labeling techniques. By inserting a quenching Trp residue on TM helix 3 and a bimane label on TM helix 6 we were able to further confirm the outward movement of TM helix 6 during rhodopsin activation (see the appendix that follows). In addition, we provide experimental evidence that this conformational change opens up a binding cleft on the cytoplasmic face of rhodopsin for the C-terminal tail of

the G_T α -subunit (257). While we and others have previously proposed such an activation mechanism, our studies are the first to provide experimental evidence supporting this theory. Furthermore, our results suggest that this binding process is mediated in part by key hydrophobic interactions and importantly, seems to require an intact retinal Schiff base linkage (257).

7. 4: Retinal release and signaling attenuation.

A final step in the rhodopsin phototransduction cascade involves the hydrolysis of the retinal Schiff base linkage and release of all-*trans*-retinal from the opsin-binding pocket. This process both terminates signaling and releases retinal to the enzymes of the retinoid cycle so 11-*cis*-retinal may be regenerated and recycled. However, as noted in the introduction, the molecular steps involved in this process remain largely unexplored. In studying MII decay and retinal release steps we find that residues G90, E122 and A295 modulate the stability of the MII state (179). The mutation G90S seems to disrupt the MI \rightarrow MII transition, while mutant E122D stabilizes the MII state and slows its decay process. We find that mutant A295S, one residue away from the retinal Schiff base linkage at K296, greatly accelerates the decay of the MII intermediate. Further, we show that while the rates of MII decay differ for these mutants, their E_a values for the overall process of retinal release were similar (179). This point suggests that the rate-limiting step in retinal release is the chemical event of Schiff base hydrolysis. Through our investigations of Schiff base hydrolysis and retinal release we find that residues T94, E113 and S186 mediate the chemistry of hydrolysis reaction. We also demonstrated that this process exhibits deuterium solvent isotope effects that are consistent with Schiff base hydrolysis proceeding through a tetrahedral carbinolamine intermediate. Based in part on

our findings we were able to propose an updated model of Schiff base hydrolysis in chapter 5 that incorporates structural information as well as recent experimental findings.

7. 5: Possible structural changes in rhodopsin during MII decay.

We also monitored conformational changes that accompany the decay of the active MII signaling state (see following appendix). Our preliminary site-directed fluorescence labeling studies suggest that following an outward movement during formation of the MII state TM helix 6 moves back toward the helical bundle during decay of the MII intermediate. In addition, our study shows that this helix resetting is linked to the retinal Schiff base linkage. The rates of MII decay and this resetting process are similar and both rates are greatly increased in the presences of hydroxylamine. Although more work remains to be done, taken together, these studies suggest that TM helix 6 resetting during MII decay may alter the $G_{T\alpha}$ binding site on the cytoplasmic face. This resetting would in turn prevent further activation of G_T by rhodopsin.

7. 6: Future studies.

Our results leave a number of questions that remain unanswered. While our studies have mapped the binding site of the $G_{T\alpha}$ C-terminus onto rhodopsin the binding sites of other portions of the α or β and γ subunits are not at present known. It is possible that binding G_T is cooperative with the binding of certain domains influencing the conformation of the receptor or the binding of the other domains.

There is also recent controversy in the field as it has been suggested that rhodopsin exists as dimers in the cell membrane (258, 259). If proven true, it is possible that the stability of rhodopsin, as well as the retinal Schiff base linkage, may also be mediated by dimerization. The presence of dimers could also have an effect on the

stoichiometry of receptor and effector proteins. The peptide quenching assays we have developed and the SDFL techniques detailed in this dissertation may prove useful in addressing these types of questions.

Dimerization in membranes raises another issue. All of the work presented in this dissertation as well as the majority of work in the rhodopsin field, conduct structure/function studies on detergent solubilized purified rhodopsin. The fact that rhodopsin is an integral membrane protein often necessitates these procedures prior to investigation. This raises the concern regarding the role of the cell membrane and specific lipids during rhodopsin activation and attenuation. Recent developments reporting the reconstitution of purified rhodopsin into lipid vesicles (260) may serve as a valuable tool to further explore the possible effects mediated by lipids and membranes.

7. 7: Concluding Statements.

The results from this dissertation study contribute to the body of knowledge regarding how rhodopsin stabilizes the Schiff base linkage of its covalently attached retinal chromophore and how the integrity of this linkage mediates receptor signaling states. G-protein coupled receptors comprise one of the largest classes of cell surface receptor proteins and are the targets of ~ 50 % of newly developed pharmaceuticals (261). Elucidating the molecular mechanisms of receptor activation and attenuation are essential for the development of new drugs as well as a fundamental understanding of cellular signal transduction. Studies on the model GPCR rhodopsin will continue to drive these efforts.

REFERENCES

1. Pierce, K.L., R.T. Premont, and R.J. Lefkowitz, Seven-transmembrane receptors. *Nat Rev Mol Cell Biol*, 2002. **3**(9): p. 639-50.
2. Wess, J., Molecular basis of receptor/G-protein-coupling selectivity. *Pharmacol Ther*, 1998. **80**(3): p. 231-64.
3. Bockaert, J. and J.P. Pin, Molecular tinkering of G protein-coupled receptors: an evolutionary success. *Embo J*, 1999. **18**(7): p. 1723-9.
4. Stenkamp, R.E., D.C. Teller, and K. Palczewski, Crystal structure of rhodopsin: a G-protein-coupled receptor. *ChemBiochem*, 2002. **3**(10): p. 963-7.
5. www.gpcr.org/7t/, *G-protein coupled receptor data base*. 2004.
6. Hamm, H.E., The many faces of G protein signaling. *J Biol Chem*, 1998. **273**(2): p. 669-72.
7. Gether, U. and B.K. Kobilka, G protein-coupled receptors. II. Mechanism of agonist activation. *J Biol Chem*, 1998. **273**(29): p. 17979-82.
8. Gether, U., S. Lin, P. Ghanouni, J.A. Ballesteros, H. Weinstein, and B.K. Kobilka, Agonists induce conformational changes in transmembrane domains III and VI of the beta2 adrenoceptor. *Embo J*, 1997. **16**(22): p. 6737-47.
9. Bourne, H.R., D.A. Sanders, and F. McCormick, The GTPase superfamily: conserved structure and molecular mechanism. *Nature*, 1991. **349**(6305): p. 117-27.
10. Bourne, H.R., D.A. Sanders, and F. McCormick, The GTPase superfamily: a conserved switch for diverse cell functions. *Nature*, 1990. **348**(6297): p. 125-32.

11. Gilman, A.G., G proteins: transducers of receptor-generated signals. *Annu Rev Biochem*, 1987. **56**: p. 615-49.
12. Arshavsky, V.Y., T.D. Lamb, and E.N. Pugh, Jr., G proteins and phototransduction. *Annu Rev Physiol*, 2002. **64**: p. 153-87.
13. Polans, A., W. Baehr, and K. Palczewski, Turned on by Ca²⁺! The physiology and pathology of Ca(2+)-binding proteins in the retina. *Trends Neurosci*, 1996. **19**(12): p. 547-54.
14. Okada, T., O.P. Ernst, K. Palczewski, and K.P. Hofmann, Activation of rhodopsin: new insights from structural and biochemical studies. *Trends Biochem Sci*, 2001. **26**(5): p. 318-24.
15. Rattner, A., H. Sun, and J. Nathans, Molecular genetics of human retinal disease. *Annu Rev Genet*, 1999. **33**: p. 89-131.
16. Nathans, J., Molecular biology of visual pigments. *Annu Rev Neurosci*, 1987. **10**: p. 163-94.
17. Nathans, J., The genes for color vision. *Sci Am*, 1989. **260**(2): p. 42-9.
18. Ebrey, T. and Y. Koutalos, Vertebrate Photoreceptors. *Prog Retin Eye Res*, 2001. **20**(1): p. 49-94.
19. Nathans, J., Rhodopsin: structure, function, and genetics. *Biochemistry*, 1992. **31**(21): p. 4923-31.
20. Nathans, J., S.L. Merbs, C.H. Sung, C.J. Weitz, and Y. Wang, Molecular genetics of human visual pigments. *Annu Rev Genet*, 1992. **26**: p. 403-24.
21. Young, R.W., Visual cells. *Sci Am*, 1970. **223**(4): p. 80-91.

22. Young, R.W. and D. Bok, Participation of the retinal pigment epithelium in the rod outer segment renewal process. *J Cell Biol*, 1969. **42**(2): p. 392-403.
23. Leskov, I.B., V.A. Klenchin, J.W. Handy, G.G. Whitlock, V.I. Govardovskii, M.D. Bownds, T.D. Lamb, E.N. Pugh, Jr., and V.Y. Arshavsky, The gain of rod phototransduction: reconciliation of biochemical and electrophysiological measurements. *Neuron*, 2000. **27**(3): p. 525-37.
24. Menon, S.T., M. Han, and T.P. Sakmar, Rhodopsin: structural basis of molecular physiology. *Physiol Rev*, 2001. **81**(4): p. 1659-88.
25. Palczewski, K. and J.C. Saari, Activation and inactivation steps in the visual transduction pathway. *Curr Opin Neurobiol*, 1997. **7**(4): p. 500-4.
26. Palczewski, K., C.L. Verlinde, and F. Haeseleer, Molecular mechanism of visual transduction. *Novartis Found Symp*, 1999. **224**: p. 191-204.
27. Sakmar, T.P., Rhodopsin: a prototypical G protein-coupled receptor. *Prog Nucleic Acid Res Mol Biol*, 1998. **59**: p. 1-34.
28. Baylor, D.A., Photoreceptor signals and vision. Proctor lecture. *Invest Ophthalmol Vis Sci*, 1987. **28**(1): p. 34-49.
29. Stryer, L., M.E. and D.A. Baylor, Activation, deactivation, and adaptation in vertebrate photoreceptor cells. *Annu Rev Neurosci*, 2001. **24**: p. 779-805.
30. Stryer, L., J.L. and D.A. Baylor, How photoreceptor cells respond to light. *Sci Am*, 1997. **276**(4): p. 40-7.
31. Stryer, L., W.L., C. Altenbach, C.M. Hubbell, and H.G. Khorana, Rhodopsin structure, dynamics, and activation: a perspective from crystallography, site-

- directed spin labeling, sulfhydryl reactivity, and disulfide cross-linking. *Adv Protein Chem*, 2003. **63**: p. 243-90.
32. Jin, S., M.C. Cornwall, and D.D. Oprian, Opsin activation as a cause of congenital night blindness. *Nat Neurosci*, 2003. **6**(7): p. 731-5.
 33. Ernst, O.P. and F.J. Bartl, Active states of rhodopsin. *ChemBiochem*, 2002. **3**(10): p. 968-74.
 34. Ridge, K.D., N.G. Abdulaev, M. Sousa, and K. Palczewski, Phototransduction: crystal clear. *Trends in Biochemical Sciences*, 2003. **28**(9): p. 479-487.
 35. Hamm, H.E., How activated receptors couple to G proteins. *Proc Natl Acad Sci U S A*, 2001. **98**(9): p. 4819-21.
 36. Beavo, J.A., Cyclic nucleotide phosphodiesterases: functional implications of multiple isoforms. *Physiol Rev*, 1995. **75**(4): p. 725-48.
 37. Palczewski, K. and P.A. Hargrave, Studies of ligand binding to arrestin. *J Biol Chem*, 1991. **266**(7): p. 4201-6.
 38. Palczewski, K., J. Buczylo, N.R. Imami, J.H. McDowell, and P.A. Hargrave, Role of the carboxyl-terminal region of arrestin in binding to phosphorylated rhodopsin. *J Biol Chem*, 1991. **266**(23): p. 15334-9.
 39. Palczewski, K. and J.L. Benovic, G-protein-coupled receptor kinases. *Trends Biochem Sci*, 1991. **16**(10): p. 387-91.
 40. Palczewski, K., Structure and functions of arrestins. *Protein Sci*, 1994. **3**(9): p. 1355-61.

41. Pepperberg, D.R., M.C. Cornwall, M. Kahlert, K.P. Hofmann, J. Jin, G.J. Jones, and H. Ripps, Light-dependent delay in the falling phase of the retinal rod photoresponse. *Vis Neurosci*, 1992. **8**(1): p. 9-18.
42. Stryer, L., Cyclic GMP cascade of vision. *Annu Rev Neurosci*, 1986. **9**: p. 87-119.
43. Stryer, L., Molecular mechanism of visual excitation. *Harvey Lect*, 1991. **87**: p. 129-43.
44. Heck, M., S.A. Schadel, D. Maretzki, F.J. Bartl, E. Ritter, K. Palczewski, and K.P. Hofmann, Signaling states of rhodopsin. Formation of the storage form, metarhodopsin III, from active metarhodopsin II. *J Biol Chem*, 2003. **278**(5): p. 3162-9.
45. McBee, J.K., K. Palczewski, W. Baehr, and D.R. Pepperberg, Confronting complexity: the interlink of phototransduction and retinoid metabolism in the vertebrate retina. *Prog Retin Eye Res*, 2001. **20**(4): p. 469-529.
46. Rando, R.R., The biochemistry of the visual cycle. *Chem Rev*, 2001. **101**(7): p. 1881-96.
47. Hargrave, P.A., J.H. McDowell, D.R. Curtis, J.K. Wang, E. Juszczak, S.L. Fong, J.K. Rao, and P. Argos, The structure of bovine rhodopsin. *Biophys Struct Mech*, 1983. **9**(4): p. 235-44.
48. Sakmar, T.P., S.T. Menon, E.P. Marin, and E.S. Awad, Rhodopsin: Insights from Recent Structural Studies. *Annu Rev Biophys Biomol Struct*, 2002. **31**: p. 443-84.
49. Okada, T. and K. Palczewski, Crystal structure of rhodopsin: implications for vision and beyond. *Curr Opin Struct Biol*, 2001. **11**(4): p. 420-6.

50. Mitchell, D.C. and B.J. Litman, Effect of ethanol on metarhodopsin II formation is potentiated by phospholipid polyunsaturation. *Biochemistry*, 1994. **33**(43): p. 12752-6.
51. Filipek, S., R.E. Stenkamp, D.C. Teller, and K. Palczewski, G Protein-Coupled Receptor Rhodopsin: A Prospectus. *Annu Rev Physiol*, 2002. **20**: p. 20.
52. Palczewski, K., T. Kumasaka, T. Hori, C.A. Behnke, H. Motoshima, B.A. Fox, I. Le Trong, D.C. Teller, T. Okada, R.E. Stenkamp, M. Yamamoto, and M. Miyano, Crystal structure of rhodopsin: A G protein-coupled receptor. *Science*, 2000. **289**(5480): p. 739-45.
53. Teller, D.C., T. Okada, C.A. Behnke, K. Palczewski, and R.E. Stenkamp, Advances in determination of a high-resolution three-dimensional structure of rhodopsin, a model of G-protein-coupled receptors (GPCRs). *Biochemistry*, 2001. **40**(26): p. 7761-72.
54. Okada, T., Y. Fujiyoshi, M. Silow, J. Navarro, E.M. Landau, and Y. Shichida, Functional role of internal water molecules in rhodopsin revealed by X-ray crystallography. *Proc Natl Acad Sci U S A*, 2002. **99**(9): p. 5982-7.
55. Birge, R.R., L.P. Murray, B.M. Pierce, H. Akita, V. Balogh-Nair, L.A. Findsen, and K. Nakanishi, Two-photon spectroscopy of locked-11-cis-rhodopsin: evidence for a protonated Schiff base in a neutral protein binding site. *Proc Natl Acad Sci U S A*, 1985. **82**(12): p. 4117-21.
56. Borhan, B., M.L. Souto, H. Imai, Y. Shichida, and K. Nakanishi, Movement of retinal along the visual transduction path. *Science*, 2000. **288**(5474): p. 2209-12.

57. Baldwin, J.M., G.F. Schertler, and V.M. Unger, An alpha-carbon template for the transmembrane helices in the rhodopsin family of G-protein-coupled receptors. *J Mol Biol*, 1997. **272**(1): p. 144-64.
58. Unger, V.M., P.A. Hargrave, J.M. Baldwin, and G.F. Schertler, Arrangement of rhodopsin transmembrane alpha-helices. *Nature*, 1997. **389**(6647): p. 203-6.
59. Nakayama, T.A. and H.G. Khorana, Orientation of retinal in bovine rhodopsin determined by cross-linking using a photoactivatable analog of 11-cis-retinal. *J Biol Chem*, 1990. **265**(26): p. 15762-9.
60. Nakayama, T.A. and H.G. Khorana, Mapping of the amino acids in membrane-embedded helices that interact with the retinal chromophore in bovine rhodopsin. *J Biol Chem*, 1991. **266**(7): p. 4269-75.
61. Karnik, S.S., T.P. Sakmar, H.B. Chen, and H.G. Khorana, Cysteine residues 110 and 187 are essential for the formation of correct structure in bovine rhodopsin. *Proc Natl Acad Sci U S A*, 1988. **85**(22): p. 8459-63.
62. Doi, T., R.S. Molday, and H.G. Khorana, Role of the intradiscal domain in rhodopsin assembly and function. *Proc Natl Acad Sci U S A*, 1990. **87**(13): p. 4991-5.
63. Kaushal, S. and H.G. Khorana, Structure and function in rhodopsin. 7. Point mutations associated with autosomal dominant retinitis pigmentosa. *Biochemistry*, 1994. **33**(20): p. 6121-8.
64. Liu, X., P. Garriga, and H.G. Khorana, Structure and function in rhodopsin: correct folding and misfolding in two point mutants in the intradiscal domain of

- rhodopsin identified in retinitis pigmentosa. *Proc Natl Acad Sci U S A*, 1996. **93**(10): p. 4554-9.
65. Cha, K., P.J. Reeves, and H.G. Khorana, Structure and function in rhodopsin: destabilization of rhodopsin by the binding of an antibody at the N-terminal segment provides support for involvement of the latter in an intradiscal tertiary structure. *Proc Natl Acad Sci U S A*, 2000. **97**(7): p. 3016-21.
66. Bourne, H.R. and E.C. Meng, Structure. Rhodopsin sees the light. *Science*, 2000. **289**(5480): p. 733-4.
67. Meng, E.C. and H.R. Bourne, Receptor activation: what does the rhodopsin structure tell us? *Trends Pharmacol Sci*, 2001. **22**(11): p. 587-93.
68. Fritze, O., S. Filipek, V. Kuksa, K. Palczewski, K.P. Hofmann, and O.P. Ernst, Role of the conserved NPxxY(x)_{5,6}F motif in the rhodopsin ground state and during activation. *Proc Natl Acad Sci U S A*, 2003. **100**(5): p. 2290-5.
69. Sakmar, T.P., R.R. Franke, and H.G. Khorana, Glutamic acid-113 serves as the retinylidene Schiff base counterion in bovine rhodopsin. *Proc Natl Acad Sci U S A*, 1989. **86**(21): p. 8309-13.
70. Zhukovsky, E.A. and D.D. Oprian, Effect of carboxylic acid side chains on the absorption maximum of visual pigments. *Science*, 1989. **246**(4932): p. 928-30.
71. Nathans, J., Determinants of visual pigment absorbance: identification of the retinylidene Schiff's base counterion in bovine rhodopsin. *Biochemistry*, 1990. **29**(41): p. 9746-52.
72. Wald, G., The chemistry of rod vision. *Science*, 1951. **113**(2933): p. 287-91.

73. Wald, G. and P.K. Brown, The molar extinction of rhodopsin. *J. Gen. Physiol*, 1953. **37**: p. 189-200.
74. Pitt, G.A., F.D. Collins, R.A. Morton, and P. Stok, Studies on rhodopsin. VIII. Retinylidenemethylamine, an indicator yellow analogue. *Biochem J*, 1955. **59**(1): p. 122-8.
75. Morton, R.A. and G.A. Pitt, Studies on rhodopsin. IX. pH and the hydrolysis of indicator yellow. *Biochem J*, 1955. **59**(1): p. 128-34.
76. Hubbard, R. and A. Kropf, Molecular isomers in vision. *Sci Am*, 1967. **216**(6): p. 64-70 passim.
77. Hubbard, R. and A. Kropf, Molecular aspects of visual excitation. *Ann N Y Acad Sci*, 1959. **81**: p. 388-98.
78. Kropf, A. and R. Hubbard, The mechanism of bleaching rhodopsin. *Ann N Y Acad Sci*, 1959. **74**(2): p. 266-80.
79. Bownds, D. and G. Wald, Reaction of the Rhodopsin Chromophore with Sodium Borohydride. *Nature*, 1965. **205**: p. 254-7.
80. Akhtar, M., P.T. Blosse, and P.B. Dewhurst, Studies on vision. The nature of the retinal-opsin linkage. *Biochem J*, 1968. **110**(4): p. 693-702.
81. Oseroff, A.R. and R.H. Callender, Resonance Raman spectroscopy of rhodopsin in retinal disk membranes. *Biochemistry*, 1974. **13**(20): p. 4243-8.
82. Baasov, T. and M. Sheves, Model compounds for the study of spectroscopic properties of visual pigments and bacteriorhodopsin. *J Am Chem Soc*, 1985. **107**(25): p. 7524-7533.

83. Steinberg, G., M. Ottolenghi, and M. Sheves, pKa of the protonated Schiff base of bovine rhodopsin. A study with artificial pigments. *Biophys J*, 1993. **64**(5): p. 1499-502.
84. Deng, H. and R.H. Callender, A study of the Schiff base mode in bovine rhodopsin and bathorhodopsin. *Biochemistry*, 1987. **26**(23): p. 7418-26.
85. Cooper, A., S. Dixon, M. Nutley, and J. Robb, Mechanism of Retinal Schiff Base Formation and Hydrolysis in Relation to Visual Pigment Photolysis and Regeneration: Resonance Raman Spectroscopy of a Tetrahedral Carbinolamine Intermediate and Oxygen-18 Labeling of Retinal at the Metarhodopsin Stage in Photoreceptor Membranes. *J Am Chem Soc*, 1987. **109**(24): p. 7254-7263.
86. Gat, Y.S., M, A mechanism for controlling the pKa of the retinal protonated Schiff base in retinal proteins. A study with model compounds. *J Am Chem Soc*, 1993. **115**(9): p. 3772-3773.
87. Rouso, I., N. Friedman, M. Sheves, and M. Ottolenghi, pKa of the protonated Schiff base and aspartic 85 in the bacteriorhodopsin binding site is controlled by a specific geometry between the two residues. *Biochemistry*, 1995. **34**(37): p. 12059-65.
88. Ebrey, T.G., pKa of the protonated Schiff base of visual pigments. *Methods Enzymol*, 2000. **315**: p. 196-207.
89. Fahmy, K., F. Siebert, and T.P. Sakmar, Photoactivated state of rhodopsin and how it can form. *Biophys Chem*, 1995. **56**(1-2): p. 171-81.
90. Fahmy, K., F. Jager, M. Beck, T.A. Zvyaga, T.P. Sakmar, and F. Siebert, Protonation states of membrane-embedded carboxylic acid groups in rhodopsin

- and metarhodopsin II: a Fourier-transform infrared spectroscopy study of site-directed mutants. *Proc Natl Acad Sci U S A*, 1993. **90**(21): p. 10206-10.
91. Barlow, R.B., R.R. Birge, E. Kaplan, and J.R. Tallent, On the molecular origin of photoreceptor noise. *Nature*, 1993. **366**(6450): p. 64-6.
92. Birge, R.R. and R.B. Barlow, On the molecular origins of thermal noise in vertebrate and invertebrate photoreceptors. *Biophys Chem*, 1995. **55**(1-2): p. 115-26.
93. Baylor, D.A., G. Matthews, and K.W. Yau, Two components of electrical dark noise in toad retinal rod outer segments. *J Physiol*, 1980. **309**: p. 591-621.
94. Baylor, D., How photons start vision. *Proc Natl Acad Sci U S A*, 1996. **93**(2): p. 560-5.
95. Kochendoerfer, G.G., S.W. Lin, T.P. Sakmar, and R.A. Mathies, How color visual pigments are tuned. *Trends Biochem Sci*, 1999. **24**(8): p. 300-5.
96. Lin, S.W., G.G. Kochendoerfer, K.S. Carroll, D. Wang, R.A. Mathies, and T.P. Sakmar, Mechanisms of spectral tuning in blue cone visual pigments. Visible and raman spectroscopy of blue-shifted rhodopsin mutants. *J Biol Chem*, 1998. **273**(38): p. 24583-91.
97. Shichida, Y. and H. Imai, Amino acid residues controlling the properties and functions of rod and cone visual pigments. *Novartis Found Symp*, 1999. **224**: p. 142-53.
98. Shichida, Y., H. Imai, Y. Imamoto, Y. Fukada, and T. Yoshizawa, Is chicken green-sensitive cone visual pigment a rhodopsin-like pigment? A comparative

- study of the molecular properties between chicken green and rhodopsin.
Biochemistry, 1994. **33**(31): p. 9040-4.
99. Fasick, J.I., N. Lee, and D.D. Oprian, Spectral tuning in the human blue cone pigment. *Biochemistry*, 1999. **38**(36): p. 11593-6.
100. Lin, S.W. and T.P. Sakmar, Specific tryptophan UV-absorbance changes are probes of the transition of rhodopsin to its active state. *Biochemistry*, 1996. **35**(34): p. 11149-59.
101. Karnik, S.S. and H.G. Khorana, Assembly of functional rhodopsin requires a disulfide bond between cysteine residues 110 and 187. *J Biol Chem*, 1990. **265**(29): p. 17520-4.
102. Davidson, F.F., P.C. Loewen, and H.G. Khorana, Structure and function in rhodopsin: replacement by alanine of cysteine residues 110 and 187, components of a conserved disulfide bond in rhodopsin, affects the light-activated metarhodopsin II state. *Proc Natl Acad Sci U S A*, 1994. **91**(9): p. 4029-33.
103. Borjigin, J. and J. Nathans, Insertional mutagenesis as a probe of rhodopsin's topography, stability, and activity. *J Biol Chem*, 1994. **269**(20): p. 14715-22.
104. Anukanth, A. and H.G. Khorana, Structure and function in rhodopsin. Requirements of a specific structure for the intradiscal domain. *J Biol Chem*, 1994. **269**(31): p. 19738-44.
105. Nathans, J., T.P. Piantanida, R.L. Eddy, T.B. Shows, and D.S. Hogness, Molecular genetics of inherited variation in human color vision. *Science*, 1986. **232**(4747): p. 203-10.

106. Jacobson, S.G., C.M. Kemp, C.H. Sung, and J. Nathans, Retinal function and rhodopsin levels in autosomal dominant retinitis pigmentosa with rhodopsin mutations. *Am J Ophthalmol*, 1991. **112**(3): p. 256-71.
107. Peteanu, L.A., R.W. Schoenlein, Q. Wang, R.A. Mathies, and C.V. Shank, The first step in vision occurs in femtoseconds: complete blue and red spectral studies. *Proc Natl Acad Sci U S A*, 1993. **90**(24): p. 11762-6.
108. Wang, Q., R.W. Schoenlein, L.A. Peteanu, R.A. Mathies, and C.V. Shank, Vibrationally coherent photochemistry in the femtosecond primary event of vision. *Science*, 1994. **266**(5184): p. 422-4.
109. Hofmann, K.P., Signalling states of photoactivated rhodopsin. *Novartis Found Symp*, 1999. **224**: p. 158-75.
110. Jager, S., I. Szundi, J.W. Lewis, T.L. Mah, and D.S. Kliger, Effects of pH on rhodopsin photointermediates from lumirhodopsin to metarhodopsin II. *Biochemistry*, 1998. **37**(19): p. 6998-7005.
111. Yan, E.C., M.A. Kazmi, Z. Ganim, J.M. Hou, D. Pan, B.S. Chang, T.P. Sakmar, and R.A. Mathies, Retinal counterion switch in the photoactivation of the G protein-coupled receptor rhodopsin. *Proc Natl Acad Sci U S A*, 2003. **100**(16): p. 9262-7.
112. Fahmy, K., T.P. Sakmar, and F. Siebert, Structural determinants of active state conformation of rhodopsin: molecular biophysics approaches. *Methods Enzymol*, 2000. **315**: p. 178-96.
113. Altenbach, C., K. Yang, D.L. Farrens, Z.T. Farahbakhsh, H.G. Khorana, and W.L. Hubbell, Structural features and light-dependent changes in the cytoplasmic

- interhelical E-F loop region of rhodopsin: a site-directed spin-labeling study. *Biochemistry*, 1996. **35**(38): p. 12470-8.
114. Farrens, D.L., C. Altenbach, K. Yang, W.L. Hubbell, and H.G. Khorana, Requirement of rigid-body motion of transmembrane helices for light activation of rhodopsin. *Science*, 1996. **274**(5288): p. 768-70.
115. Sheikh, S.P., T.A. Zvyaga, O. Lichtarge, T.P. Sakmar, and H.R. Bourne, Rhodopsin activation blocked by metal-ion-binding sites linking transmembrane helices C and F. *Nature*, 1996. **383**(6598): p. 347-50.
116. Dunham, T.D. and D.L. Farrens, Conformational changes in rhodopsin. Movement of helix f detected by site-specific chemical labeling and fluorescence spectroscopy. *J Biol Chem*, 1999. **274**(3): p. 1683-90.
117. Yeagle, P.L. and A.D. Albert, A conformational trigger for activation of a G protein by a G protein-coupled receptor. *Biochemistry*, 2003. **42**(6): p. 1365-8.
118. Han, M., M. Groesbeek, T.P. Sakmar, and S.O. Smith, The C9 methyl group of retinal interacts with glycine-121 in rhodopsin. *Proc Natl Acad Sci U S A*, 1997. **94**(25): p. 13442-7.
119. Han, M., M. Groesbeek, S.O. Smith, and T.P. Sakmar, Role of the C9 methyl group in rhodopsin activation: characterization of mutant opsins with the artificial chromophore 11-cis-9-demethylretinal. *Biochemistry*, 1998. **37**(2): p. 538-45.
120. Han, M., S.W. Lin, M. Minkova, S.O. Smith, and T.P. Sakmar, Functional interaction of transmembrane helices 3 and 6 in rhodopsin. Replacement of phenylalanine 261 by alanine causes reversion of phenotype of a glycine 121 replacement mutant. *J Biol Chem*, 1996. **271**(50): p. 32337-42.

121. Han, M., S.W. Lin, S.O. Smith, and T.P. Sakmar, The effects of amino acid replacements of glycine 121 on transmembrane helix 3 of rhodopsin. *J Biol Chem*, 1996. **271**(50): p. 32330-6.
122. Shieh, T., M. Han, T.P. Sakmar, and S.O. Smith, The steric trigger in rhodopsin activation. *J Mol Biol*, 1997. **269**(3): p. 373-84.
123. Wald, G., Molecular basis of visual excitation. *Science*, 1968. **162**(850): p. 230-9.
124. Lewis, J.W., F.J. van Kuijk, J.A. Carruthers, and D.S. Kliger, Metarhodopsin III formation and decay kinetics: comparison of bovine and human rhodopsin. *Vision Res*, 1997. **37**(1): p. 1-8.
125. Vogel, R., F. Siebert, G. Mathias, P. Tavan, G. Fan, and M. Sheves, Deactivation of Rhodopsin in the Transition from the Signaling State Meta II to Meta III Involves a Thermal Isomerization of the Retinal Chromophore C=N Double Bond. *Biochemistry*, 2003. **42**(33): p. 9863-9874.
126. Jencks, W.P., *Catalysis in Chemistry and Enzymology*. 1987, Mineola, N.Y.: Dover Publications Inc.
127. Kuhne, H., *On the Photochemistry of the Retina and on Visual Purple*. 1878, London: Macmillan Press Ltd.
128. Wald, G.D., J. and St. George, C. C., The light reaction in the bleaching of rhodopsin. *Science*, 1950. **111**: p. 179-182.
129. Archila, J.B., H. Lagenaur, C. and Cordes, E.H., Substituent and secondary deuterium isotope effects for hydrolysis of Schiff bases. *J Org Chem*, 1971. **36**(10): p. 1345-1347.

130. Bruault, M.P., R.M. and Bevins, C.L., Kinetics and mechanism of the hydrolysis of 2,2,2-trifluoro-N-(3-methyl-2-cyclohexenylidene)ethyamine - an α,β -unsaturated Schiff base. *J Org Chem*, 1976. **41**(2): p. 346-350.
131. Doukas, A.G., B. Aton, R.H. Callender, and T.G. Ebrey, Resonance Raman studies of bovine metarhodopsin I and metarhodopsin II. *Biochemistry*, 1978. **17**(12): p. 2430-5.
132. Hargrave, P.A., H.E. Hamm, and K.P. Hofmann, Interaction of rhodopsin with the G-protein, transducin. *Bioessays*, 1993. **15**(1): p. 43-50.
133. Merbs, S.L. and J. Nathans, Role of hydroxyl-bearing amino acids in differentially tuning the absorption spectra of the human red and green cone pigments. *Photochem Photobiol*, 1993. **58**(5): p. 706-10.
134. Oprian, D.D., A.B. Asenjo, N. Lee, and S.L. Pelletier, Design, chemical synthesis, and expression of genes for the three human color vision pigments. *Biochemistry*, 1991. **30**(48): p. 11367-72.
135. Khorana, H.G., Rhodopsin, photoreceptor of the rod cell. An emerging pattern for structure and function. *J Biol Chem*, 1992. **267**(1): p. 1-4.
136. Helmreich, E.J. and K.P. Hofmann, Structure and function of proteins in G-protein-coupled signal transfer. *Biochim Biophys Acta*, 1996. **1286**(3): p. 285-322.
137. Wald, G., The molecular basis of visual excitation. *Nature*, 1968. **219**: p. 800-807.
138. Motto, M., M. Sheves, V. Balogh-Nair, K. Tsujimoto, and K. Nakanishi, Opsin shifts in bovine rhodopsin and bacteriorhodopsin. Comparison of two external point-charge models. *J Am Chem Soc*, 1980. **102**: p. 7947-7949.

139. Asenjo, A.B., J. Rim, and D.D. Oprian, Molecular determinants of human red/green color discrimination. *Neuron*, 1994. **12**(5): p. 1131-8.
140. Neitz, M., J. Neitz, and G.H. Jacobs, Spectral tuning of pigments underlying red-green color vision. *Science*, 1991. **252**(5008): p. 971-4.
141. Yokoyama, R. and S. Yokoyama, Convergent evolution of the red- and green-like visual pigment genes in fish, *Astyanax fasciatus*, and human. *Proc Natl Acad Sci U S A*, 1990. **87**(23): p. 9315-8.
142. Chan, T., M. Lee, and T.P. Sakmar, Introduction of hydroxyl-bearing amino acids causes bathochromic spectral shifts in rhodopsin. Amino acid substitutions responsible for red-green color pigment spectral tuning. *J Biol Chem*, 1992. **267**(14): p. 9478-80.
143. Kochendoerfer, G.G., Z. Wang, D.D. Oprian, and R.A. Mathies, Resonance Raman examination of the wavelength regulation mechanism in human visual pigments. *Biochemistry*, 1997. **36**(22): p. 6577-87.
144. Wang, Z., A.B. Asenjo, and D.D. Oprian, Identification of the Cl(-)-binding site in the human red and green color vision pigments. *Biochemistry*, 1993. **32**(9): p. 2125-30.
145. Kleinschmidt, J. and F.I. Harosi, Anion sensitivity and spectral tuning of cone visual pigments in situ. *Proc Natl Acad Sci U S A*, 1992. **89**(19): p. 9181-5.
146. Baehr, W., E.A. Morita, R.J. Swanson, and M.L. Applebury, Characterization of bovine rod outer segment G-protein. *J Biol Chem*, 1982. **257**(11): p. 6452-60.

147. Ferretti, L., S.S. Karnik, H.G. Khorana, M. Nassal, and D.D. Oprian, Total synthesis of a gene for bovine rhodopsin. *Proc Natl Acad Sci U S A*, 1986. **83**(3): p. 599-603.
148. Yang, K., D.L. Farrens, W.L. Hubbell, and H.G. Khorana, Structure and function in rhodopsin. Single cysteine substitution mutants in the cytoplasmic interhelical E-F loop region show position- specific effects in transducin activation. *Biochemistry*, 1996. **35**(38): p. 12464-9.
149. Fong, T.M., *Overview of Mutagenesis Techniques*, in *Structure-Function Analysis Of G Protein-Coupled Receptors*, J. Wess, Editor. 1999, Wiley-Liss: New York. p. 1-20.
150. Oprian, D.D., R.S. Molday, R.J. Kaufman, and H.G. Khorana, Expression of a synthetic bovine rhodopsin gene in monkey kidney cells. *Proc Natl Acad Sci U S A*, 1987. **84**(24): p. 8874-8.
151. Reeves, P.J., J. Hwa, and H.G. Khorana, Structure and function in rhodopsin: kinetic studies of retinal binding to purified opsin mutants in defined phospholipid-detergent mixtures serve as probes of the retinal binding pocket. *Proc Natl Acad Sci U S A*, 1999. **96**(5): p. 1927-31.
152. Sakamoto, T. and H.G. Khorana, Structure and function in rhodopsin: the fate of opsin formed upon the decay of light-activated metarhodopsin II in vitro. *Proc Natl Acad Sci U S A*, 1995. **92**(1): p. 249-53.
153. Yang, K., D.L. Farrens, C. Altenbach, Z.T. Farahbakhsh, W.L. Hubbell, and H.G. Khorana, Structure and function in rhodopsin. Cysteines 65 and 316 are in

- proximity in a rhodopsin mutant as indicated by disulfide formation and interactions between attached spin labels. *Biochemistry*, 1996. **35**(45): p. 14040-6.
154. Farrens, D.L. and H.G. Khorana, Structure and function in rhodopsin. Measurement of the rate of metarhodopsin II decay by fluorescence spectroscopy. *J Biol Chem*, 1995. **270**(10): p. 5073-6.
155. Fahmy, K., T.A. Zvyaga, T.P. Sakmar, and F. Siebert, Spectroscopic evidence for altered chromophore--protein interactions in low-temperature photoproducts of the visual pigment responsible for congenital night blindness. *Biochemistry*, 1996. **35**(47): p. 15065-73.
156. Phillips, W.J. and R.A. Cerione, The intrinsic fluorescence of the alpha subunit of transducin. Measurement of receptor-dependent guanine nucleotide exchange. *J Biol Chem*, 1988. **263**(30): p. 15498-505.
157. Rao, V.R., G.B. Cohen, and D.D. Oprian, Rhodopsin mutation G90D and a molecular mechanism for congenital night blindness. *Nature*, 1994. **367**(6464): p. 639-42.
158. Fasick, J.I., T.W. Cronin, D.M. Hunt, and P.R. Robinson, The visual pigments of the bottlenose dolphin (*Tursiops truncatus*). *Vis Neurosci*, 1998. **15**(4): p. 643-51.
159. Ridge, K.D., S. Bhattacharya, T.A. Nakayama, and H.G. Khorana, Light-stable rhodopsin. II. An opsin mutant (TRP-265----Phe) and a retinal analog with a nonisomerizable 11-cis configuration form a photostable chromophore. *J Biol Chem*, 1992. **267**(10): p. 6770-5.
160. Hoffmann, K.P., Photoproducts of rhodopsin in the disk membrane. *Photobiochem. Photobiophys.*, 1986. **13**: p. 309-338.

161. Lewis, J.W. and D.S. Kliger, Photointermediates of visual pigments. *J Bioenerg Biomembr*, 1992. **24**(2): p. 201-10.
162. Resek, J.F., Z.T. Farahbakhsh, W.L. Hubbell, and H.G. Khorana, Formation of the meta II photointermediate is accompanied by conformational changes in the cytoplasmic surface of rhodopsin. *Biochemistry*, 1993. **32**(45): p. 12025-32.
163. Imai, H., D. Kojima, T. Oura, S. Tachibanaki, A. Terakita, and Y. Shichida, Single amino acid residue as a functional determinant of rod and cone visual pigments. *Proc Natl Acad Sci U S A*, 1997. **94**(6): p. 2322-6.
164. Fahmy, K. and T.P. Sakmar, Regulation of the rhodopsin-transducin interaction by a highly conserved carboxylic acid group. *Biochemistry*, 1993. **32**(28): p. 7229-36.
165. Zvyaga, T.A., K. Fahmy, F. Siebert, and T.P. Sakmar, Characterization of the mutant visual pigment responsible for congenital night blindness: a biochemical and Fourier-transform infrared spectroscopy study. *Biochemistry*, 1996. **35**(23): p. 7536-45.
166. Vogel, R., G.B. Fan, M. Sheves, and F. Siebert, The molecular origin of the inhibition of transducin activation in rhodopsin lacking the 9-methyl group of the retinal chromophore: a UV- Vis and FTIR spectroscopic study. *Biochemistry*, 2000. **39**(30): p. 8895-908.
167. Ganter, U.M., E.D. Schmid, D. Perez-Sala, R.R. Rando, and F. Siebert, Removal of the 9-methyl group of retinal inhibits signal transduction in the visual process. A Fourier transform infrared and biochemical investigation. *Biochemistry*, 1989. **28**(14): p. 5954-62.

168. Meyer, C.K., M. Bohme, A. Ockenfels, W. Gartner, K.P. Hofmann, and O.P. Ernst, Signaling states of rhodopsin. Retinal provides a scaffold for activating proton transfer switches. *J Biol Chem*, 2000. **275**(26): p. 19713-8.
169. Nagata, T., A. Terakita, H. Kandori, D. Kojima, Y. Shichida, and A. Maeda, Water and peptide backbone structure in the active center of bovine rhodopsin. *Biochemistry*, 1997. **36**(20): p. 6164-70.
170. Jung, K.H., E.N. Spudich, P. Dag, and J.L. Spudich, Transducer-binding and transducer-mutations modulate photoactive-site-deprotonation in sensory rhodopsin I. *Biochemistry*, 1999. **38**(40): p. 13270-4.
171. Albert, A.D. and P.L. Yeagle, Structural studies on rhodopsin. *Biochim Biophys Acta*, 2002. **1565**(2): p. 183-95.
172. Lewis, J.W. and D.S. Kliger, Absorption spectroscopy in studies of visual pigments: spectral and kinetic characterization of intermediates. *Methods Enzymol*, 2000. **315**: p. 164-78.
173. Schertler, G.F. and P.A. Hargrave, Projection structure of frog rhodopsin in two crystal forms. *Proc Natl Acad Sci U S A*, 1995. **92**(25): p. 11578-82.
174. Fukuda, M.N., Papermaster, D.S., Hargrave, P.A., Structural analysis of carbohydrate moiety of bovine rhodopsin. *Methods in Enzymology*, 1982. **81**: p. 214-23.
175. Sung, C.H., B.G. Schneider, N. Agarwal, D.S. Papermaster, and J. Nathans, Functional heterogeneity of mutant rhodopsins responsible for autosomal dominant retinitis pigmentosa. *Proc Natl Acad Sci U S A*, 1991. **88**(19): p. 8840-4.

176. Sung, C.H., C.M. Davenport, J.C. Hennessey, I.H. Maumenee, S.G. Jacobson, J.R. Heckenlively, R. Nowakowski, G. Fishman, P. Gouras, and J. Nathans, Rhodopsin mutations in autosomal dominant retinitis pigmentosa. *Proc Natl Acad Sci U S A*, 1991. **88**(15): p. 6481-5.
177. Sung, C.H., C. Makino, D. Baylor, and J. Nathans, A rhodopsin gene mutation responsible for autosomal dominant retinitis pigmentosa results in a protein that is defective in localization to the photoreceptor outer segment. *J Neurosci*, 1994. **14**(10): p. 5818-33.
178. Resek, J.F., D. Farrens, and H.G. Khorana, Structure and function in rhodopsin: covalent crosslinking of the rhodopsin (metarhodopsin II)-transducin complex--the rhodopsin cytoplasmic face links to the transducin alpha subunit. *Proc Natl Acad Sci U S A*, 1994. **91**(16): p. 7643-7.
179. Janz, J.M. and D.L. Farrens, Engineering a functional blue-wavelength-shifted rhodopsin mutant. *Biochemistry*, 2001. **40**(24): p. 7219-27.
180. Laemmli, U.K., Cleavage of structural proteins during the assembly of the head of bacteriophage T4. *Nature*, 1970. **227**(259): p. 680-5.
181. Andres, A., A. Kosoy, P. Garriga, and J. Manyosa, Mutations at position 125 in transmembrane helix III of rhodopsin affect the structure and signalling of the receptor. *Eur J Biochem*, 2001. **268**(22): p. 5696-704.
182. Vogel, R. and F. Siebert, Conformation and stability of alpha-helical membrane proteins. 1. Influence of salts on conformational equilibria between active and inactive states of rhodopsin. *Biochemistry*, 2002. **41**(11): p. 3529-35.
183. Segel, I.H., *Enzyme Kinetics*. 1975, New York: Wiley. 931-941.

184. Sakmar, T.P., R.R. Franke, and H.G. Khorana, The role of the retinylidene Schiff base counterion in rhodopsin in determining wavelength absorbance and Schiff base pKa. *Proc Natl Acad Sci U S A*, 1991. **88**(8): p. 3079-83.
185. Kaushal, S., K.D. Ridge, and H.G. Khorana, Structure and function in rhodopsin: the role of asparagine-linked glycosylation. *Proc Natl Acad Sci U S A*, 1994. **91**(9): p. 4024-8.
186. Yan, E.C., M.A. Kazmi, S. De, B.S. Chang, C. Seibert, E.P. Marin, R.A. Mathies, and T.P. Sakmar, Function of extracellular loop 2 in rhodopsin: glutamic acid 181 modulates stability and absorption wavelength of metarhodopsin II. *Biochemistry*, 2002. **41**(11): p. 3620-7.
187. Hubbard, R., Bownds, D., and Yoshizawa, T., The Chemistry of Visual Photoreception. *Cold Spring Harb Symp Quant Biol*, 1965. **30**: p. 301-315.
188. Karnik, S.S., K.D. Ridge, S. Bhattacharya, and H.G. Khorana, Palmitoylation of bovine opsin and its cysteine mutants in COS cells. *Proc Natl Acad Sci U S A*, 1993. **90**(1): p. 40-4.
189. Sung, C.H., C.M. Davenport, and J. Nathans, Rhodopsin mutations responsible for autosomal dominant retinitis pigmentosa. Clustering of functional classes along the polypeptide chain. *J Biol Chem*, 1993. **268**(35): p. 26645-9.
190. Kemp, C.M., S.G. Jacobson, A.J. Roman, C.H. Sung, and J. Nathans, Abnormal rod dark adaptation in autosomal dominant retinitis pigmentosa with proline-23-histidine rhodopsin mutation. *Am J Ophthalmol*, 1992. **113**(2): p. 165-74.
191. Hwa, J., P. Garriga, X. Liu, and H.G. Khorana, Structure and function in rhodopsin: packing of the helices in the transmembrane domain and folding to a

- tertiary structure in the intradiscal domain are coupled. *Proc Natl Acad Sci U S A*, 1997. **94**(20): p. 10571-6.
192. Hwa, J., P.J. Reeves, J. Klein-Seetharaman, F. Davidson, and H.G. Khorana, Structure and function in rhodopsin: further elucidation of the role of the intradiscal cysteines, Cys-110, -185, and -187, in rhodopsin folding and function. *Proc Natl Acad Sci U S A*, 1999. **96**(5): p. 1932-5.
193. Hwa, J., J. Klein-Seetharaman, and H.G. Khorana, Structure and function in rhodopsin: Mass spectrometric identification of the abnormal intradiscal disulfide bond in misfolded retinitis pigmentosa mutants. *Proc Natl Acad Sci U S A*, 2001. **98**(9): p. 4872-6.
194. Illing, M.E., R.S. Rajan, N.F. Bence, and R.R. Kopito, A rhodopsin mutant linked to autosomal dominant retinitis pigmentosa is prone to aggregate and interacts with the ubiquitin proteasome system. *J Biol Chem*, 2002. **28**: p. 28.
195. Reuter, T., Photoregeneration of rhodopsin and isorhodopsin from metarhodopsin III in the frog retina. *Vision Res*, 1976. **16**(9): p. 909-17.
196. Landin, J.S., M. Katragadda, and A.D. Albert, Thermal destabilization of rhodopsin and opsin by proteolytic cleavage in bovine rod outer segment disk membranes. *Biochemistry*, 2001. **40**(37): p. 11176-83.
197. Vogel, R. and F. Siebert, Conformation and stability of alpha-helical membrane proteins. 2. Influence of pH and salts on stability and unfolding of rhodopsin. *Biochemistry*, 2002. **41**(11): p. 3536-45.
198. Swinbourne, E.S., *Analysis of Kinetic Data*. Studies in Modern Chemistry, ed. W.A. Agosta. 1971, London: Thomas Nelson and Sons Ltd.

199. Hiroyuki Matsumoto, K.H., and Toru Yoshizawa, Effect of Digitonin Concentration on Regeneration of Cattle Rhodopsin. *Biochim Biophys Acta*, 1978. **501**: p. 257-268.
200. Ridge, K.D., Z. Lu, X. Liu, and H.G. Khorana, Structure and function in rhodopsin. Separation and characterization of the correctly folded and misfolded opsins produced on expression of an opsin mutant gene containing only the native intradiscal cysteine codons. *Biochemistry*, 1995. **34**(10): p. 3261-7.
201. Cooper, A. and C.A. Converse, Energetics of primary processes in visula escitation: photocalorimetry of rhodopsin in rod outer segment membranes. *Biochemistry*, 1976. **15**(14): p. 2970-8.
202. Harosi, F.I. and C. Sandorfy, Retinylidene-opsin schiff base chromophores and their accessibility to water. *Photobiochemistry and Photobiology.*, 1995. **61**(5): p. 510-517.
203. Blazynski, C. and S.E. Ostroy, Pathways in the hydrolysis of vertebrate rhodopsin. *Vision Res*, 1984. **24**(5): p. 459-70.
204. Szundi, I., T.L. Mah, J.W. Lewis, S. Jager, O.P. Ernst, K.P. Hofmann, and D.S. Kliger, Proton transfer reactions linked to rhodopsin activation. *Biochemistry*, 1998. **37**(40): p. 14237-44.
205. Starace, D.M. and B.E. Knox, Activation of transducin by a *Xenopus* short wavelength visual pigment. *J Biol Chem*, 1997. **272**(2): p. 1095-100.
206. Babu, K.R., A. Dukupati, R.R. Birge, and B.E. Knox, Regulation of phototransduction in short-wavelength cone visual pigments via the retinylidene Schiff base counterion. *Biochemistry*, 2001. **40**(46): p. 13760-6.

207. Janz, J.M., J.F. Fay, and D.L. Farrens, Stability of dark state rhodopsin is mediated by a conserved ion pair in intradiscal loop E-2. *J Biol Chem*, 2003. **278**(19): p. 16982-91.
208. Gross, A.K., V.R. Rao, and D.D. Oprian, Characterization of rhodopsin congenital night blindness mutant T94I. *Biochemistry*, 2003. **42**(7): p. 2009-15.
209. Garriga, P. and J. Manyosa, The eye photoreceptor protein rhodopsin. Structural implications for retinal disease. *FEBS Lett*, 2002. **528**(1-3): p. 17-22.
210. Ramon, E., L.J. del Valle, and P. Garriga, Unusual thermal and conformational properties of the rhodopsin congenital night blindness mutant Thr-94 --> Ile. *J Biol Chem*, 2003. **278**(8): p. 6427-32.
211. Gross, A.K., G. Xie, and D.D. Oprian, Slow binding of retinal to rhodopsin mutants G90D and T94D. *Biochemistry*, 2003. **42**(7): p. 2002-8.
212. del Valle, L.J., E. Ramon, X. Canavate, P. Dias, and P. Garriga, Zinc-induced decrease of the thermal stability and regeneration of rhodopsin. *J Biol Chem*, 2003. **278**(7): p. 4719-24.
213. Rousso, I., I. Brodsky, A. Lewis, and M. Sheves, The role of water in retinal complexation to bacterio-opsin. *J Biol Chem*, 1995. **270**(23): p. 13860-8.
214. Vogel, R., G.B. Fan, M. Sheves, and F. Siebert, Salt dependence of the formation and stability of the signaling state in G protein-coupled receptors: evidence for the involvement of the Hofmeister effect. *Biochemistry*, 2001. **40**(2): p. 483-93.
215. Shi, L.a.J., J.A., The binding site of aminergic G protein-coupled receptors: The transmembrane segments and second extracellular loop. *Annual Review of Pharmacology and Toxicology*, 2002. **42**: p. 437-467.

216. Schadel, S.A., M. Heck, D. Maretzki, S. Filipek, D.C. Teller, K. Palczewski, and K.P. Hofmann, Ligand Channeling within a G-protein-coupled Receptor: The Entry and Exit Of Retinals in Native Opsin. *J Biol Chem*, 2003. **278**(27): p. 24896-24903.
217. Baehr, W., S.M. Wu, A.C. Bird, and K. Palczewski, The retinoid cycle and retina disease. *Vision Research*, 2003. **43**(28): p. 2957-2958.
218. Stenkamp, R.E., S. Filipek, C.A. Driessen, D.C. Teller, and K. Palczewski, Crystal structure of rhodopsin: a template for cone visual pigments and other G protein-coupled receptors. *Biochim Biophys Acta*, 2002. **1565**(2): p. 168-82.
219. Janz, J.M. and D.L. Farrens, Assessing structural elements that influence Schiff base stability: mutants E113Q and D190N destabilize rhodopsin through different mechanisms. *Vision Research*, 2003. **43**(28): p. 2991-3002.
220. Zhukovsky, E.A., P.R. Robinson, and D.D. Oprian, Transducin activation by rhodopsin without a covalent bond to the 11- cis-retinal chromophore. *Science*, 1991. **251**(4993): p. 558-60.
221. Nagata, T., A. Terakita, H. Kandori, Y. Shichida, and A. Maeda, The hydrogen-bonding network of water molecules and the peptide backbone in the region connecting Asp83, Gly120, and Glu113 in bovine rhodopsin. *Biochemistry*, 1998. **37**(49): p. 17216-22.
222. Lewis, J.W., I. Szundi, W.Y. Fu, T.P. Sakmar, and D.S. Kliger, pH dependence of photolysis intermediates in the photoactivation of rhodopsin mutant E113Q. *Biochemistry*, 2000. **39**(3): p. 599-606.

223. Sun, H., T. Tsunenari, K.W. Yau, and J. Nathans, The vitelliform macular dystrophy protein defines a new family of chloride channels. *Proc Natl Acad Sci U S A*, 2002. **99**(6): p. 4008-13.
224. Schowen, K.B. and R.L. Schowen, Solvent isotope effects of enzyme systems. *Methods Enzymol*, 1982. **87**: p. 551-606.
225. Klein-Seetharaman, J., E.V. Getmanova, M.C. Loewen, P.J. Reeves, and H.G. Khorana, NMR spectroscopy in studies of light-induced structural changes in mammalian rhodopsin: applicability of solution (19)F NMR. *Proc Natl Acad Sci U S A*, 1999. **96**(24): p. 13744-9.
226. Shi, L., G. Liapakis, R. Xu, F. Guarnieri, J.A. Ballesteros, and J.A. Javitch, Beta2 adrenergic receptor activation. Modulation of the proline kink in transmembrane 6 by a rotamer toggle switch. *J Biol Chem*, 2002. **277**(43): p. 40989-96.
227. Liu, J., N. Blin, B.R. Conklin, and J. Wess, Molecular mechanisms involved in muscarinic acetylcholine receptor-mediated G protein activation studied by insertion mutagenesis. *J Biol Chem*, 1996. **271**(11): p. 6172-8.
228. Ghanouni, P., J.J. Steenhuis, D.L. Farrens, and B.K. Kobilka, Agonist-induced conformational changes in the G-protein-coupling domain of the beta 2 adrenergic receptor. *Proc Natl Acad Sci U S A*, 2001. **98**(11): p. 5997-6002.
229. Hamm, H.E., D. Deretic, A. Arendt, P.A. Hargrave, B. Koenig, and K.P. Hofmann, Site of G protein binding to rhodopsin mapped with synthetic peptides from the alpha subunit. *Science*, 1988. **241**(4867): p. 832-5.

230. Martin, E.L., S. Rens-Domiano, P.J. Schatz, and H.E. Hamm, Potent peptide analogues of a G protein receptor-binding region obtained with a combinatorial library. *J Biol Chem*, 1996. **271**(1): p. 361-6.
231. Aris, L., A. Gilchrist, S. Rens-Domiano, C. Meyer, P.J. Schatz, E.A. Dratz, and H.E. Hamm, Structural requirements for the stabilization of metarhodopsin II by the C terminus of the alpha subunit of transducin. *J Biol Chem*, 2001. **276**(4): p. 2333-9.
232. Dratz, E.A., J.E. Furstenau, C.G. Lambert, D.L. Thireault, H. Rarick, T. Schepers, S. Pakhlevaniants, and H.E. Hamm, NMR structure of a receptor-bound G-protein peptide. *Nature*, 1993. **363**(6426): p. 276-81.
233. Kisselev, O.G., J. Kao, J.W. Ponder, Y.C. Fann, N. Gautam, and G.R. Marshall, Light-activated rhodopsin induces structural binding motif in G protein alpha subunit. *Proc Natl Acad Sci U S A*, 1998. **95**(8): p. 4270-5.
234. Koenig, B.W., G. Kontaxis, D.C. Mitchell, J.M. Louis, B.J. Litman, and A. Bax, Structure and orientation of a G protein fragment in the receptor bound state from residual dipolar couplings. *J Mol Biol*, 2002. **322**(2): p. 441-61.
235. Brabazon, D.M., N.G. Abdulaev, J.P. Marino, and K.D. Ridge, Evidence for structural changes in carboxyl-terminal peptides of transducin alpha-subunit upon binding a soluble mimic of light-activated rhodopsin. *Biochemistry*, 2003. **42**(2): p. 302-11.
236. Konig, B., A. Arendt, J.H. McDowell, M. Kahlert, P.A. Hargrave, and K.P. Hofmann, Three cytoplasmic loops of rhodopsin interact with transducin. *Proc Natl Acad Sci U S A*, 1989. **86**(18): p. 6878-82.

237. Acharya, S., Y. Saad, and S.S. Karnik, Transducin-alpha C-terminal peptide binding site consists of C-D and E- F loops of rhodopsin. *J Biol Chem*, 1997. **272**(10): p. 6519-24.
238. Cai, K., Y. Itoh, and H.G. Khorana, Mapping of contact sites in complex formation between transducin and light-activated rhodopsin by covalent crosslinking: use of a photoactivatable reagent. *Proc Natl Acad Sci U S A*, 2001. **98**(9): p. 4877-82.
239. Cai, K., J. Klein-Seetharaman, D. Farrens, C. Zhang, C. Altenbach, W.L. Hubbell, and H.G. Khorana, Single-cysteine substitution mutants at amino acid positions 306-321 in rhodopsin, the sequence between the cytoplasmic end of helix VII and the palmitoylation sites: sulfhydryl reactivity and transducin activation reveal a tertiary structure. *Biochemistry*, 1999. **38**(25): p. 7925-30.
240. Klein-Seetharaman, J., J. Hwa, K. Cai, C. Altenbach, W.L. Hubbell, and H.G. Khorana, Single-cysteine substitution mutants at amino acid positions 55-75, the sequence connecting the cytoplasmic ends of helices I and II in rhodopsin: reactivity of the sulfhydryl groups and their derivatives identifies a tertiary structure that changes upon light-activation. *Biochemistry*, 1999. **38**(25): p. 7938-44.
241. Mansoor, S.E., H.S. McHaourab, and D.L. Farrens, Mapping proximity within proteins using fluorescence spectroscopy. A study of T4 lysozyme showing that tryptophan residues quench bimane fluorescence. *Biochemistry*, 2002. **41**(8): p. 2475-84.

242. Struthers, M., H. Yu, and D.D. Oprian, G protein-coupled receptor activation: analysis of a highly constrained, "straitjacketed" rhodopsin. *Biochemistry*, 2000. **39**(27): p. 7938-42.
243. Abdulaev, N.G. and K.D. Ridge, Light-induced exposure of the cytoplasmic end of transmembrane helix seven in rhodopsin. *Proc Natl Acad Sci U S A*, 1998. **95**(22): p. 12854-9.
244. Terakita, A., T. Yamashita, N. Nimbari, D. Kojima, and Y. Shichida, Functional interaction between bovine rhodopsin and G protein transducin. *J Biol Chem*, 2002. **277**(1): p. 40-6.
245. Natochin, M., K.G. Gasimov, M. Moussaif, and N.O. Artemyev, Rhodopsin Determinants for Transducin Activation: A Gain-of-Function Approach. *J Biol Chem*, 2003. **278**(39): p. 37574-81.
246. Clackson, T. and J.A. Wells, A hot spot of binding energy in a hormone-receptor interface. *Science*, 1995. **267**(5196): p. 383-6.
247. Alexiev, U., I. Rimke, and T. Pohlmann, Elucidation of the nature of the conformational changes of the EF-interhelical loop in bacteriorhodopsin and of the helix VIII on the cytoplasmic surface of bovine rhodopsin: a time-resolved fluorescence depolarization study. *J Mol Biol*, 2003. **328**(3): p. 705-19.
248. Krishna, A.G., S.T. Menon, T.J. Terry, and T.P. Sakmar, Evidence that helix 8 of rhodopsin acts as a membrane-dependent conformational switch. *Biochemistry*, 2002. **41**(26): p. 8298-309.

249. Mielke, T., U. Alexiev, M. Glasel, H. Otto, and M.P. Heyn, Light-induced changes in the structure and accessibility of the cytoplasmic loops of rhodopsin in the activated MII state. *Biochemistry*, 2002. **41**(25): p. 7875-84.
250. Franke, R.R., B. Konig, T.P. Sakmar, H.G. Khorana, and K.P. Hofmann, Rhodopsin mutants that bind but fail to activate transducin. *Science*, 1990. **250**(4977): p. 123-5.
251. Franke, R.R., T.P. Sakmar, R.M. Graham, and H.G. Khorana, Structure and function in rhodopsin. Studies of the interaction between the rhodopsin cytoplasmic domain and transducin. *J Biol Chem*, 1992. **267**(21): p. 14767-74.
252. Matsumoto, H., K. Horiuchi, and T. Yoshizawa, Effect of digitonin concentration on regeneration of cattle rhodopsin. *Biochim Biophys Acta*, 1978. **501**(2): p. 257-68.
253. Nathans, J., Determinants of visual pigment absorbance: role of charged amino acids in the putative transmembrane segments. *Biochemistry*, 1990. **29**(4): p. 937-42.
254. Weitz, C.J. and J. Nathans, Histidine residues regulate the transition of photoexcited rhodopsin to its active conformation, metarhodopsin II. *Neuron*, 1992. **8**(3): p. 465-72.
255. Wall, M.A., D.E. Coleman, E. Lee, J.A. Iniguez-Lluhi, B.A. Posner, A.G. Gilman, and S.R. Sprang, The structure of the G protein heterotrimer Gi alpha 1 beta 1 gamma 2. *Cell*, 1995. **83**(6): p. 1047-58.

256. Lambright, D.G., J. Sondek, A. Bohm, N.P. Skiba, H.E. Hamm, and P.B. Sigler, The 2.0 Å crystal structure of a heterotrimeric G protein. *Nature*, 1996. **379**(6563): p. 311-9.
257. Janz, J.M. and D.L. Farrens, Rhodopsin activation exposes a key hydrophobic binding site for the transducin α -subunit C-terminus. *J Biol Chem*, Submitted.
258. Fotiadis, D., Y. Liang, S. Filipek, D.A. Saperstein, A. Engel, and K. Palczewski, Atomic-force microscopy: Rhodopsin dimers in native disc membranes. *Nature*, 2003. **421**(6919): p. 127-8.
259. Liang, Y., D. Fotiadis, S. Filipek, D.A. Saperstein, K. Palczewski, and A. Engel, Organization of the G protein-coupled receptors rhodopsin and opsin in native membranes. *J Biol Chem*, 2003. **278**(24): p. 21655-62.
260. Niu, L., J.M. Kim, and H.G. Khorana, Structure and function in rhodopsin: asymmetric reconstitution of rhodopsin in liposomes. *Proc Natl Acad Sci U S A*, 2002. **99**(21): p. 13409-12.
261. Schwalbe, H. and G. Wess, Dissecting G-protein-coupled receptors: structure, function, and ligand interaction. *ChemBiochem*, 2002. **3**(10): p. 915-9.
262. Vogel, R. and F. Siebert, Conformations of the active and inactive states of opsin. *J Biol Chem*, 2001. **276**(42): p. 38487-93.
263. Cai, K., J. Klein-Seetharaman, J. Hwa, W.L. Hubbell, and H.G. Khorana, Structure and function in rhodopsin: effects of disulfide cross-links in the cytoplasmic face of rhodopsin on transducin activation and phosphorylation by rhodopsin kinase. *Biochemistry*, 1999. **38**(39): p. 12893-8.

Appendix I

Retinal Schiff Base Hydrolysis Regulates Resetting of TM Helix 6 During Rhodopsin Signal Attenuation.

A. 1: SUMMARY

In this appendix I report preliminary results suggesting that the integrity of the retinal Schiff base linkage determines the conformation of TM helix 6 during decay of the MII state. The data suggest helix 6 “resets” or moves back toward the helical bundle in tandem with hydrolysis of the retinal Schiff base linkage. Preliminary work on this project was carried out in collaboration with Tom Dunham and data for mutant V139W-K248B shown here was collected and analyzed by Tom. Jon Fay also helped with the preparation of some of the rhodopsin mutants used in this study. Steve Mansoor provided technical assistance with setting-up the fluorescence spectrophotometer for the dual-emission recordings.

A. 2: INTRODUCTION

The light activated Metarhodopsin II (MII) photointermediate represents the active conformation of rhodopsin that can bind and activate the G-protein transducin (14, 27, 48, 67, 161). Following signaling, the active MII state is deactivated either by becoming phosphorylated at its C-terminal tail by rhodopsin kinase and then bound by the protein arrestin, which blocks further interaction and activation of transducin (37-40), or by decaying through hydrolysis of the retinal Schiff base and release of all-*trans*-retinal from the opsin-binding pocket (31, 45, 154). *In vivo* opsin is recycled and reconstituted with 11-*cis*-retinal provided through the retinoid cycle to reform a photosensitive pigment (16, 20, 45, 46). FTIR studies on the conformation of MII decayed opsin suggest no large scale unfolding occurs but rather indicate that the protein adapts a “loose helical bundle” conformation (262), and the decayed opsin can rapidly

rebind exogenously added 11-*cis*-retinal to reform native state rhodopsin in a detergent solubilized system (152, 154).

Site-directed labeling provides an excellent means to investigate these kinds of dynamic processes (31). Cysteine-scanning mutagenesis, in combination with sulfhydryl-directed spectroscopic probes (for fluorescent or EPR studies) enables specific monitoring of changes in protein domains of interest (31, 116). Such methodology has been used extensively in the study of the activation mechanism of rhodopsin (31, 116), and have shown that a key movement in the transition to the MII state involves an outward movement of transmembrane helix 6 in the rhodopsin cytoplasmic face (31, 114, 116). This movement increases the exposure of residues on the inner face of this helix (Figure A. 1) and is needed for transducin (G_T) activation (114-116, 225). In addition, similar movements appear to occur in ligand activated GPCRs as well (8, 226-228).

We recently showed that this movement provides a binding site for the C-terminal tail of the α -subunit of the transducin G-protein by opening up a cleft on the cytoplasmic face of rhodopsin (257). These studies also found that this binding does not occur in the opsin form that results from complete decay of the MII species (257). One interpretation for these results would be that helix 6 returns toward the helical bundle as part of a resetting process during MII decay, thus closing the cleft between helices 3 and 6 and thereby preventing further binding and activation of transducin.

This appendix reports experiments designed to test the above hypothesis and monitor conformational changes in TM helix 6 that occur during the MII decay process. These studies utilize a new methodology to monitor these movement based upon the quenching effect tryptophan residues have on the small fluorescent probe bimane when

the two are within near contact distance (241). Using this technique in combination with other assays it is shown that following an outward movement of TM helix 6 during receptor activation, helix 6 moves back toward the helical bundle of the protein during MII decay. The kinetics of this resetting process are shown to be similar to that of the Schiff base hydrolysis and retinal release process and both rates are dramatically shown to increase upon the addition of hydroxylamine. Taken together these results suggest that the resetting of helix 6 during MII decay is dependent upon 1) the integrity of the retinal Schiff base linkage and 2) the occupation of the retinal-binding pocket.

A. 3: MATERIALS and METHODS

A. 3. 1: Materials

For materials used in this chapter please refer to sections 3. 3. 1 and 6. 3. 1 in chapters 3 and 6.

A. 3. 2: Construction, expression and purification of rhodopsin and recombinant rhodopsins.

For construction, expression and purification of rhodopsin mutants please refer to section 2. 3. 3 and 2. 3. 4 in chapter 2.

A. 3. 3: PDT-bimane labeling of rhodopsin mutants, and determination of labeling efficiency

For labeling protocol and efficiency assessment please refer to section 6. 3. 3 in chapter 6.

A. 3. 4: UV/vis Absorption Spectroscopy

For UV-Vis absorption spectroscopy please refer to section 2. 3. 5 and 6. 3. 4 in chapters 2 and 6.

A. 3. 5: Measurement of the rate of retinal release and/or MII decay by fluorescence spectroscopy.

For MII decay assay conditions please refer to section 3. 3. 9 in chapter 3.

A. 3. 6: Dual emission fluorescence spectroscopy.

The experimental set up for the dual emission assays are similar to that used to measure MII stability and utilizes a Photon Technologies QM-1 steady-state fluorescence spectrophotometer. The fluorescence of emission of both tryptophan and bimane were monitored by slewing the excitation wavelength between 295 and 380 nm and monitoring the emission at 330nm (tryptophan) and 460 nm (bimane), respectively. Each measurement was carried out using 100 μ L of a 0.25 μ M mutant sample in 0.05 % DM, 5 mM MES pH 6.0, and sample temperature was maintained at 10 $^{\circ}$ C using a water-jacketed cuvette holder connected to a circulating water bath. After the samples were photobleached to the MII state, the retinal release measurements were carried out by exciting the sample for 2 s by exciting at 295 nm, $\frac{1}{4}$ nm bandwidth slit setting, and monitoring emission at 330 nm, 12-nm bandwidth slit setting. The excitation monochromator then slewed to excite the same sample at 380 nm for 2 s and monitor emission at 480 nm using the same bandwidth settings. The excitation beam was blocked for 45 s between recordings to prevent further photobleaching of the samples. In this manner the rates of retinal release and Trp/bimane quenching were simultaneously recorded on the same sample under the same conditions. To determine the $t_{1/2}$ values for

retinal release and Trp/bimane quenching experimental data was analyzed using a mono-exponential rise to maxima fit in Sigma Plot (Jandel Scientific Software).

A. 4: RESULTS

A. 4. 1: Rational for choice of mutants generated.

Sites for monitoring conformational changes. To investigate possible conformational changes occurring in helix 6 during the course of MII decay we employed a site-directed fluorescence (SDFL) labeling strategy. Previous spin-label studies of rhodopsin illustrate that residue 250 (on helix 6) moves toward residue 139 (on helix 3), while 248 (helix 6) moves away from 139 during receptor activation (114, 263). These same residues are utilized in the SDFL experiments shown in the present study. In the θ^3 background of rhodopsin we introduced a tryptophan mutation at site V139 and mutated residue V250 to a cysteine for labeling with the sulfhydryl-directed probe PDT-bimane, generating mutant V139W-V250B (where the “B” indicates the site is labeled with bimane). In a similar manner, mutant V139W-V248C was also constructed. To serve as controls for the quenching studies (described below), single mutants lacking the Trp quenching residue, K248C and V250C were utilized. A model depicting the locations of these modifications on the cytoplasmic face of rhodopsin is shown in Figure A. 1.

Mutant E113Q to account for FRET. The rhodopsin counter-ion mutant E113Q exhibits pH dependency of its dark state λ_{\max} value (69, 70, 184). As a result, the λ_{\max} value can range between 380 at higher pH to 505 nm at lower pH (69, 70, 184). To utilize the unique absorbance properties of E113Q as a control of fluorescence resonance

³ The θ mutant of rhodopsin has the reactive cysteine residues at positions C140, C316, C322 and C323 replaced with serines (see chapter 6).

energy transfer (FRET) in the bimane emission experiments mutant E113Q-V139W-V250C was constructed. This was carried out because the activation process of rhodopsin results in substantial alterations in its absorption properties, with the dark state λ_{max} of 500 nm shifting to 380 nm in the transition to the MII state (4, 25, 33, 48). As a result, it is important to account for the resulting change in spectral overlap of the fluorescence probe and retinal, as this will effect the inherent FRET that occurs from the probe to the retinal chromophore. As can be seen in figure A. 2A the fluorescence emission of PDT-bimane overlaps with the absorbance of dark state (DS) rhodopsin. As such, when exciting the bimane attached to rhodopsin in the DS, FRET takes place between the probe (donor) and the DS protein (acceptor). This FRET results in a lower level of bimane fluorescence emission intensity in the dark state (Figure A. 2B). Photoconversion from dark to the MII state relieves a substantial portion of this spectral overlap (Figure A. 2A), resulting in less FRET, which in turn results in substantially higher levels of fluorescence intensity in the MII state relative to the emission in the dark state (Figure A. 2B).

A. 4. 2: Characterization of rhodopsin mutants.

All mutants could be expressed in a COS cell system, with yields slightly below that of WT rhodopsin and all were able to bind the 11-*cis*-retinal chromophore and be purified to homogeneity following standard procedures (179, 207). In addition, the introduction of these mutations had little effect on the dark state and MII state λ_{max} values, see Table A. 1. Each mutant was readily labeled with PDT-bimane, and for those tested, exhibit molar label ratios of ~ 1.2 to 0.7 labels per rhodopsin, with minimal contaminating free label present following purification (Table A. 1).

Photobleaching experiments were next performed on the PDT-bimane labeled mutants. All mutants could form a MII like photointermediate upon illumination with light and acid denaturation of this species confirmed the presence of an intact protonated retinal Schiff base linkage (data not shown). Importantly, mutants K248B, V139W-K248B, V250B and V139W-V250B do not show any abnormal photobleaching absorption intermediates during the time course of MII decay (Figure A. 3). As mentioned above, anomalous absorption species could lead to altered FRET during bimane emission assays and complicate any results obtained.

A. 4. 3: Monitoring TM Helix 6 movement using fluorescence spectroscopy.

The active MII state decays both through the MIII intermediate and directly to opsin and all-trans retinal (48, 124, 125). To minimize formation of the ~ 480 nm MIII intermediate, assays were conducted at 10 °C, pH 6.0 under buffering conditions which minimize the formation of the MIII species (Figure A. 3). Previously, we have shown that movement of helix 6 during rhodopsin activation may be detected by chemical reactivity and fluorescence spectroscopy (116, 257). We further confirmed this finding using Trp/bimane quenching SDFL and also used these methods to investigate conformational changes in helix 6 taking place during MII decay, as outlined below.

The dynamics of helix 6 may be monitored using a bimane probe at residue V250. In the absence of a Trp quenching group the level of bimane fluorescence for V250B increases significantly upon conversion from the dark to the MII state, then remains steady over the duration of the assay (Figure A. 4A). As noted above, the large intensity increase observed during the DS → MII transition may be attributed to relief of the

spectral overlap and FRET between the bimane label and the dark state absorbance of the protein.

In contrast a V250B mutant that also contains a Trp quenching group at the end of TM helix 3 (see Figure A. 1), V139W-V250B, initially exhibits an initial quenching in fluorescence intensity during the DS \rightarrow MII transition immediately following photobleaching (Figure A. 4B). This quenching of the bimane fluorescence is slowly mitigated over the course of the assay and eventually reaches a plateau (Figure A. 4B). Importantly, no abnormal absorption photoproducts form during the course of the assay in this mutant, which might complicate interpretation of the fluorescence spectra (Figure A. 4D). Plotting these results as bimane fluorescence intensity *vs.* time suggests the rate of helix 6 resetting may occur on a similar time scale to that of the rate of MII decay (Figure A. 4).

In order for quenching to occur the bimane residue at V250B must come within near contact distance of the tryptophan residue located at V139. We interpret our results to indicate that the bimane label on V250B moves toward the Trp quenching group at V139W to within near contact distance, resulting in significant quenching of bimane fluorescence, which counteracts the normal increase in fluorescence observed due to relief of FRET between the probe and dark state absorbance of rhodopsin (compare Figures A. 4A, C with A. 4B, D).

As another control we also monitored dynamics of helix 6 were also monitored using a bimane probe at site K248. Similar to V250B, the level of bimane fluorescence for K248B increases significantly from the dark to the MII state (due to relief of FRET) then remains steady over the duration of the assay (Figure A. 5A). When a Trp

quenching group is added to helix 3 (V139W) a small amount of quenching occurs in V139W-248B following photobleaching (Figure A. 5B). While subtle, the slow quenching occurs during the decay of the MII state while again no anomalous absorbing species are detected during the course of the assay (Figure A. 5C, D).

As a final control we performed similar experiments on rhodopsin mutant E113Q-V139W-V250B (Figure A. 6). This mutant was studied because relative to the other mutants tested, E113Q-V139W-V250B shows considerably less spectral overlap with bimane emission in the dark state (Figure A. 6A). Similar to the other bimane labeled mutants, E113Q-V139W-V250B does not exhibit any anomalous absorbance intermediates during the decay of the MII state (Figure A. 6B). However, as a result of substantially less energy transfer from the bimane probe to the dark state absorbance, this mutant exhibits interesting emission features following bleaching and during the decay of the MII state. Upon bleaching, the bimane emission decreases by ~ 50 % then slowly increases over the course of the experiment. Following the initial drop in emission, the behavior of E113Q-V139W-V250B is similar to V139W-V250B except the rate of fluorescence increase is much slower ($t_{1/2} = 59$ min). This slow rate of change is expected — mutant E113Q has a very long lived MII state (69, 219), and the retinal release rate of E113Q-V139W-V250B occurs with a $t_{1/2}$ of 62 min (Table A. 1). As these values again suggested a link between MII decay and helix 6 resetting we further explored this possibility as described below.

A. 4. 4: TM Helix 6 resetting is coupled to retinal Schiff base hydrolysis.

To determine if the rate of helix 6 resetting is coupled to retinal Schiff base hydrolysis dual emission fluorescence experiments were performed. By slewing the

excitation beam between 295 and 380 nm and monitoring the sample emission fluorescence at 330 and 460 nm both tryptophan and bimane fluorescence were monitored simultaneously on the same sample. In this manner both the rate of retinal release (tryptophan) and helix 6 resetting (bimane) were monitored for labeled mutant V139W-V250B following photobleaching at 10 °C (Figure A. 7A, C). The rates obtained from this experiment for MII decay ($t_{1/2} = 29$ min) and helix resetting ($t_{1/2} = 26$ min) are very similar. Hydroxylamine readily reacts with rhodopsin in the MII state and rapidly hydrolyzes the retinal Schiff base linkage, greatly expediting the retinal release process (154). As expected, the presence of 50 mM hydroxylamine greatly increases the rate of the retinal release for the labeled mutant V139W-V250B ($t_{1/2} = 0.6$ min), (Figure A. 7B). In addition, the rate of TM helix 6 resetting is also increased by a similar magnitude ($t_{1/2} = 0.4$ min), (Figure A. 7D).

A. 5: DISCUSSION

In the present work we confirm previous reports of TM helix 6 movement during MII formation through SDFL studies. The Trp/bimane fluorescence quenching observed during the formation of the MII species for mutants V139W-V250B and E113Q-V139W-V250B is consistent with prior reports of TM helix 6 movement (114-116). Importantly, we find that this quenching is relieved over time (Figures A. 4, A. 6C). We attribute the relief of quenching to movement of the bimane label on residue V250B away from the quenching Trp at site V139W. Similarly, the quenching observed for V139W-K248B during the decay of the MII state may be explained as the bimane on K248 moving closer

to the Trp residue at site V139. It is important to note that there are no Trp residues in this region of the protein except the one engineered in at residue V139.

Previous EPR studies suggested movements occur around TM helix 3 during receptor activation, though not to the extent of helix 6 (31). To a first approximation, we propose our results could be interpreted as movement of TM helix 6 away from helix 3 during activation and back toward the helical bundle during MII decay.

Conformational changes that occur during the decay of the MII intermediate are not well understood. Previous studies have documented the ability of purified decayed rhodopsin (opsin) to rebind exogenously added 11-*cis*-retinal and form a photosensitive pigment in detergent (152). In addition, decayed MII opsin is thought not to fully unfold following retinal release (262). Furthermore, solution ^{19}F NMR spectroscopy studies illustrate that chemical shifts which occur following photobleaching gradually return to near dark state levels during MII decay (225). These studies indicated that the rate of these shifts parallel the rate of MII decay and retinal release (225). Importantly, the findings from this NMR study also suggest that while the decaying MII state does not return fully to a dark state conformation it does return to a state that is quite similar structurally. Taken together these previous results are consistent with our model of TM helix 6 resetting during the course of MII decay.

To investigate the link between TM helix 6 resetting and retinal Schiff base hydrolysis and retinal release we utilized dual fluorescence emission spectroscopy. During the decay of the MII signaling state the retinal is hydrolyzed and released from the opsin-binding pocket, which can be monitored as an increase in the fluorescence of intrinsic rhodopsin tryptophans (154). Thus by simultaneously monitoring Trp

fluorescence (330 nm) and bimane fluorescence (460 nm) from the same sample we obtained rate information on both MII decay and TM helix 6 resetting. Mutant V139W-250B shows that the rate of helix 6 resetting occurs on a similar scale to the rate of MII decay for this same sample (Figure A. 7A, C), and importantly, in the presence of 50 mM hydroxylamine retinal release and helix movement are dramatically increased (Figure A. 7B, D). Hydroxylamine is well known to hydrolyze Schiff bases, and as such greatly increases the rate of MII decay and retinal release (154). Thus our results suggest that resetting of TM helix 6 is dependent on both the retinal Schiff base linkage and the occupancy of the opsin-binding pocket by retinal. Finally, our finding on mutant E113Q-V139W-V250B further corroborates this theory. This mutant exhibits a very slow rate of MII decay, and the rate of helix 6 resetting is also greatly slowed for this mutant (A. 6).

We have recently shown that a peptide analogous to the C-terminal tail of $G_{T\alpha}$ binds to a cleft on the cytoplasmic face of rhodopsin that opens as a result of TM helix 6 movement (257). This binding interaction only occurs upon formation of the MII intermediate, as no binding was detected in the dark state or following the complete decay of the MII species (257). In addition, we found that the binding interaction could be abolished by the addition of hydroxylamine, which rapidly cleaved the MII retinal Schiff base linkage. These results together with our current work, suggest that during MII decay the cleft opened on the cytoplasmic face of rhodopsin during activation closes and as a result, the C-terminus of $G_{T\alpha}$ is no longer able to bind. We note however, that our simplistic interpretation does not account for additional binding interactions that take place between rhodopsin and the $G_{T\alpha\beta\gamma}$ heterotrimer, nor possible conformational changes that may occur as a result of $GTP \rightarrow GDP$ exchange and release of the $G_{T\alpha}$ subunit

following activation. Furthermore, we have not studied possible conformational changes in TM helix 6 associated with the formation and decay of the MIII photointermediate.

The results discussed here in conjunction with those from other groups provides the basis for proposing a mechanistic model that relates TM helix 6 movement to the MII decay process (Figure A. 8). This model illustrates the orientation of the helices for dark state rhodopsin with 11-*cis*-retinal bound within the opsin-binding pocket. Absorption of light causes isomerization of the retinal to the all-*trans* configuration and is accompanied by rigid body movement of TM 6 during the formation of the active MII signaling intermediate. This active MII state slowly decays over time in a process that involves the hydrolysis of the Schiff base linkage as well as release of all-*trans*-retinal from the opsin-binding pocket. During decay of the MII state TM helix 6 moves back toward the helical bundle, possibly to prevent further interaction with and activation of G_T . The completion of the MII decay process results in the empty opsin apoprotein and free all-*trans*-retinal. 11-*cis*-retinal provided by the retinoid cycle may bind to opsin to reform the dark state photosensitive pigment rhodopsin. Note that this model does not account for the possible formation and decay of the MIII photointermediate.

In summary we propose that following outward movement during the formation of the active MII signaling state TM helix 6 of rhodopsin moves back toward the helical bundle during MII decay. This helix resetting appears to be regulated by the integrity of the retinal Schiff base linkage. We speculate that this movement may close a cleft that is at least partially involved in binding the C-terminal tail of $G_{T\alpha}$ during receptor activation. This study illustrates the relationship between the “ligand-binding” domain and the

cytoplasmic face of the receptor, which must communicate to enable efficient signaling activation and attenuation.

Table A. 1: Characterization of PDT-bimane labeled rhodopsin mutants (DS and MII λ_{\max} , spectral ratio, labeling ratio, % free label, $t_{1/2}$ of retinal release).

Sample ^a	Dark State λ_{\max} (nm) ^b	II State λ_{\max} (nm) ^b	A_{280}/A_{500} ^c	Labeling Ratio ^d	% Free Label ^e	II Decay $t_{1/2}$ (min) ^f
K248B	500	383	1.7	1.2 ± 0.1	3.4 ± 0.1	36.2
V139W-K248B	499	381	1.8	nd ^g	nd	29
V250B	500	381	1.7	0.7 ± 0.1	4.2 ± 1.3	36.5
V139W-V250B	500	382	1.7	0.7 ± 0.1	6.2	22.5
E113Q-V139W-V250B	385/485 ^h	380	nd ^h	nd	nd	62 ⁱ

^a All samples are rhodopsin mutants generated in the theta background and labeled specifically at the introduced cysteine residue with the PDT-bimane probe.

^b Absorbance λ_{\max} determined from the 1st derivative of the raw spectral data.

^c Pure rhodopsin typically exhibits a protein (A_{280} nm) to chromophore (A_{500} nm) absorbance ratio of 1.6 to 1.8. ^d The amount of PDT-bimane label incorporated into the rhodopsin single cysteine mutants are presented as the number of labels per rhodopsin mutant (label/sample). Error values are standard error of the mean ($n = 2$). ^e The amount of free label remaining in each sample following labeling and purification is presented as a percentage of the total sample. ^f The MII decay rate of the labeled samples was determined at either 10 °C for all mutants except E113Q. Under these identical conditions the MII decay $t_{1/2}$ for unlabeled WT rhodopsin is 37.5 min at 10 °C and 13 min at 20 °C. ^g nd = not determined. ^h The λ_{\max} of mutant E113Q is pH dependent (see Results). ⁱ MII decay $t_{1/2}$ for mutant E113Q was determined at 20 °C.

Figure A. 1: Three-dimensional model of rhodopsin viewed toward the cytoplasmic face indicating sites of bimane label and tryptophan-quenching group

incorporation. (A) Model of labeled mutant V139W-K248B, indicating the PDT-bimane fluorophore (purple) attached at K248B on helix 6 and the tryptophan-quenching group (green) engineered in at site V139 on helix 3. (B) Model of labeled mutant V139W-V250B, indicating the PDT-bimane fluorophore (purple) attached at V250 on helix 6 and the tryptophan-quenching group (green) engineered in at site V139 on helix 3. In each model, the large arrow indicates the proposed movement helix 6 and the smaller arrow denotes possible movement of helix 3 thought to occur during formation of the MII state. The model was prepared using the coordinates from the rhodopsin crystal structure (PDB# F188, (52)) and portions of the extracellular domain and intracellular loops have been removed for clarity.

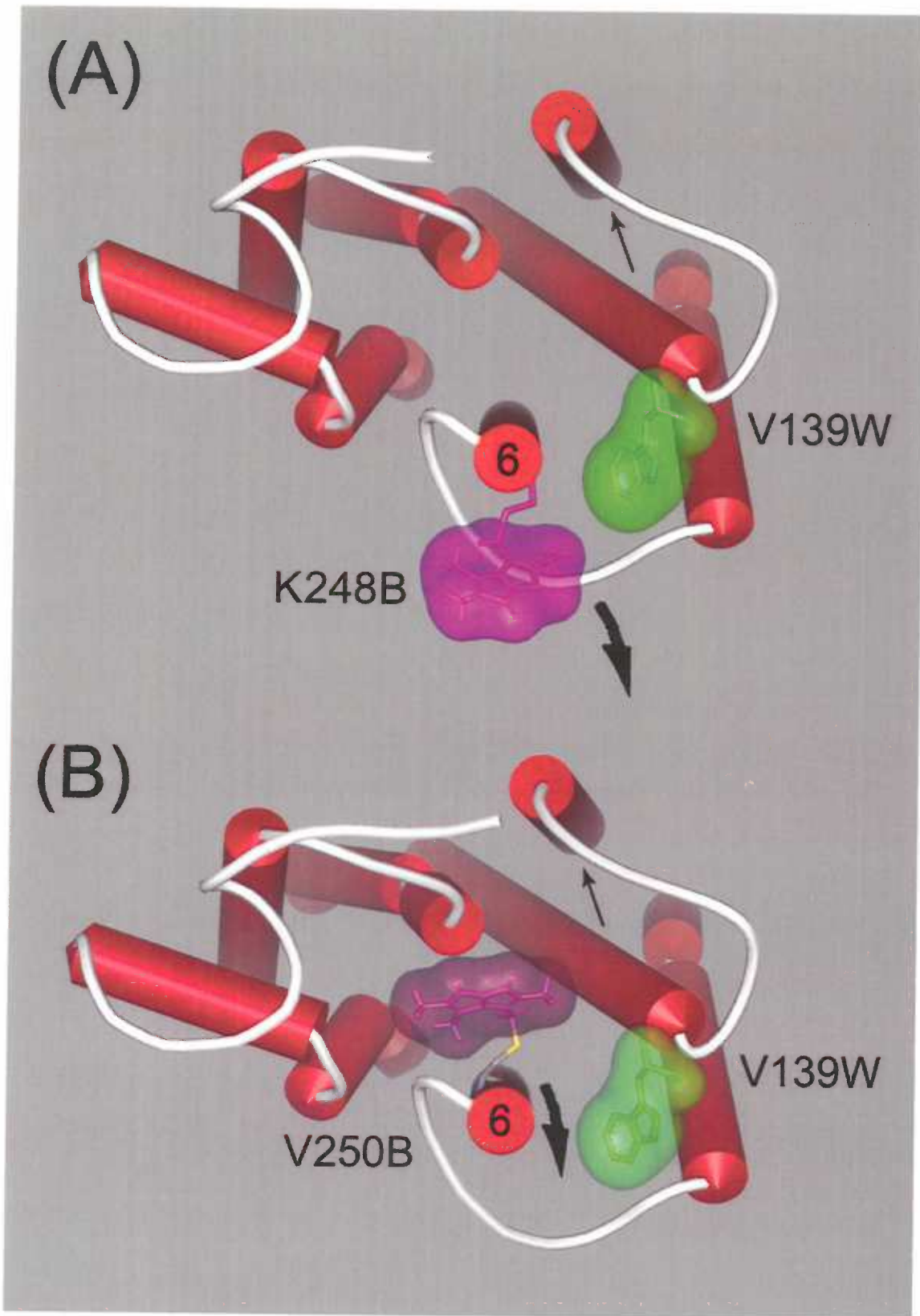


Figure A. 2: Fluorescence resonance energy transfer between bimane fluorescence emission and rhodopsin absorbance. (A) The fluorescence emission spectrum of PDT-bimane overlaid with the absorbance profiles of dark state (DS) and MII rhodopsin. As can be seen, significant spectral overlap of bimane emission occurs with DS rhodopsin (shaded gray and black) resulting in substantial energy transfer from bimane to retinal and thus a quenching of fluorescence. This overlap is greatly reduced upon photoconversion to the MII state (black only). (B) Fluorescence emission properties of a bimane-labeled rhodopsin mutant, K248B. The sample (500 nM) was excited at λ_{380} nm and scanned in the DS and following bleaching to the MII state. Note the large state-dependent change in fluorescence emission due to relief of energy transfer.

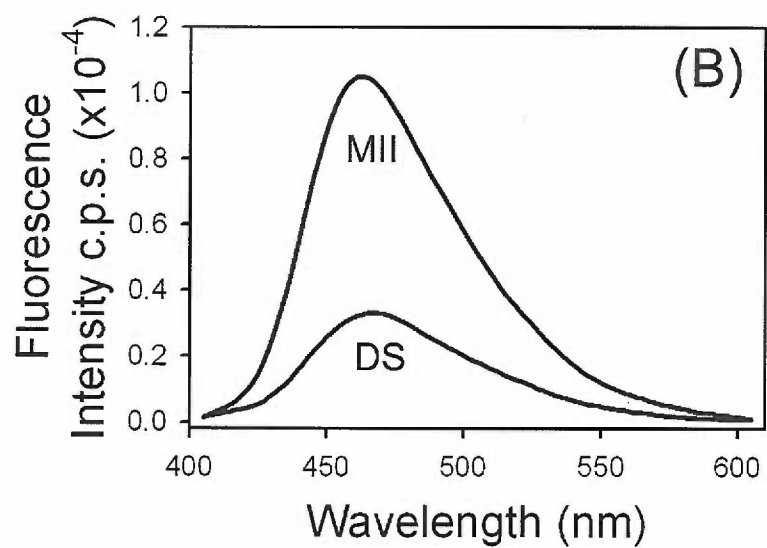
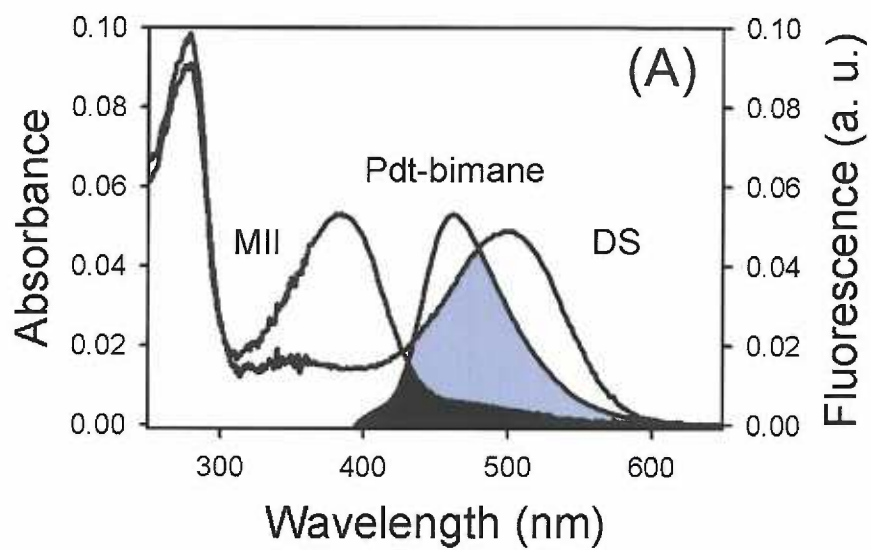


Figure A. 3: UV/vis bleaching profiles of PDT-bimane labeled rhodopsin mutants during MII decay. Absorbance spectra for PDT-bimane labeled samples were recorded in the dark state (red) and in 2.5 to 5 min intervals following 30 s photobleaching (black) over the duration of one hour. In this manner spectra were obtained during the course of MII decay under the same conditions used for fluorescence experiments, samples were in buffer containing 0.05 % DM, 5 mM MES, pH 6.0 at 10 °C (see Figure 7. 4 and 7. 5). No anomalous spectral species are present in any of the labeled samples V250B, V139W-V250B, K248B, **(D)** V139W-K248B.

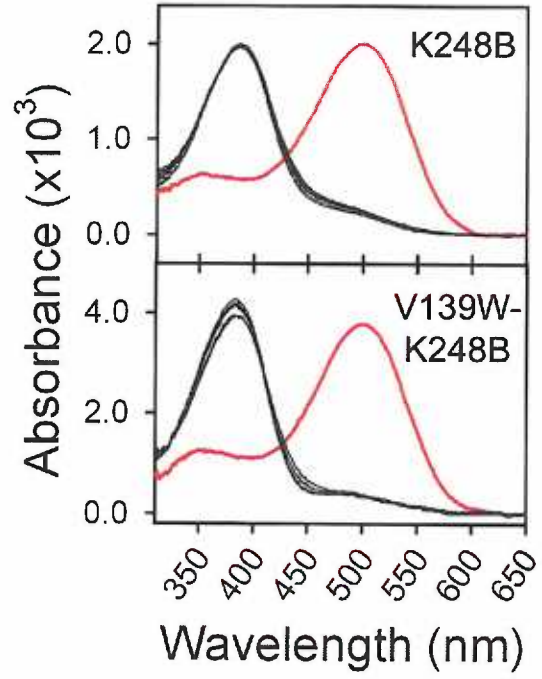
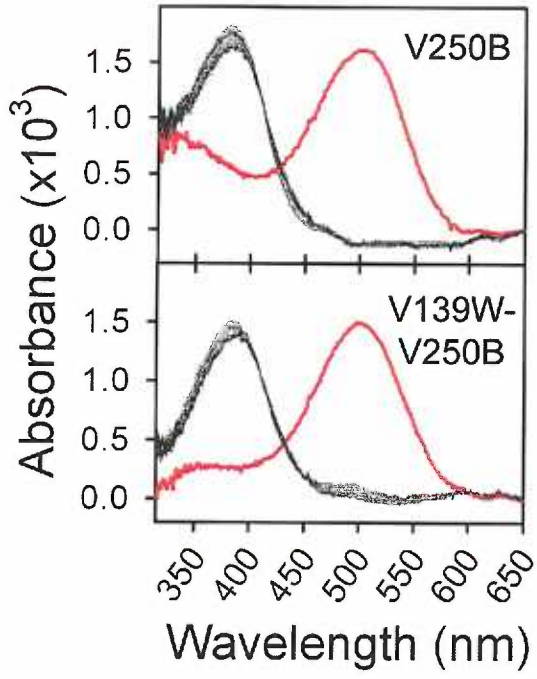


Figure A. 4: Movements in TM helix 6 during MII decay detected at site 250 from bimane fluorescence. **Top**, steady-state fluorescence emission spectra for rhodopsin mutants **(A)** V250B and **(B)** V139W-V250B recorded in 0.05% DM, 5 mM MES, pH 6.0 at 10 °C. An emission scan was first taken in the dark state (black) then following photobleaching with > 490 nm light for 30 s (red), with subsequent scans taken in 150 to 300 s intervals for the duration of the experiment (60 min). A large increase in emission intensity occurs upon bleaching mutant V250B **(A)** and remains steady over time. In contrast, the emission intensity of V139W-250B **(B)** decreases slightly after bleaching and slowly increases over time. **Bottom**, the emission intensity at 460 nm is plotted as a function of time for **(C)** V250B and **(D)** V139W-V250B in relation to the MIII absorbance (480 nm, gray triangles). Very little MIII intermediate is formed under these conditions.

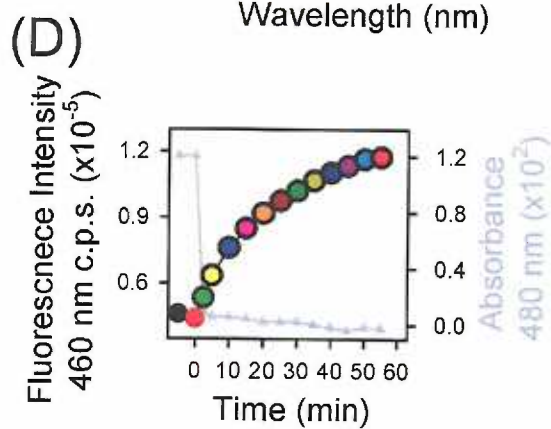
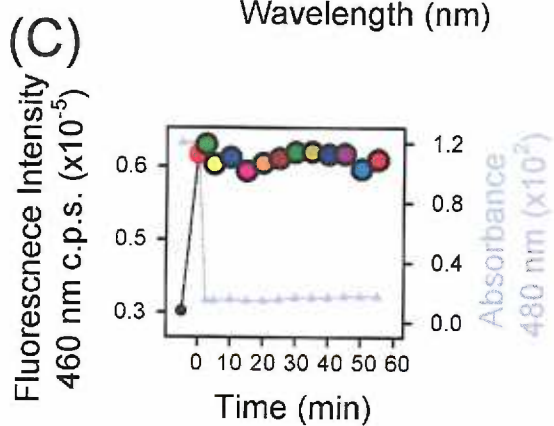
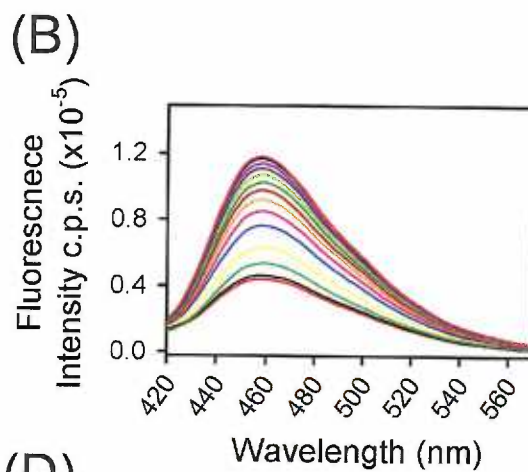
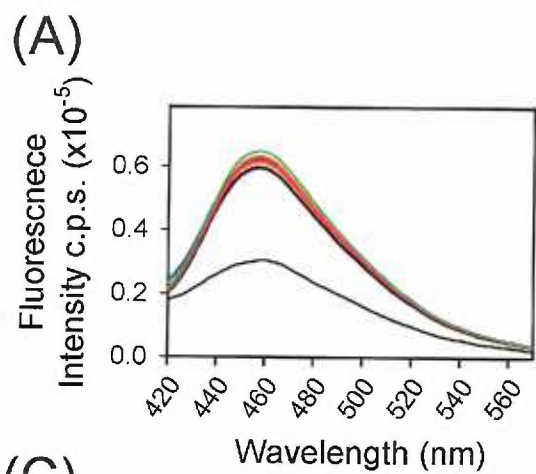


Figure A. 5: Movements in TM helix 6 during MII decay detected at site 248 from bimane fluorescence. **Top**, steady-state fluorescence emission spectra for rhodopsin mutants **(A)** K248B and **(B)** V139W-K248B recorded in 0.05% DM, 5 mM MES, pH 6.0 at 10 °C. An emission scan was first taken in the dark state (black) then following photobleaching with > 490 nm light for 30 s (red), with subsequent scans taken in 150 to 300 s intervals for the duration of the experiment (60 min). Similar to V250B A large increase in emission intensity occurs upon bleaching mutant K248B **(A)** and remains steady over time. While a similar initial increase also occurs in V139W-K248B **(B)**, the emission decreases slightly over time. **Bottom**, the emission intensity at 460 nm is plotted as a function of time for K248B **(C)** and V139W-V248B **(D)** in relation to the MIII absorbance (480 nm, gray triangles). Similar to the V250B mutants very little MIII intermediate is formed under these conditions.

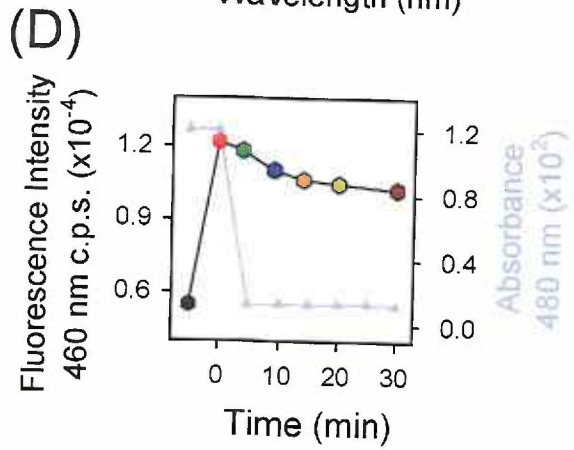
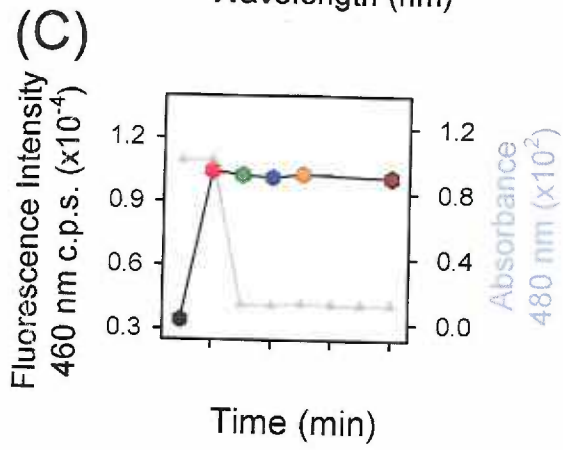
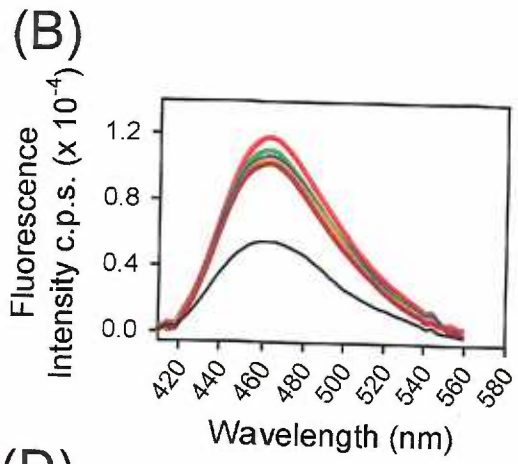
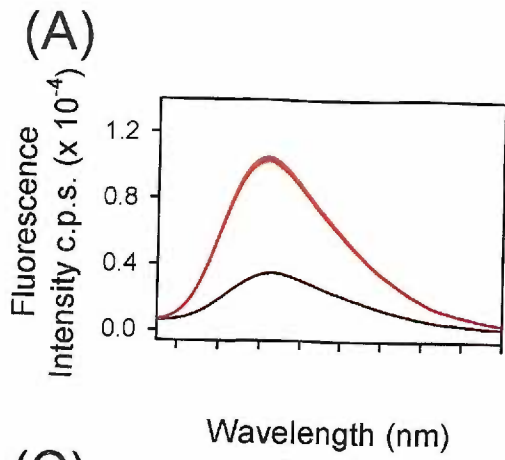
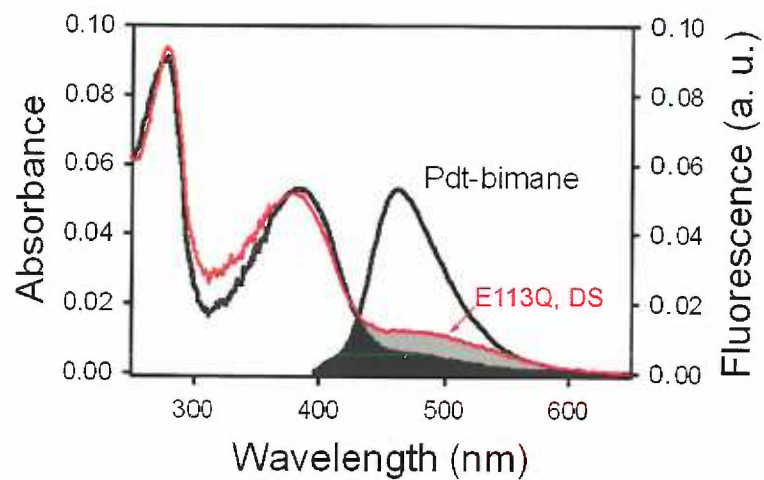
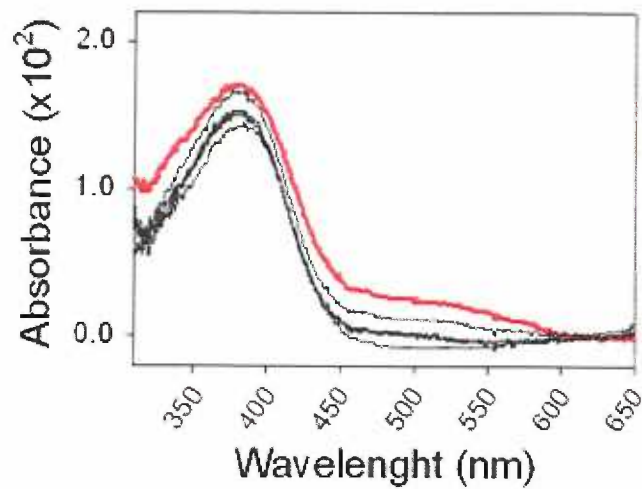


Figure A. 6: UV/vis bleaching profile and Steady state emission spectra of mutant E113Q-V139W-V250B. (A) The fluorescence emission spectrum of PDT-bimane overlaid onto the absorbance profiles of E113Q-V139W-V250B in the dark state (DS, red) and MII states (black). The altered dark state absorbance caused by the E113Q mutation results in substantially less spectral overlap between the absorbing states of this mutant and bimane fluorescence emission (gray and black shading) and less FRET between the two groups. (B) Absorbance profile for E113Q-V139W-V250B during MII decay. The sample was recorded in the dark state (red) and in 2.5 to 5 min intervals following 30 s photobleaching (black) over the duration of one hour at 20 °C. No anomalous spectral species are present during decay of the MII state. (C) Steady-state bimane emission (460 nm) spectra of E113Q-V139W-V250B monitoring TM helix 6 movement during MII decay at 20 °C. Photobleaching the sample (arrow) causes an initial 50% decrease in emission intensity, which then slowly increases over time. The $t_{1/2}$ for the rate of bimane fluorescence increase is 59 min, which is close to the 62 min measured for retinal release/MII decay for this mutant.

(A)



(B)



(C)

